ABSTRACT

Title of Thesis: Bioimprovement of geotechnical properties of sandy soils

Degree candidate: Chiung-Wen Chou

Degree and year: Master of Science, 2007

Thesis directed by: Dr. Eric A. Seagren (Chair) and Dr. Ahmet H. Aydilek (Co-Chair)
Department of Civil and Environmental Engineering

Biological processes may provide great and previously unexplored opportunities for *in situ*, cost effective soil improvement. A laboratory research study was conducted to evaluate the changes in geomechanical properties of sand due to microbial precipitation of calcium with *Bacillus pasteurii*. Direct shear tests and California bearing ratio (CBR) were conducted on the soils subjected to microbial calcite precipitation in the completely stirred tank reactors and completely mixed biofilm reactors, respectively. Scanning electron microscopy (SEM) analyses were conducted to evaluate the performance of microbial precipitation.

Results of the study show that: (1) the bioinduced calcites effectively improve geomechanical properties of sand, (2) live cells significantly improve the properties due to biotic conditions and related pore volume changes, while both dead and resting cells act like organic fibers and cause lower but notable increases in friction angle and bearing strength, and (3) bio-plugging of the column is mostly due to calcite formation, and not biomass accumulation, as evidenced in SEM analyses.

BIOMODIFICATION OF GEOTECHNICAL PROPERTIES OF SAND

by

Chiung-Wen Chou

Thesis submitted to the Faculty of the Graduate School of the
University of Maryland,College Park in partial fulfillment
of the requirements for the degree of
Master of Science
2007

Advisory Committee:

Associate Professor Eric A. Seagren, Chair
Associate Professor Ahmet H. Aydilek, Co-Chair
Professor Deborah J. Goodings
Professor Oliver J. Hao

ACKNOWLEDGEMENT

First of all, it is my pleasure to acknowledge a lot of people who assist me during these one and half years. I would like to thank Dr. Seagren and Dr. Aydilek for giving this great opportunity to join this research. Their guidance, encourage, and patience mean a lot to me, especially to a girl who never leave her home country. Also, I would like to thank Dr. Goodings and Dr. Hao for being my thesis committee members, and giving me valuable comments for this topic. I also appreciate National Science Foundation for supporting this research topic and partial financial aid as well as the staff of Civil and Environmental Engineering Department for providing assistance.

Next, I truly appreciate fellow graduate students, Doina, Lan, Melih, Philip, Houng Li, Eliea, Eunyoung and Michael for their assistance whenever I needed. I am grateful to have them in the laboratory such that the time in the laboratory was enjoyable to me. Also, I am grateful to have helps from Mr. Alfredo L. Bituin, Mr. Timothy K. Maugel, and Mr. Howard Grossenbacher for guiding me specific laboratory testing, and fabrication of specialized devices.

Finally, I would like to thank Jason and my family, who always support me. Their love makes me strong and be able to challenge all difficulties without feeling lonely here.

TABLE OF CONTENTS

LIST OF TABLES

LIST OF FIGURES

SECTION 1

INTRODUCTION

There is an increasing interest in engineering to mimic and maximize the benefits of natural processes. The aim is to achieve an engineering end that has minimal impact on the environment and that may also be less expensive to implement. Whereas environmental engineers have been leaders among the civil engineering profession in this initiative, there are new possibilities being explored in geotechnical engineering. The growing pressures for development of less desirable engineering sites, especially as urban areas grow into densely developed megacities, have focused attention on new possibilities for technologies to achieve soil improvement and stabilization. Such new soil stabilization technique has other important applications outside of urbanized areas, such as ground stabilization against earthquake damage, and prevention of landslides arising from natural causes, such as hurricanes. These measures will be particularly attractive if they can be implemented over wide areas and at low cost.

In situ soil improvement has the ability to alter the strength, hydraulic conductivity, and stiffness of soil. Since it can be designed to cause minimal disruption at the surface, the process is advantageous for use in urban areas or areas of difficult access. The ability to improve soil strength *in situ* has several important implications. For example, increasing the bearing capacity of soils can reduce settlement of structures such as in earthquakes, thus resulting in site improvement. Furthermore, construction on marginal soils such as loose sands, fills, mine spoils, collapsible soils, and expansive soils

will be enabled due to strengthening of subsurface materials. Strengthening soils will also lead to increased load-carrying capability, which plays an essential role in slope stability. *In situ* soil improvement techniques can also be applied to controlling groundwater flow, e.g., via alteration of the hydraulic conductivity. It may be desirable to increase permeability with soil improvement; however, it is more typical that a reduction in permeability is sought (Wartman and Riemer 2002). For example, reduction of permeability in a cut-off wall of soil surrounding an excavation, a tunnel, or the foundation of a structure, can be an effective way to control seepage and achieve a degree of waterproofing. It can also be used in design for containment of contaminated leachate, encapsulating hazardous waste, and initiating or enhancing *in situ* biodegradation of harmful substances (Shackelford and Jefferis 2000, Gates et al. 2001).

In addition to these examples, biological processes may provide cost effective solutions to *in situ* site improvement that are largely unexplored. There is ample evidence of natural cementation of geological formations occurring constantly over time due to physiochemical and biological reactions (Tooth and Fairchild 2003, Smith and Compton 2004). Precipitation of minerals is not an unusual process in nature, and examples of microbiologically-mediated mineralization (biomineralization) in the natural soil environment have been documented (Ghiorse 1984, Banfield and Nealson 1997, Douglas and Beveridge 1998, Le Métayer-Levrel et al. 1999, Castanier et al. 2000, Ehrlich 2002).

Microbial reactions can result in relatively insoluble compounds that can contribute to soil cementation (Buczynski and Chafetz 1991, Folk 1993, Gonzalez-Muñoz et al. 2000). One of these natural processes is microbiological $CaCO_3$ precipitation. The bacteria-induced calcite precipitation process, especially using urea as

a microbial substrate, has also been successfully implemented in the laboratory for improvement of permeable construction materials and plugging of fractured rocks (Gollapudi et al. 1995, Urzi et al. 1999, Ross et al. 2001, Bang et al. 2001, Day et al. 2003, DeJong et al. 2006). Despite the possibility of using microbial cementation of soils via $CaCO_3$ precipitation, the relationship between the bio-catalysis of urea and soil geomechanical properties is still not well-understood. There is a need to study the range of possible conditions necessary to recreate these natural processes *in situ,* and to evaluate the magnitude and the longevity of the effects on soil properties. This experimental research program was undertaken in response to this need. The objectives of the study were to create geotechnically beneficial effects, to assess the geomechanical and hydraulic benefits that are a product of these microbiological processes, and to evaluate abiotic factors on the geotechnical properties of soils.

To accomplish these objectives, a series of laboratory tests were conducted to investigate the impact of factors such as relative concentrations of calcite-oxidizing bacteria on the entire process, the duration of each stage of the process, as well as the resulting improvement in soil strength, and possible changes in hydraulic conductivity. An optimum mineralization environment for the microbial studies was designed using completely stirred tank reactors (CSTR) and completely mixed biofilm reactors (CMBR) specially fabricated for the study. Direct shear tests and California bearing ratio (CBR) were conducted on the soils subjected to microbial $CaCO_3$ precipitation in the CSTRs and CMBRs, respectively. The effects of soil density, cell types (i.e., dead, resting, and live cells), and cell concentration on soil geomechanical properties were studied. Finally, existing CSTR and pseudo-analytical CMBR models were used to describe the behavior

of microbes within the sandy soil matrix during steady state conditions.

Section 2 is a literature review with respect to the origin and mechanisms of microbially mediated $CaCO_3$ precipitation and their influences on soil properties. Subsequently, section 3 provides the experimental materials and design, as well as the analytic methods. Next, the efficiency of the CSTR and CMBR systems and the results of the direct shear and CBR tests using the specimens prepared in the CSTR and CMBR system are presented in Sections 4 and 5. Finally, the conclusions are provided in Section 6, along with suggestions for practical applications and recommendations for future studies.

SECTION 2

LITERATURE REVIEW

2.1 SOIL STABILIZATION AND IMPROVEMENT OVERVIEW

Soil is the most used of construction materials. When engineers have difficulties with on-site construction onto or within soils, the possible solutions are to either cause a positive change in the properties of the soil, i.e., so-called soil improvement, or to change the soil properties adequately to allow field construction to occur, i.e., so-called soil stabilization. As introduced in Section 1, methods for improving the properties of soil by physical or chemical applications were developed during the twentieth century. For example, traditionally, chemical additives such as lime or other materials like fly ash are used to upgrade the engineering properties of a soil through chemical reactions. This method could further be coupled with use of a mechanical device to enhance the soil's load-bearing capacity (US Army Corps of Engineers 1984).

Interestingly, biological applications for improving the mechanical properties of soil have rarely been applied. This is surprising given that microbial activities are ubiquitously present in surface and subsurface soils. In addition, microbial activities in the soil drive numerous reactions such as catalysis, biodegradation, precipitation, and so on, which have great potential for modifying soil properties in field applications. Furthermore, microbes have been recognized to participate in some geochemical reactions such as mineralization in surface soils, rock or marine environment (Klappa 1979, Monger et al. 1991). Activation of biological processes in which precipitation or

mineralization is induced and the byproduct of those reactions acts a small particle within soil matrix could be applied such that the arrangement of treated soils is consolidated effectively. Generally, these reactions can contributed with varying degrees of impact, to properties such as low hydraulic conductivity, extraordinary compressibility or exclusively high friction angle (Mitchell and Santamarina 2005). Through such influences on geomechanical properties, some researchers and engineers have applied this concept for the remediation of materials, stone restoration or microbial enhanced oil recovery (Tiano et al. 1999, Banat 1995), all of which are example of so-called bio-mediation of soil properties.

Nevertheless, the concept of using biological activities in the geotechnical field has not been developed well to date. As a result, the effects of geoenvironmental limiting factors on microbial activities in soil and their impact on soil mechanical behavior remains relatively unknown. On the other hand, chemical addition is very common geotechnical method used to alter the engineering properties of soils or materials through cementation or precipitation processes. Therefore, the effect of microbial activities on precipitation on sandy soils, in particular on calcification, and the possibility for biomediation of calcification in sandy soils was the focus in this study. The goal of this chapter is to review the current state of knowledge and practice for conventional soil improvement/ stabilization in geotechnical engineering, the effect of biological processes on soils, and the concepts and applications of bioclogging and biocalcification as catalyzed by urease.

2.2 CONVENTIONAL METHODS FOR SOIL IMPROVEMENT

Several conventional methods are widely used to effectively improve or control compressibility or hydraulic conductivity of on-site soils in order to support foundational structures. This method can be divided two wide categories: mechanical stabilization and chemical additives. Overall, both methods can increase strength, reduce hydraulic conductivity, liquid, plastic limits, or control swelling potential of soils (Broderick and Daniel 1990, Bell 1996, Al-Rawas et al. 2005, Venaktarama et al. 2007, Hélène et al. 2002, Ambarish and Chillara 2007, Celestine 2007). However, compared to chemical additives, mechanical stabilization techniques, either using mechanical devices or non-reactive materials, do not need to consider the side effects such as chemical reactions along with native components of the on-site soils. Furthermore, mechanical stabilization is more cost effective and has less time consuming than chemical additive stabilization. Nevertheless, some limiting factors must be considered, including compaction pressure and recurrence of contaminant migration. For instance, when applying a high compaction pressure, the compaction device may crush aggregates that are added or naturally remaining, thereby losing the engineering properties of the soils (US Army Corps of Engineers 1984). Or, without any chemical bonding, contaminants may migrate to other uncontaminated sites once environmental factors such as moisture or pH change.

With regard to chemical additions, several common stabilizers are widely used. These include lime, cement, fly ash, calcium chloride or other stabilizers. After addition, through chemical reactions such as hydrolysis, the moisture content in soils would decrease to effectively reduce plastic limits or increase bearing strength. However, to achieve significant improvements, some limiting factors need to be avoided including

inappropriate stabilizer content/ types, incorrect types of soils, high concentrations of organic matters and inappropriate water content/temperature (Bell 1996, Al-Rawas et al. 2005, Venaktarama et al. 2007, Hélène et al. 2002). For example, with an appropriate amount of lime and optimum moisture and temperature, treated clay soils can be improved significantly, otherwise, the improvement would be restricted or negative effects could take place (Bell 1996). Time also plays an important role. Generally, the length of the curing period is long, taking over 7 or 28 days (Ambarish and Chillara 2007). In terms of sustainability, improved strength of treated soils via addition of woodash may decay after a cured period (Celestine 2007), implying that additive stabilizers do not ensure resistance to weathering.

2.3 BIOMEDIATED METHODS FOR SOIL IMPROVEMENT

Microorganisms, in particular bacteria, can alter the particle size distribution of soils, influence the arrangement of the soil matrix by forming a biofilm on the surface of the particles, or promote crystallization or precipitation within soil matrix. Subsequently, after these activities the soil may behave differently, e.g., there may be a decrease in hydraulic conductivity, or an increase in hydrodynamic dispersion, chemical retardation, or the migration of fine particles (Mitchell et al. 2005). For convenience, the following discussion is separated into two subsections: the effect of biofilm formation on the behavior of soils, and evolution and mechanisms of biocrystallization.

2.3.1 The effect of biofilm formation

Biofilm formation on the surface of particles or soils can sometimes cause a decrease in the hydraulic conductivity, a phenomenon that is referred to as bioclogging. Obviously, biological activities control the efficiency of bioclogging; therefore, transport of nutrients and bacteria, the accumulation and deattachment of biomass onto and off of soil particles, and shear detachment by transport flow play important roles in promoting microbially mediated plugging (Mitchell et al. 2005). For instance, some researchers have demonstrated under limited substrate loading condition, it was difficult for bacteria to accumulate and cement themselves together; thus, the attachment of biofilm onto the soil became weak and resulted in washing out (Vandevivere et al. 1992, Rittmann 1993). In particular, Rittmann (1993) developed a conceptual model based on normalized surface loading to describe the effect of substrate loading on the accumulation of biofilm biomass and the reduction of hydraulic conductivity. Furthermore, with limiting nutrients, a biofilm may be unstable and form mushroom-like shapes, so the detachment rate by any interference such as sloughing or erosion will increase (Picioreanu et al. 2000). In particularly, it is an arising interest that some biofilm induced by specific bacteria (e.g., *Bacillus indica*) can be resistant in extreme environment such as in a wide range of pH (Dennis et al. 1998).

In addition to the effects of hydrological factors, which directly affect nutrient supply and attachment/ detachment of biomass by flow shear stress, the byproducts of biological activities (e.g., gas bubbles) can retard flow transport and, therefore, result in a decrease in hydraulic conductivity; however, these effects do not contribute to compressibility or shear strength (Seki et al. 1998). The distribution of particle sizes in

the soil could also play another key role in bioclogging. For example, within a fine particle matrix, the formation of biofilm could bind cations in the soils and stimulate crystallization due to the strong interaction between the bacteria and particle surfaces (Konhauser and Urrutia 1999), and then those cations or dislike metals can be captured (Gollapudi et al. 1995, Warren et al. 2001). On the other hand, microorganisms may not cause a significant effect on soil properties in a large particle matrix compared to in a fine particle matrix. Nevertheless, the accumulation of biomass or crystals onto the surfaces of the large particle will alter the particle surface properties, although those influences are still underexplored. Hence, the pore sizes of soil can be significantly affected by bioclogging processes, resulting of either the formation of aggregations or biofilms or entrapment of organisms and limitation of nutrient transport. Mitchell et al. (2005) identified the bounded region in which bioclogging can take place (Figure 2) as a function of organism sizes and soil D_{10}. Moreover, they concluded that gravel well-graded (GW), gravel poorly-graded (GP), sand well-graded (SW), sand poorly-graded (SP), silt with less 50% of liquid limit (ML) and organic soils, as defined by soil classification, are applicable to bio-stabilization. As noted above, whatever or not continuous biofilm formation occurs or not depends on the substrate loading (Rittmann 1993).

2.3.2 The evolution and mechanisms of biocrystallization

Crystallization driven by microorganisms is ubiquitous on earth, especially calcification processes. Indeed, Boquet et al. (1973) reported that calcium carbonate precipitation induced by soil bacteria is a common phenomenon. Some microbes induce calcite crystals in the aquatic environment, such as *Pseudomonas* in saline medium

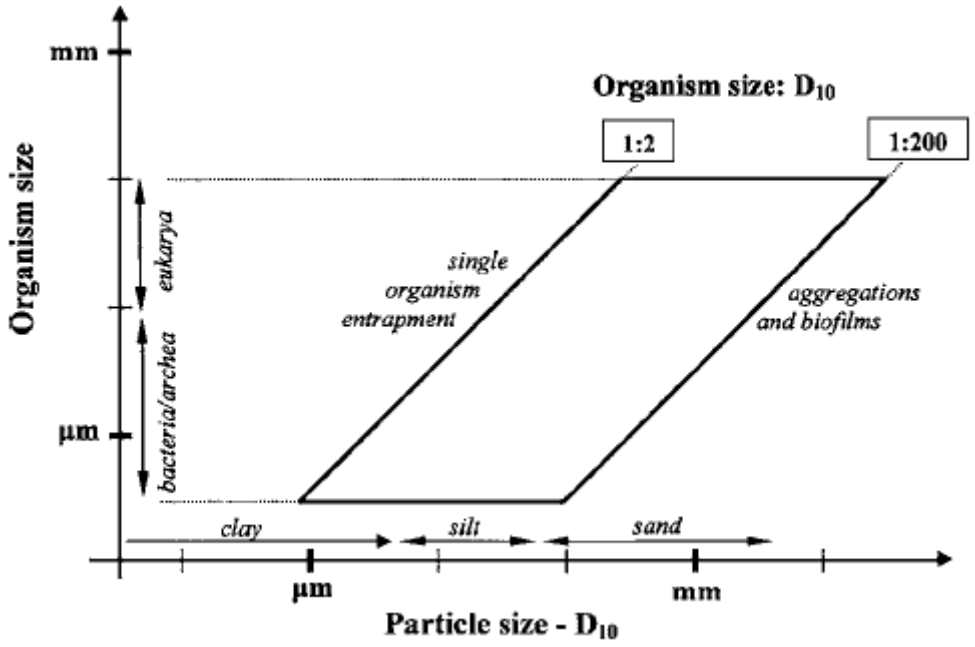

Figure 2.1 The bounded region of soil sizes in which biologically clogging occurs (Mitchell et al., 2005)

(Greenfield 1963), while some bacteria have been discovered to cause the formation of calcite deposits in solid medium (Lian et al. 2006). Phillips et al. (1987) observed lithological aspects of calcareous soils and calcretes from South Australia via scanning electron microscope (SEM) methods and found that the formation and pattern of microcrystals in certain calcified filaments were consistent; however, adjoining filaments were varied. Thus, they suggested that calcification was involved and caused mainly by biochemical mechanisms within cells.

Generally speaking, biologically mediated calcification is generated mainly by an increase in alkalinity through ammonia production resulting from either dissolution of carbon dioxide in autotrophic metabolism or an increase of carbonate in heterotrophic metabolism (Castanier et al. 1999). Among those possible pathways of microbially mediated calcification, heterotrophic metabolic processes are the major focus of this study. There are several different heterotrophic pathways existing in natural environments that may be associated with calcification, such as biodegradation of urea, reduction reactions of nitrate and sulphate or ammonification of amino-acid (see Figure 2.2). All of these processes would increase the pH and swift the bicarbonate and carbonate system so that carbonate precipitation becomes favorable when free calcium is present in the environment (Castanier et al., 1999). Correspondingly, calcite precipitation induced by microbes isolated from soils has been reported in both aerobic and anaerobic environments. Under aerobic conditions, *Bacillus* family has proven to be the most commonly selected group of bacteria from soil environments in previous calcification studies (Ciurli et al., 1996; Bang et al., 2001; Lian et al., 2006). As a given aerobic example, *Myxococcus Xanthus*, an aerobic soil bacterium, has been discovered to have a

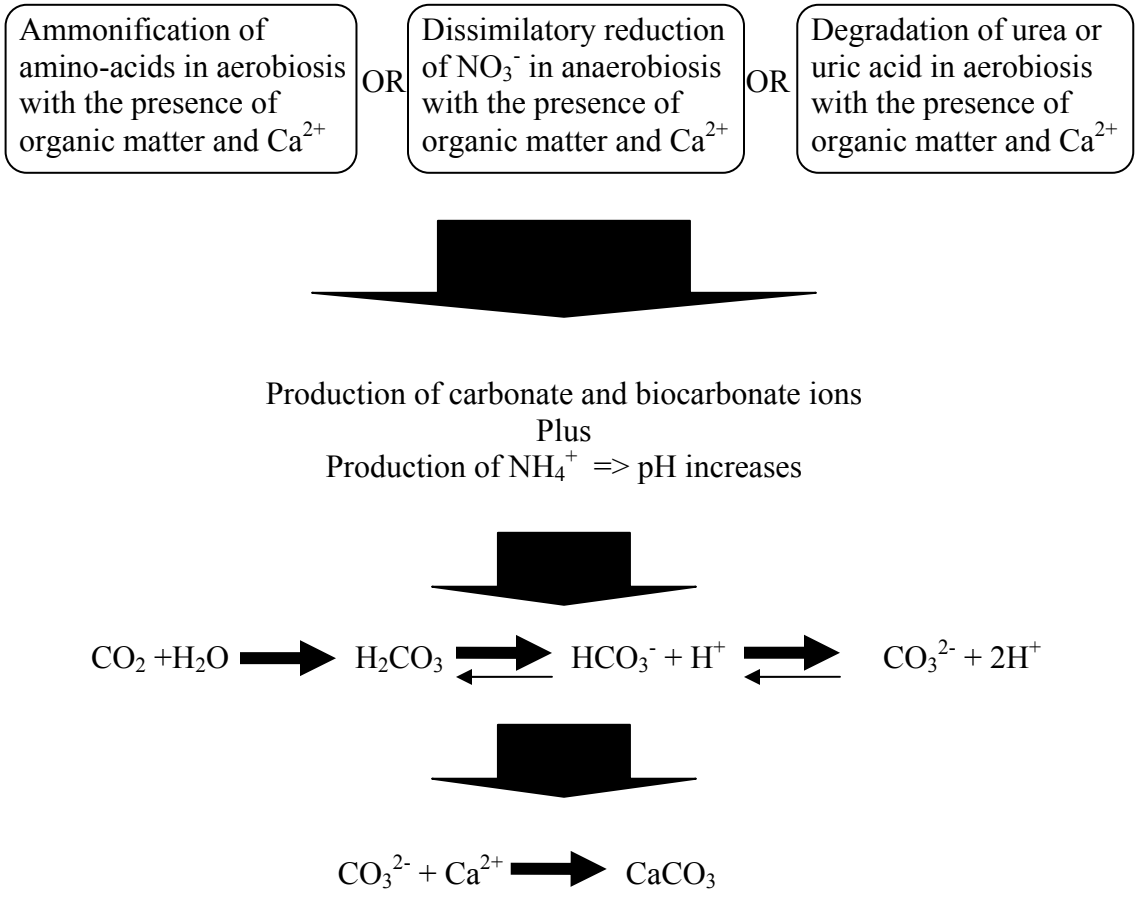

Figure 2.2 The occurrence of calcium carbonate precipitation in nitrogen cycle (Castanier et al. 1999)

strong ability to initiate calcification (Rodriguez-Navarro et al. 2003). Scanning electronic microscopy analysis of *B. pasteurii* (Figure 2.3) and *M. Xanthus* (Figure 2.4), indicate that the formation of calcite is strongly associated with accumulation of the bacterial community (Bang et al. 2001), and that the bio-induced calcite crystals developed epitaxially (Rodriguez-Navarro et al., 2003). Under anaerobic conditions, Hammes et al. (2003) designed bio-catalytic calcification reactors (BCC), coupled with anaerobic sludge, to remove calcium form wastewater. When BCC reactor was in optimal performance, the microbial population of autochthonous bacteria revealed dynamic evolutions, and was dominated by three anaerobic bacteria (e.g., *Porphyromonas* sp., *Arcobacter sp*. and *Bacteroides sp*.). They found that the occurrence of calcite precipitation was in the localized micro-environment (i.e., calcareous sludge) where most precipitating microbes colonized.

2.4 UREA AS A SUBSTRATE FOR BIOCLOGGING

Among those different mechanisms described above (e.g., ammonification, dissimilatory reduction of nitrate, urea hydrolysis), degradation of urea or uric acid is the focus of this study, because urease is ubiquitous and environmental friendly in the environment. Enzymatically, it has been demonstrated that urease has at least two roles: (1) uptake urea as a nitrogen source (Nielsen et al. 1998, Swensen et al. 1998), or (2) utilize urea to generate ATP as an energy source (Mobley and Hausinger 1989).

The degradation of urea and initiation of biocalcification can be summarized by the following reactions (2.1-2.4). The production of ammonium and carbonate and dissolution of carbonate ion are associated with accumulation of urease and meanwhile,

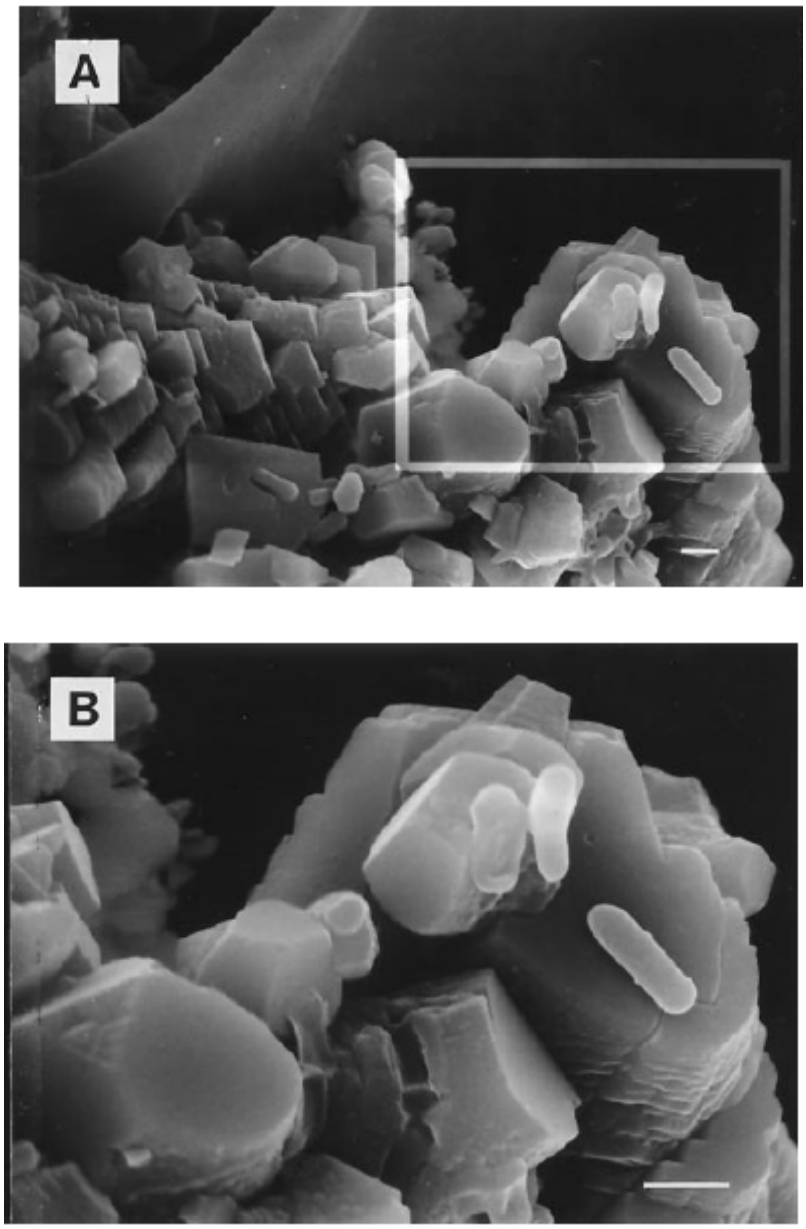

Figure 2.3 The observation of morphology of calcite induced by *B. pasteurii* through scanning electron microscopy studies. (Bang et al. 2001)

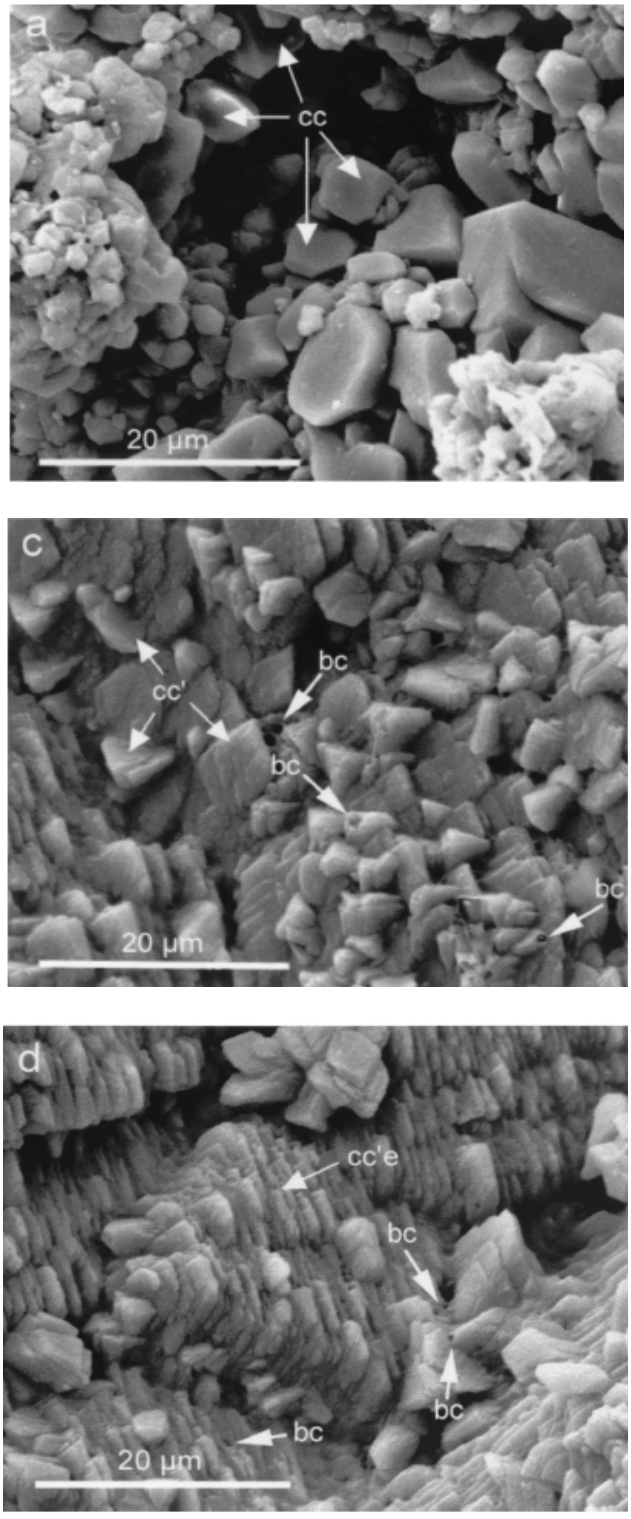

Figure 2.4 The formation of calcite crystals (cc and cc'), bacterial cell (bc), and calcite crystals epitaxially (cc'e) by *Myxococcus Xanthus* were observed from SEM photographs. (Rodriguez-Navarro et al. 2003)

an alkaline environment is generated.

$$NH_2CONH_2 \xrightarrow{Urease} NH_3 + H_2O + CO_2 \text{.....(2.1)}$$

$$NH_3 + H_2O + CO_2 \leftrightarrow NH_4^+ + OH^- + CO_3^{2-} \text{.....(2.2)}$$

If free calcium is available, the conditions are favorable for it to attach on cells due to attractive force between the cations and the negatively charged cell membrane:

$$Ca^{2+} + Cell \rightarrow Cell - Ca^{2+} \text{.....(2.3)}$$

In the presence of carbonate, $CaCO_3$ precipitates thus form on the cells as following:

$$Cell - Ca^{2+} + CO_3^{2-} \rightarrow Cell - CaCO_3 \downarrow \text{.....(2.4)}$$

Urease has been acknowledged to have some properties that are different from normal enzymes (Pettit et al. 1976). For instance, the existence of urease in soil may indicate that it is resistant to proteolysis (Takishima et al. 1988) or gamma irradiation (Skujins et al. 1969, Gurel et al. 1997), possibly due to a high affinity of urease for adsorption onto organic matters or organo-mineral precipitates (Huang et al. 1997). Furthermore, immobilized urease generally is more favorable for sorbing substrates and promoting mineral precipitation based on kinetics studies (Huang et al. 1997, Ciurli et al. 1996).

In trying to understand the performance of biocalcification by urease, it is helpful to model the behavior of urea hydrolysis by urease in soils. Michaelis-Menten kinetics has been used by several researchers (Pettit et al. 1976, Makboul and Ottow 1979) and to satisfactionly describe urease enzymatic activities in soils. These studies have shown that the half saturation coefficient (Km) values were in a range of 6.4 mM to 55.8 mM urea and that the concentration of the calcareous substrate (i.e., the calcium content) has a

certain impact on urease activity. Since urea hydrolysis can switch the ambient pH and promote calcification, it is reasonable to suggest that urea concentrations and pH may effect on urease activities. For example, Cabrera et al. (1991) modeled urease activities in the soils with varied pH via two enzymatic reactions (i.e., high affinity reaction and low affinity reaction) modified from Michaelis-Menten kinetics. These analysis indicated that both K_m either in the high affinity or low affinity reaction were reaching maximum at pH 6.5 (e.g., 18 mM and 31.39 M for low affinity and high affinity reactions, respectively) and dropped to the minimum at pH 9.5 (e.g., 3.92 mM and 3.55 M for low affinity and high affinity reactions, respectively) due to possible substrate inhibition. Moreover, Rachhpal-Singh and Nye (1984) conducted a series of experiments with various urea concentrations up to 10 M and observed that urea hydrolysis rate increased with increasing urea concentration, until reaching a peak hydrolysis rate, hydrolysis rate decreased for higher urea concentrations.

Other than using the Michaelis-Mention equation, some experimental studies (Ferris et al. 2003, Mitchell et al. 2005, Nielsen et al. 1998, Swensen and Bakken 1998) have shown that urea hydrolysis can sometimes be simply described with a first order reaction. First order rate constants in these studies ranged from 0.01 to 1.68 day^{-1}, depending on soil types and temperature.

2.5 APPLICATIONS OF BIOCALCIFICATION

In the last decade, many researchers (Bang et al. 2001, Ramachandran et al. 2001, Dejong et al. 2006, Rodriguez-Navarro et al. 2003) have investigated the feasibility of biomediation of calcification in soils (e.g., sand), geotechnical materials (e.g concrete) or

ornamental stone/building for various purposes. The efficiency of all applications was dependent on environmental factors such as cell number, nutrient and oxygen supply, and the porosity of the particles, consistent with the factors limiting microbial activities, as discussed in the previous section.

For example, in the case of sand or sand mixture, which is of interest in this reasearch, bio-induced calcite can effectively decrease porosity of mediated sand, reduce the permeability by up to 90%, and also contribute to sand consolidation (Stocks-Fischer et al. 1999, Kantzas et al. 1992). In addition, bio-mediated sand may behave similarly to gypsum-cemented soil in terms of response to shear wave velocity in consolidated undrained traxial test (Dejong et al. 2006).

In a test of the biotreatment of the cracks in concrete treated by live cells gained higher compressibility than untreated concrete after a certain period of curing time (e.g., by providing nutrient as an incubation period) due to occurrence of bio-calcification (Rammachandran et al. 2001). Interestingly, concrete treated with dead cells also had improved in compressive strength, which was possibly caused by the the microbial cells acting as organic fibers (Rammachandran et al. 2001). In the case of the biomediation of ornamental stone, Rodriguez-Navarro et al. (2003) reported that the carbonate precipitates induced by *Myxococcus Xanthus* had more resistant strength than the original calcite of the stone. An alternative approach for biomediation of cracks or fractures in concrete or calcareous stone is to apply immobilization technique (i.e., the use of encapsulated cells), which some researchers think can be expected to result a relative high metabolic activity (Klein and Kluge 1981, Wang and Ruchenstein 1993). For instance, Bang et al. (2001) inoculated cells into polyurethane (PU) foam to immobilize

cells as cell-laden PU foam, and placed immobilized cells in the cement mortar cubes (i.e., simulated cracks in concrete). They reported that among a series of experiments with various cell concentrations (i.e., $5x\ 10^7$, $5x\ 10^8$ and $5x\ 10^9$) and incubation periods (i.e., 7 and 28 days), the highest compressive strength improvement was observed in the 7 days of curing period in the presence of $5x\ 10^9$ cells/crack.

2.6 MOTIVATION FOR CURRENT RESEARCH

As described above, the occurrence of biocalcification is ubiquitous and plays an important role in natural systems, including soils, sediments, and minerals (Buczynski and Chafetz 1991, Défarge et al. 1996, Monger et al. 1991). Therefore, it is not surprising that modification of the properties of soil or engineered materials by using microbially-mediated processes like biocalcification may have lower costs than other techniques in a suitable environment (Martin et al. 1996, Cookson 1995). For example, in the geoenvironmental application, such as capping of soft sediments and sludges, biomediation of the soils hydraulic conductivity via biologically induced plugging processes can efficiently affect the infiltration of surface water or storm water (Aydilek and Edil 2002). Biomediation of soil properties, such as reducing the hydraulic conductivity or enhancing the strength of capping materials by microbial plugging processes, can be equally applicable to other geotechnical techniques. Further, compared with synthesis materials for repairing cracks of concrete, such as structural epoxy, resins, epoxy mortar, and other mixture materials that are widely used in the geotechnical field, the use of microbially mediated processes can effectively reduce the length of the curing time and quickly remedy those cracks. Finally, those bio-induced precipitates are

environmental friendly and innocuous.

Among the numerous soil bacteria associated with biocalcification, participation of *Bacillus pasteurii* in calcification have been demonstrated by several scientists (e.g., Ferris et al. 1996, Stocks-Fischer et al. 1999, Bang et al. 2001, Ramachandran et al. 2001, Dejong et al. 2006). Furthermore, the calcite induced by *Bacillus pasteurii* has been shown to result in creation impermeable channels, which modify the properties of soils *in situ* and can be used to control excess water flow or quarantine undesirable substances in a specific zone by limiting migration (Gollapudi U.K. et al., 1995, Warren et al. 2001).

Therefore, *Bacillus pasteurii*, an alkalophilic bacterium that forms endospores and may be able to survive in extreme environments, was selected as the calcification catalytic agent in this study. To evaluate the performance of bio-calcification mediated by *B. pasteurii* within a sand matrix, specially designed experimental system were used (e.g., completely stirring tank reactor (CSTR) and completely mixing biofilm reactor (CMBR). In an attempt to optimize the calcite precipitation via complete-mixing of substrate, while providing a specimen that could be used directly in direct shear tests and California bearing ratio tests, both of which are widely employed in the field. The details of methods, materials, and designs are discussed in the Section 3.

SECTION 3

MATERIALS AND METHODS

As described in Section 2, in which the applications of biomineralization to soil improvement are discussed, capping applications have a high potential for improvement via biological precipitation processes. Because sandy soils are typically chosen as capping materials, sand was therefore used as the sole type of soil in this study. To experimentally investigate the applicability of sandy soil improvement via biomineralization of urea by urease, this research the experiment was divided into three experimental components: (1) a determination of two geomechanical properties, specifically, direct shear strength and bearing capacity, of biologically-treated sand using *Bacillus pasteurii 11859*; (2) an evaluation of the effect of dead and resting cells on the geomechanical characteristics of sand; and (3) a study of the kinetics of *Bacillus pasteurii 11859*. Importantly, determination of the geomechanical properties of the sand with, and without biological treatment required design of special completely stirred tank reactors (CSTRs) and completely mixed biofilm reactors (CMBRs) that could be directly used in geomechanical testing equipment. The materials and methods used to perform these experiments are described in this section.

3.1 EXPERIMENTAL MATERIALS

3.1.1 Sand

The sand used in these experiments was acquired from U.S. Silica Company, West Virginia (product number #1 Q-Rok unground silica). The chemical components of the sand are shown in Table 3.1. Because the investigations conducted in this study examined the change in engineering properties of the sand as a result of biological mediation, sterilization of the sand was required. To prepare the sand, several kilograms of sand were placed in a plastic tray and were washed with acidic solution (0.25 N of HCl) for 12 hours with periodic stirring. Then, the acidic solution was poured out, and a basic solution (0.25 N of NaOH) was added to the sand for another 12 hours with periodic mixing. Subsequently, the sand was extensively rinsed with deionized water until pH 7 was reached. Before use, the sand was autoclaved at 121^{o}C and 21 psi for about 30 minutes.

3.1.2 *Bacillus pasteurii 11859*/Growth/ Stock conditon

As shown by previous studies (Ramachandran et al. 2001, Ferris et al. 2003), the family of *B. pasteurii* has a high potential to contribute to soil improvement via microbially-mediated precipitation process, especially *B. pasteurii 11859*. During bioinduced calcite precipitation, *B. pasteurii* utilizes urea as nitrogen and energy sources (Mobley and Hausinger 1989) to release ammonium as a byproduct, and then the increase of ambient pH significantly changes bicarbonate-carbon species. Therefore in this study, *Bacillus pasteurii 11859* was used in all of the biotic experiments. According to Bang et al. (2001), *B. pasteurii 11859* can degrade urea more effectively if *B. pasteurii 11859*

Table 3.1 Typical chemical components of the sand in the experimental program (U.S. Silica Company, WV)

Components	%
SiO_2	99.7
Fe_2O_3	0.022
Al_2O_3	0.07
TiO_2	0.02
CaO	0.01
MgO	<0.01
Na_2O	<0.01
K_2O	0.01
Others (Loss on ignition)	0.2

stores in BPU medium (ATCC 1832) rather than in Tris-YE medium, because the presence of urea in BPU medium can effectively promote urea hydrolysis. Thus, *B. pasteurii 11859* was preserved in BPU medium as stock cultures while Tris-YE medium was only used as a growth medium and a plate-count medium. The original strain *11859* cells used in these experiments were provided by Professor Sookie S. Bang (South Dakota School of Mines and Technology, Rapid City, SD, USA).

For pilot cultures, a stock *B. pasteurii 11859* culture was maintained by transferring from the original cultures to streak plates with BPU medium (Table 3.2). The plates were incubated at 30℃ for about 2 days, and then preserved in refrigerator. The same procedure was followed to transfer the cultures to fresh BPU plates every month in order to keep a high enzymatic activity. Regarding to the preparation of BPU medium, two 500 mL medium bottles were prepared. One contained trypticase peptone 10 g/L, yeast extract 5 g/L, tricine 4.5 g/L, ammonium sulfate 5g/L, glutamic acid 2g/L, urea 10 g/L, and deionized water 500 mL. Next, the solution was mixed well, adjusted pH to 8.6± 0.1 and did filter-sterilize afterward by using 0.2μm autoclaved filter. Another medium bottle contained a mixture of 15 g agar with 500 mL of deionized water and autoclaved at 121℃ and 21 psi for 15 minutes. While the solution contained agar was cool down to 50℃, both solutions mixed together and poured equally to 100 mm×15 mm (diameter× height) Petri dishes. Once the media of Petri dishes became solid, dishes were stacked up and stored at 4℃. Before using plates, these plates should be warm up in the incubator at 30℃ for 24 hours.

To prepare the inoculation for the geomechanical tests described below, a colony of *B. pasteurii 11859* was aseptically transferred in to 5 mL autoclaved Tris-YE medium

Table 3.2 Stock BPU Medium (ATCC 1832, Ramachandran et al., 1999)

Ingredient (L^{-1})	
Solution A	
Trypticase peptone	10 g
Yeast extract	5 g
Tricine	4.5 g
$(NH_4)_2SO_4$	5 g
Glutamic acid	2 g
Urea	10 g
Deionized water	500 mL
Solution B	
Agar	15 g
Deionized water	500 mL

Table 3.3 Typical Growth Medium (Stocks-Fischer et al., 1999)

Ingredient (L^{-1})	
Tris-HCl	130 mM (pH 9)
$(NH_4)_2SO_4$	10 g
Yeast Extract	20 g
Agar	1.6%

without agar in a 15 mL centrifuge tube, in which the components of Tris-YE medium (Table 3.3) have to be autoclaved separately and added afterward. Note that no growth occurs in Tris-YE medium if autoclaving caused a mixing of ingredients.

The tubes were incubated at 30℃ in the reciprocal shaking water bath with a speed of 110 rpm, and the growth monitored using turbidity at 600 nm as a wavelength in a spectrophotometer (Spectronic 21 from Bausch & Lomb). The cells were harvested when cells reached the late exponential phase, in order to have a high concentration of active cells. Since a large amount of cell suspension was needed in this study, after first incubation, those 5 mL cultures in 15 mL of centrifuge tubes were transferred aseptically to 1 L of Tris-YE medium in order to obtain more cell suspensions. Next, the culture broth was centrifuged at 4500 rpm for 10 minutes, the cell pellets removed and then were washed twice using 0.13 M of pH 9 Tris-HCl buffer. After washing, the cells were resuspended in the buffer depending on which reactors would be conducted. For example, completely stirring tank reactor required 6 L of suspension solution while completely mixing biofilm reactor needed 2 L of suspension volume. To give the desired cell concentration, a correlation curve between optical density at 600 nm of wavelength of spectrophotometer (Spectronic 21 from Bausch & Lomb) and cell number was set up by preparing a cell suspension and recording corresponding absorbence values, and then plate count method using Tris-YE plates was used for determination of cell number. Therefore, for each biotical experiment, initial cell suspension could be controlled in the same concentration. Alternatively, for the preparation of dead cells, 1L cell solution containing 10^8 cells/mL was autoclaved 30 minutes per day in 3 consecutive days. Then, this autoclaved cell suspension was diluted into the volume of 2 L or 6 L to achieve

desired concentrations of 10^3 and 10^7 cells/mL for the current study.

3.1.3 Bio-catalysis medium

As mentioned before, urea plays a very important role in microbial calcite mineralization for *B. pasteurii 11859*. All biotical experiments were carried out with a bio-catalysis medium including nutrient broth 3 g, urea 20 g, NH_4Cl 10 g, $NaHCO_3$ 2.12 g, and $CaCl_2$ 2.8 g per L of solution (Table 3.4). In order to prepare the medium, all components, except $CaCl_2$, were dissolved and mixed together in a 20 L autoclavable bottle for preventing precipitates. The pH of the solution was adjusted to below 6 before autoclaving. To obtain sterilized media, 45 minutes of autoclaving was necessary to 20 L of the solution. Once the solution cooled down to room temperature, $CaCl_2$ was added and mixed well with the solution.

3.2 EXPERIMENTAL DESIGN AND METHODS

3.2.1 Geotechnical index properties of the sand

The particle size distribution of the sand was determined through by sieve analysis, following the procedures outlined in ASTM D421-422 (Figure 3.1). The sand had no fine particles passing the U.S. No. 200 sieve (<0.074 mm) and was classified as pooly-graded sand (SP) according to the Unified Soil Classification System (USCS) and gravel or fine sand according to the American Association of State Highway and Transportation Officials (AASHTO) Classification System. A summary of the physical properties of the sand used in this study are provided in Table 3.5.

Table 3.4 Bio-catalysis medium/ Urea-$CaCl_2$ medium (Stock-Fisher et al., 1999)

Ingredient (L^{-1})	
Nutrient broth (Bacto)	3 g
Urea	20 g
NH_4Cl	10 g
$NaHCO_3$	2.12 g
$CaCl_2$	2.8 g

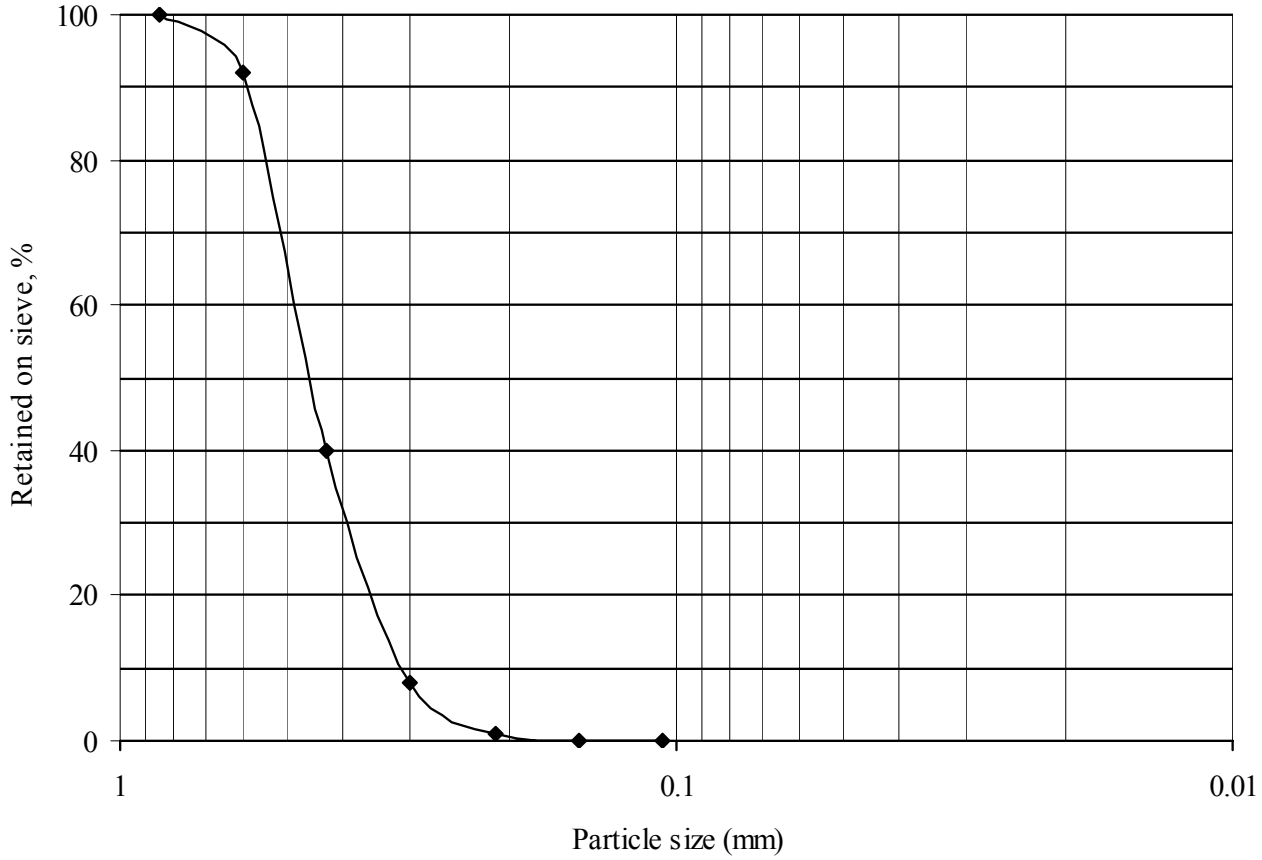

Figure 3.1 Particle size distribution of tested sand

Table 3.5 Typical physical properties of the sand used in the experimental program

Property	Typical Value
USCS classification	Poorly-graded sand (SP)
Specific gravity	2.655
Maximum density, g/cm^3	1.57
Minimum density, g/cm^3	1.37
Maximum void ratio, e_{max}	0.93
Minimum void ratio, e_{min}	0.68
Coefficient of uniformity, C_u	1.67
Mean diameter, D_{50}, mm	0.46
Coefficient of curvature, C_c	1.01
Grain Fineness	34
Grain shape	Subangular
Hardness (Mohs scale)	7
Mineral type	Quartz
pH	6.5

Note: Duplicate tests were used for determination of specific gravity, and the ratio of Gs_{larger} to $Gs_{smaller}$ is less than 1.02 so the result of specific gravity was reasonable according to Bowles (1992). Grain fineness, shape hardness and mineral type are taken from the material data sheets provided by the U.S. Silica Company.

3.2.2 Direct shear tests

The direct shear test was selected as the geomechanical method to determine the shear strength parameters (i.e., friction angle and cohesion coefficient) of the untreated and the biotreated sand specimens. The challenge was to prepare the treated specimen for testing. If the soil was first treated separately via biomediated reaction, it would have to be diseparated to place it in the shear box testing equipment. Therefore, it was decided to place the untreated sand in the shear box apparatus and then place the box with sand under condition to promote the desired microbially-mediated reaction. Considering the fact that the conventional shear boxes are made of metal, which may react with experimental medium and may be toxic to the microbes, or cause chemical reactions with experimental media to interfere with the expected biological reaction, new shear boxes were constructed using polyurethane board (Freeman Manufacturing & Supply Company, Ohio) as shown Figure 3.2. The box dimensions are the same as that of the conventional shear boxes (10 cm× 10 cm). A completely mixing flow was through these boxes designed to provide a completely stirred tank system.

3.2.2.1 Reactor design-Completely stirred tank reactors (CSTRs)

It was necessary to create a controlled environment that could allow the aseptic introduction of the bacteria as growth media into the shear boxes, and induce the uniform calcite formation within the pore spaces of the sand. To facilitate investigation of the effect of biological precipitation between particles of sand under different microbial (e.g., bacterial concentrations) and geotechnical conditions (e.g., the length of reaction time, and compaction), a completely stirred tank reactor (CSTR) was employed to provide an

environment that allowed completely mixing as good distribution of cell and substrate, therefore promote uniform bio-precipitation reactions to take place. The CSTR was created from a 10×18×5 inches of plastic tub (McMaster-Carr Supply Company, Robbinsville, NJ) contained two Masterflex platinum-cured silicone L/S 16 tubings (Cat. EW-96410-16, Cole-parmer Instrument Company) as an influent and an effluent, two peristaltic pump drivers (L/S Easy-load pump, Cole-parmer Instrument Company) to control flow rates, a magnetic bar to create an ideal flow, a mixer to provide a mixing speed, and an air diffuser connected with house air to diffuse air bubbles (Figure 3.3). First, to avoid contamination occurring, it is necessary to have an aseptic environment before any biotic experiments are conducted. All components of the CSTR were required to sterilize by being in 0.1% of HNO_3 of acid bath for 24 hours and autoclaving 15 minutes at 121 ℃ and 21 psi. Then, three shear box specimens were placed aseptically in the sterilized plastic tub covered with aluminum foil. Regarding to the set-up of a feed bottle, a 20 L of urea-$CaCl_2$ was prepared as described before, connected with influent tubing, and covered with aluminum foil to prevent photodegradation of urea. To have the same hydraulic retention time in both CSTR and CMBR systems corresponding with different compaction of sands (e.g., loose and dense), two design flow rates of influent and effluent were employed in CSTR, 8.3 mL/min and 9.5 mL/mL for dense and loose compaction, respectively. Moreover, the volume of CSTR in the plastic tub was designed to 6 L. A magnetic bar was placed in the center of the tub, and the tub was located on a magnetic stirrer for approaching completely mixing conditions. Tracer studies were conducted to establish the suitable mixing speed.

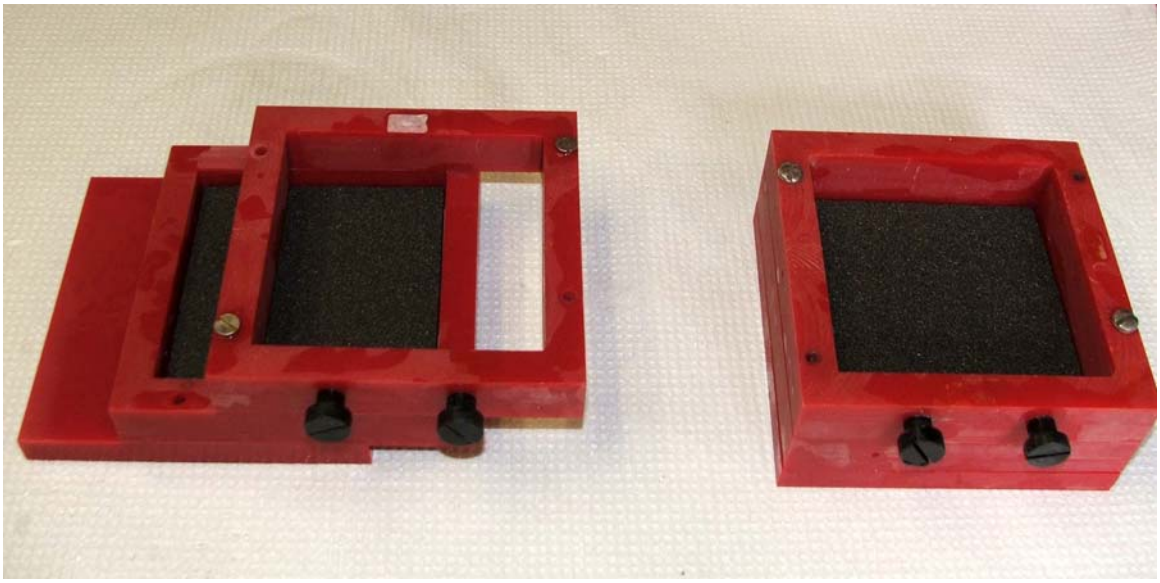

Figure 3.2 Left: the assembly of direct shear box, including upper part of the box, lower part of the box, a riser, and porous plates (in the lower box.); Right: the combination of shear box parts held together with clamping screws. (Note that these boxes were fabricated by Howard Grossenbacher from aerospace engineering machine shop of the University of Maryland, College Park)

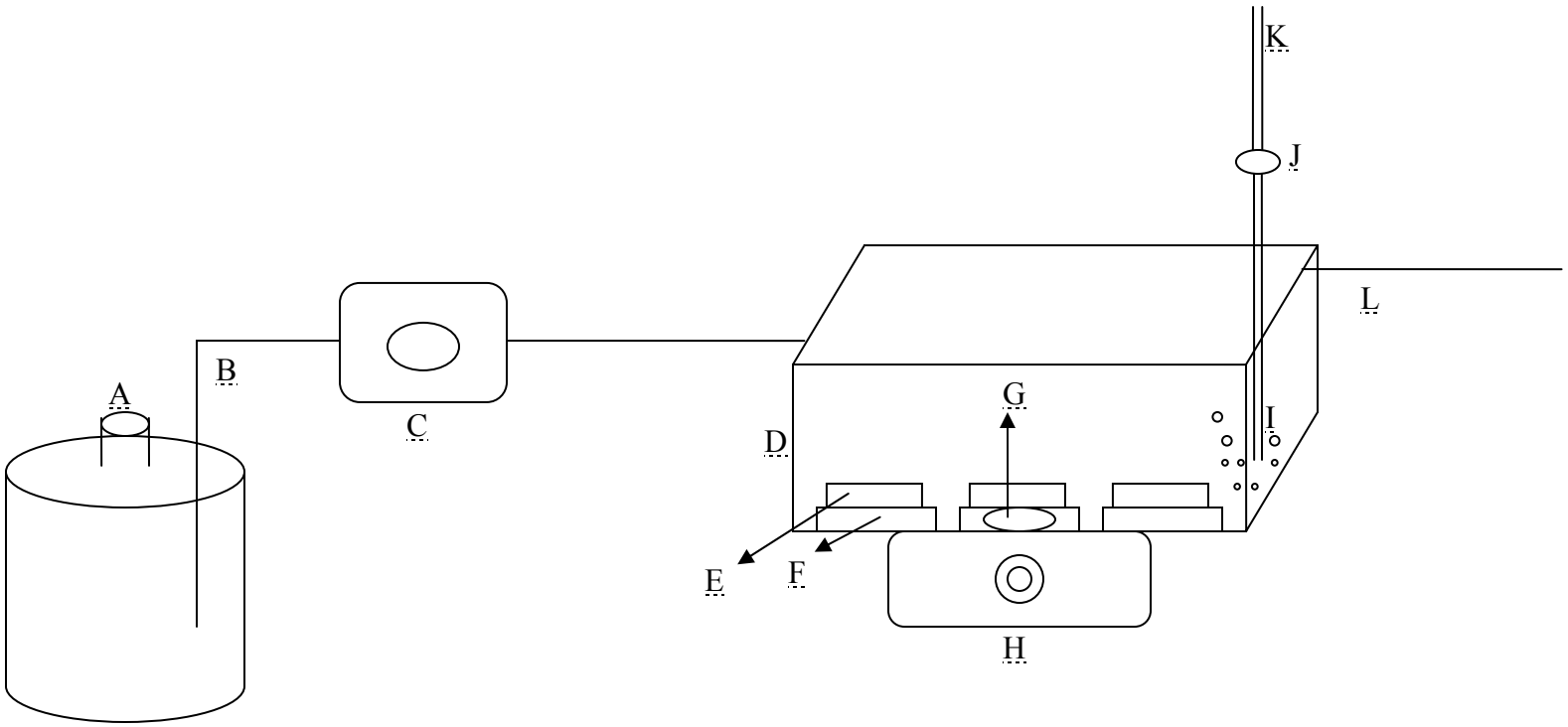

A: Feed bottle
B: Influent tubing
C: Influent pump
D: Plastic tub
E: Direct shear box
F: A riser
G: A magnetic bar
H: A mixer
I: Air supply tubing
J: A filter
K: House air supply
L: Effluent tubing

Figure 3.3 The schematic drawing of the CSTR/ Direct shear boxes system

3.2.2.2. Tracer studies

To verify if the CSTR design actually approached completely-mixed conditions, tracer studies were conducted using a non-reactive treacer (sodium bromide). To initiate the test, the system was first filled with 6 L of deionized water and there were three shear boxes placed inside for simulation of biotic or aseptic experiments. Then flow rate of influent was adjusted to such that the system had a same hydraulic retention time (HRT) of 12 and 10.5 hours with the column system (CMBR) described below. The bromide concentration in the tank effluent was monitored periodically until effluent concentration reached initial bromide concentration (1000 mg/L). The resulting data was modeled with the ideal complete mixing curve to determine if the tank with the selected HRT were a completely mixed system.

3.2.2.3. The preparation of specimens with and without bio-catalysis

All the laboratory devices for the direct shear test were sterilized (including the shear box and clamping screws) prior to performing the biological experiments. Specifically, acid washing and autoclaving were the sterilization procedures employed. First, an acid bath was prepared with 0.1% of HNO_3 and the shear boxes were disassembled and submerged in the acidic solution for 24 hours. Later, the shear boxes were rinsed with deionized water and the shear boxes were carefully reassembled to avoid contamination. Finally, the equipment was sterilized by autoclaving at 121 ^{o}C and 21 psi for 15 minutes.

Once the shear boxes were sterilized, they were packed with the sand to achieve

the desired relative densities by applying gradual compaction on the layers of sand formed. The two relative densities were used for this study 35% and 85%, which were chosen as representative of the loose and dense conditions in the field. For compaction of the loose sand specimen, the sterilized sand was sprayed aseptically into the shear box using a funnel at a height of 0.2 cm above the surface of the previously deposited sand layer. To provide a uniform specimen, the funnel with the sterilized sand was held upright (i.e., vertically) and a constant pouring speed was applied. According to the preparation of dense specimens, vibration or compaction are the most common methods (Oliviera et al. 1996). Moreover, the height of spraying sand would contribute the compaction of the sand due to gravity (Waleed 1995). In this study, dense compaction was therefore accomplished by aseptically spraying sterilized sand into the shear box at above 30 cm the surface of sand. In this fashion the sand was applied in four layers divided in the shear box. After introduction of each layer, 40 blows were applied to the sand surface using a 10 by 10 cm wood compactor with square base. For each experiment, triplicate specimens were prepared in this fashion so as to obtain a friction angle and cohesion stress provided by application of three different normal stresses as discussed further below.

For with biocatalysis experiments, the triplicate specimens were aseptically placed in the plastic tub CSTR along with 6L of bacterial suspension, which was prepared as described above. To ensure the shear boxes were inoculated, 3 L of the inoculums was equally poured through each box. The system was then left undisturbed for 24 hours to allow bacteria to attach onto the sand particles. After 24 hours, urea-$CaCl_2$ medium was fed into the batch system with a hydraulic retention time of 12 or 10.5

hours, for the loose and dense compaction, respectively. During feeding period, mixing was applied and several parameters (i.e., pH, urea, ammonium, calcium, dissolved oxygen and cell numbers) were measured periodically until all parameters approached a steady-state.

For the specimens without bio-catalysis, either dead cells or resting cells were introduced into instead of the live cells. The main difference between dead cells and resting cells was the application of autoclaving. Dead cells were prepared by following the procedure presented in Section 3.1.2 with autoclaving while resting cells were the live bacterial suspension except they were suspended in Tris-HCl buffer without a substrate supply. The specimens with specific loose or dense compaction were placed in 6 L of the dead or resting cell suspension and allowed to sit for 24 hours with completely mixing using a magnetic bar. Subsequently, the shear stress of the specimens was determined using the direct shear device (Figure 3.4).

3.2.2.4. The procedure of shear tests

To rapidly estimate the strength of the micro-biologically remedied sand, a direct/ residual shear apparatus was used (EL26-2114, ELE international, UK). There were three components in the direct shear device: a robustly constructed case, microprocessor controlled drive system, and a computer. Moreover, force, horizontal and vertical displacement parameters were monitored by three linear variable differential transformers (LVDT) during the tests.

Prior to running the shear tests, the three shear boxes were drained by gravity. Three LVDTs were connected to the computer and calibrated. Either untreated or treated

specimen was placed into the shear device, covered with a metal loading hander and attached to the vertical displacement LVDT. Then, the desired normal load such as 10, 20, or 30 kg, was applied by placing desired weights onto the arm of the shear device and the consolidation stage was initiated. Once the change in vertical displacement was leveled off, the consolidation stage was completed and shear stage was applied next. During the preparation of shearing stage, two clamping screws which hold upper and lower boxes together were taken off, and shear box was then separated by screwing the spacing screws in the upper of box to provide a proper space to allow two half boxes to move freely. Note that the space is generally lightly larger than largest soil particles. Next, the other LVDT were then reset to measure shear displacement and horizontal shear force. Finally, shear stage was started with a constant speed (1 mm/min) until testing specimen reached the estimated failure (10 mm). The data from the three LVDTs were recorded by the Ds7 software.

The shear strength was determined by monitoring the change of the shear force versus cross-sectional area of the specimen. The shear strength of a tested specimen reached a peak value, which would be defined as the maximum shear stress. Three tests under three separate normal stresses were performed to determine the cohesion and friction angle of the specimen. The following equation was used to calculate shear strength.

$$\tau' = c' + \sigma' \tan\varphi' \quad \text{..... (3.1)}$$

Where τ' is shear strength, c' is cohesion coefficient, σ' is effective stress, and φ' is in degree of friction angle.

Figure 3.4 Direct shear tests set-up

3.2.3 California bearing ratio tests

The California Bearing Ratio (CBR) procedure, developed by the California Division of Highways in 1929, was chosen as the geomechanical method used to determine the bearing capacity of sand in this study. Generally, CBR tests are useful to estimate the suitability of a soil for road way and foundation design, and an increase in CBR indicates an increase in the overall strength of the soil.

Similar to the direct shear test, the challenge for this study was to modify the CBR equipment to provide an environment within the testing apparatus in which the sand could be biologically stabilized while simultaneously providing an apparatus in which the CBR could be measured directly without remolding. The details of the reactor design and experimental conditions are presented in the following paragraphs.

3.2.3.1. Reactor design-Completely mixed biofilm reactors (CMBRs)

To allow stimulation of the microbial processes within the CBR equipment, the concept of complete mixed biofilm reactors (CMBRs) was introduced and combined with the function of CBR equipment. The components of CMBR system included a column whose size was similar to a conventional CBR device, along with an influent provided at a constant substrate flow, and an effluent that was also recycled through the system to enhance the efficiency of mixing (Figure 3.5). All components of the CMBR system such as tubing, feeding bottles, and CBR column were autoclavable. The 152 mm CBR column was fabricated from 6” PVC, and the top and bottom plates were made of polyurethane board (Figure 3.6).

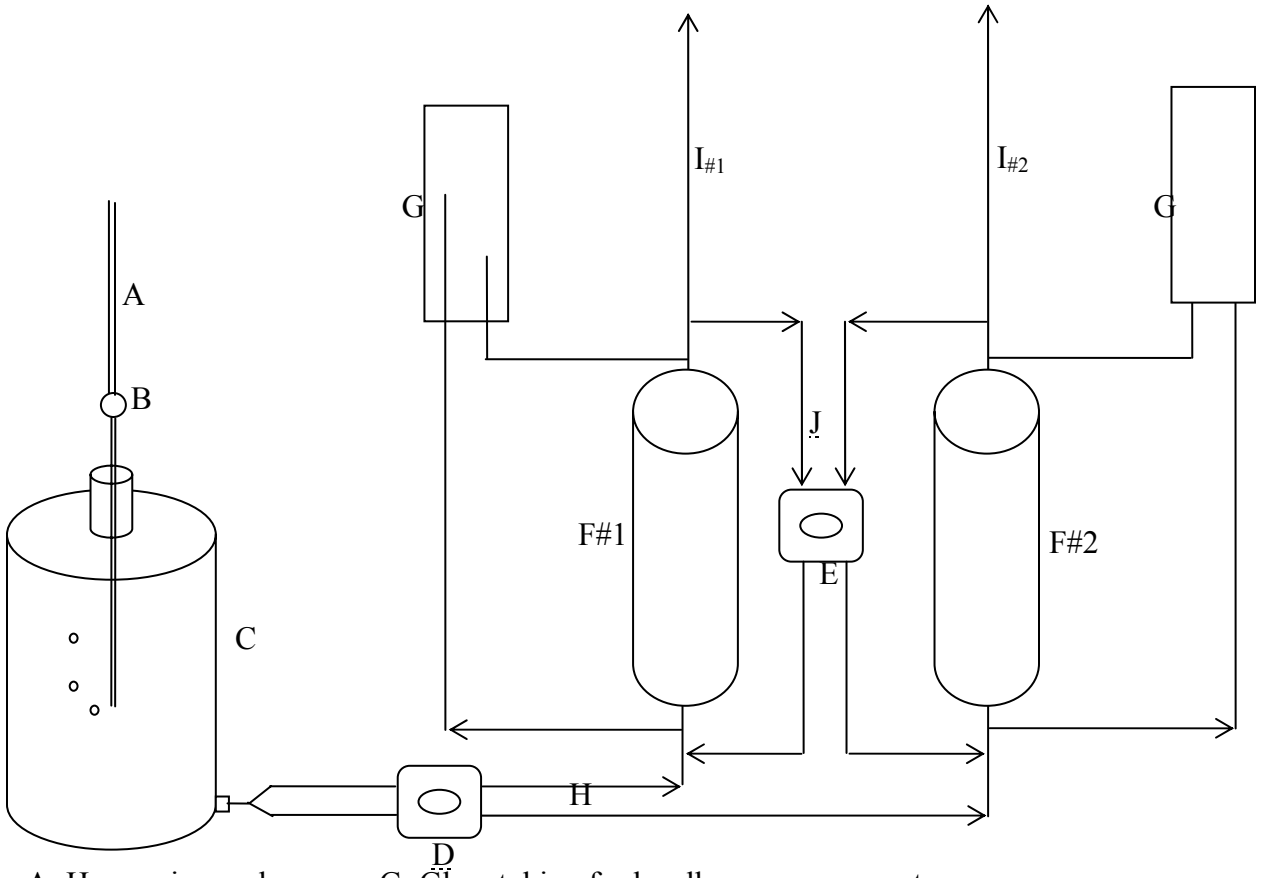

A: House air supply
B: Air filter
C: Feed bottle
D: Influent pump
E: Recycle pumps
F: CBR column
G: Glass tubing for headloss measurement
H: Influent
I: Effluent
J: Recycle flow

Figure 3.5 The schematic drawing of the CMBR/CBR system.

Figure 3.6 The column for California Bearing Ratio tests.

As mentioned above, CBR was modified and combined with the CMBR system. Therefore, some requirements for CMBR system and the procedures of setup were described below. First, three were three main parts in CMBRs: substrate supply, CBR columns, and a series of piezometers setup. Regarding the preparation of substrate supply, a 4 L aspirator with a spigot used for providing urea-$CaCl_2$ medium was connected with an air diffuser. In addition to the connection of air diffuser with the aspirator, a glass tubing was used as well to release excess air pressure from the media. To avoid contamination from house air which was the source of air supply, there was one filter used between the connection of air diffuser and air supply (0.2 μm). The set-up required three connections from the feeding bottle, a recycle flow to provide a well-mixed flow, and a set of piezometers to monitor the change of head pressures of the column. The conjunction of the influent and recycle flow used a peristaltic pump to control the influent flow rate as 1.5± 0.1 ml/min to create a HRT of 12 hours and 10.5 hours for dense and loose compaction conditions, respectively, and another pump was used to maintain the selected recycle flow rate. The optimum recycle flow rate would be determined by tracer tests described below and be followed in biotic CMBR experiment. A series of constant rate-of-flow hydraulic conductivity tests were performed using the CMBR system set-up. Headloss across the column was measured using a series of piezometers attached to the system. The piezometers were made of 12 inches long glass tubing, placed on aboard adjacent to the columns (Figure 3.5)

Once the head loss across the column was determined, Darcy's law (equation 3.2) was used to determine the hydraulic conductivities:

$$K = \frac{QL}{A\Delta H} \quad \text{.....(3.2)}$$

Where K is hydraulic conductivity, Q is flow rate, L is specimen length, A is cross-sectional area of sample, and ΔH is hydraulic head. The flow rate and hydraulic head were monitored periodically during the experiments.

3.2.3.2. Tracer studies

To ensure completely mixed condition in the CMBR system conditions, it is necessary to select an appropriate ratio of the recycle flow (Q_R) to the influent flow rate (Q). Theoretically, a ratio of Q_R to Q should be sufficient to achieve completely mixed condition and the general Q_R/Q ratio ranges from 10 to 70 (Rittman and Manem 1992). To overcome this difficulty in selecting the appropriate recycle rate, tracer studies were conducted in the current study to determine the appropriate recycle flow rate. For example, first, sterilized sand was aseptically packed into the column with desired densities, and was then saturated with deionized water. During the saturation, the influent flow rate (Q) was set to about 1.5 mL/min. Next, a trial recycle flow, 20 ml/min, was set providing a Q_R/Q ratio of 13. A bromide solution with a concentration of 1000 ppm was then injected into the system as a step input. The bromide concentration was then periodically monitored in the effluent samples until steady state flow condition were reached. In subsequent experiment the Q_R/Q ratio was systematically adjusted by repeating above steps until experimental bromide concentration matched to ideal bromide concentration. Therefore, the trial recycle rate would be adopted in the further experimental tests.

3.2.3.3 The preparation of specimens with and without bio-catalysis

All experimental conditions used in the CSTR system were also adopted for the CMBRs, including the variability of bacterial concentrations with loose or dense sand compaction, and dead, resting, and live cell treatments. To simulate loose or dense compaction in the field, columns with loose condition were prepared aseptically by using a funnel to pour sterilized sand into as loosely as possible from above 0.2 cm of the surface of sand while columns with dense condition were achieved by spraying the sterilized sand from the height of 45 cm above the surface of sand and applying 40 blows for each layer using a metal compactor.

For each bio-catalysis experiment, the specimen was first prepared with selected specific density. Next, the column was saturated by pumping in 0.13 M Tris-HCl buffer at flow rate of 1.5 ml/min for 24 hours, after which the column was inoculated by pumping in 2 L 10^7 cells/mL of bacterial suspension. Then, the column was sit stagnant for 12 hours to allow organisms to attach onto sand. After the stagnant period, the urea-$CaCl_2$ medium was fed into the column using the peristaltic pump at an influent flow rate of 1.5± 0.1 ml/min flow rate with a recycle flow rate which was determined from tracer studies. Subsequently, the key parameters (urea, ammonium, calcium, pH, flow rate, hydraulic conductivity, dissolved oxygen, and cell numbers) were monitored until the column was completely plugged, suggested by the high head loss across the column based on piezometer readings.

Specimens without bio-catalysis (i.e., with dead and resting cells) also followed the same preparation procedure as the specimens with bio-catalysis; however, no substrate supply was employed in these experiments to prevent the dead cells or resting

cells from being washed out.

3.2.3.4 The procedure for California bearing ratio tests

After the sand specimens prepared as described above, the CBR tests were carried out immediately using a compression machine (S-5840 Multi-Loader Compression Machine was fabricated by Geotest Instrument Corp) as shown in Figure 3.7. Prior to CBR test, the CBR column was drained for few minutes, and then was placed on the platform of the compression machine. About 2.27 kg of slotted weights was applied on the specimen to simulate 11.7 kPa of field overburden stress that typically exists in geotechnical application. Next, the piston was positioned on the specimen and the reading of loading dial was zeroed as well as LVDT of penetration. The penetration and the loading readings were simultaneously recorded with a constant penetration rate of 0.05 inches/ min. The machine should be stopped while the distance of the penetration reached 6 mm. The CBR number was determined in the percentage by comparing the bearing stress of the specimen with the standard unit stress at the specific penetration such as 2.5 mm, 5.0 mm or 7.5 mm (Table 3.6). Note that if the CBR value at the deeper penetration is greater than the one at the shallow penetration, the greater CBR value should be used.

3.3 MICROBIAL KINETICS

To apply biomediation of soil improvement or stabilization by *B. pasteurii 11859* in the field, microbial kinetics are very useful tools help engineers to predict and

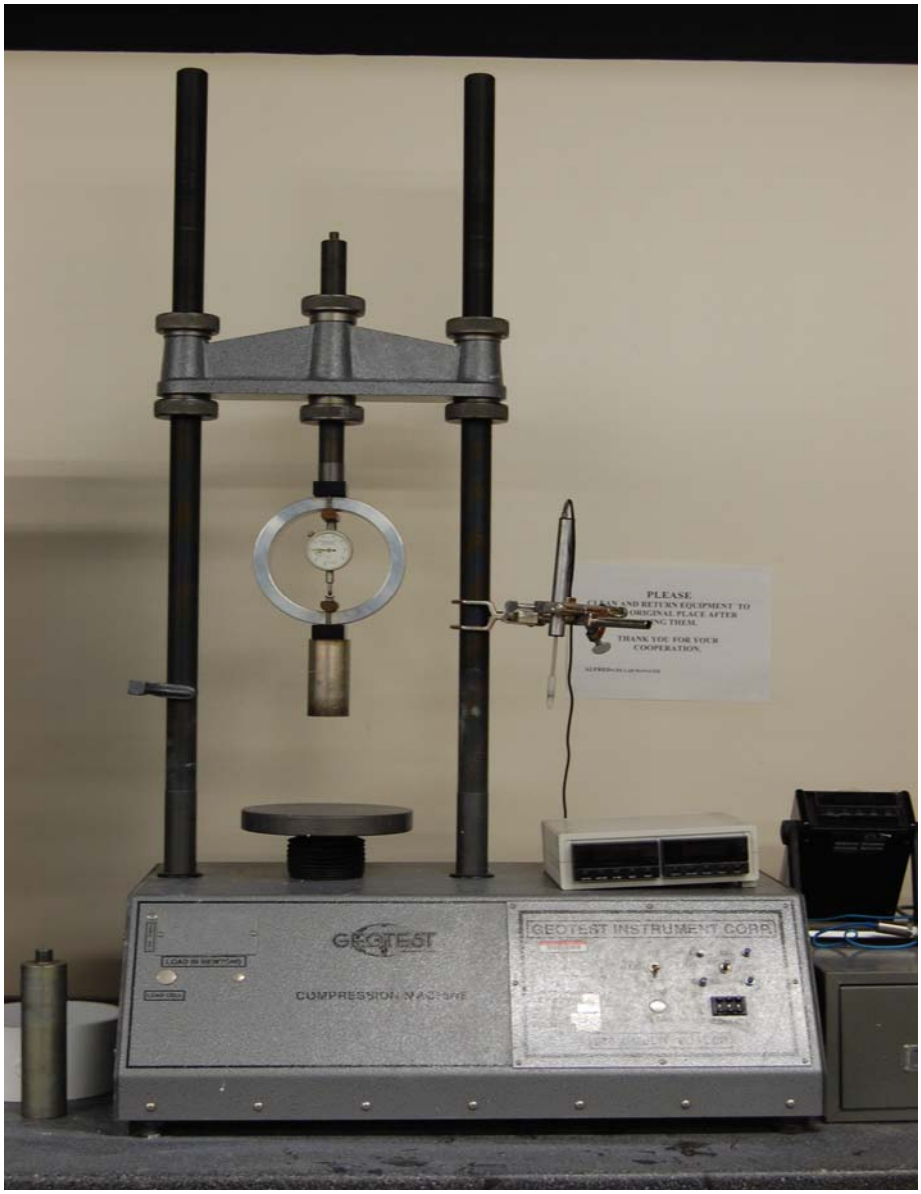

Figure 3.7 California Bearing Ratio (CBR) test set-up.

Table 3.6 The relationship between standard unit stress and penetration (Bowles 1992)

Penetration		Standard unit stress	
mm	in	MPa	psi
2.5	0.1	6.9	1000
5	0.2	10.3	1500
7.5	0.3	13.0	1900
10	0.4	16.0	2300
12.7	0.5	18.0	2600

understand how the microbial system will perform. In particular, the relationship between the microbial catalyst and the primary substrate is the most basic element in a microbial kinetic study. Microbial kinetic parameters including the maximum specific substrate utilization rate (q_{max}), one-half saturation coefficient (K), maximum specific growth rate (μ_{max}), true yield for cell synthesis (Y), and endogenous decay coefficient (b) can be estimate using with batch growth system or continuous flow chemostats. The latter approach was chosen in this study and the resulting kinetics parameters were used to evaluate the CSTR and CMBR reactors used in this research.

3.3.1 CSTR kinetics

The microbial parameters for *B. pasteurii* obtained from chemostat studied were used to model the experimental data for the primary substrate (i.e., urea) when the CSTR used in the desired shear box experiments was at steady state. Note that the parameters were calculated based on the steady-state urea condition and were assumed to represent the kinetic for growth on urea. However, the urea-$CaCl_2$ medium also included nutrient broth, which also support of cell growth.

As mentioned above, microbes and primary substrate play key roles in microbially enzymatic activities. Therefore, the concept of writing mass balance on the biomass in the chemostat results in the following equation:

$$V\frac{dX}{dt} = Q_{in}X_{in} - Q_{out}X_{out} + V\mu X \quad \text{.....(3.3)}$$

where V is the volume of the reactor, X is the biomass concentration in the reactor, t is time, Q_{in} is influent flow rate, X_{in} is the biomass in the influent, Q_{out} is effluent flow rate,

and, X_{out} is the biomass in the effluent and concentration of flow, and μ is the specific growth rate. Assuming completely mixing in chemostat, $X_{out} = X$, $Q_{in}=Q_{out}=Q$ and volume of the reactor is a constant. If, in addition, it is assumed that $X_{in} = 0$, then equation 3.3 can rewrite.

$$\frac{dX}{dt} = -\frac{Q}{V}X + \mu X = (\mu - D)X \quad \text{.....(3.4)}$$

where D is defined as the dilution rate (Q/V).

Similarly, writing the mass balance on the primary substrate in the chemostat produces the following equation:

$$V\frac{dS}{dt} = Q_{in}S_{in} - Q_{out}S_{out} - VqX \quad \text{.....(3.5)}$$

where S_{in} is substrate concentration in the influent, S_{out} is the substrate concentration in the effluent, and q is the specific substrate utilization rate (μ/Y). Applying the same assumptions that were used to create equation 3.4, equation 3.5 can be rewritten as,

$$\frac{dS}{dt} = \frac{Q}{V}(S_{in} - S_{out}) - (\frac{\mu}{Y}X) = D(S_{in} - S_{out}) - (\frac{\mu}{Y}X) \quad \text{.....(3.6)}$$

Assuming that all of the components in the chemostat are at steady state then dX/dt = 0 and dS/dt= 0. For this condition, the steady state biomass, $X^{'}$, and substrate, $S^{'}$, concentration in the chemostat can be calculated by solving equations 3.4 and 3.6.

$$S' = \frac{K(D+b)}{\mu - (D+b)} \quad \text{.....(3.7)}$$

$$X' = \frac{D(S_{in} - S')Y}{\mu} \quad \text{.....(3.8)}$$

By inventing equation 3.7, the following equation can be developed:

$$\frac{1}{D+b} = \frac{1}{\mu} + \frac{K}{\mu}\frac{1}{S'} \quad \text{.....(3.9)}$$

If b can be ignored by assuming b<< D, the equation 3.9 becomes a linear equation that is used to create a data plot known as the Lineweaver-Burke plot in which 1/S' is plotted as a function of 1/D. By plotting the data from a series of experiments with different dilution rates in the form of the Lineweaver-Burke plot, the microbial parameters μ and K can be determined from the y-intercept (μ) and slope (K).

To determine the other two required microbial parameters, Y and b, it is necessary to set up another equation as a function of Y and b via combining equations of 3.7 and 3.8:

$$D = Y\frac{D(S_{in} - S')}{X'} - b = YU - b \quad \text{.....(3.10)}$$

where U is $D(S_{in}-S')/X'$.

By plotting D versus U, Y and b can then be determined from the slope of the equation 3.10 and the y-intercept, respectively.

To study the microbial kinetics of *B. pasteurii 11859* in this research, a series of chemostat experiments were performed at several different hydraulic retention times as follows: 2, 4, 6, 8, 12 and 16 hours. The set-up of the chemostat as ysed in these experiments is shown in Figure 3.8. This reactor used a 1 L flask as a reactor, two peristaltic pumps to control the influent and effluent flow rate as a constant, a magnetic mixing device, and a house air supply. Before use, all parts of the chemostat were sterilized by autoclaving, including the tubing, air filter, and the flask containing a magnetic stir bar and covered by a cotton ball. To initiate the experiment, 500 mL cell suspension containing 10^4 cells/mL in 0.13 M of Tris buffer was prepared in the sterilized

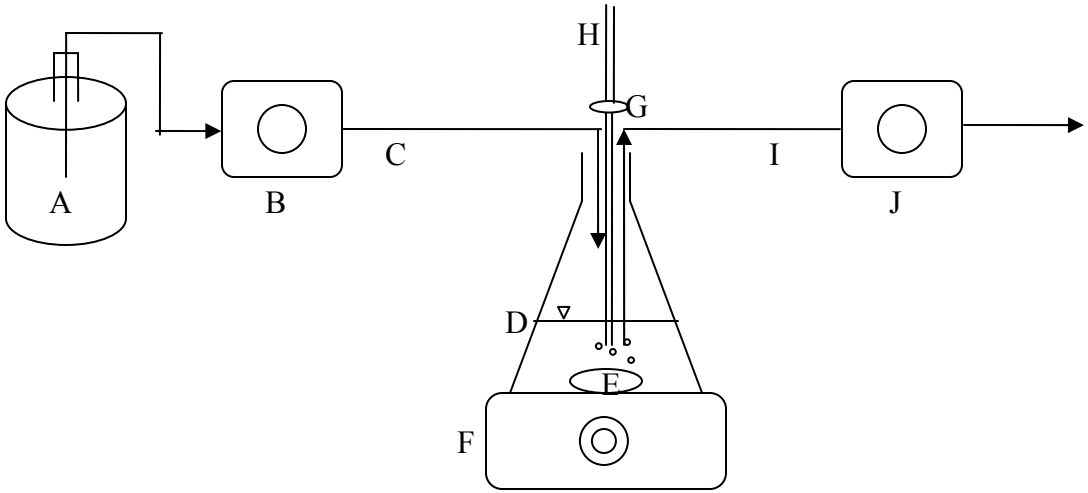

A: Feed bottle
B: Influent pump
C: Influent
D: Reactor (1L flask)
E: Magnetic stir bar
F: Mixer
G: Air filter
H: House air supply
I: Effluent
J: Effluent pump

Figure 3.8 The schematic drawing of the Chemostat system used for the kinetic determination

reactor. Then, 4 L of the urea-$CaCl_2$ medium aseptically was prepared and flow started at time 0 of the incubation. After 2 HRTs, the cell numbers, urea, pH and DO were monitored until all parameters reached steady-state concentrations. Subsequently, the steady-state data were used within equations 3.9 and 3.10 to estimate the culture's kinetic parameters for growth on urea.

3.3.2 CMBR kinetics

To evaluate a CMBR's performance at steady state, a convenient tool is to compare the normalized surface loading of the experimental CMBR system with that of an ideal CMBR system. The concept of normalized surface loading was developed by Rittmann and co-workers (e.q., Rittmann 1982a, Rittmann 1982b, Rittmann and McCarty 1980a, Sáez and Rittmann 1988, 1992, Rittmann 1993) to model how materials (e.g., nutrient, substrate, or dissolved oxygen) are transported through a biofilm. Application of the normalized surface loading approach requires knowledge of the steady-state flux into the biofilm (J_{ss}), as well as several other parameter describing key characteristics of the biofilm (e.g., aqueous diffusion coefficient (D), thickness of biofilm (L_f) and effective diffusion layer (L), and active biomass density (X_f)). The relationship plotted in a normalized surface loading curve is based on the normalized substrate flux (J_{ss}/J_R) as a function of normalized steady-state substrate concentration (S/S_{min}) in which S is the steady-state substrate concentration in the effluent of a completely mixed control volume, S_{min} is the minimum substrate concentration to support steady-state cell synthesis, J_R is the minimum substrate flux to form steady-state deep biofilm, and J_{ss} is actual substrate flux into the biofilm.

S_{min}, J_{ss} and J_R can be determined by pseudo-analytical method from Sáez and

Rittmann (1992), and Rittmann and McCarty, (2001) as follows.

$$S_{\min} = K\frac{b + b_{\det}}{\mu - b_{\det}} \quad \text{.....(3.11)}$$

$$J_{ss} = J_{ss}^{*}[KqX_f D_f]^{1/2} = \frac{Q(S_0 - S)}{aV} \text{.....(3.12)}$$

$$J_R = J_R^{*}\left[KqX_f D_f\right]^{1/2} \text{.....(3.13)}$$

where b_{det} is the specific biofilm detachment coefficient, Q is flow rate, a is the surface specific surface are of the particles, V is the volume of the reactor, S_0 is the initial substrate concentration, J_{ss}^{*} is the dimensionless reference flux for a deep biofilm, J_R^{*} are the reference flux and the dimensionless reference flux, respectively, when the biofilm is not deep, and D_f the diffusion coefficient in the biofilm is proportional to the aqueous diffusion coefficient (e.g., generally, $D_f = 0.8$ D). To compute S_{min}, b_{det} must be determined as assuming the other parameters are known. Rittmann (1982a, b) showed that b_{det} was related to the thickness of the biofilm (L_f) and shear stress (σ), and developed the following simple equations (3.14-3.15) to determine b_{det}:

For $L_f < 0.003$ cm,

$$b_{\det} = 8.42 * 10^{-2}\sigma^{0.58} \text{.....(3.14)}$$

For $L_f > 0.003$ cm,

$$b_{\det} = 8.42 * 10^{-2}\left(\frac{\sigma}{1 + 433.2(L_f - 0.003)}\right)^{0.58} \text{.....(3.15)}$$

in which shear stress can be calculated by,

$$\sigma = \frac{200\mu u(1-\varepsilon)^2}{d_p^2\varepsilon^3 a(7.46 * 10^9)} \text{.....(3.16)}$$

where μ is absolute viscosity, u is superficial liquid velocity, ε is porosity of the particles in the CMBR, d_p is the diameter of the solid particles, and a is the specific surface area of the particles. L_f can be calculated by assuming for a biofilm at steady state, the growth rate of new biomass per unit area is equal to the loss rate of biomass per unit area. Therefore, the following equation can be developed by assuming $b >> b_{det}$:

$$L_f = \frac{J_{ss} Y}{X_f b} \quad \text{.....(3.17)}$$

Once L_f is quantified, we can decide whether to use equation 3.14 or 3.15 to obtain b_{det}. Then, to evaluate if the assumption of $b >> b_{det}$ is correct, we have to compare b and b_{det}. If the assumption is wrong (e.g., $b < b_{det}$), it means the other equation should be used and it is necessary to recalculate L_f by equation 3.17 using $b+b_{det}$ instead of b.

However, without knowing J_{ss}, L_f can not be obtained. To quantify J_{ss} , equation 3.12 can be used. To quantify J_{ss} from equation 3.12, J_{ss}^* should be defined first as follows:

$$J_{ss}^* = K^*(S^* - S_s^*) \quad \text{.....(3.18)}$$

where K^* is the ratio of the external mass transport to the maximum substrate utilization rate, S^* is normalized substrate concentration, and S_s^* at substrate concentration at the boundary of biofilm and the liquid phase under the experimental conditions. K^* can be determined from,

$$K^* = \frac{D}{L}\left[\frac{K}{qX_f D_f}\right]^{1/2} \quad \text{.....(3.19)}$$

in which the diffusion coefficient in water (D), diffusion coefficient in biofilm (D_f), and thickness of the effective diffusion layer (L) are biofilm characteristics that can be

estimated by the fluid properties (equation 3.20~3.24). For example, D can be estimated using the Wilke-Chang equation,

$$D = 1.279(V_b)^{-0.6} \quad \text{.....(3.20)}$$

in which V_b is the molar volume of the compound (e.g., primary substrate) at its boiling point, which can be obtained from a chemistry reference book. According to Williamon and McCarty (1976) a typical D_f is estimated by,

$$D_f = 0.8D \quad \text{.....(3.21)}$$

Finally, Jennings (1975) illustrated that L can be quantified by using the Reynolds number, Schmidt number, and other fluid properties:

$$L = \frac{D(\mathrm{Re}_m)^{0.75} Sc^{0.67}}{5.7u} \quad \text{.....(3.22)}$$

where u is the superficial liquid velocity, and Re_m and Sc are calculated by,

$$\mathrm{Re} = \frac{\rho u d_p}{\mu} \quad \text{.....(3.23)}$$

$$Sc = \frac{\mu}{\rho D} \quad \text{.....(3.24)}$$

After estimating K^* using equation 3.19 to 3.20, S^* is easily computed as follows:

$$S^* = S / K \quad \text{.....(3.25)}$$

Furthermore, S_s^* is estimated by doing trial and error solution on S_s^* until both sides of the equation below are equal:

$$S_s^* = S^* - \frac{\left(\tanh\left[\alpha\left(\frac{S_s^*}{S_{\min}^*} - 1\right)^{\beta}\right]\right)\left(2\left[S_s^* - \ln(1+S_s^*)\right]\right)^{1/2}}{K^*} \quad \text{.....(3.26)}$$

where S_{min}^* is the normalized S_{min}, and α and β are the coefficients as a function of S_{min}^*:

$$S^*_{\min} = S_{\min} / K \quad \text{……..……(3.27)}$$

$$\alpha = 1.5557 - 0.4117 \tanh[\log S^*_{\min}] \text{……..(3.28)}$$

$$\beta = 0.5035 - 0.0257 \tanh[\log S^*_{\min}] \text{……..(3.29)}$$

Using equations 3.19 to 3.29, K^*, S^* and S_s^* can be estimated and J_{ss}^* can be solved for by equation 3.18. Then, from equation 3.12, J_{ss} can be obtained in order to determine appropriate the range of L_f and calculate b_{det} . Finally, S_{min} can be defined through equation 3.11.

As discussed above, the ratios of S/S_{min} and J_{ss}/J_R are required in order to develop the ideal normalized surface loading curve for modeling the performance of a CMBR. Up to this point, relationships for S_{min} and J_{ss} have been determined, leaving J_R as the only unknown factor. Using equation 3.13, J_R can be computed as long as J_R^* is known. To determine J_R^*, it is necessary to define the substrate concentration, S_R^* at the boundary of biofilm and the liquid phase when the biofilm is deep:

$$J_R^* = \sqrt{2(S_R^* - \ln(1 + S_R^*))} \quad \text{…….(3.30)}$$

To compute S_R^*, a reduced safety ratio (f) multiplied by the actual flux is used. Generally f is equal to set a 0.99 for reference flux:

$$f = 0.99 = \tanh\left[\alpha\left(\frac{S_R^*}{S_{\min}^*} - 1\right)^{\beta}\right] \text{……..(3.31)}$$

where S_{min}^*,α and β can be found through equations 3.27 to 3.29.

Through the analyses above, the experimental S/S_{min} versus J_{ss}/J_R in steady-state CMBR could be determined and compared to the theoretical, ideal normalized loading curve. For this work, the ideal normalized loading curve was taken from the reference book, Rittmann and McCarty (2001).

3.3.3 Determination of Biofilm characteristics

As discussed above, the biofilm characteristics are critical parameters for simulating the performance of a CMBR. In particular, the density of biomass (X_f) and thickness of the biofilm (L_f) are strongly related to the behavior of mechanical stress in a biofilm (Laspidou et al. 2005). Therefore, to accurately evaluate the pattern of bacteria and substrate interactions and the mechanical behavior of the biofilm accumulation within sand matrix, X_f and L_f were determined in duplicate by using following procedures adopted from Seagren (1994), Rittmann et al. (1986), Raskin (1993).

First, samples of the sand porous media were aseptically removed from the CMBR which was deformed after CBR measurement (i.e., one from the top of the column, and another from the bottom of the column) and stored in sterilized jars at 4℃ until they were analyzed. Then, two subsamples of sand removed and placed in two clear aluminum weighing planchets and weighed to obtain the "wet" weight. Then, those planchets with the wet samples were dried at the 105℃ for 24 hours which was assumed to be sufficient time for the samples to dry to a stable weight. Subsequently, the samples plus planchets were cooled in a desiccator, and weighed to obtain the "dry" weight. Finally, those dry samples were put into the muffle furnace with a temperature 550℃ for 1 hour, cooled in the desiccator, and the weight recorded as "ignited" weight. These data were then used for the determination of L_f and X_f. The biofilm thickness, L_f, was calculated using the following equations:

$$L_f = \frac{W}{\rho n A(0.99)} \quad \text{.....(3.32)}$$

where W is the difference between dry and wet sample masses, ρ is the water density at 20℃, 998.2 kg/m^3, n is the number of dry sand particles, A is the surface area of a sand

particle, and 0.99 is the fraction number assuming that 99% of the biofilm was water. In this study, n was impossible to determine directly. Therefore, it was estimated by dividing the dry weight of the sand by the mass per sand particle. The mass of a single sand particle was in turn estimated by multiplying the specific gravity of sand the volume of a sand particle assuming that the particle is a sphere with the average diameter of a sand particle (D_{50}). Similarly, the volume of A was also calculated by assuming a spherical sand particle with diameter, D_{50}. Finally, the biofilm densitywas calculated as follows (Seagren 1994, Raskin 1993):

$$X_f = \frac{B}{nAL_f} \quad \text{.....(3.33)}$$

where B is the difference between dry and ignited sample weights.

3.4 ANALYTICAL METHODS

3.4.1 Bromide

Bromide was measured by using a bromide combination electrode (Orion 94-35, Thermo Electron Corporation, Beverly, MA) connected with a ion meter (Orion Model 520A. Thermo Electron Corporation, Beverly, MA). For each use, the slope of electrode was first checked by measuring the difference between the probe readings for 10 mL of 10 ppm and 100 ppm bromide standard solution, which was prepared by sodium bromide, with 0.2 mL reagent of 5 M $NaNO_3$. If a value of 57 ±3 was obtained according to manufacture manual, the electrode was ready to be used. Following the same procedure as for the slope check, the calibration curve was performed by preparing 10 mL of different bromide standard solutions ranging from 1 ppm to 1000 ppm, each with 0.2 mL

of reagent solution added. The values of the meter reading were recorded in units of mV, and plotted versus corresponding bromide concentrations. A curve that fits the data was obtained by regression analysis. Because the bromide standard concentration was set between 1 ppm to 1000 ppm as a calibration curve, detection limitation in this method was 1 ppm.

3.4.2 Ammonium

Ammonium content in aqueous solutions was determined using an ammonium combination electrode (Cat. 27502-03, Cole-parmer Instrument Company) connected to a ion meter (Orion Model 720A.Thermo Electron Corporation, Beverly, MA). Similarly as above, the slope check for the ammonium electrode probe was performed by measuring the differences between probe readings for 10 mL of 10 ppm and 100 ppm standard solutions, and each solution was added 0.2 mL of 5 M of NaCl reagent. Once the difference in mV was confirmed to be in the range of 56± 2 mV according to manufacture manual, the electrode was ready to be used. Then, a series of ammonium standard solutions ranging from 1 ppm to 1000 ppm were prepared and analyzed all with 0.2 mL of 5 M NaCl added. The calibration curve was set up by which the meter readings were recorded in units of mV, and plotted in a log scale versus corresponding to standard solutions. Detection limitation was 1 ppm NH_4^+ based on the border of calibration curve.

3.4.3 Urea

A colorimetric method described by Jung et al. (1975) was employed in this study

to determine urea in aqueous solution. Three reagents were required, o-phthalaldehyde, naphthylethylenediamine, and BRIJ 35 (Ricca Chemical products). While the BRIJ 35 was used as is, preparation was required for the other two reagents. O-phthalaldehyde reagent was prepared by mixing 74 mL of concentrated H_2SO_4 with 800 mL of deionized water, allowing the solution to cool down, and then adding 200 mg of o-phthalaldehyde (Sigma Chemical Co. products) with 1 mL of BRIJ 35. The naphthylethylenediamine reagent (NED) was obtained by dissolving 5 g of boric acid in 600 mL of deionized water and then adding 222 mL of concentrated H_2SO_4. After mixing well and cooling down to room temperature, 600 mg of n-(1-naphthyl)ethylenediamine dihydrochloride (Eastman Organic Chemicals products) and 1 mL of BRIJ 35 were added to the solution , which was then diluted to 1 L. Both the o-phthalaldehyde and NED reagents are stable and can be stored in a brown bottle for at least three years.

Once all the reagents were prepared, the urea content in a sample solution was measured using the following procedure. First, several 10 mL test tubes that were able to fit into the spectrophotometer (Spectronic 21 from Bausch & Lomb) were prepared. Then reagent solutions were added to each tube the following the sequence: first 2.5 mL of o-phthalaldehyde reagent, followed by 50 μL of sample, and then 2.5 mL of NED reagent. Subsequently, the mixture was vortexed and incubated at 37℃ for 30 minutes to allow for the color development. A blank tube was prepared by adding 2.5 mL of BRIJ 35 instead of 50 μL of sample, and used to zero the spectrophotometer. Additionally, a regent blank was prepared by adding 50 μL of deionized water. Then, the optical densities of each tube were recorded at a wavelength of 505 nm. A calibration curve of urea concentrations versus absorbance values, which was calculated by deducting from

the absorbance of the regent blank, could be set up following the same procedures. Detection limitation was 0.2 g/L depended on the limitation of calibration curve.

3.4.4 Calcium

Calcium concentrations in water sample were measured using the EDTA titration method (APHA 3500-Ca). First, a A 0.01 M EDTA solution was prepared and placed in a 50 mL burette. Then, 50 mL of sample were diluted to appropriate concentrations (e.g between 5 to 10 mg per 50 mL sample) below limit of detection. Subsequently, 2 mL of 1M NaOH and few drops of the indicator, Murexide, were added to the solutions until a pink color was observed. Finally, the sample was titrated with the EDTA solution until color of the solution changed from pink to purple, and the volume of EDTA titrant used was recorded. The calcium concentration was calculated by the following equation:

$$mg \quad Ca/L = \frac{A * B * 400.8}{mL \ sample} \text{.....(3.34)}$$

where A is the volume of 0.01 M EDTA titrant, and B is mg $CaCO_3$ equivalent to 1 mL titrant at the end point of titration.

3.4.5 Content of calcium carbonate onto the soils

As part of the evaluation of the nature of the bio-induced precipitates attached onto the soil particles and modified soil properites.,the calcium carbonate content was measured by the following steps. First, subsamples of the porous media samples taken from the CMBR (see section 3.3.3) were taken and placed in duplicate in the aluminum planchets, dried at 105℃ for 24 hours, cooled in the desiccator, and weighed. The

difference between dry sample mass and that of empty aluminum planchet was taken as the mass of dry sand. Those dry sand samples were placed in 250 mL flasks and rinsed with up to 100 mL of 0.1 N H_2SO_4 acid solution to allow the precipitates to dissolve into the liquid phase from the surface of the sand particles. The flasks plus sand and acid solution were shook by hands for 10 minutes, and then filtered through 0.45μm filter paper. Subsequently, the content of calcium in the liquid sample was determined by using EDTA titration method as described in Section 3.4.4. The calcium in the liquid was assumed to represent the content of calcium in the solid and was converted to the percentage of mass as $CaCO_3$.

3.4.6 Dissolved oxygen

Dissolved oxygen was determined directly by using a dissolved oxygen probe connected to a meter (model Section 6, Hach, Loveland, CO). Before starting the measurements, the dissolved oxygen probe was calibrated using air-saturated water following the manufactures instruction. Then, the dissolved oxygen concentration was measured by completely submerging the DO probe tip into the sample solution. Detection limitation is 0.01 mg/L.

3.4.7 Cell number

In this study, cell density was quantified as the number of colony forming units (CFUs) /mL by using the dilution plating method. Petri dishes with growth medium (Table 3.5) in solid form were prepared in advance and were placed in the incubator at

30^0C for 24 hours in order to dry. Sterilized dilution tubes and pipet tips were prepared by autoclaving for 15 minutes at 121 ^{0}C, 21 psi. A 0.85% NaCl solution was prepared for dilution of the samples. To quantify the cell numbers, serial dilution of the original culture was prepared with dilution 10 factor of. Subsequently, 0.1 mL of sample with different dilution factors was aseptically pipetted into duplicate Petri dishes and spread on the agar surface with a sterile glass spreader. Finally, the number of CFUs in the agar plates was counted after 2 days of incubation at 30^0C.

3.4.8 Scanning electronic microscopy (SEM) and Energy dispersive X-ray spectroscopy (EDS)

Scanning electron microscope (SEM, which is capable of creating a three-dimensional image with a high resolution as high as 1 μm, was used to examine the formation of bio-induced precipitation and biofilms on the surface of the sand matrix. To perform the electronic microscopy, suitable specimens were required. The preparation of specimens includes five stages: fixation, dehydrating, drying, mounting, and coating (as guided by Mr. Timothy K. Maugel, University of Maryland College Park, Biological Ultrastructure Laboratory).

In the fixation step, several grains of samples were first put in a plastic container, and a few drops of 10 mM piperazine-N,N′-bis-2-ethanesulfonic acid (PIPES) buffer were added until the whole grains of specimens were submerged. Then the container was placed on a rotating stage for 10 minutes. Next, a glass pipet was used to remove and waste PIPES buffer and replaced few drops of 10 mM PIPES buffer. The steps described above were repeated 3 times. Subsequently, a 2% by volume solution of glutaraldehyde,

the primary fixation reagent, was prepared by using 10 mM pipes buffer. This solution was used to chemically fix the specimen and prevent distortion during the SEM analysis, by placing few drops of the primary fixation reagent into the samples. Then, the specimens were placed on the rotating stage for 60 minutes at room temperature. After finishing the primary fixation stage, those specimens were washed three times using 10 mM PIPES buffer, for 10 minutes per wash. Next, the second fixation solution, a 1% by volume of osmium tetroxide, was prepared in 10 mM pipes buffer. A few drops of the second fixation solution were then added into the previous samples, which were washed for 45 minutes. Then, after completing the second fixation, those specimens were washed again with 10 mM PIPES buffer three times, with 10 minutes per wash. After finishing the washing stages using 10 mM PIPES buffers, the fixation stage was completed.

In the dehydrating stage, ethanol was selected as the main organic solvent. First, the PIPES solution was wasted, and 70% ethanol was used to wash the fixed specimens for 10 minutes. Next, 95% ethanol was used to wash the specimens for 10 minutes. Finally, 100% ethanol was added in the specimens, which were washed for 10 minutes, in 3 consecutive washes.

In the drying stage, the hexamethyldisilazane (HMDS) method was used in this study instead of the critical point drying. First, a mixture of 100% ethanol and HMDS in a ratio of 2 to 1 (by volume) was added in the dehydrated specimens, which were washed for 10 minutes. Next, a mixture of 100% ethanol and HMDS was prepared in a volume ratio of 1 to 1, and the specimens were washed for 10 minutes. Then, another addition of the mixture of 100% ethanol and HMDS was made, again by a volume ratio of 1 to 2, and

the specimens washed for 10 minutes. Finally, HMDS was added individually to the specimens for washing time of 15, 30, and 45 minutes, respectively. When those consecutive steps were finished, a few drops of HMDS were added to the specimens, which placed in the dessicator to dry for few days.

In the mounting stage, several stubs were labeled depending on the number of samples to be examined. Then, a piece of sticking membrane was added onto the stubs to allow some grains of specimens to adhere to the stubs. Note that if the stub was full of samples, the charges of coated samples could interfere with SEM analysis.

In the final coating stage, gold and palladium were employed as a coating metal. To achieve the coating stage, a high vacuum evaporator (Denton DV 502/503) was used. The purpose of coating is to prevent the collection of static electric fields on the surface of the specimens, and also to enhance the electronic conductivity. The coat thickness was 25 nm as recommended by the operator of Biological Ultrastructure Laboratory. Therefore, 6" of gold/palladium wire was used, convolved, and placed in the tungsten basket of the vacuum chamber. Next, the samples were placed on the rotating stage. Via application of a high vacuum which was produced by an oil diffusion pump and mechanical rotary pump, the evaporated metal was sputtered onto specimens. Once the specimens were coated, they were ready for SEM analysis and EDS analysis. The operations of SEM analysis and energy dispersive X-ray spectroscopy were conducted by Mr. Timothy K. Maugel of the University of Maryland College Park, Biological Ultrastructure Laboratory. These analyses were used to examine the surface condition of the specimens and also to define chemical characterization on the surface of the particles.

SECTION 4

COMPLETELY STIRRED-TANK REACTORS AND DIRECT SHEAR TESTS

The objective of this section is to present and discuss the results of the experiments evaluating the effect of bio-calcification mediated by *B. pasteurii* on the shear strength of the sand media. First, the results of the study of the kinetics for growth of *B. pasteurii* on urea are discussed. Then the performance of flow, transport and bio-catalysis by *B. pasteurii* in completely stirred tank reactors (CSTR) which were fabricated to prepare sample for direct shear tests. Finally, the results of the investigation of the effects of different types of cells, compaction, and cell number on shear strength of the tested sand are examined. The shear tests were performed to evaluate the tested sand after biotic or abiotic experiments.

4.1 UREOLYSIS KINETICS

The microbial kinetic parameters (e,g., μ_{max}, K_s, Y, b) for describing growth of *B. pasteurii 11859* on urea were estimated in chemostats operated until steady-state was reached for varied hydraulic retention times (HRTs) (e.g., 2, 4, 6, 8, 10.5, 12, and 16 hours). Of the tests with hydraulic retention times, 2 hours was sufficiently short that the washed out of inoculated cells occurred and urea concentration was essentially equal to the influent concentration. Therefore, the data for 2 hour HRT was not used in the data analysis. The microbial kinetic coefficients μ_{max} and K were ontained using the so-called

Linewaver-Burke plot, in which the inverse steady state substrate concentrations are plotted versus hydraulic retention (Figure 4). Based on Equation 3.9 and Figure 4.1, K_s and μ_{max} are calculated to equal 470 mM, and 11.1 day^{-1}, respectively. This K_s value is higher than the value of 140 mM reported by Bang (2004) for the same bacterial culture and same incubated medium. There are two possible reasons for the observed difference. First, Bang (2004) used a batch system rather than a chemostat system, such as used in the current study, the batch kinetic experiments must be performed and evaluated very carefully to obtain valid parameter estimates. The second possible reason is the pH. The initial pH in this study was pH=9 versus pH=8 in the study by Bang (2004). It is well-known that pH plays an important role on urease enzymatic activity, and the change in pH may have significant effects on microbial activity (Cabrera et al. 1999).

The dilution rate (D= 1/HRT) is plotted versus substrate utilization rate per steady-state biomass per day (U) in Figure 4.2, in order to obtain the Y and b parameters as per Equation 3.10. The resulting values forY and b are calculated as 0.55 and 0.1 day^{-1}, respectively. Rittmann and McCarty (2001) reported that Y and μ range typically from 0.42 to 0.49 and 8.4 to 13.2 day^{-1}, respectively, for aerobic heterotrophic organisms. These values are comparable to the ones obtained in the current study, suggesting that these kinetic parameter estimates are reasonable. Thus, the kinetic parameters obtained above are adopted in the evaluation of performance of bio-catalysis in the CSTR and CMBR systems.

4.2 TRACER STUDIES

A requirement for CSTR design is the complete mixing condition provided in the continuous flow reactor so that the concentration of a particular element inside the basin

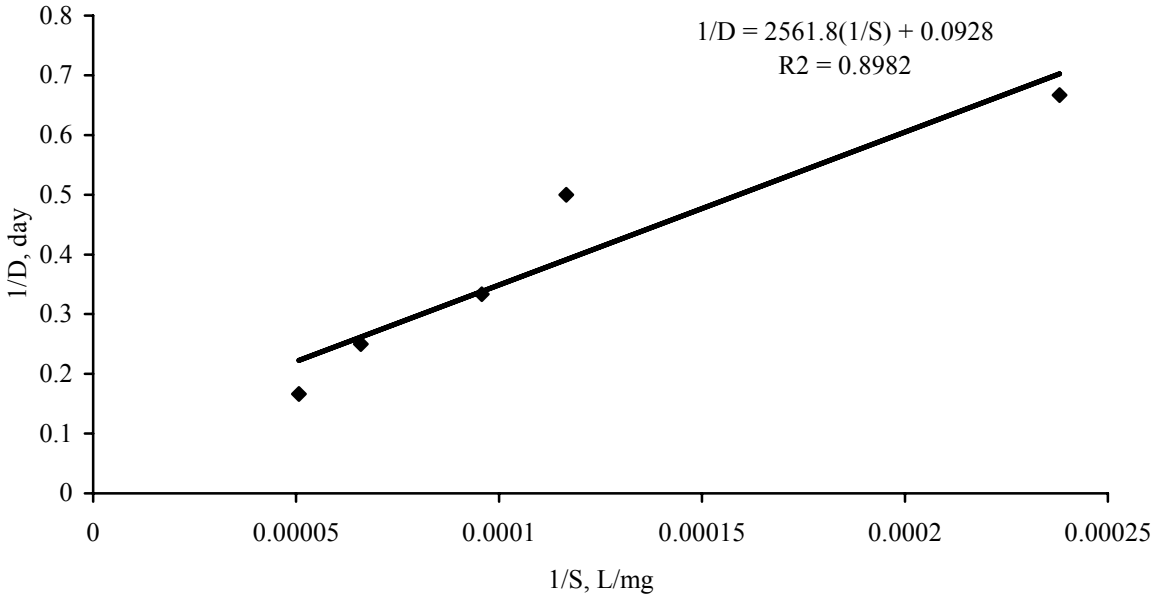

Figure 4.1 Lineweaver-Burke plot for the *B. pasteurii* chemostat data.

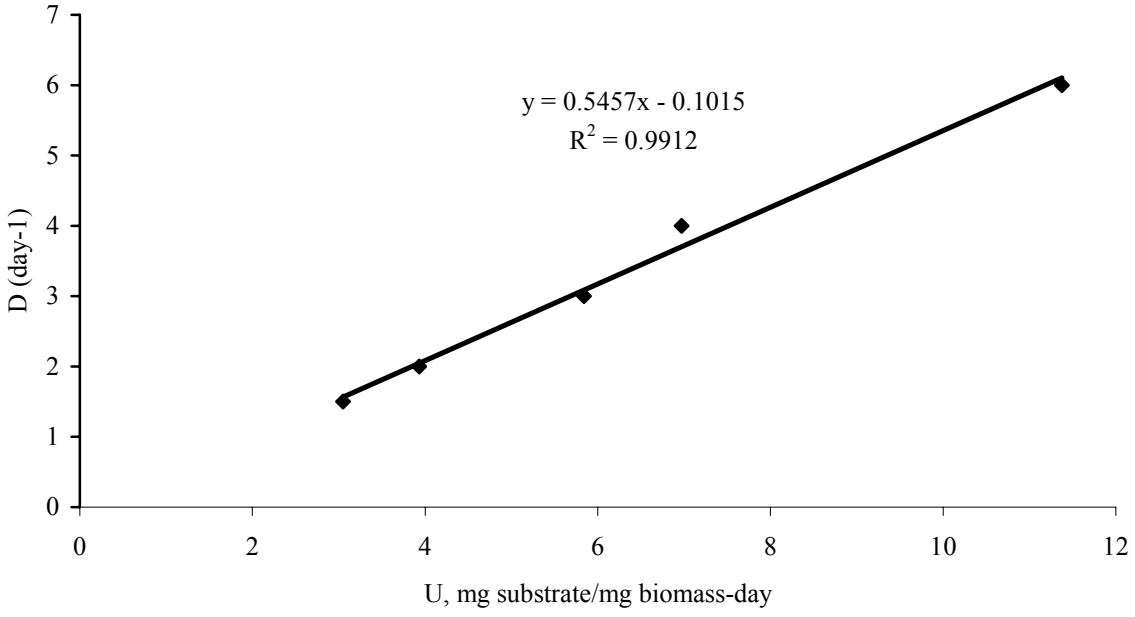

Figure 4.2 Determining Y and b values for the *B. pasteurii* chemostat data by using equation D= YU-b

is equal to its concentration in the effluent. In this study the mixing was provided by magnetic stirred bar. To evaluate whether or not the mixing system provided homogeneous flow conditions, tracer tests were conducted using bromide as a non-reactive tracer. The results of these tests are presented in Figure 4.3. These experiments were performed with the direct shear boxes placed inside the CSTR basin. The results indicate that ideal mixing flow conditions were achieved regardless of the relative density of the sand inside the shear boxes. The hydraulic retention times calculated based on volume and flow rate were 10.5 hours and 12 hours for specimens prepared at 35% (loose) and 85% (dense) relative density, respectively.

4.3 BIO-CATAYLSIS

After ensuring that the ideal flow conditions can be achieved in the basins, sand specimens prepared at target relative densities in the shear boxes were placed in the basin of the CSTR system. After initiation of continuous flow of growth media into the CSTR, all four parameters--urea, calcium, pH and cell count-- were monitored periodically until the system reached steady-state. The data presented Figures 4.4 and 4.5 show the temporal variations in these parameters for specimens inoculated with cell concentrations of 10^3 and 10^7 cells/mL, respectively. From the data in Figure 4.4, it can be seen that the changes in pH, urea, and calcium corresponds well with the cell growth for bacteria concentration of 10^3 cells/mL. For instance, an increase in pH and decrease in calcium and urea can be observed starting at 54 hours corresponding to sharp change in the cell growth curve. These observations are similar to the ones reported in previous studies by Fujita et al. (2000) and Bang et al. (2001).

(a)

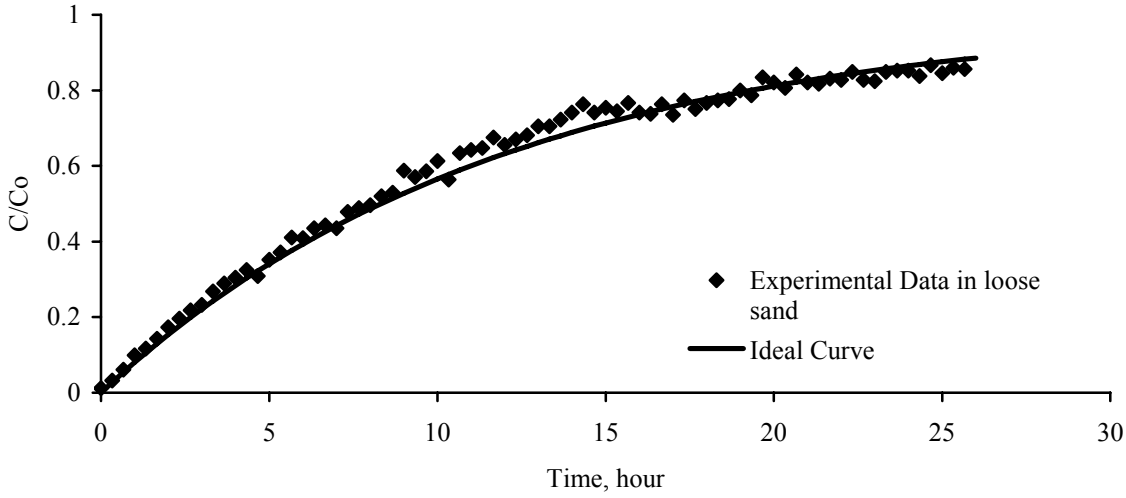

(b)

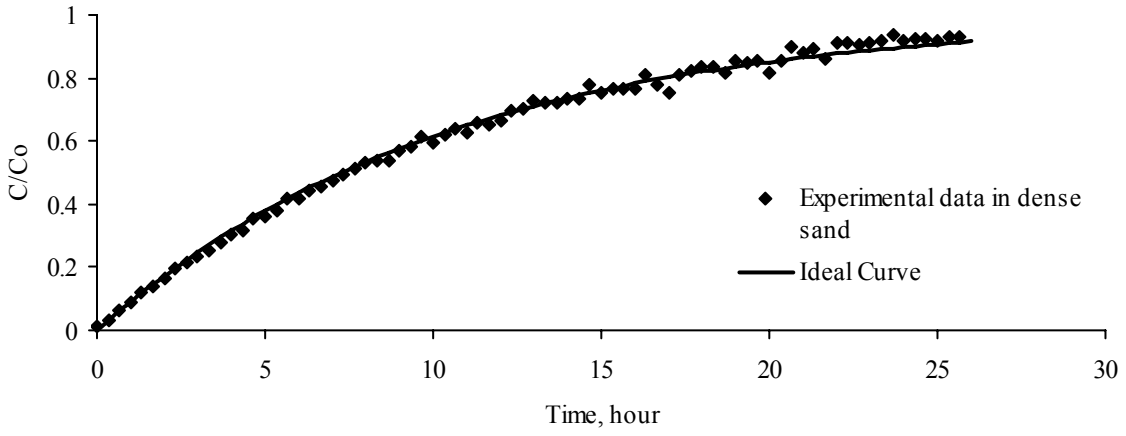

Figure 4.3 Tracer curve for a step injected tracer into the CSTR basin direct shear boxes packed with (a) loose sand, and (b) dense sand.

For the low bacteria concentration (10^3 cells/mL), the CSTR completes the dilution stage in about 18 hours followed by a lag period of 36 hours, after which *B. pasteurii* start to degrade urea (Figure 4.4). Once the degradation of urea occurs, the pH in the system increases to 9.1 due to ammonia production (see Equation 2.3). On the other hand, for the specimen treated with a high bacteria concentration (10^7 cells/mL), the consumption of urea and calcium occurs immediately after CSTR completes the dilution stage, within 18 hours of incubation (Figure 4.5). The CSTR system inoculated by 10^3 cell/mL bacteria reaches steady state conditions within 47 hours (i.e., equal to 4 HRTs) of reaching the dilution stage, whereas the one inoculated by 10^7 cells/mL bacteria reaches steady state within 11 hours (i.e., about 1 HRT) of reaching the dilution stage mainly due to relatively higher inoculum size. Bang et al. (2001) conducted batch experiments with *B. pasteurii* at a cell concentration 5 x 10^7 cells/mL and observed that calcite precipitation reached to a quasi-steady state within 6 hours. The observed difference between the two studies is probably primarily due to the different experimental system and the higher bacteria concentration (10^7 cells/mL versus 5 x 10^7 cells/mL).

4.4 EVALUATION THE PERFORMANCE OF BIO-CATALYSIS USING CSTR MODEL

With the occurrence of bio-catalysis, the urea was degraded effectively in the CSTR, as illustrated in Figures 4.4 and 4.5 with the system ultimately reaching a steady-state. To evaluate the steady-state data, the simple model developed in Section 3.3 was used to describe the ureolysis by *B. pasteurii 11859* in the CSTR. To achieve this, several parameters were required, including the reactor and microbial characteristics as

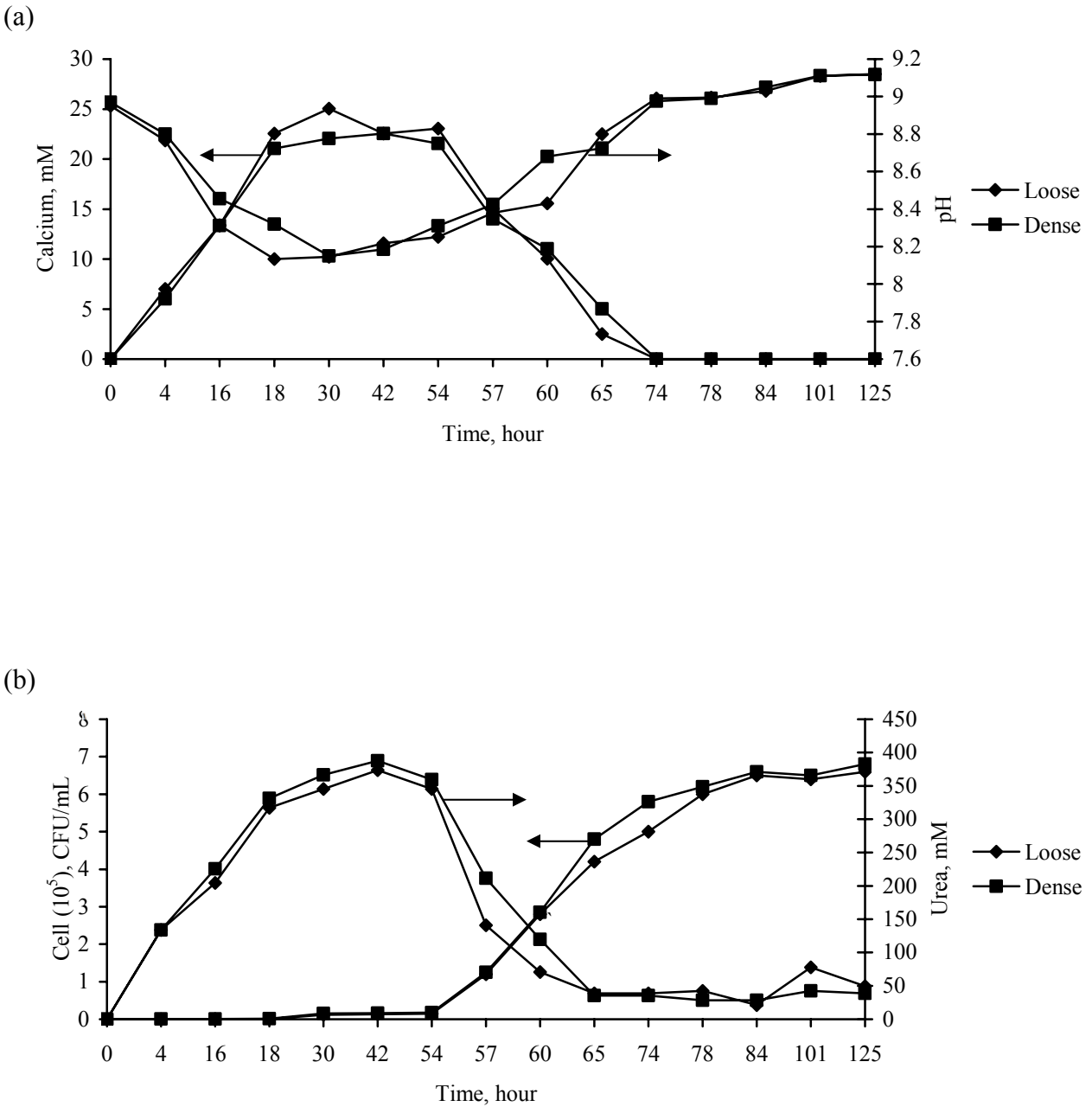

Figure 4.4 Temporal variations in (a) calcium and pH, and (b) urea and cell growth during bio-catalysis by 10^3 cells/mL of *B. pasteurii* in CSTRs containing direct shear boxes with loose and dense packed sand.

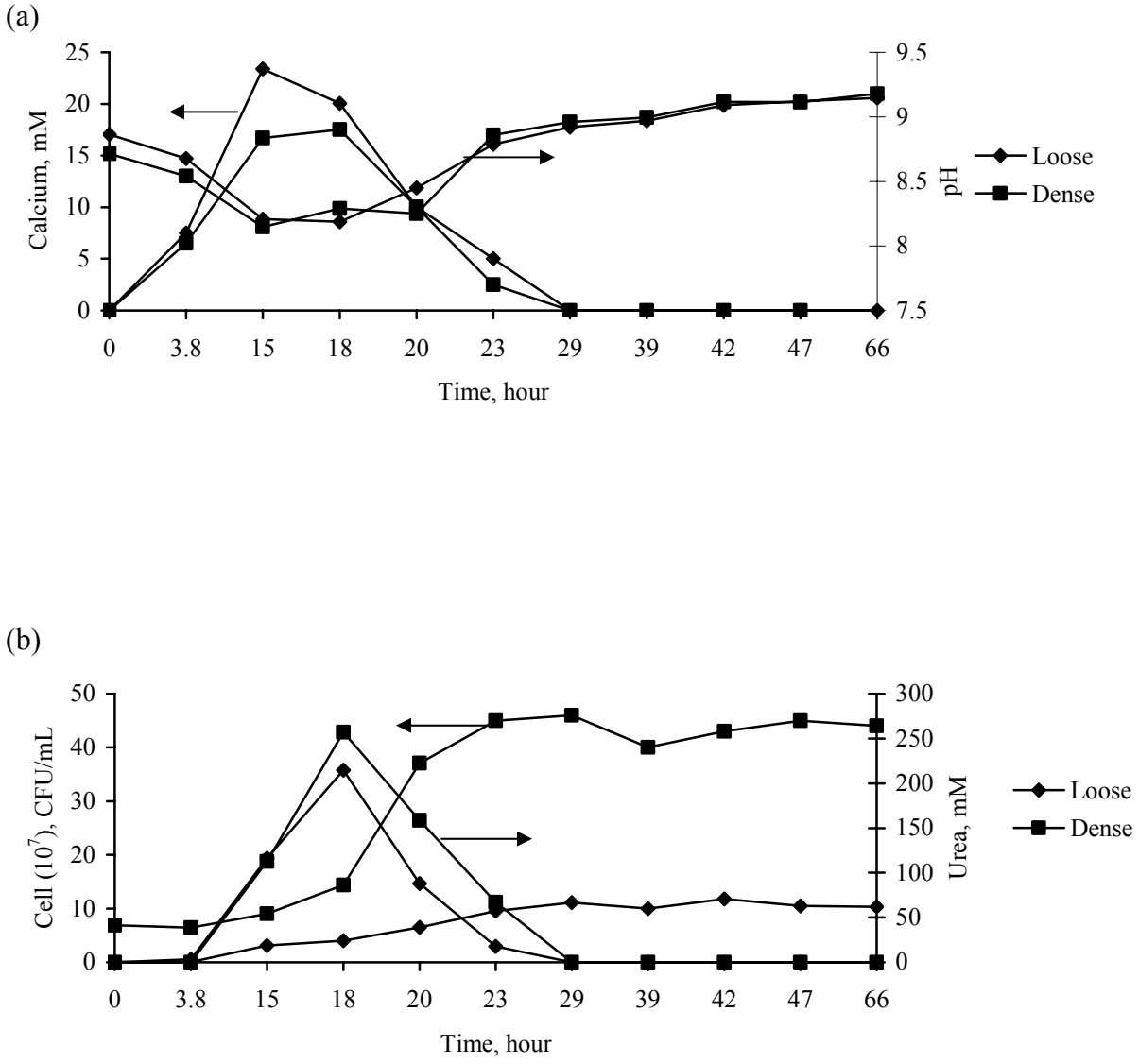

Figure 4.5 Temporal variations in (a) calcium and pH, and (b) urea and cell growth during bio-catalysis by 10^7 cells/mL of *B. pasteurii* in CSTRs containing direct shear boxes with loose and dense packed sand.

summarized in Table 4.1 and 4.2. Using these parameters and equation 3.7, the steady-state urea concentration can be predicted, and compared with actual steady-state substrate concentrations, as shown Figure 4.6 for the two hydraulic retention times evaluated in this portion of the study. In both cases, the experimental urea concentrations are lower than the ones predicted by equation 3.7, indicating a higher than expected efficiency of urea removal rate in the experimental conditions. Furthermore, based on equation 3.8, predicted biomass concentration can be estimated, showing that the experimental biomass concentrations did not have an obvious trend as compared with modeled biomass concentration. These observations may due to several possible reasons, related to the presence of the shear boxes packed with sand in the CSTR system which allowed for the attachment and accumulation of bacteria. Most importantly, the impact of this attached biomass on the urea concentration is not accounted for in equation 3.7. In addition, this attached biomass efficiency also affect the suspended biomass concentrations. Finally the attached biomass may also indirectly affect substrate utilization rate because it has been proven that attached bacteria have a relative high metabolic activity (Klein and Kluge 1981, Wang and Ruchenstein 1993).

The CSTR simulations in Figure 4.6 and sample preparation can be used to achieve the optimal biocalcification. The fundamental controlling parameter for the conditions in the CSTR is the hydraulic residence time. The value selected for the hydraulic residence time depends on the desired balance of substrate removal, biomass production, and other process (Rittmann and McCarty 2001). For example, when the hydraulic retention time is very small $S=S^0$ and $X_a=0$ (i.e., Xa =0 at about 6 hours of HRT in Fig. 4. 6), which is so-called washout. The hydraulic residence time at which

Table 4.1 Reactor characteristics considered in simulating ureolysis in CSTR

Reactor types	Volume, L	Hydraulic retention time, hrs	Flow rate, L/hr
Reactor 1 (with shear boxes containing loose sands)	6	10.5	0.57
Reactor 2 (with shear boxes containing dense sands)	6	12	0.5

Table 4.2 Input model parameters of ureolysis obtained from chemostat studies

Kinetic parameters	Values
Half saturated concentration for urea, K, mg/cm^3	27.6
Substrate utilization rate, q, mg_s/mg_a-d	20.2
Maximum specific growth rate, μ, day^{-1}	11.1
Overall decay coefficient, b', day^{-1}	0.1
Yield for biomass synthesis, Y, mg_a/mg_s	0.55

washout begins is called HRT_{min}. When HRT is operated longer than HRT_{min}, which was estimated to be about 2.2 hours in this work by using 1/(Yq-b), the substrate decreases with increasing HRT. For very large HRT, S approaches another limiting values, S_{min}, which is the minimum substrate concentration that can support steady state biomass. In this work, S_{min} was estimated to be about 0.25 mg/cm^3. Finally, as seen in Figure 4.6, when HRT is longer than HRT_{min} biomass initially increases with decreasing substrate concentration; however, biomass it eventually reaches a maximum value (at 40 hours of HRT at this work and then declines as decay becomes dominant. Based on these observations from the CSTR simulation, if optimal biological calcification is to be achieved in the sample specimen, it is recommended that the HRT should be based on the accumulation of biomass, and not the substrate utilization.

4.5 EFFECT OF CELL TYPE AND NUMBER ON STRENGTH IMPROVEMENT

Up to this point, the focus has been on lives biomediating calcalification. However, in the real environment, bacteria may die due to lack of nutrients or oxygen, or eventually form endospores, which may act as organic fibers. As a result, live and dead bacteria may influence the soil properties differently. In order to study the effect of different types of cells on the shear properties of the silica sand (i.e., friction angle and cohesion), live, dead and resting *B. pasteurii* cells were prepared and incubated in the sand following the methods described in Section 3.2.2.3. In case of live cells, direct shear tests were conducted once the utilization rate of urea in the CSTR basin reached steady state. In this case, the urea was the primary nitrogen and energy source for the microorganisms (Mobley and Hausinger 1989). On the other hand, in case of dead and

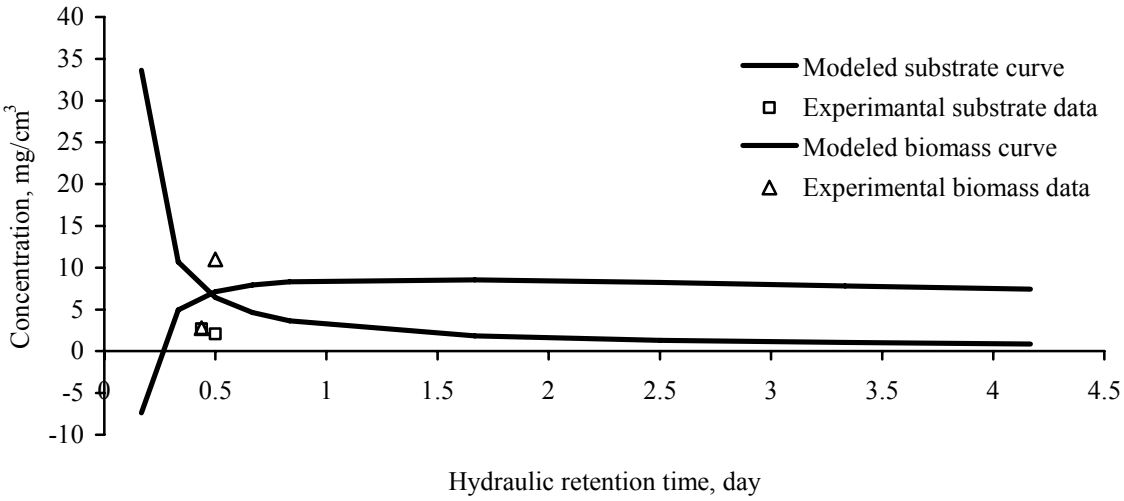

Figure 4.6 Modeled and observed substrate and biomass concentrations versus hydraulic retention time for steady state concentrations in the CSTR.

resting cells, the cells were inoculated in the sand and shear tests were performed after 1 day of curing time. This short curing time was selected to give enough time for the cells to attach onto the surface of the sand particles while minimizing the decay of the resting cells.

A summary of direct shear test results for these differed specimens are given in Tables 4.3 and 4.4. The friction angles of the untreated loose and dense sands are 27^{o} and 33^{o}, respectively. The same soils exhibited cohesions of 2.6 kPa and 4.6 kPa, respectively. Bardet (1997), Ashford et al. (2001) and FEMA Coastal Construction Manual (2005) reports friction angles of 26^{o}-30^{o} and 32^{o}-39^{o} for loose and dense poorly-graded sands. These parameters are comparable with the ones obtained in the current study. Table 4.3 shows that the shear strength parameters of the specimens, in general, have been significantly improved as a result of the treatment, regardless of the cell types, with the improvement primarily reflected in the increased friction angles. However, the live-cell treatment seems to have a more profound effect on the friction angles as compared to the other two cell types. For instance, the increase is 1% and 2% for sands treated with 10^{3} cells/mL. dead cells and prepared at relative densities of 35% and 85%, respectively. In comparison, for the same initial cell concentration, cell type and relative densities, the changes are 7% and 5%, respectively, in case of resting cells, and 25% and 20%, respectively, for live cells. Figure 4.7 is given as an example to show the changes in friction angle and cohesion of sand treated with 10^{7} cells/mL concentrations. The improvement in friction angle with live cells can be attributed to the formation of crystals

Table 4.3 Summary of shear strength parameters for treated and untreated sands in the cases of loose sand

Experimental conditions / Geomechanical Properties	Loose (35% of relative density)						
	Blank	Dead cells		Resting cells		Live cells	
		10^3 cells/mL	10^7 cells/mL	10^3 cells/mL	10^7 cells/mL	10^3 cells/mL	10^7 cells/mL
Friction angle	27°	27.3°	34.6°	25.1°	33°	33.8°	38.4°
Cohesion, kPa	2.6	3.9	0	3.9	0	0.6	0

Table 4.4 Summary of shear strength parameters for treated and untreated sands in the cases of dense sand

Experimental conditions / Geomechanical Properties	Dense (85% of relative density)						
	Blank	Dead cells		Resting cells		Live cells	
		10^3 cells/mL	10^7 cells/mL	10^3 cells/mL	10^7 cells/mL	10^3 cells/mL	10^7 cells/mL
Friction angle	33°	33.5°	41.2°	34.7°	39.7°	39.6°	43.3°
Cohesion, kPa	4.6	8.1	4.6	4.6	3.1	3.7	0
Residual Friction angle	23.4°	22.8°	36.3°	34.7°	33.1°	38.2°	32.1°
Residual cohesion, kPa	4	7.6	2.7	1.0	1.9	0	1.3

(i.e., calcite or other calcareous crystals) induced by *B.pasteurii*, which may in turn cement the pore surfaces , as shown in Figure 4.8. Existing studies also showed that calcium carbonate can deposit onto the cell wall when free carbonate ion is present in the environment. Beveridge et al. (1997) suggests that live *B. pasteurii* cells promote the formation of calcite by forming a biofilm and extracellular polymeric substance (which have been proven as nucleation sites), and allowing the cation (i.e., Ca^{2+} in this study) to be effectively adsorbed onto sand particles and form mineral deposits. Similarly, Silver et al. (1975) demonstrated that calcium is predominantly adsorbed and accumulated on cell membranes. The same crystal formations may also be responsible for the observed increase in peak strength of the sand in the current study (Figure 4.7). The increase in the peak (ultimate) strength has also been observed by previous researchers in microbiological treatment of concrete (Ramachandran et al. 1999), and monumental carbonate stones (Rodriguez-Navarro et al. 2003).

The expected mechanisms are different in case of dead and resting cells. According to Ramachandran et al. (1999), dead cells act as organic fibers, which may simply stay within the porous matrix and decompose with age. Most probably, the same mechanism is responsible for the observed strength and friction angle increase with dead may explain the results with resting cells in the current study. Resting cells are live cells without a food supply, meaning that bacterial activity remains low. However, these cells may decay and die due to lack of nutrients and act like organic fibers as well. Table 4.3 and 4.4 also shows that the friction angle increases with increasing cell number for all of the compaction conditions and cell types. Figure 4.9 is given as an example to demonstrate the effect of bacterial concentration on shear properties in case of the loose

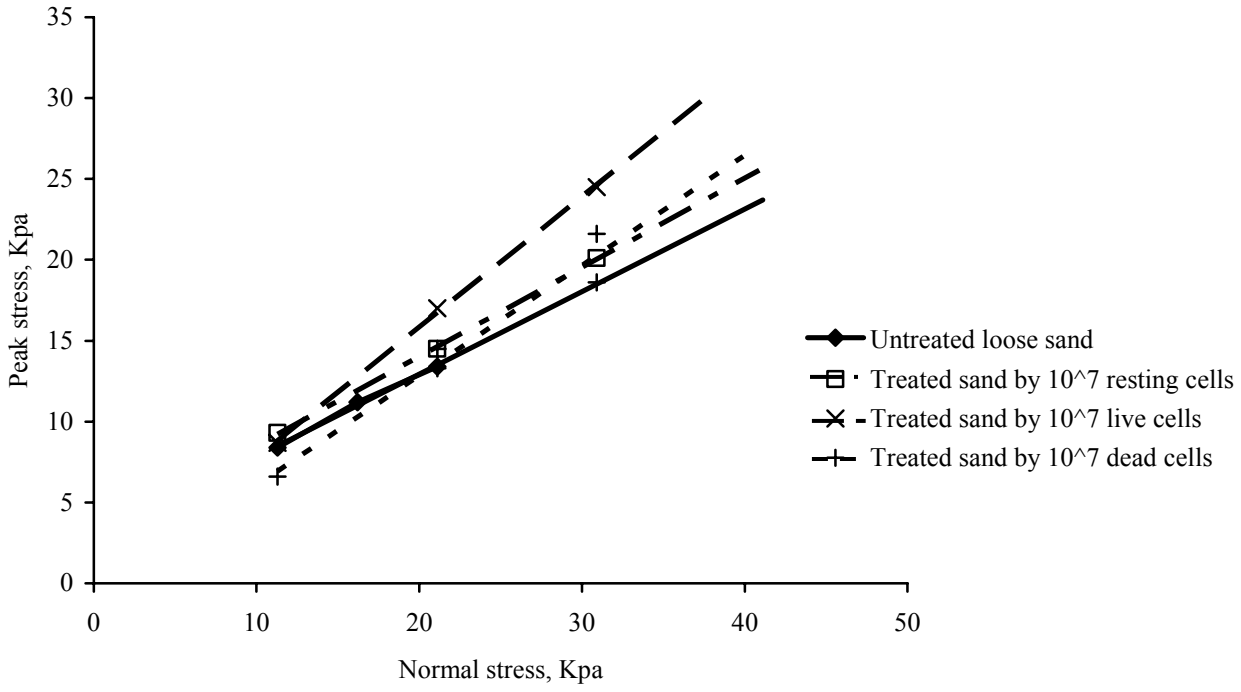

Figure 4.7 Effect of cell types on friction angle and cohesion of loose sand (bacteria concentration= 10^7 cells/mL)

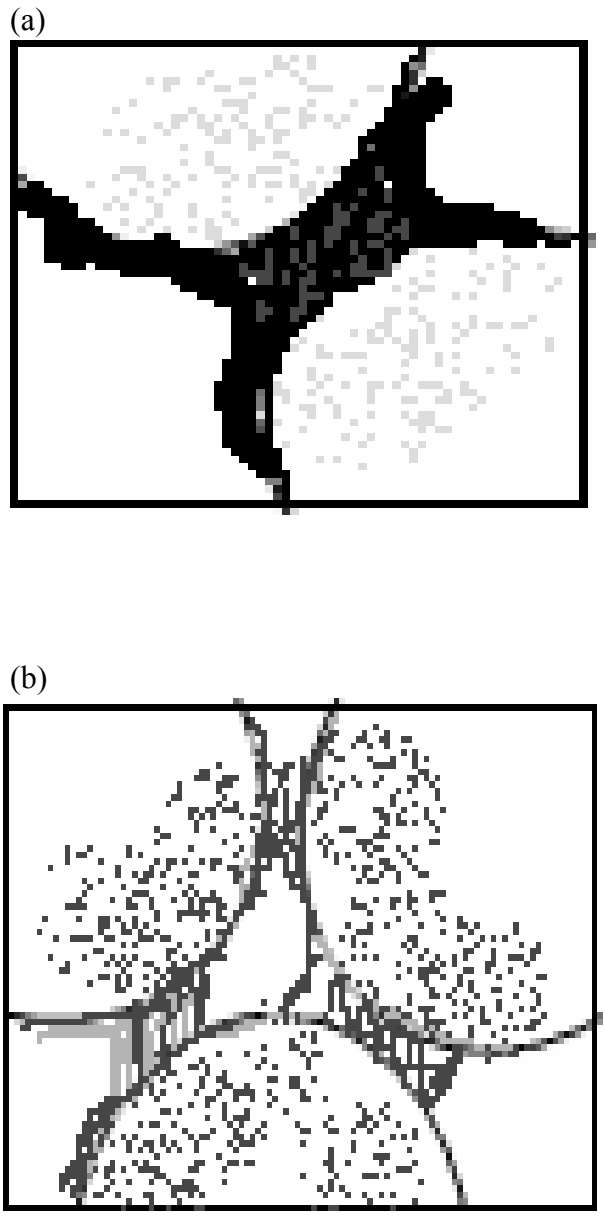

Figure 4.8 Schematic of crystals deposition onto the surface of sand particles and plugging within sand matrix: (a) heavy deposit and (b) light deposit. (Modified from Hillgärtner et al. 2001).

sand. As explained above, resting and dead cells are likely to act like organic fibers and contribute to shear strength. Live cells, on the other hand, produce precipitates that ultimately plug the pore spaces. As a result, an increase in the concentration of live cells increases the amount of precipitates which directly contribute to friction angle. Similar observations were made by Gollapudi et al. (1995) and Ramachandran et al. (2001) in testing of sands and concrete. Note that while the dead and resting cells clearly are affecting the friction angle, the impact of the live cells is more dramatic as expected.

4.6 THE EFFECT OF COMPACTION ON STRENGTH IMPROVEMENT

The direct shear tests were conducted on sand specimens prepared at 35% and 85% relative densities. In all cases, the friction angle increases as a result of density increase. The increase is in a range of 19-23%, 21-38% and 13-17% for dead, resting and live cells, respectively. Figure 4.10 is given as an example to demonstrate the effect of compaction on sands treated with different cell types prepared at 10^7 cells/mL concentration. This shows that the friction angle improvement in the loose compaction is similar to the one in the dense compaction in the cases of dead and resting cells, whereas in the case of live cells, the friction angle improvement in the loose compaction is more significant than in the dense compaction. The possible reason is that the improved friction angle of treated sand by dead or resting cells is simply contributed by the biomass density in the pore volume. It is obvious that biomass densities of dead or resting cells are very small (i.e., 9.5×10^{-3} mg/cm^3), as compared with biomass density of live cells (i.e., 0.95~3.8 mg/cm^3). In addition, in the case of live-cell mediated sand, the friction angle improvement is not only due to a relative high biomass density, which results from

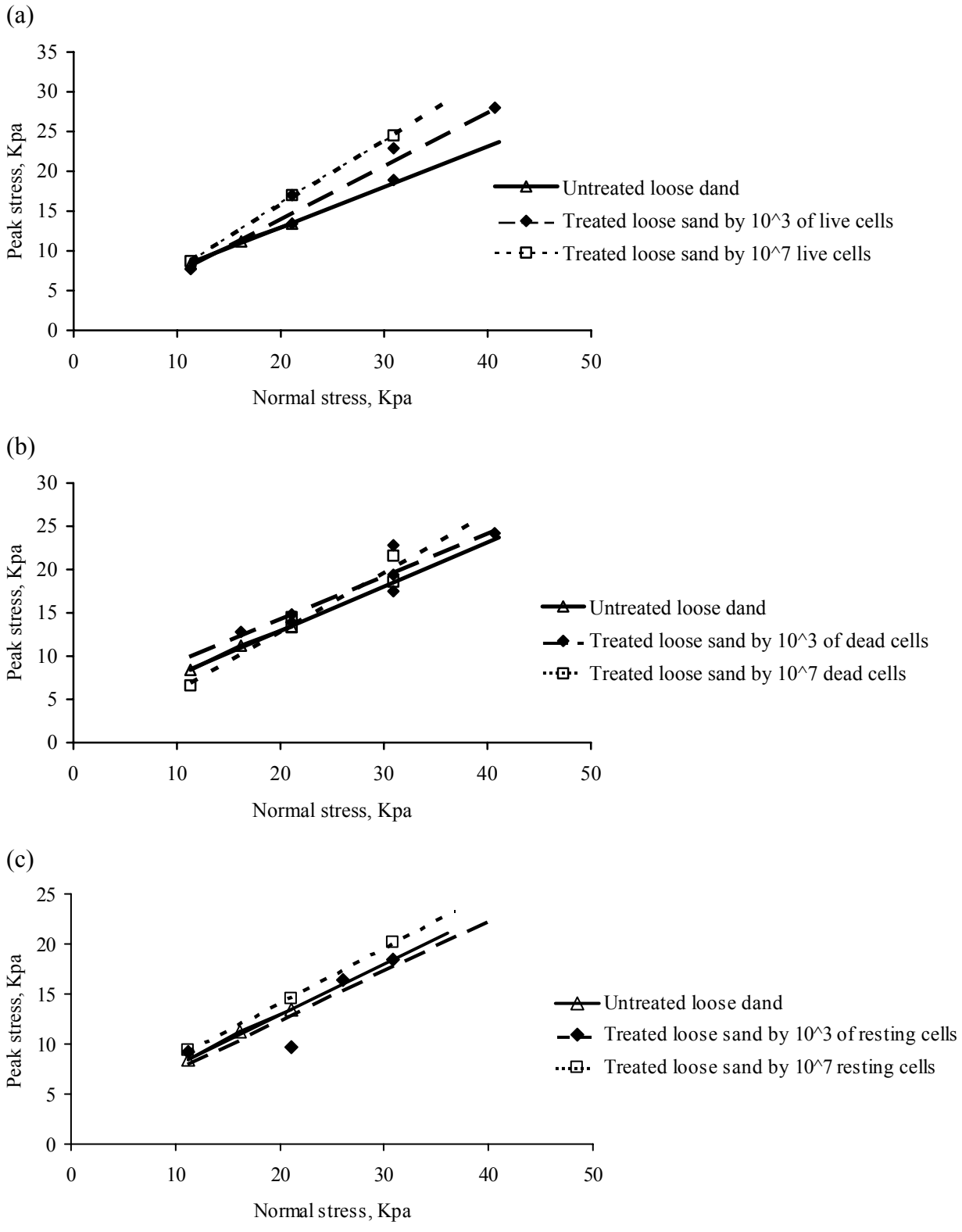

Figure 4.9 Effect of cell number on friction angle and cohesion coefficient sand prepared at D_r=35% and treated with (a) live, (b) dead, and (c) resting cells.

biomass synthesis, but also due to calcite crystal precipitation, which plugged within the sand matrix. Thus, the compaction factor does affect the efficiency of bio-mediated processes, this is, the more available pore volume within sand matrix, the more precipitates induced to plug into pore spaces between sand particles.

During shearing stages, unit volume change of each specimen was also recorded. Figure 4.11 is given as an example to demonstrate the effect of compaction on the volume changes of the specimens that were treated with different cell types prepared at 10^7 cells/mL concentration. As expected, dense sand experienced higher volume change as compared to the loose sand, and the treated ones accompany their untreated pairs. Figure 4.11 also shows that the live cells resulted in higher volume changes than the dead cells for both dense and loose sands. Moreover, the volume change of resting cells has a similar behavior to that of dead cells in the loose compaction. This is attributed to the fact that the improvement with live cells is due to the formation of calcite or other calcareous crystals whereas the dead or resting cells act like organic fibers.

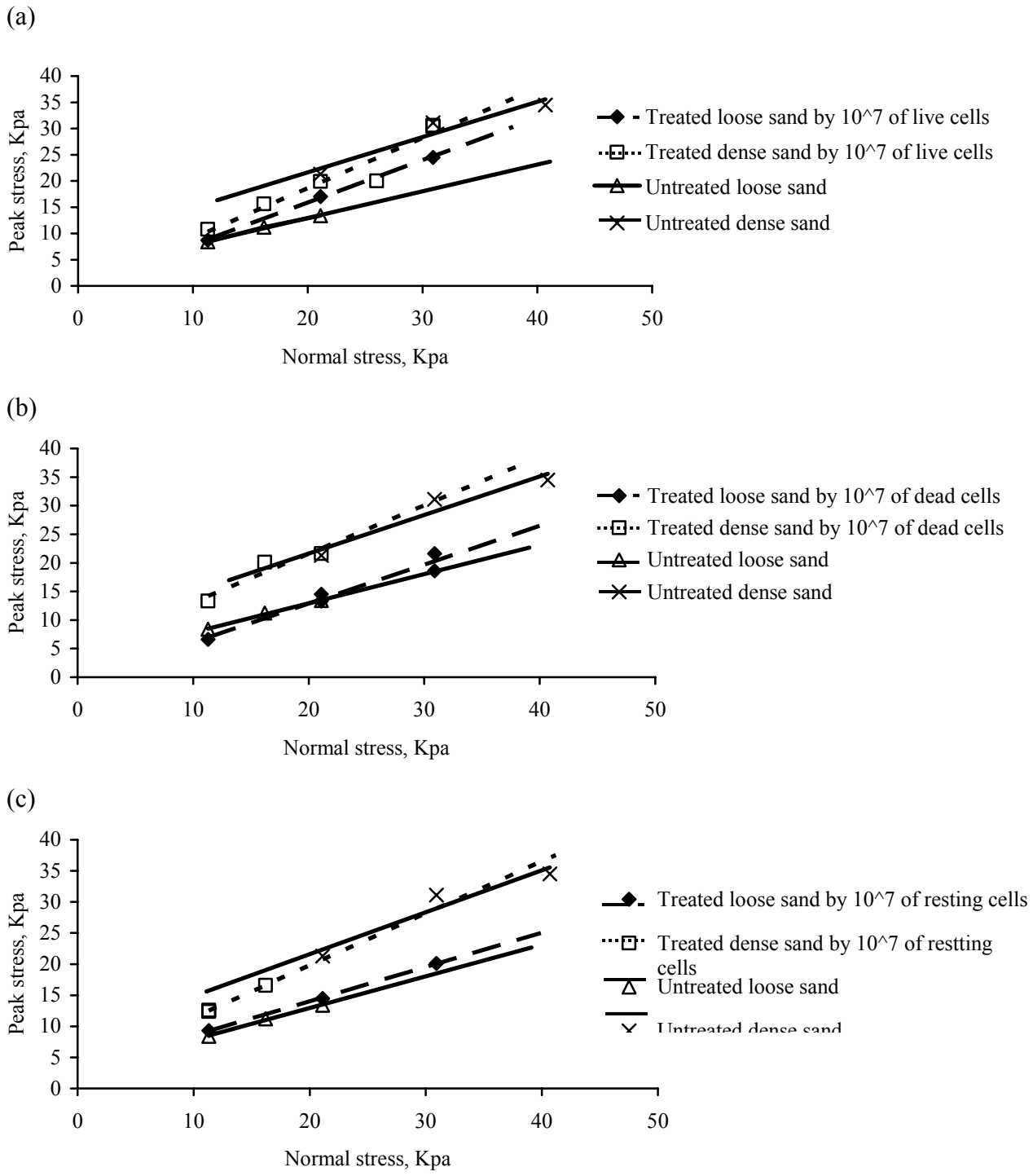

Figure 4.10 Effect of relative densities on friction angle and cohesion coefficient in the presence of 10^7 cells/mL of (a) live cells, (b) dead cells, and (c) resting cells.

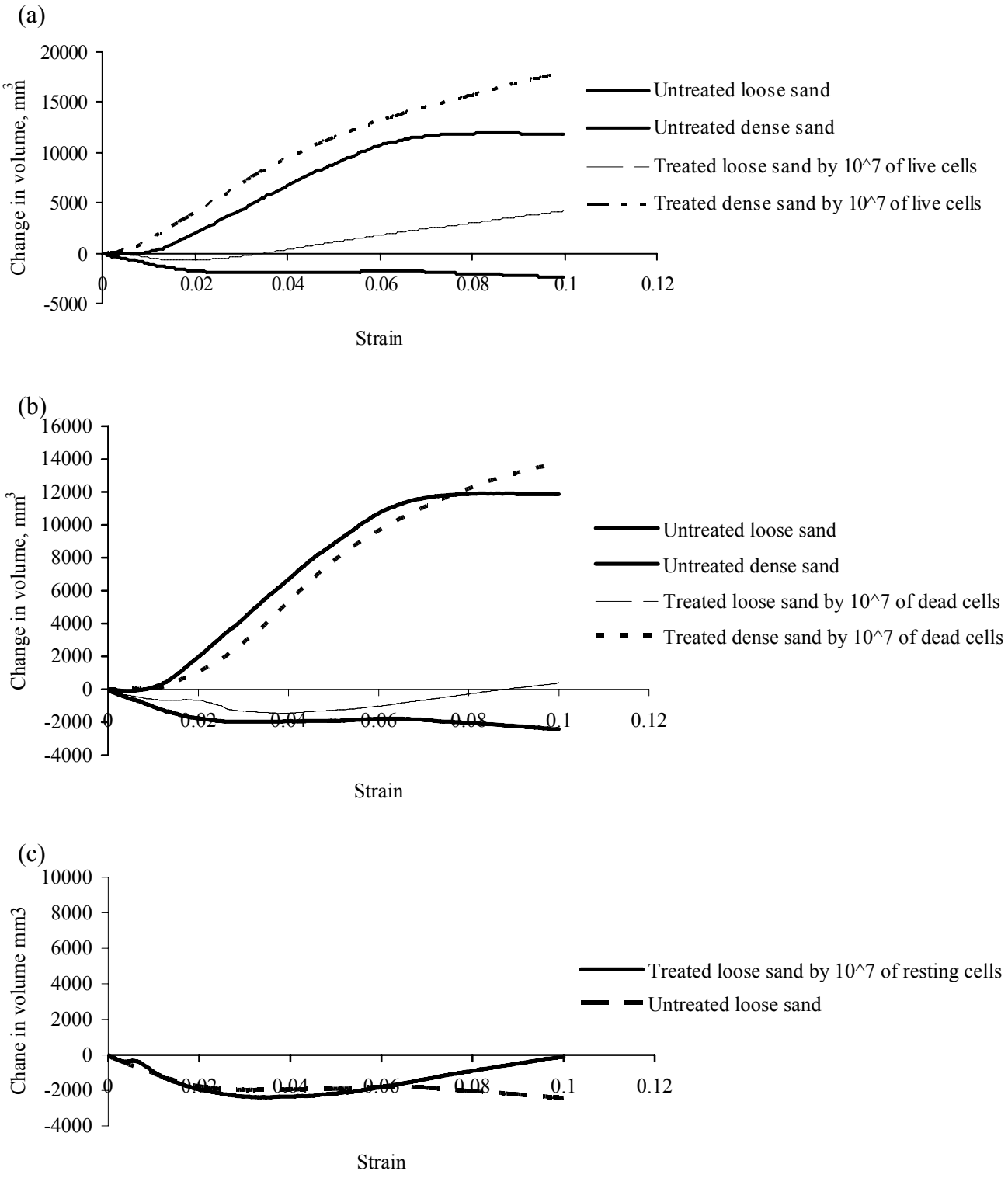

Figure 4.11 Effect of relative densities on volume change of sand in the presence of 10^7 cells/mL of (a)live cells, (b) dead cells, and (c) resting cells. All curves are based on a normal stress of 21.1 kPa.

SECTION 5

COMPLETELY MIXING BIOFILMS REACTORS AND CALIFORNIA BEARING RATIO TESTS

As mentioned in the Section 3.2.3.1, hydraulically completely-mixed biofilm reactors (CMBRs) were designed to provide an optimal environment for precipitation of calcite throughout the sand. The CMBR columns were then subjected to ASTM D 3668 California Bearing Ratio (CBR) tests to study the effect of the microbiological treatment method on soil strength. In this section, hydraulic the performance of the CMBR, the preparation of the sand specimen inside the CMBR columns, and the mechanisms of bio-catalysis in the CMBR system are discussed. The section also includes a discussion of the effects of different types of cells and cell numbers on the bioimprovement process reflected by the changes in the CBR data.

5.1 TRACER TESTS AND CBR ANALYSIS OF UNTREATED SAND

The purpose of the bromide tracer tests was to study the hydraulic performance of the column reactor with recycle flow. A recycle flow rate of 20 mL/min was chosen based on the trial-run tracer studies as providing approximately completely mixed conditions in the column. For example, based on the tracer data in Figure 5.1a, a completely mixed flow condition was successfully achieved for the loose sand (D_r =35%), due to the availability of pore spaces. In case of dense sand (D_r=85%), on the other hand (Figure 5.1b), the ideal tracer curve stays below experimental bromide concentrations

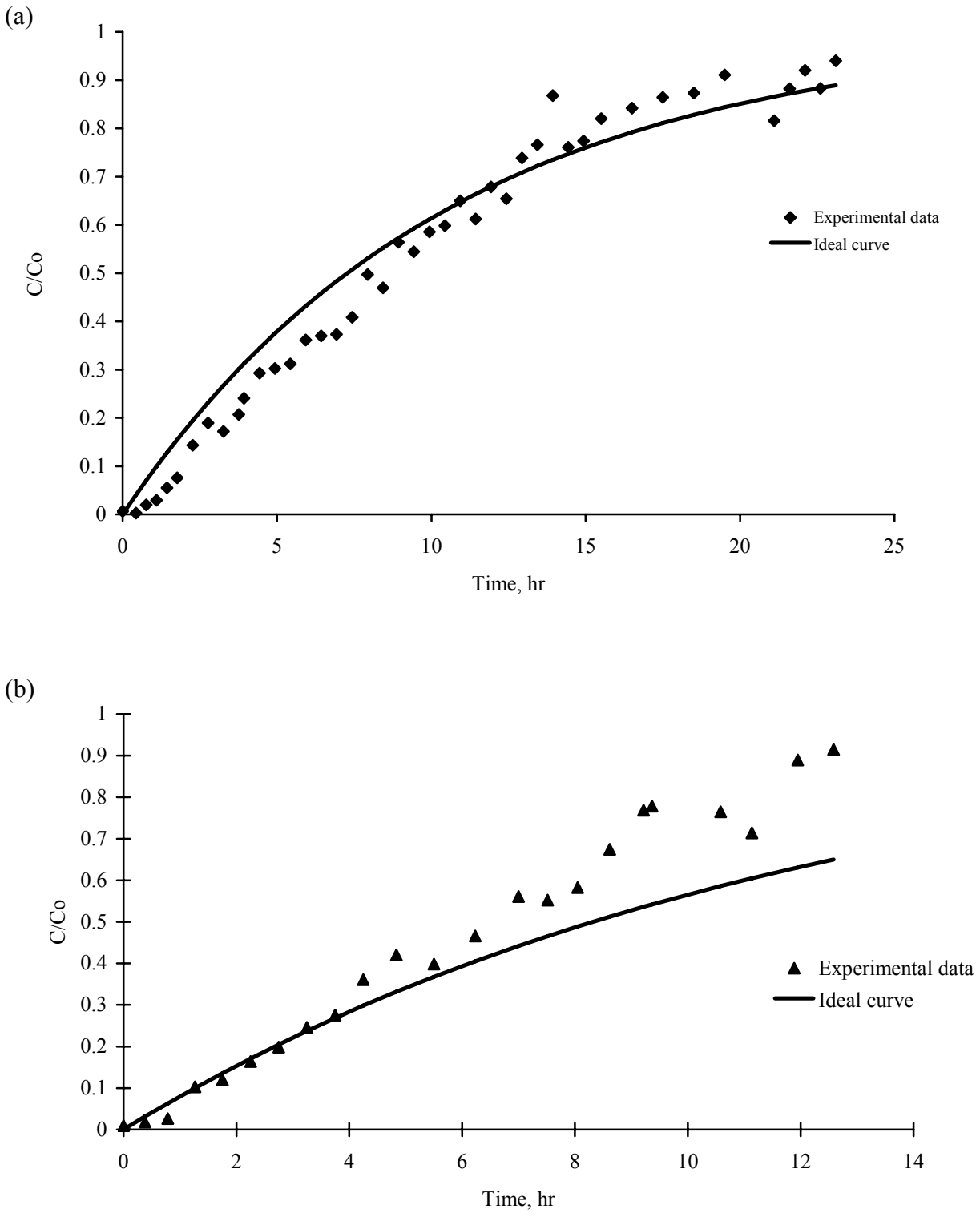

Figure 5.1 The tracer curves in CMBR systems with a flow rate 1.5~1.6 ml/min and recycle flow rate 20 ml/min for different sand compactions: (a) loose and (35% relative density) (b) dense sand (85% relative density).

starting at 6 hours of operation, probably due to the occurrence of the short circuitry flow along the column walls.

The results of CBR analysis of untreated sand samples are presented in Figure 5.2. The data suggests that the variation of the CBR along the height of the column for either loose or dense sand is small. The calculated standard deviations of CBR for specimens prepared at relative densities of 35% and 85% were less than 0.5%, and the average CBR number was 9.76% and 21% for loose and dense compaction, respectively. Thus, it was concluded that the method of specimen preparation was acceptable.

5.2 THE BIOCATALYSIS OF CALCIFICATION BY *B. PASTEURII 11859* IN CMBR

The CMBR data from the effluent calcium, pH, cell number, and urea concentrations are presented in Figures 5.3 and 5.4. These data show that calcium and urea, which were added in the feed solution, increased initially and then dropped after around 20 hours of operation, indicating that the dilution of those substrates is dominant between the first and the second hydraulic retention times (e.g., 10.5 and 12 hours as 1 HRT for loose and dense compactions, respectively), after which urea degradation and carbonate precipitation induced by *B. pasteurii 11859* becomes dominant. Specifically, as urea degradation starts to result in a concentration decrease, the pH increases due to production of ammonia according to Equation (2.1). As seen in Figures 5.3 and 5.4, pH arises from approximately 8 to 9.1 for dense and loose compaction. Similar trends were observed in previous studies of bioinduced carbonate precipitation (Bang et al. 2001,

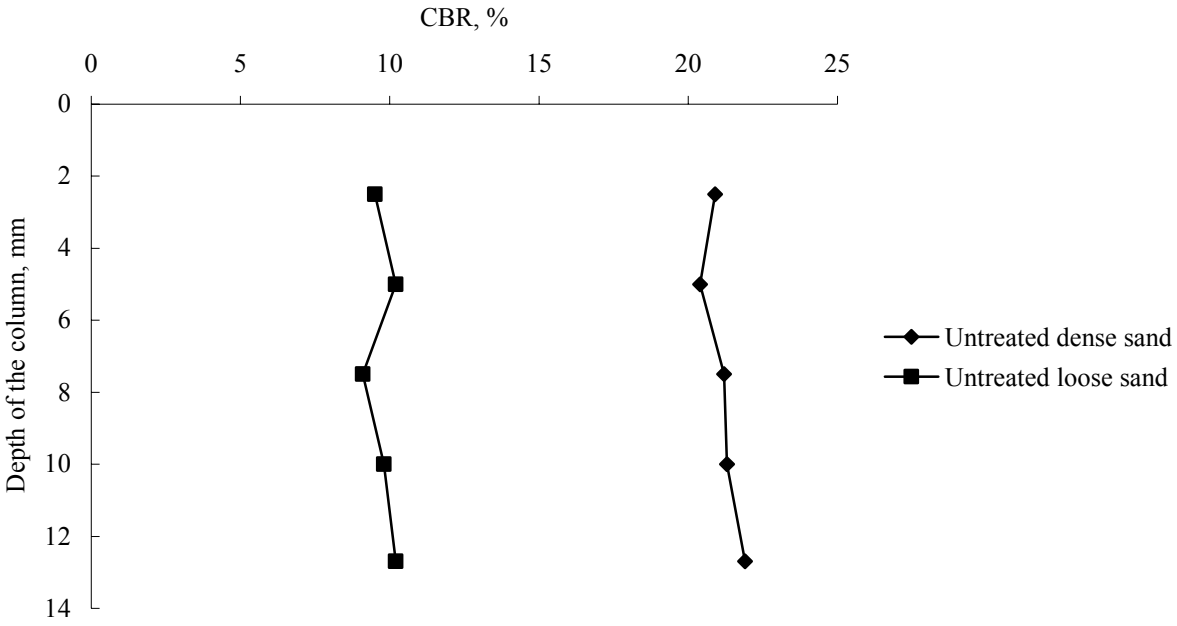

Figure 5.2 The CBR number of untreated dense and loose sands at different depths in the CMBR columns.

Rodriguez-Navarro et al. 2003). Based on enzymatic activity point of view, *B. pasteurii* can be able to locally change chemical and physical properties such as pH, or urea solubility, in the surrounding environment by reducing the required activation energy of calcification. Hence, carbonate precipitation becomes favorable and supersaturation of precipitation becomes possible in the local environment (Párraga et al.1998). Correspondingly, once the drop in urea concentration begins, the calcium concentrations start to decrease, demonstrating that calcium carbonate precipitation is occurring and is associated with bacterial activity. Several possible mechanisms responsible for the carbonate crystallization induced by bacteria have been reported in previous studies. For example, it has been demonstrated that Gram-positive bacteria such as *B. pasteurii* have numerous surface functional groups, such as carboxyl or hydroxyl, which are negatively charged in an alkaline environment. Therefore, a powerful electrostatic affinity is expected (Fein 2000, Rodriguez-Navarro et al. 2003), and it is reasonable to assume that the biomass grown is capable of adsorbing cations. Additionally, extracellular polymeric substances (EPS) generally induced by bacteria during biofilm formation have been shown to act as heterogeneous nucleation sites during the mineralization (Decho 2000). Note that in both columns the effect of calcium was below detection limit after 33~35 hours, suggesting that further biologically induced calcification was limited by the calcium concentration.

The biocalcification resulted in changes in head-loss and flow rate as shown in Figure 5.5 (a) and (b). Correspondingly, as the head-loss increased and flow rate decreased (Eq. 3.2), the hydraulic conductivity decreased in both sand columns (Figure 5.5 (c) ultimately reading about 2×10^{-5} cm/s after approximately after 9 hours and 28

(a)

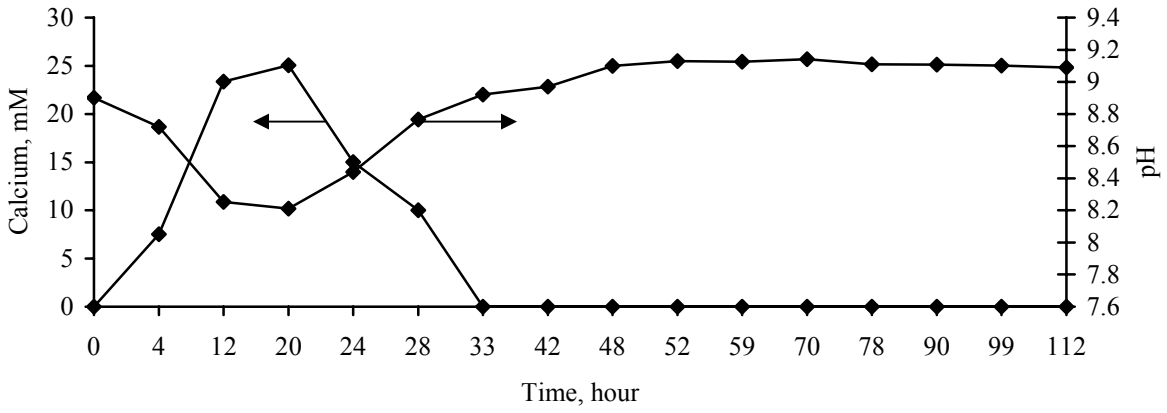

(b)

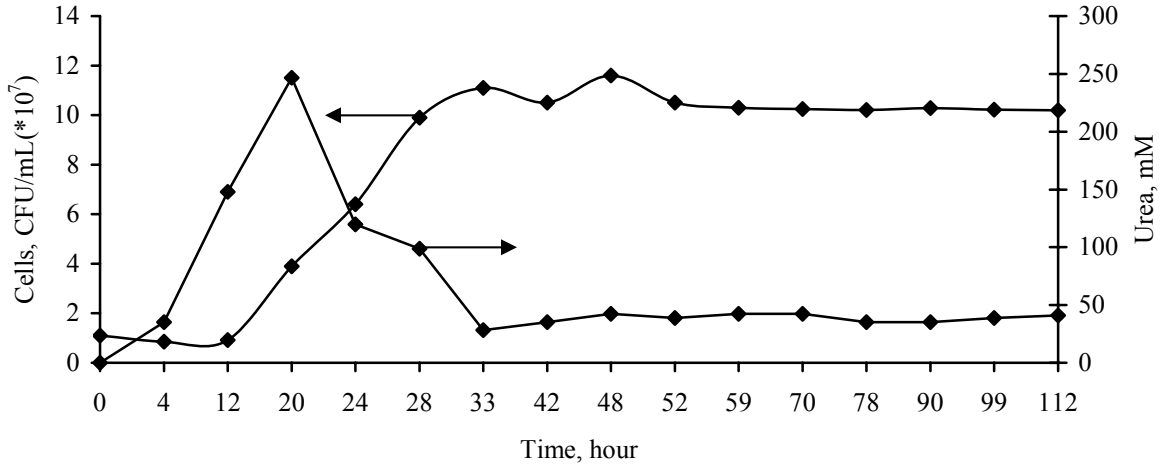

Figure 5.3 CMBR effluent data (a) calcium and pH, and (b) cell number and urea concentration with the loosely compacted sand.

(a)

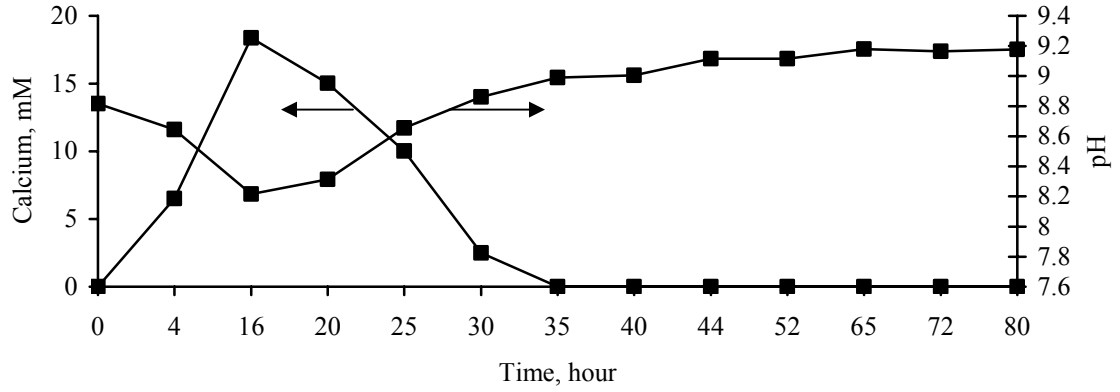

(b)

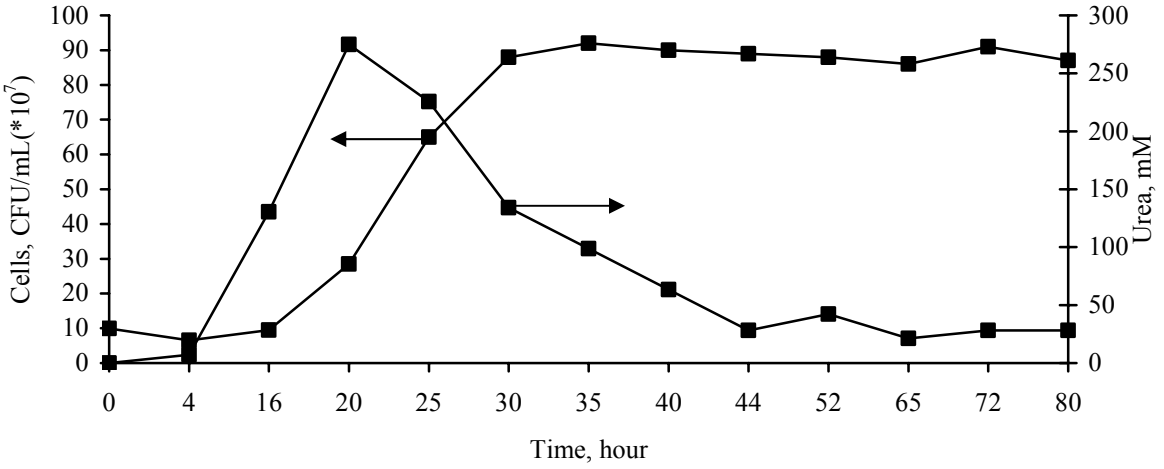

Figure 5.4 CMBR effluent data (a) calcium and pH, and (b) cell number and urea concentration with the loosely compacted sand.

hours of nutrient injection in the dense and loose sand columns, respectively. This value is equal to the detection limit for rigid-wall permemeters like the CMBRs. Interestingly, in the loose sand column, the hydraulic conductivity decreased initially, but then reached a steady state between 15 to 30 hours of incubation. Such steady state conditions were not observed in the dense sand column, but head loss measurements only possible during the first 10 hours due to equipment limitation. Indeed, under both conditions eventually the head-loss became too large to measure with the piezometers (after 10 hours and 30 hours, respectively, for dense and loose compaction). After that point it was no longer possible to calculate the K values. Flow rate was monitored until the column was completely plugged, i.e., Q=0. As illustrated in Figure 5.5, the observed flow rate and hydraulic conductivity trends for a particular sand specimen were generally comparable. However, there was a period during the first 30~40 hours of the experiment during which the flow rates were relatively constant despite the drops in head-loss and K. Presumably the head gradient by the pump was sufficient to overcome the head loss due to bioplugging during this period although the trends with the two densities of compaction were not exactly the same. For example, Figure 5.5 (b) shows that the effluent flow rate in the loose sand started to decline at the onset of incubation, and then plateaus until about 30 hours, while the effluent flow rate in the dense sand remained steady state for the first 45 hours of incubation, after which it declines. This is contrary to the experiment that the flow rate would decrease faster in the dense sands due to the relatively lower porosity. This phenomenon can probably be attributed to the occurrence of short-circuiting of flow in the dense sand along the walls of the column, consistent with the observations made in tracer studies as shown in Figure 5.1. The effluent flow rates

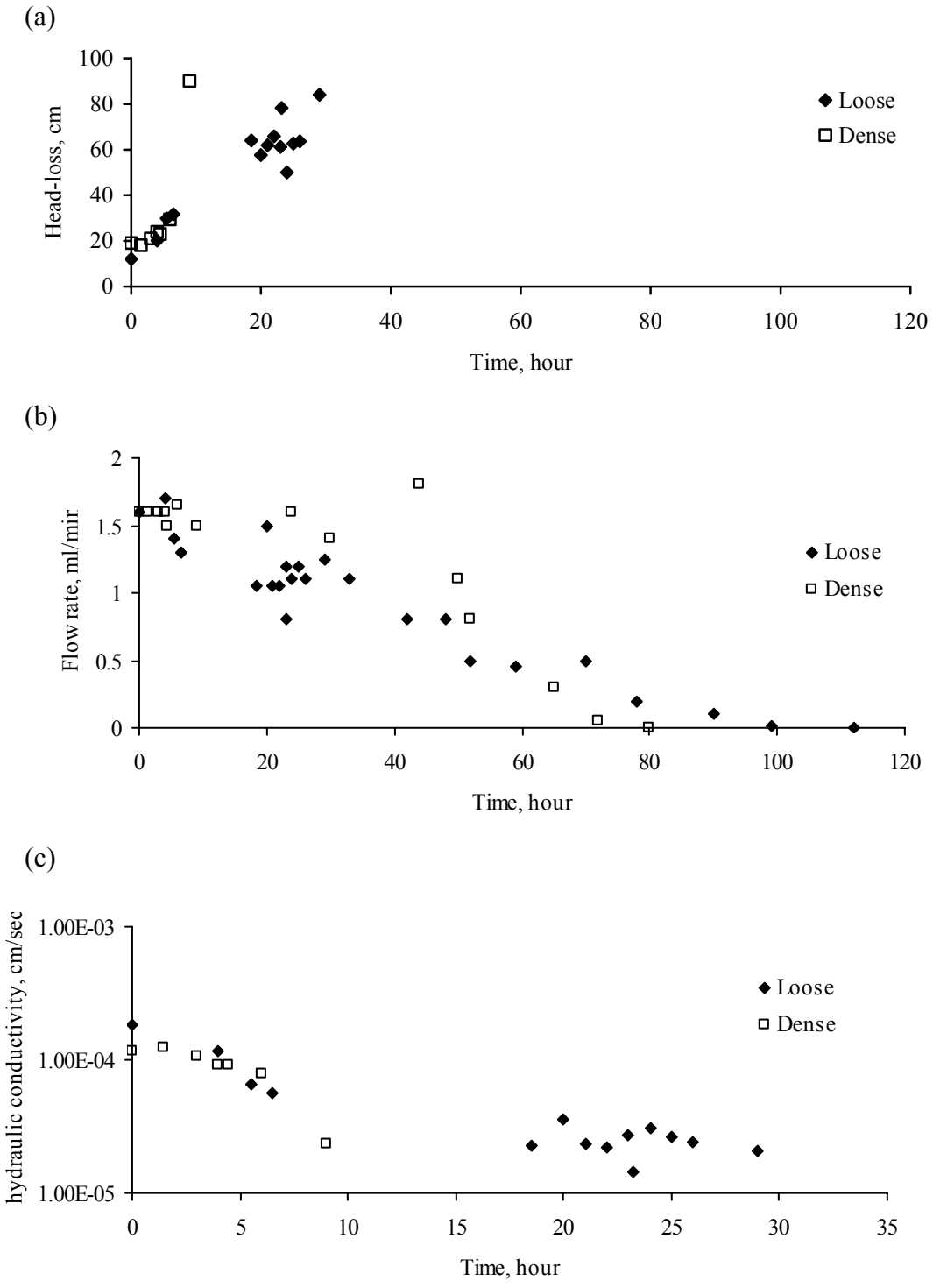

Figure 5.5 Changes in (a) head-loss (b) flow rate and (c) hydraulic conductivity and in CMBR system with loose and dense compactions.

decrease to about zero after 75 hours and 100 hours of incubation in the dense and loose compaction columns, respectively, mainly due to plugging in the porous media.

5.3 EVALUATION PERFORMANCE OF BIO-CATALYSIS IN CMBR BY USING A PSEUDO-ANALYTICAL BIOFILM MODEL

The behavior of the CMBR reactor was modeled during the period in which it was at steady-state with respect to urea utilization and cell growth by using the normalized loading curve approach based on the pseudo-analytical biofilm model developed by Rittmann et al. (1993) and described in Section 3.3.2. The four types of input parameters for the model-- microbial parameters, soil properties, fluid parameters, and biofilm characteristics-- are summarized in Table 5.1. Among these parameters, biofilm density and biofilm thickness were measured as described in Section 3.3.3 and were estimated to be about 11 mg/cm^3 and 0.0074 cm, respectively. These values differ significantly from the typical values of 40 mg/cm^3 and 0.003 cm, respectively, reported by Rittmann (1982b) and Rittmann and McCarty (2001). Specifically, the biofilm developed in the CMBR was thick, which can protect cells from detachment caused by fluid shear stresses; however, the biofilm density, X_f, was lower than typically reported. The implications of this are explained further below.

According to Equations 3(11)-3(27), via normalization of the substrate concentration and flux, normalized loading curves can be constructed as shown in Figure 5.6. Although only one condition was carried out in the current study to compare with the ideal normalized loading curve, this condition closely matches to the predicted normalized loading curve. The experimental conditions resulted in a $J_{ss}/J_R > 1$; thus, the

Table 5.1 Required parameters in simulating ureolysis in CMBR

Kinetic parameters	**Values**
K, mg/cm^3	27.6
q, mg_s/mg_a-d	20.2
μ, day^{-1}	11.1
b', day^{-1}	0.1
Y, mg_a/mg_s	0.55
Biofilm characteristics	**Values**
Thickness of the diffusion layer, L, cm	0.032
Diffusion coefficient, D, cm^2/day	1.296
Diffusion coefficient in biofilm, D_f, cm^2/day	1.0376
Mass density, X_f, mg/cm^3	11.1
Biofilm thickness, L_f , cm	0.0074
Soil parameters	**Values**
Diameter of sand particle, cm	0.046
Porosity,ε	0.57
Fluid parameters	**Value**
Flow rate, Q, cm^3/d	2282
Absolute viscosity at 20℃, g/cm-d	1.158
Water density at 20℃, g/cm^3	0.998
Superficial flow velocity, cm/d	12.51
Reynolds number	2.31
Schmidt number	0.895
Steady state substrate concentration, S, mg/cm^3	1.8

Table 5.2 Parameters obtained from the pseudo-analytical model for using in normalized substrate loading curve

Parameters	**Value**
Dimensionless of S_{min} , S_{min}^*	$9.1*10^{-3}$
The ratio of external mass transport to maximum utilization rate, K^*	14
Dimensionless substrate conc., S^*	0.065
Coefficient for S_s^*, and S_R^*, α	1.954
Coefficient for S_s^*, and S_R^*, β	0.5283
Dimensionless of S at the biofilm/liquid boundary, S_s^*	0.061
Reference actual steady state flux, J_{ss}^*	0.056
Actual steady-state flux, J_{ss}, mg_s/cm^2-d	4.467
Dimensionless of S at the biofilm/liquid boundary at f=0.99, S_R^*	0.0253
Dimensionless of reference flux, J_R^*	0.0266
Reference flux, J_R, mg_s/cm^2-d	2.12

Note that S^* and J_{ss} are obtained by using steady-state CMBR data (e.g., S is 1.8 mg/cm^3).

current CMBR is classified as being in the high-load region according to Rittmann and McCarty (2001). In this region, any changes in flux can have a significant impact on steady-state substrate concentrations, due to the system being governed by mass-transport resistance (Rittmann and McCarty 2001). In addition, according to Rittmann (1993) with $J_{ss}/J_R>1$, continuous biofilm formation is expected consistent with the thick biofilm, L_f = 0.0074 cm/ However, the low X_f value of 11 mg/cm^3 suggests that the "biofilm" is not entirely due to biomass accumulation, but rather also contains mineral deposits due to biocalcification. This hypothesis is supported by the fact that the percentage of calcium crystals attached onto the sand grains (i.e., 68% by weight as $CaCO_3$) was much higher than that of the biomass density (i.e., 0.4% weight as VSS). Furthermore, according to the X-ray analysis, the compositional profile of the crystal on the surface of the sand grains indicates that the total calcium content is 25% by weight, which is also much higher than the biomass density (this is discussed further in the SEM and EDS Analysis Section). These observations suggest that the plugging of the column in the current study was mostly due to the formation of $CaCO_3$, and not biomass accumulation, which has been the significant factor in previous studies (Taylor and Jaffé 1990, Rittmann et al. 1993).

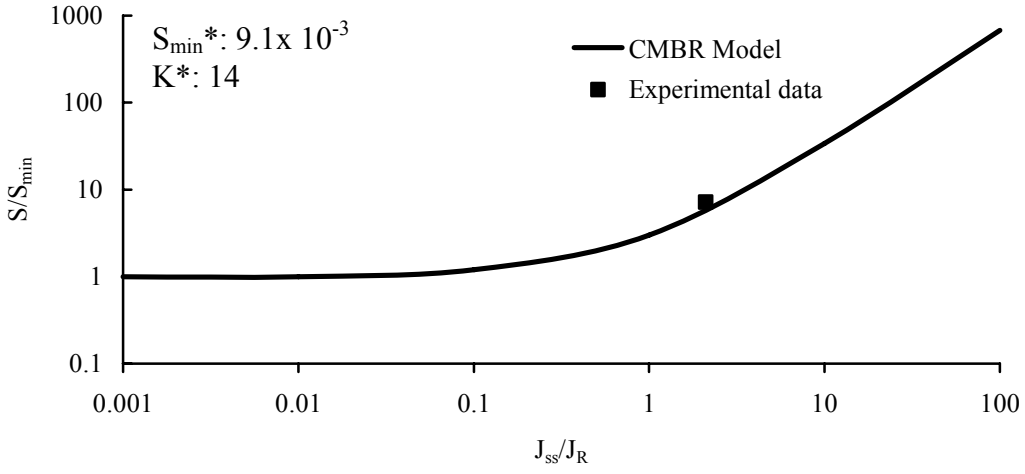

Figure 5.6 Modeled and observed normalized substrate and flux in the steady-state biofilm.

5.4 THE EFFECT OF TYPES OF *B. PASTEURII 11859* ON BIOLOGICAL TREATMENT

There were three types of cells, resting, dead and live cells, used in the CMBR system. Figure 5.7 presents the CBR test curves for one of the cell concentrations utilized (i.e.,10^7 cells/mL). As seen in Figure 5.7, the stress increases with piston penetration due to an ongoing biomineralization in testing of loose sand (D_r=35%) treated with live cells while the recorded stress value is pretty constant throughout the column if the treatment is performed with dead or resting cells. It is believed that the presence of biotic conditions is not the only reason and porosity of the sand also has an effect on the observed behavior. This can be clearly seen when the stress is plotted versus penetration depth for dense sand (D_r=85%) in Figure 5.8. Higher relative density of the soil contributes to efficiency of bio-cementation in the case of live cell treatment and, as a result, stress increases with depth. Figure 5.7 shows the CBR values for the upper 12.7 mm (0.5 inch) penetration depth inside the columns. The results are also summarized in Table 5.3. Both loose and dense sands gain strength as a result of microbial treatment. Among three types of cells, live cells increase the CBR especially in case of dense sands due to possible formation of bio-induced crystals (Ramachndran et al. 2001, DeJong et al. 2006). This crystallization process increases the CBR of sand by up to 5.8 times, similar to an increase observed in shear testing of gypsum-cemented sands by DeJong et al. (2006). There are two other possible reasons for the relatively lower CBR values observed for loose sands. First, generation of CO_2 and NH_3 can retard the pore-scale flow in the columns and slow down the precipitation process. Second, the microbiologically formed calcium precipitates may attach themselves onto the gas

molecules and thereby decrease the efficiency of the entire biomineralization process (Seki et al. 1998). However, the attachment of calcites onto the gas bubbles may not contribute to the compressive strength since gas generation influence the bacterial crystallization and those crystals may be unstable (Mitchell et al. 2005). Lian et al. (2006) studied the interaction between calcite induced bacteria and crystal formation and indicated that bacterial colonization could either promote or prevent the further development of the crystal faces. Ramachandran et al. (2001) made similar observations in testing of concrete cracks treated with *B. pasterurii*. Their analyses showed that limited pore spaces in the treated concrete affected the distribution of compressive strengths along the depth.

The resting and dead cells, on the other hand, do not significantly contribute to CBR. The only exception to that is the dead-cell treatment of loose sand. As explained in Section 3, the flow in the columns is from bottom to top. The bacteria at the bottom of the column are likely to take the nutrient or oxygen and therefore there is a possible nutrient and oxygen limitation for the bacteria at the top of the column. For instance, the average dissolved oxygen concentrations in the columns were 8 ppm and 3.5-6 ppm at the bottom and top of the columns, respectively during the incubation. As a result, the live cells at the top of the column do not exhibit the expected behavior and result in lower CBR than the dead or resting cells. On the other hand, this phenomenon is not observed in testing of dense sand as the relatively low porosity of the sand offsets this negative effect introduced by the lack of nutrients and oxygen at the top of the column.

As seen in Figures 5.7 and 5.8, the dead and resting cells increase the CBR of the dense sand at deeper parts of the columns (i.e., penetration depths greater than 40 mm).

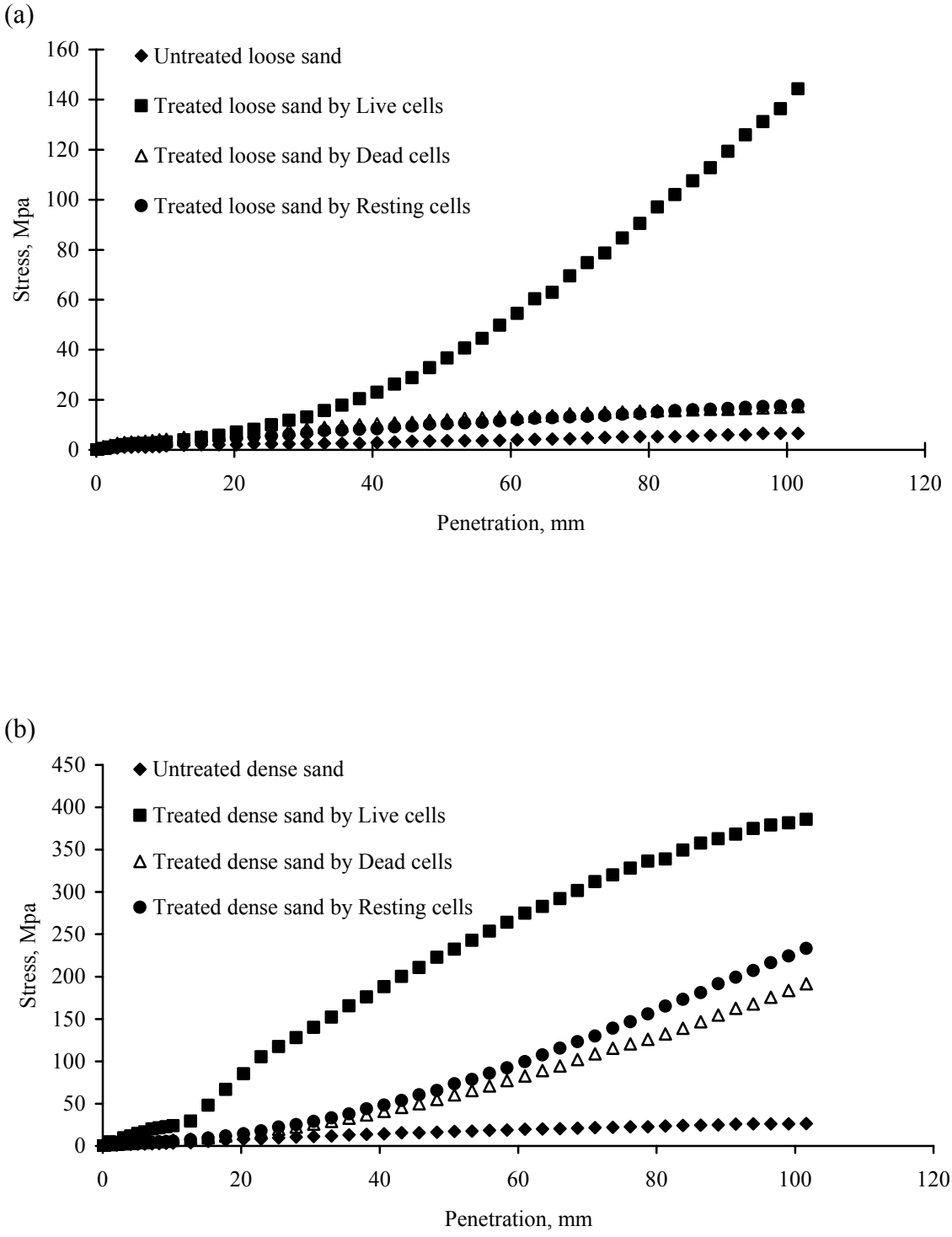

Figure 5.7 The stress of treated sands with 10^7 cells/mL of cell number corresponding to penetration in California bearing ratio test either for (a) the loose compaction or for (b) the dense compaction.

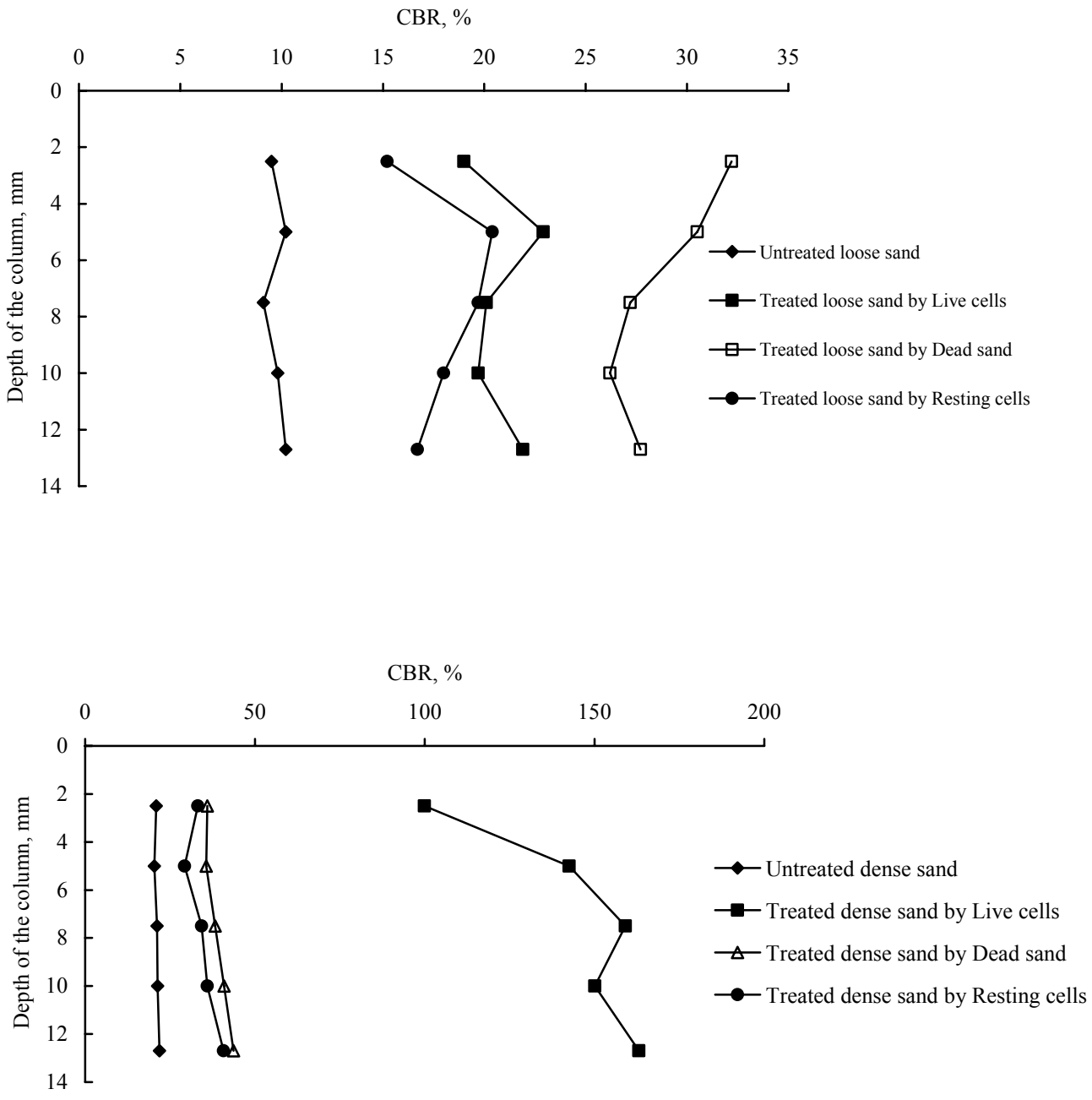

Figure 5.8 The variation of CBR number determined with different depths of CMBR columns in presence of dead cells, resting cells or live cells

Table 5.3 The summary of California Bearing Ratio tests of CMBR systems with different experimental conditions.

Experimental conditions	Loose					
	Blank	Dead cells		Resting cells		Live cells
Depth, mm	0 cells/mL	10^3 cells/mL	10^7 cells/mL	10^3 cells/mL	10^7 cells/mL	10^7 cells/mL
CBR @ 2.5 mm, %	9.5	13.3	32.2	17.1	15.2	19
CBR @ 5 mm, %	10.2	15.3	30.5	17.8	20.4	22.9
CBR @ 7.5 mm, %	9.1	18.1	27.2	18.1	19.7	20.1
CBR @ 10 mm, %	9.8	18	26.2	16.4	18	19.7
CBR @ 12.7 mm, %	10.2	17.5	27.7	14.6	16.7	21.9
Avg	9.76	16.44	28.76	16.8	18	20.72
STD	0.47	2.08	2.49	1.39	2.13	1.62

Experimental conditions	Dense					
	Blank	Dead cells		Resting cells		Live cells
Depth, mm	0 cells/mL	10^3 cells/mL	10^7 cells/mL	10^3 cells/mL	10^7 cells/mL	10^7 cells/mL
CBR @ 2.5 mm, %	20.9	13.3	36	22.7	33.2	100
CBR @ 5 mm, %	20.4	15.3	35.7	22.9	29.3	142
CBR @ 7.5 mm, %	21.2	14.1	38.3	22.1	34.3	159
CBR @ 10 mm, %	21.3	13	40.9	29.5	36	150
CBR @ 12.7 mm, %	21.9	13.1	43.7	29.8	40.8	163
Avg	21.14	13.76	38.92	25.4	34.72	143
STD	0.55	0.96	3.39	3.89	4.19	25.4

It is believed that these cells acted like organic fibers and contributed to the overall strength of the treated sand. Similar observations were made by Ramachandran et al. (2001) in a study conducted for microbial treatment of concrete cracks. Improvement of sandy soils with polypropylene (PP) fibers is a commonly used technology in geotechnical construction (Consoli et al. 2003). Various laboratory studies have been conducted to evaluate the effectiveness of this stabilization technology (Lawton et al. 1993, Maher and Gray 1990, Santoni et al. 2001, Santoni and Webster 2001, Consoli et al. 2003, Michalowski and Čermák 2003, Consoli et al. 2007). In one of these studies, Lawton et al. (1993) added polypropylene fibers to uniform Ottawa sand at different percentages by weight and conducted CBR tests to study the success of fiber-treatment technology. A comparative evaluation is made by converting the bacteria concentrations used in this study to bacteria contents per weight and the results are summarized in Table 5.4. The bacteria cells have significantly lower percentage by weight values as compared to PP fibers due to a difference in their densities (i.e, the densities of cells and PP fibers are 0.011 g/cm^3 and 0.91 g/cm^3, respectively). However, the contribution to the CBR is clear. For instance, CBR of untreated loose sand increases 2.35 times as a result of 0.3% addition of dead cells while the increase is 1.85 times when the sand was blended with PP fibers at 5% by weight. In general, the increase in CBR of microbiologically treated sand is in a range of 112 to 576% while the range stays between 133 and 414% for PP-treated sand. These results suggest that the dead/resting cells are likely to act like organic fibers and contribute to the overall strength of the sand.

Table 5.4 Comparison of reinforced sand by different types of elements with various contents.

Content of different types of reinforcing elements	Types of testing sand	Reinforced Stress at 25.4 mm on CBR penetration curve, Mpa	Reference
5 % random Homopolymer polypropylene	Loose Ottawa sand/ SP	0.69	Lawton et al. 1993
10 % random Homopolymer polypropylene		1.24	
Non-reinforced sand		0.24	
10 % random Homopolymer polypropylene/ smooth	Dense Ottawa sand/ SP	3.79	
10 % random Homopolymer polypropylene/ rough		2.41	
Non-reinforced sand		1.03	
0.3×10^{-4}% uniformed dead cells	Loose sand/ SP	4.72	Current study
0.3% uniformed dead cells		7.86	
0.3×10^{-4}% uniformed resting cells		4.21	
0.3% uniformed resting cells		5.52	
Non-reinforced sand		2.34	
2.1×10^{-5} % uniformed dead cells	Dense sand/ SP	4.73	
0.21% uniformed dead cells		19.72	
2.1×10^{-5} % uniformed resting cells		10.48	
0.21% uniformed resting cells		22.27	
Non-reinforced sand		9.45	

5.5 THE EFFECT OF RELATIVE DENSITY OF THE SAND AND CELL NUMBER ON BIOLOGICAL TREATMENT

As mentioned above, the change in compressive stress corresponding to 100 mm of penetration is monitored to identify the effect of relative density of the sand on biological treatments. An example relationship between stress and penetration depth for a bacteria concentration of 10^7 cells/mL is provided in Figure 5.9. Two of the cell treatments (i.e., dead cells and resting cells) have a similareffect on CBR values. In case of loose sand, the D_r is low, the pore spaces are large and neither the dead nor resting cells fully attach onto the sand particles and, therefore, the CBR of treated sand is only 16 to 28% higher than that of untreated sand. As mentioned in Section 5.3, retardation of the flow as a result of CO_2 and NH_3 generation, and attachment of microbiologically formed calcium precipitates onto the gas molecules are two possible reasons for the decrease in the efficiency of the biomineralization process in loose sands. However, for dense specimens, the recycling flow can effectively provide the nutrient and oxygen into the relatively smaller pore spaces and the bearing strength increases from 26 MPa to 185-375 MPa (7 to 14 times increase) as a result of microbiological treatment.

Figure 5.10 shows that the CBR increases with increasing cell concentrations, regardless of cell type (i.e., dead or resting) or relative density of sand. For instance, the average stress at the 100-mm depth of the loose and dense sands treated with 10^3 cells/mL dead and resting cells is about 13 MPa and 35 MPa, respectively. The average stresses increase to 16 MPa and 200 MPa when the bacteria concentration is increased to10^7 cells/mL. Similar increases can be observed at different depths.

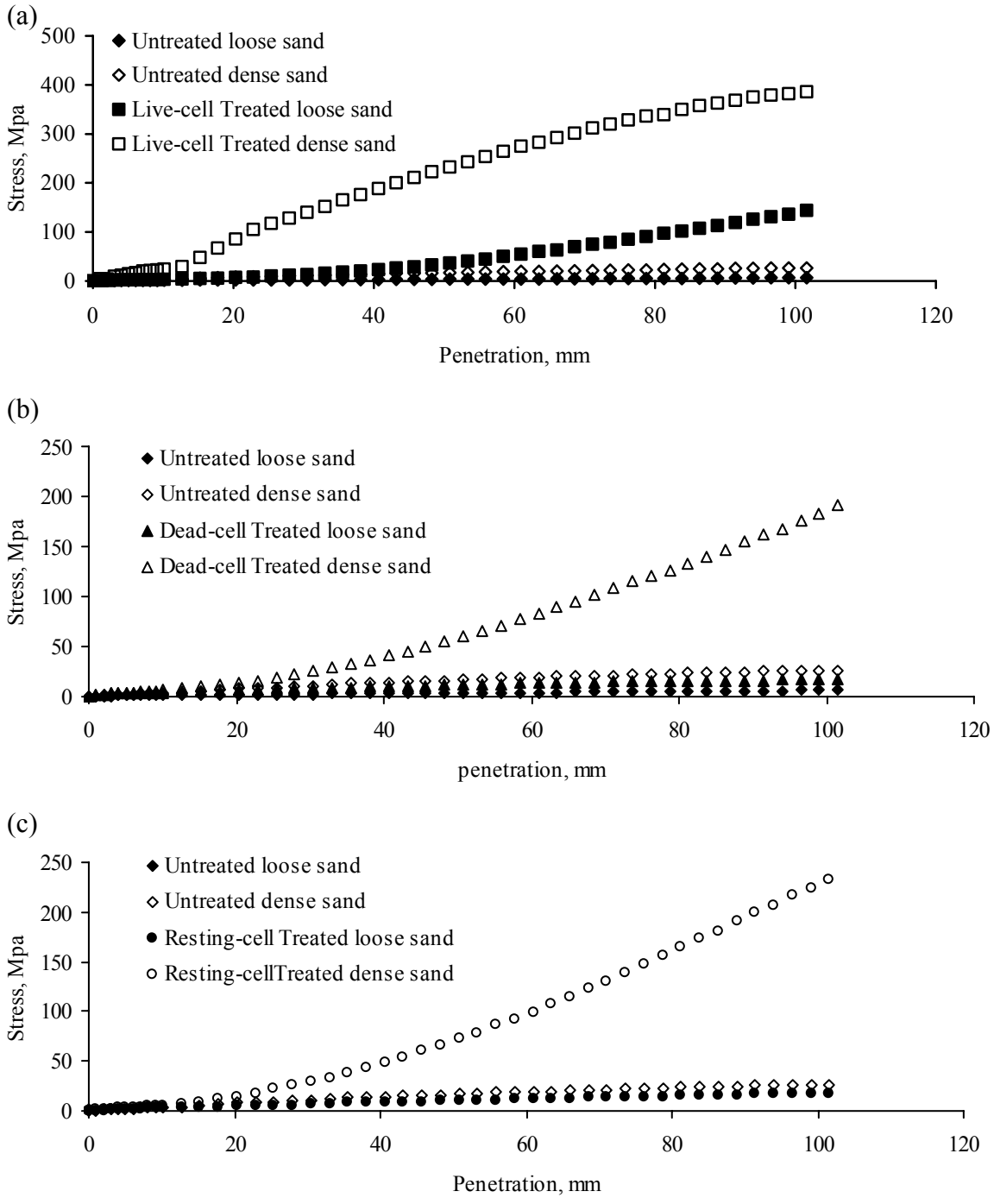

Figure 5.9 The effect of compaction on CBR stress curves in different treatments along with 10^7 cells/mL of inoculation: (a) live cells treatment, (b) dead cells treatment, and (c) resting cells treatment.

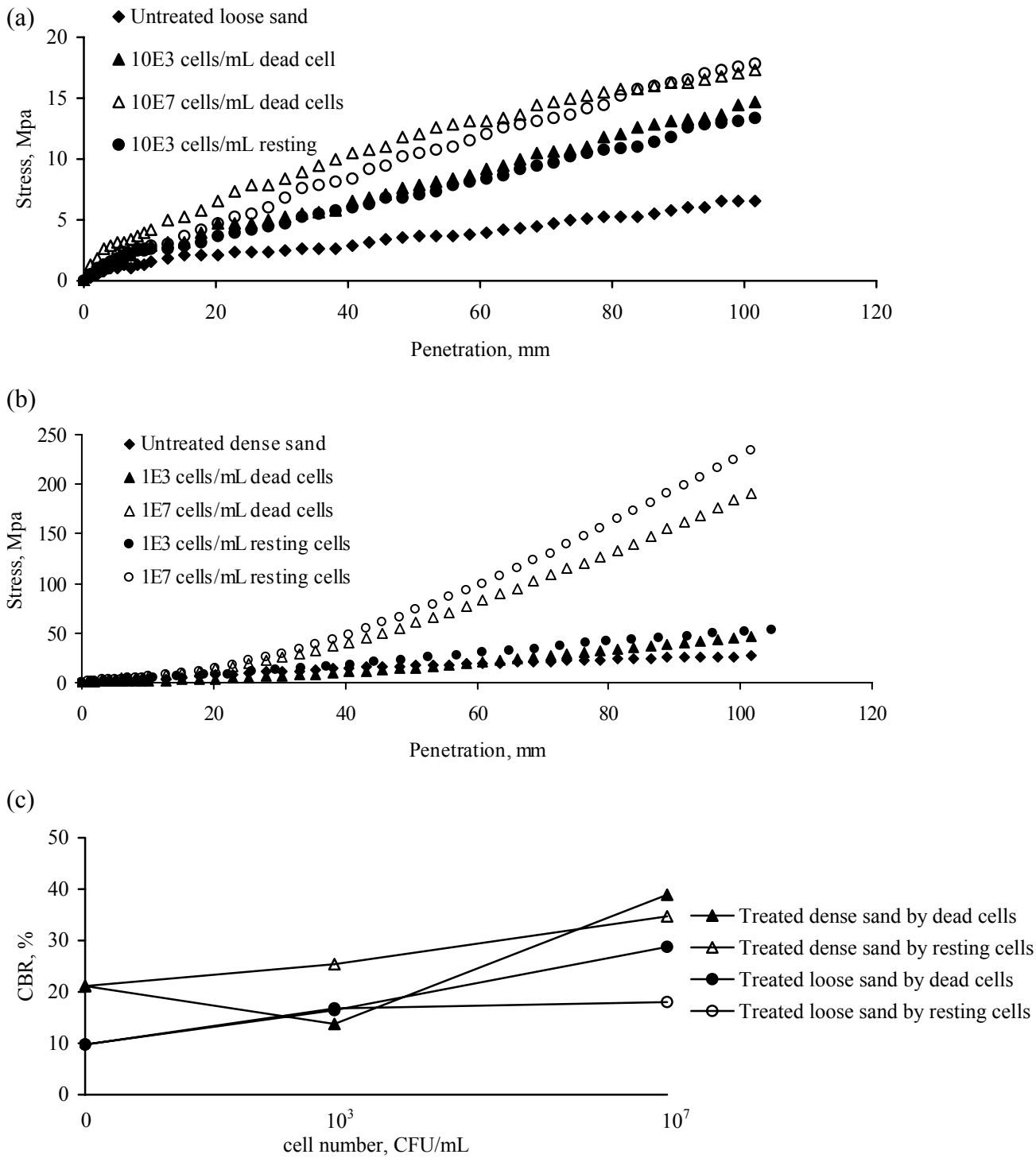

Figure 5.10 The influence of cell number on CBR stress penetration curves (a, b) and CBR number (c).

5.6 SEM AND EDS ANALYSIS

In order to examine the bonding between the sand particles occurred due to microbial cementation, the samples of untreated and treated sand were subjected to environmental electron scanning microscopy (ESEM) analysis. Chemical compositions of the samples were examined using the energy dispersive X-ray spectrometry (EDS) technique. All samples were subjected to microbial treatment with live cells prepared at 10^7 cells/mL in the CBR columns. The microbiologically cemented specimens show evidence of cementation on the particle surface and at particle contacts (Figures 5.11 and 5.12) . The calcite crystal faces formed as a result of treatment with *Bacillus pasteurii* are apparent in the highly magnified images. Similar observations were made by Dejong et al. (2006) for microbial cementation of Ottawa sand.

In order to investigate the presence of bacteria attachment onto sand particles, samples of treated sand were washed by following the procedures listed in Section 3.4.8 before SEM analysis. This step was necessary to obtain clear SEM images of bacteria attachment by eliminating some of the residues due to heavy cementation. One of the SEM images is given in Figure 5.12b. Bacteria attachment onto the sand particle surface is clearly visible. The observation is similar to the ones reported by Fujita et al. (2000) and Bang et al. (2001) for calcification of sand with *B. pasteurii*.

Further confirmation of the biological calcification was made by analyzing the presence of calcium crystals via EDS coupled with SEM. The EDS analysis was conducted on magnified SEM images of untreated and treated samples of sand and the results are given in Figure 5.13. High percentages of silica are evident as the sand contains 99.7% silica by weight. The high percentage of calcium in EDS plot of treated

(a)

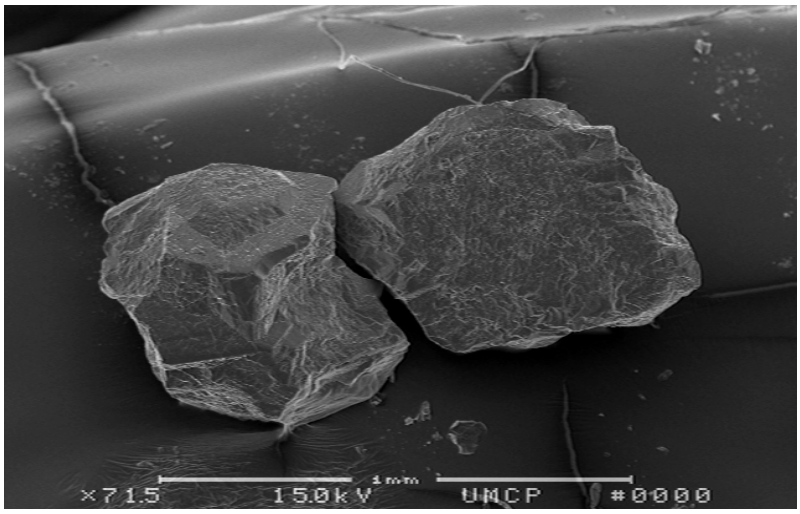

(b)

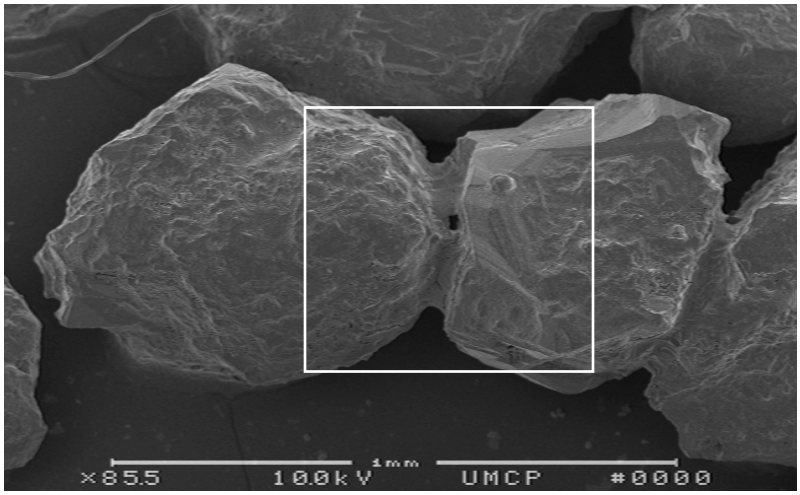

(c)

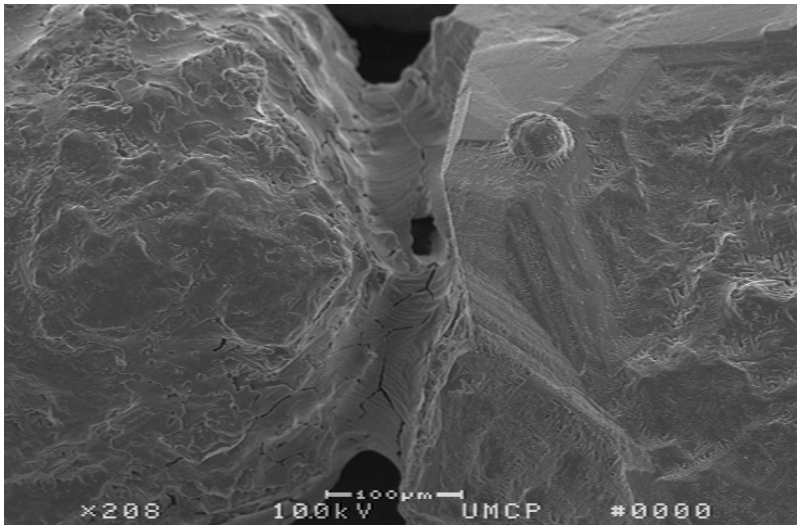

Figure 5.11 Scanning electronic micrographs of (a) untreated sand (1 mm), (b) treated sand (1 mm), and (c) treated sand (100 μm).

(a)

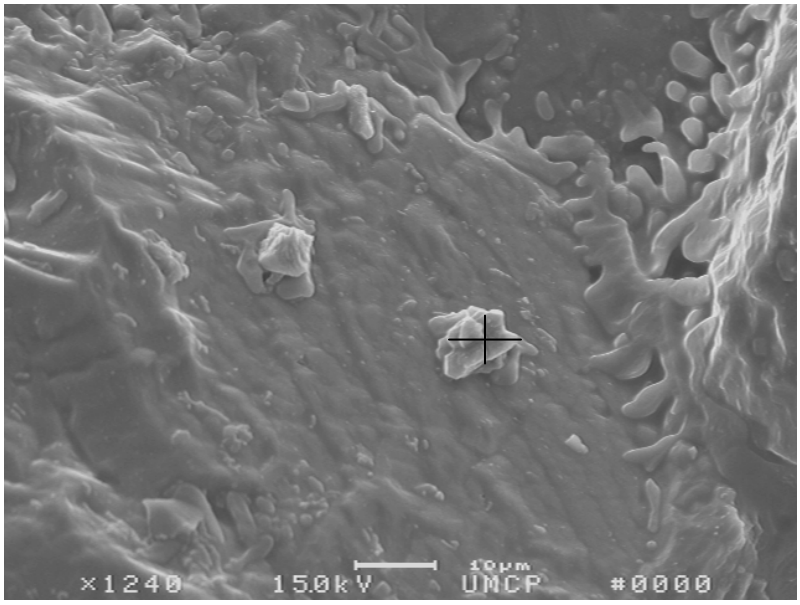

(b)

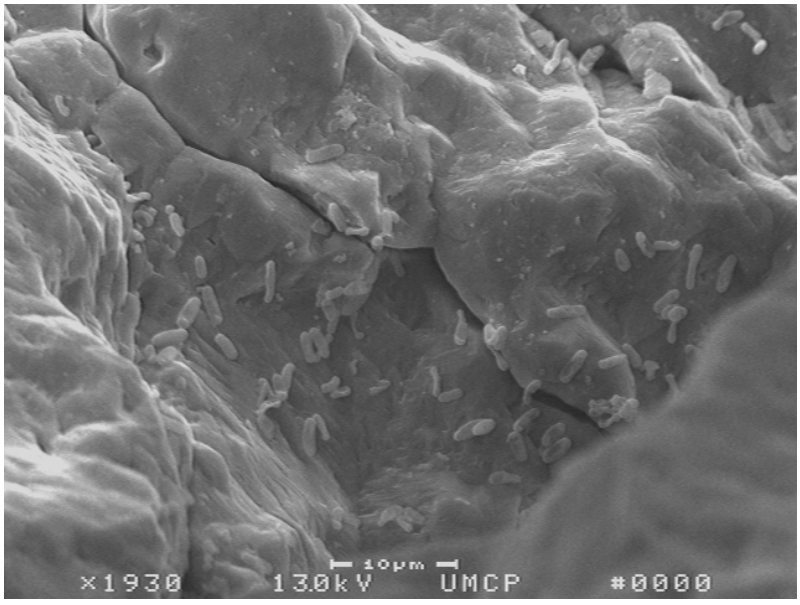

Figure 5.12 Scanning electro micrographs of (a) crystal formation (10 μm) and *B. pasteurii* attachments (10 μm).

specimen indicates that the cementation was due to microbial precipitation of calcite. It should be noted that peaks of gold and oxygen are due to specimen coating during preparation, and continuous intrusion of oxygen during SEM operation, respectively. The SEM analyses confirm CMBR model predictions that the bio-precipitation is the primary cause for pore-scale plugging of the sand inside the column.

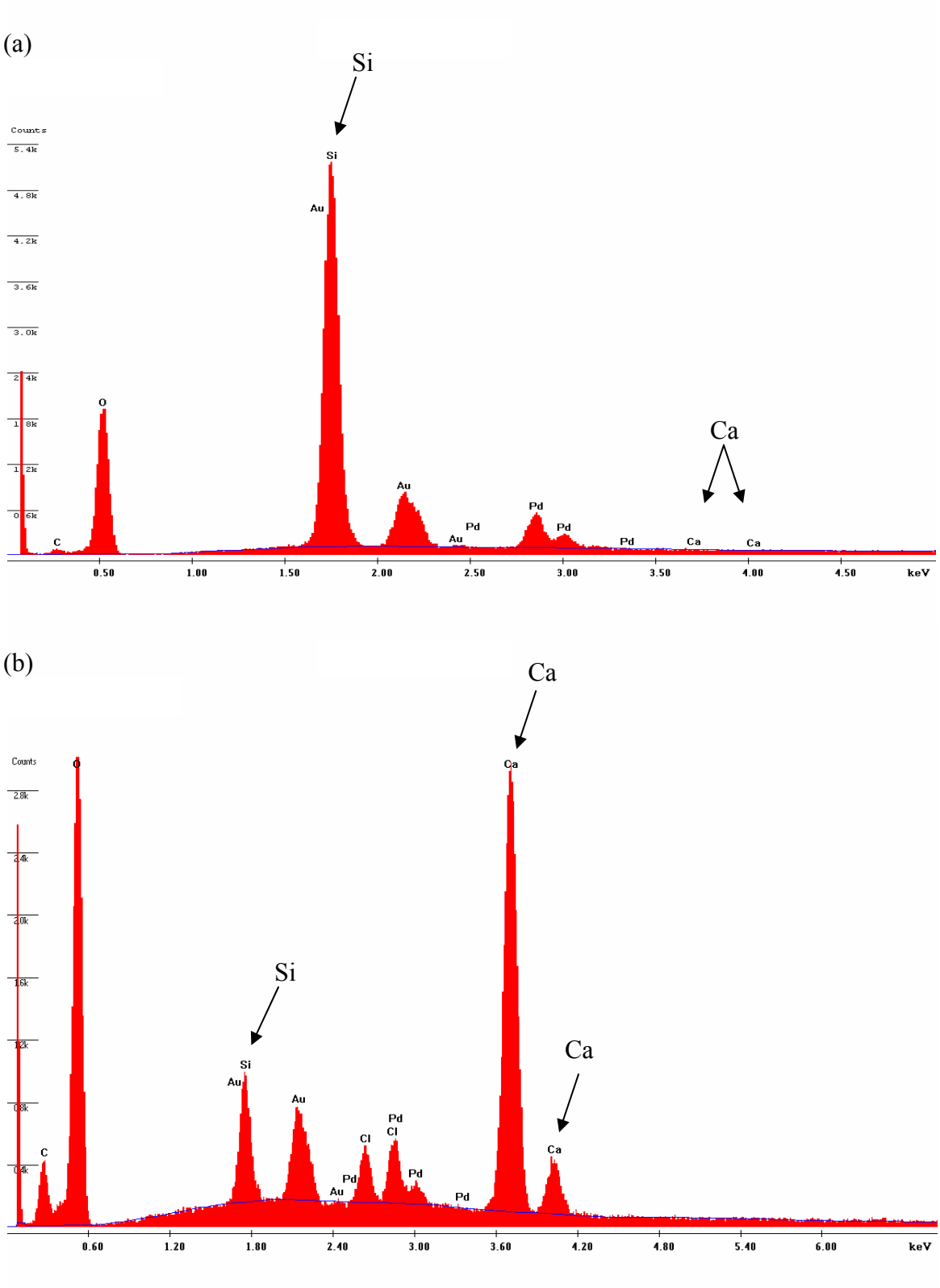

Figure 5.13 Composite profile of (a) untreated sand grains and (b) live-cell treated sand grains by using energy dispersive X-ray spectroscopy.

SECTION 6

CONCLUSIONS AND RECOMMENDATIONS

6.1 SUMMARY AND CONCLUSIONS

A series of laboratory tests were conducted to investigate the impact of soil density, cell types (i.e., dead, resting, and live cells), and cell concentration on soil geomechanical properties. An optimal mineralization environment was created in completely stirred tank reactors (CSTR) and completely mixed biofilm reactors (CMBR) specially fabricated for the study. Direct shear tests and California bearing ratio (CBR) were conducted on the soils subjected to microbial $CaCO_3$ precipitation in the CSTRs and CMBRs, respectively. Finally, scanning electron microscopy study (SEM) and energy dispersive spectrometry (EDS) techniques were utilized to examine the cementation by microbiological process within sandy soil matrix and identify the composition of crystals, respectively. The following conclusions are derived from the study:

1. The bio-catalysis of urea in the CSTR system was achieved after 74 and 29 hours of incubation by the low and high concentrations of bacteria, respectively. For the low bacteria concentration, a lag period of 36 hours was observed. Overall, when the degradation of urea occurred, the pH in the system increased to 9.1 due to ammonia production and free calcium decreased, presumably due to $CaCO_3$ precipitation.

2. All specimens treated by different types of *B. pasteurii* cells under different conditions (i.e., live, dead, resting) experienced an increase in their shear strength. The strength improvement was mainly reflected in friction angles, and the effect on cohesion was minimal. However, the live-cell treatment seems to have a more profound effect on the friction angles as compared to the other two cell types. The increase in friction angles with live, resting, and dead cells was 42-31%, 20-22%, and 25-28%, respectively. It is believed that the dead cells probably contributed to strength by acting like organic fibers. The resting cells most probably also died due to a lack of nutrients and acted like organic fibers as well. Regardless of cell types, a more significant improvement was observed at high cell concentrations.
3. During shearing stages, the specimens treated by live cells resulted in higher volume changes than the dead cells for both dense and loose sands due to a formation of crystals. Moreover, the volume change of specimens treated with resting cells has a similar behavior to that of specimens treated with dead cells in the loose compaction, suggesting that both act like organic fibers.
4. The bio-catalysis of urea in the CMBR system was completed after about 35 hours of incubation regardless of the relative density of the soil. The trends for pH and calcium due to degradation of urea were similar to the ones observed for the CSTR system. Hydraulic conductivity of the treated sand decreased to about 2.5×10^{-5} cm/sec, and no flow was observed after 75 and 100 hours of incubation in dense and loose compactions, respectively (i.e., biological plugging of sand occurred). The biomass density and biofilm thickness in the CMBR systems were about 11 mg/cm^3 and 0.0074 cm, respectively, which differ significantly from the

typical values of 40 mg/cm^3 and 0.003 cm, respectively, reported by Rittmann (1982b) and Rittmann and McCarty (2001). Thus, the biofilm produced in the current study was physically thick and could protect the cells from detachment caused by fluid shear stresses. However, the density of the biofilm was low, suggesting the film orgconsist of materials other than biomass. Consistent with this relatively higher percentage of calcium crystal attached onto the sand grains compared to the biomass density (i.e., 68% $CaCO_3$ by weight versus 0.4% volatile suspended solids by weight), and the EDS analysis of the SEM images suggested that the specimen plugging inside the columns was mostly due to the formation of $CaCO_3$, and not biomass accumulation as in previous studies (Taylor and Jaffé 1990, Rittmann et al. 1993).

5. Similar to the observations made in the direct shear tests, a more profound increase in California bearing ratio (CBR) values was evident for the live-cell treatment than other treatments by dead or resting-cells. The dead cells acted like organic fibers; however, the observed strength increase was 1.27 times higher than the increase reported for sands treated with polypropylene fibers in the existing literature.
6. In all cases, CBR increased with increasing cell concentrations, regardless of cell type (i.e., dead or resting) or relative density of sand. A significant increase was observed in case of dense sands, and especially under biotic conditions the strength increased by 100 to 142%. The increase was relatively small in case of loose sand (16 to 28%) possibly due to retardation of the pore-scale flow and slowing of the precipitation process as a result of generation of CO_2 and NH_3 in

the columns. Another reason could be the formation of the microbiologically formed calcium precipitates which may attach themselves onto the gas molecules and thereby decrease the efficiency of the entire biomineralization process.

6.2 PRACTICAL IMPLICATIONS

As proven in current study, microbially plugged process by precipitating $CaCO_3$ does not only decrease hydraulic conductivity of the sandy soil, but also increase bearing capacity and friction angle of the sandy soil. The process has potential for use in geoenvironmental capping applications. The retirement of large industrial waste storage facilities in accordance with environmental regulations has become a critical cost issue for industry and a challenge to the geotechnical community. Many facilities were constructed prior to the emergence of modern environmental regulations and contain a variety of contaminated high water content materials. Some examples are PCB (polychlorinated biphenyls) containing wastewater treatment sludges, contaminated harbor dredgings, waste pickle liquor sludges, asbestos-containing sediments, mine tailings, and contaminated river bottom sediments. These materials are contained typically in surface impoundments such as lagoons, ponds or old quarries.

Capping, if practical, often offers the least expensive solution to remediation of facilities contaminated with sludges or similar high water content geomaterials contained in surface impoundments. In this approach, the material is left in place and isolated so that accidental falling of humans and animals and ingestion of contaminated material is prevented and, if required, infiltration of rain and surface water is impeded. Caps can be impervious if infiltration of water and generation of leachate is to be limited or pervious

when leachate generation is not a concern such as in natural attenuation sites and/or with certain type of contaminants (e.g., PCBs are quite insoluble and do not transport with water). While formation of a surface crust is an important function for providing a good construction platform on soft geomaterial, effective drainage is another function that is critical for long-term performance. Bacteria-induced calcite precipitation is expected to provide these duties in capping applications, by increasing the strength and slightly decreasing the hydraulic conductivity of the candidate capping material, which is typically a sandy soil.

Moreover, Knobel et al. (1992) suggested that, some metal contaminants, especially divalent metals (i.e., Pb, Zn, and Cd) or even radionuclide (i.e., ^{90}Sr or ^{60}Co) can be captured as co-precipitates or adsobates during calcite precipitation. This can have a clear advantage if the capped soil is contaminated with one of the metals. Furthermore, the moicrobially-induced calcite precipitation can be coupled with bioremediation (i.e., and integrated remediation technology) to quarantine the undesired substances. For instance, these unwanted substances can be isomorphically replaced with Ca^{2+} in the lattice structure or integrate into interstitial sites of calcite precipitates (Warren et al. 2001).

Microbiological processes can also assist in the control of dust in heavy haul roads (e.g., mine roads), and repair of aircraft runways. The rapid and controlled improvement of soils using cost-effective solutions in these applications is particularly important in military operations, such as fast construction of military bunkers, barracks and helicopter landing pads, landing of military aircraft, and deployment of tanks and military vehicles. For instance, the rapid landing of airplanes in very brief intervals of

time applies dynamic loads to the soil resulting in very intense compression and decompression cycles. The foundation, being thus subjected to fatigue stresses, then may undergo fracturing up to the point of collapse. Under these conditions, both very thick layers of aggregate, and frequent and expensive maintenance are required. Although the maintenance costs are high, by far the most important cost factor is the reduction in revenue caused by the disruption of services. The problem becomes more cumbersome and expensive when the rapid reconstruction of the system and repair of the runways are needed. Increase of soil strength, especially near the surface, can be very beneficial in these types of applications. It is believed that calcite precipitation occurring as a result of microbiological reactions is highly likely to provide this strength increase.

Finally, the process has potential for use in erosion control of naturally occurring surfaces, such as slopes, whether they have been deforested or naturally exposed, with application to dust control at construction sites, especially when issues of dust raise environmental concerns, and in military operations. Secondary potential applications for use exist at campgrounds, on trails, in parks, and on race tracks, to name only a few. In these cases, a light temporary surface crust that is permeable to water can be created for dust control or large quantities may generate results similar to the lime stabilization.

6.3 LIMITATIONS OF THE METHODOLOGY

There appear to be certain limitations on the potential for these effects. Firstly, the process is effective in calcium-rich soils, which are abundant in arid and semi-arid regions in the U.S, mainly in the western states and some parts of the Great Plains. These soils contain free carbonates near the surface and throughout, typically ranging from 5 to

25% carbonate by weight (Brady and Weil 2002). The process has not been found to be effective in clayey soils, which have low hydraulic conductivity in nature and do not have the aerobic conditions necessary for microbiological reactions to occur. Secondly, aerobic zone in soils is about 15-20 cm that is critical for *Bacillus pasteurii* in order to keep the aerobic bacteria alive (Reichenbach 1999). Therefore, geotechnical applications that benefit from shallow effects of increased strength and decreased permeability are the primary ones at this stage. As understanding of the processes develops, however, other applications are expected to present themselves.

In situ contamination can decrease the effectiveness of bacteria-indiced calcite precipitation. For example, MTBE, and BTEX are common contaminants in the aquifer due to their relatively high solubility. These contaminants are toxic to human beings as well as bacteria; therefore, the bacterial activity can be significantly inhibited presenting the soils contaminated with these compounds or other similar petroleum hydraocarbons. The level inhibition is related to the aqueous concentration level for these contaminants.

As discussed in Section 2, the efficiency of biological plugging process is related to particle size of the soil employed. While the *Bacillus pasteurii*-induced calcite precipitation process seems to be effective in coarse sandy soils, shear stresses induced high field flow rates can affect the accumulation of biofilm (Taylor and Jaffé 1990, Rittmann et al. 1993) as well as the crystallization of calcite.

6.4 RECOMMENDATIONS FOR FUTURE RESEARCH

The following subjects can be beneficial to enhance the efficiency of bio-mediation of calcification in soils.

1. Crack developments resulting from freezing and desiccation may also affect biomineralization. Assessment of the durability of the microbiologically treated soils when exposed to such climatic stresses will be the topic of future research, considering the exploratory nature of the proposed work.
2. In the field application, moisture is one of environmental factors that can significantly affect bacterial activities. Saturation as designed in current study is not a normal case in the nature environment. In addition, high water content somehow retards biological mechanisms (Cookson 1995). The optimum moisture for biocalcification in soils shall be studied in the future.
3. As presented in this study, the availability of pore volume can positively affect the deposition of calcites, nevertheless, the deposition of calcites can not directly response to strength improvement in soils due to interfere with gas generation that can be nucleation sites. Thus, in order to maximize biocalcification, optimum relative density can be the topic of future research.

APPENDIX A

The determination of soil properties and their measurements

Before use this testing sand, three physical properties were needed to determine for the further experiment design, including soil classification, specific gravity, maximum and minimum of densities. Each measurement procedure was described as follows.

A.1 SOIL CLASSIFICATION

The particle size distribution of the sand was performed by sieve analysis, following procedures of particle-size analyses (ASTM D421-422). First, 1 kg of sand was prepared and oven dried for 24 hours at 105℃ to eliminate the effect of moisture on the soil classification. Then, a stack of sieves varying from larger opening sizes to smaller opening sizes was built, and a collecting pan was placed under the stack of sieves for collection of the particles passing the #200 sieve. The sieve stack was placed on the sieve shaker and shaken for 5 to 10 minutes. Subsequently, the residual weight of sand on each sieve was quantified, and the percent passing through each sieve was calculated.

A.2 SPECIFIC GRAVITY

For determination of specific gravity of sand, Standard Test Methods for Specific Gravity of Soil Solids methods were used (ASTM D854 and AASHTO T 100) The procedures are described below. Two representative samples between 5 and 6 g were

added to two 25 mL volumetric flasks, respectively. Next, the flasks were filled to about two-thirds of the total volume with deaerated water. Subsequently, vacuum was applied to the flasks for at least 10 minutes until boiling of the water in the flask was observed due to the decrease of the air pressure. When no air bubbles were observed, the flasks were detached from the vacuum device and filled with deaerated water. Finally, the weight of flasks and temperature were recorded, and weigh the weight of sand with water afterward. The determination of specific gravity was computed by following equations.

$$Gs = \frac{\alpha M_s}{M_{bw} + M_s - M_{bws}} \quad \text{.....(A-1)}$$

$$\alpha = \frac{\rho_T}{\rho_{20^\circ c}} \quad \text{.....(A-2)}$$

where Gs is Specific gravity, M_s is Mass of dry soil, M_{bw} is Mass of the flask filled with water at the same temperature, M_{bws} is Mass of the flask with water and soils, α is Temperature correction coefficient, ρ_T is The density of distilled water at temperature T, and $\rho_{20℃}$ is The density of distilled water at 20℃.

A-3 MAXIMUM AND MINIMUM OF DENSITIES OF TESTING SAND

For the geomechanical tests described below, specimens with appropriate densities to mimic either loose or dense compactions as used in the field. To achieve these densities, several experimental trials were performed to determine the adequate minimum and maximum densities of the sand. Specifically, to attain the minimum and maximum densities laboratory tests were conducted by following the procedures described by standard test methods for minimum index density method (ASTM 4254) and standard test methods for maximum index density method using vibratory table

(ASTM 4253). First, the standard mold was filled up with oven-dried sand as loosely as possible by using a funnel. Next, the surplus sand from the surface of the mold was trimmed off using a straightedge without compressing the sand in the mold. Finally, the mass of sand in the mold and the weight of empty mold were recorded and the minimum density was calculated.

For determination of maximum density, the standard mold was filled up with oven-dried sand and stroked the sides of mold so that the surcharge base plate is able to be set into the mold tightly before application of vibration. Next, the surcharge base-plate handle was taken off and the standard mold was attached to the vibration table. The dial indicator gauge holder was set up in each side of the brackets and the initial reading was recorded as the average of brackets. Then, the mold was attached to the guide sleeve tightly and surcharge weight was placed onto surcharge base plate. The dial readings were recorded in the same positions as described above after 8 minutes of vibration and averaged. Finally, the mass of sand and mold were recorded and the volume of the sand was calculated to determine the maximum density.

APPENDIX B

THE DIRECT SHEAR TEST RESULTS

The direct shear test was selected as the geomechanical method to determine the shear strength parameters (i.e., friction angle and cohesion coefficient) of the untreated abiotic treated and the biotic treated sand specimens. In each test, the data from consolidation stage was recorded in the format of vertical deformation versus time while shearing strength versus relative horizontal displacements corresponding to thickness change was recorded in the shear stage. To clearly understand how the specimen prepared in different treatment performs during the shearing tests, the data of all specimens in various experimental conditions are listed as follows of untreated, abiotic, and biotic experiments.

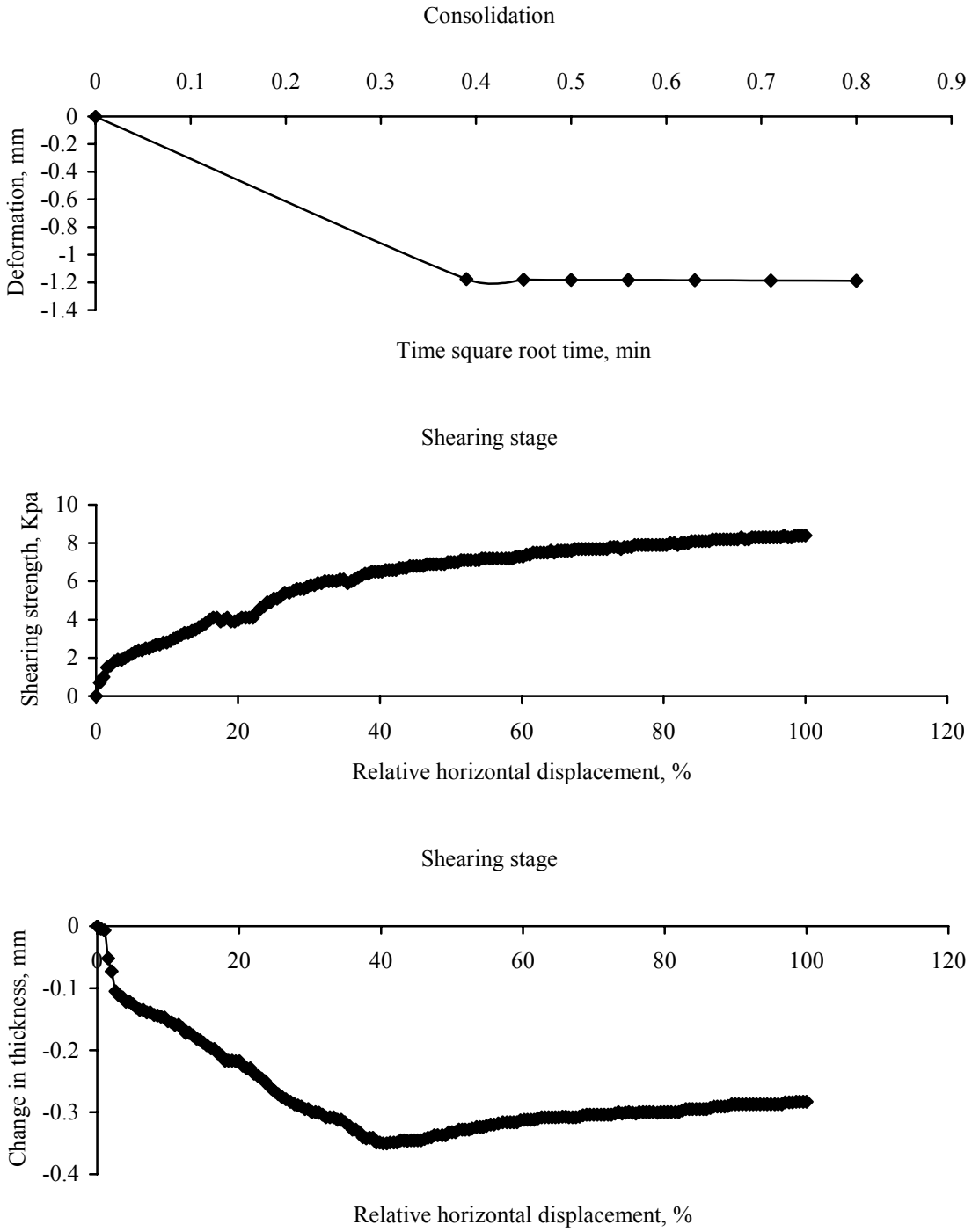

Figure B.1 11.3 kPa of normal stress was conducted in the untreated specimen with 35% of relative density, and data was recorded in (a) consolidation and (b) shearing stage, respectively. Note that vertical deformation, horizontal deformation, and peak strength were -1.648 mm, 10.725 mm and 8.4 kPa, respectively.

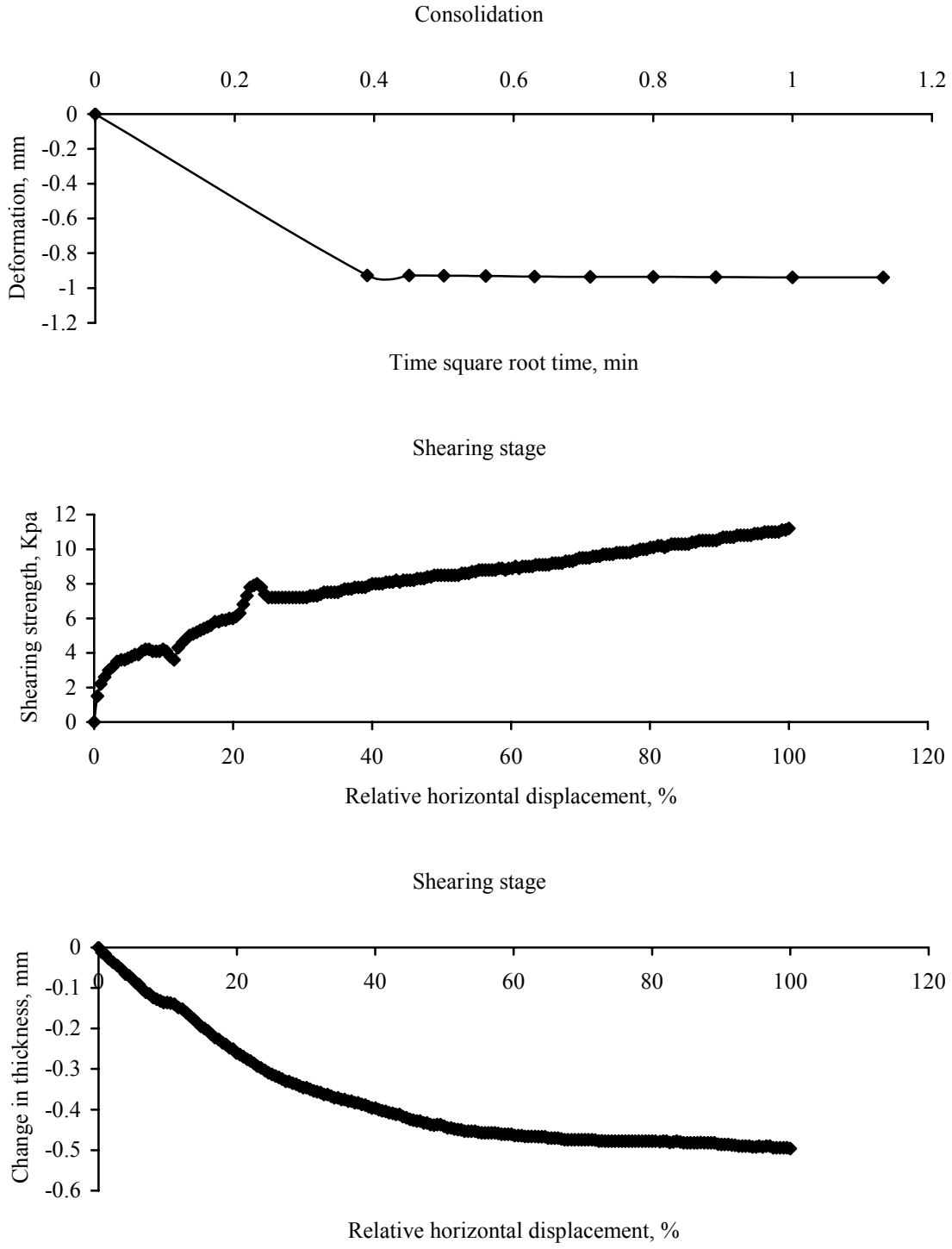

Figure B.2 16.2 kPa of normal stress was conducted in the untreated specimen with 35% of relative density, and data was recorded in (a) consolidation and (b) shearing stage, respectively. Note that vertical deformation, horizontal deformation, and peak strength were -1.571 mm, 10.716 mm and 11.2 kPa, respectively.

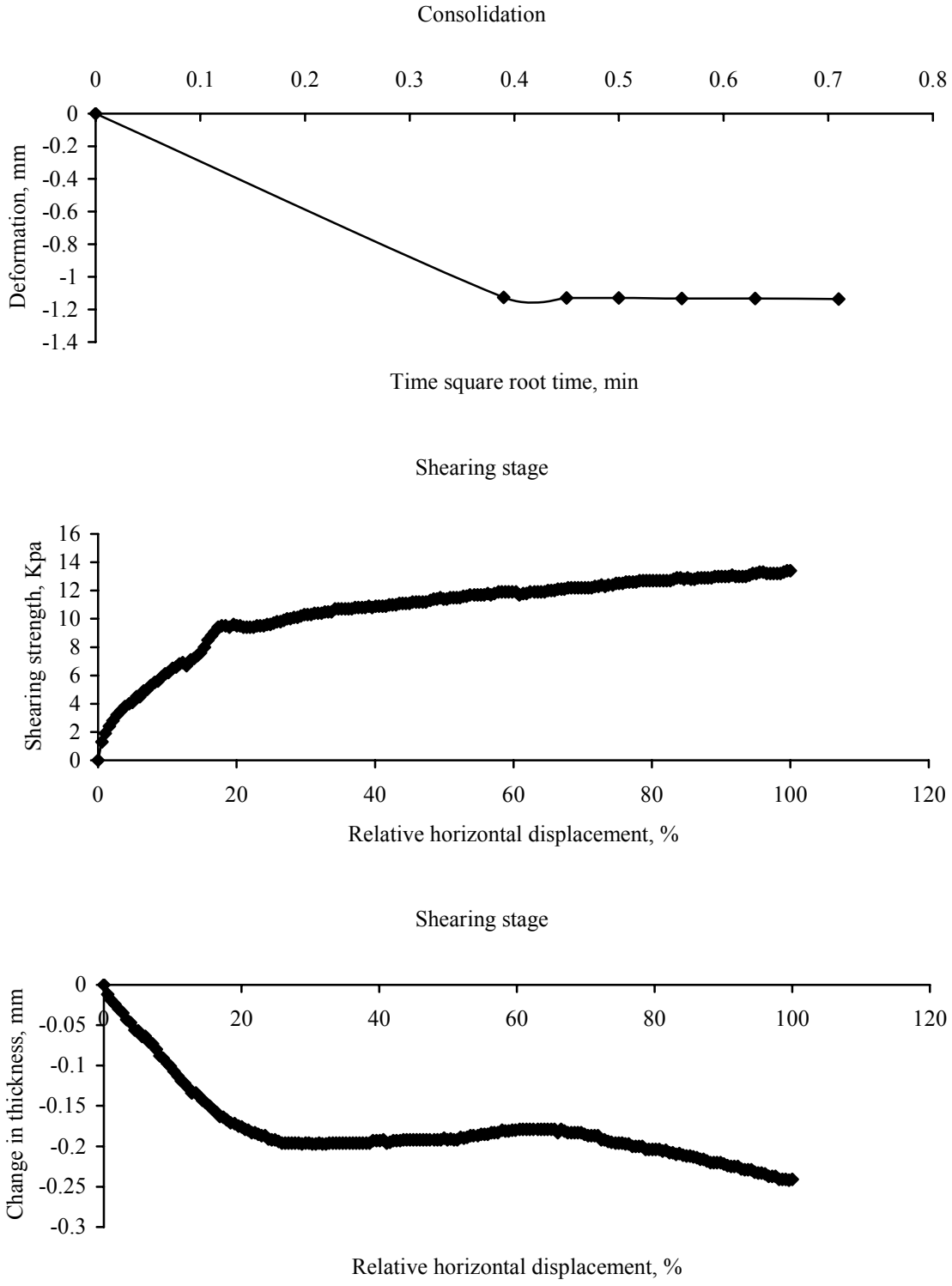

Figure B.3 21.1 kPa of normal stress was conducted in the untreated specimen with 35% of relative density, and data was recorded in (a) consolidation and (b) shearing stage, respectively. Note that vertical deformation, horizontal deformation, and peak strength were -1.442 mm, 10.781 mm and 13.4 kPa, respectively.

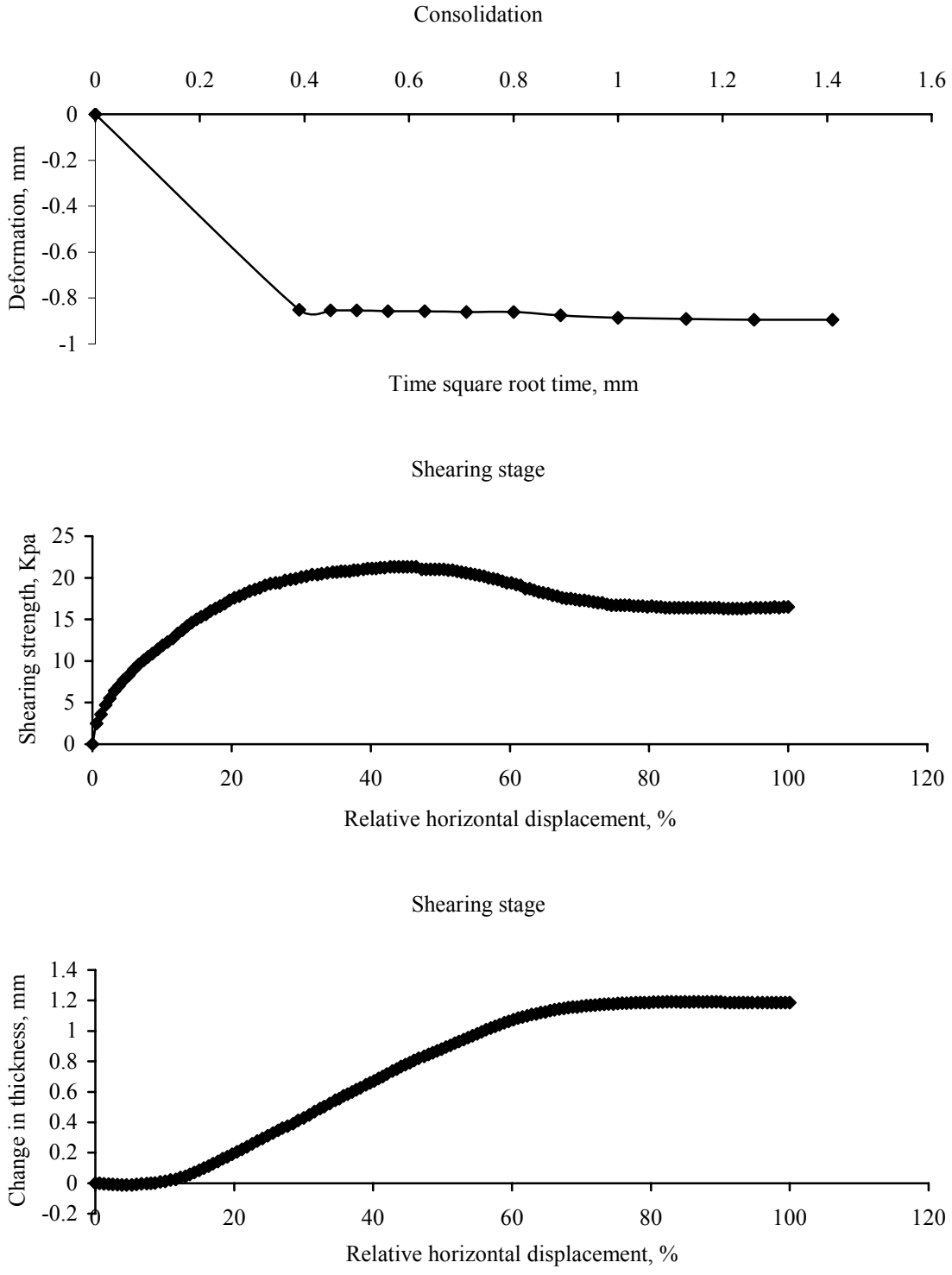

Figure B.4 21.1 kPa of normal stress was conducted in the untreated specimen with 85% of relative density, and data was recorded in (a) consolidation and (b) shearing stage, respectively. Note that vertical deformation, horizontal deformation, residual strength, and peak strength were -0.144 mm, 3.748 mm, 16.4 kPa and 21.3 kPa, respectively.

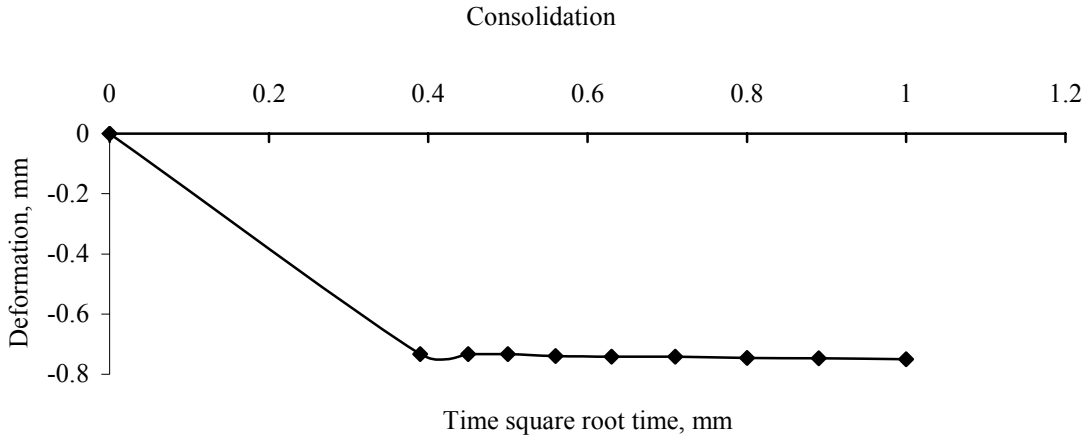

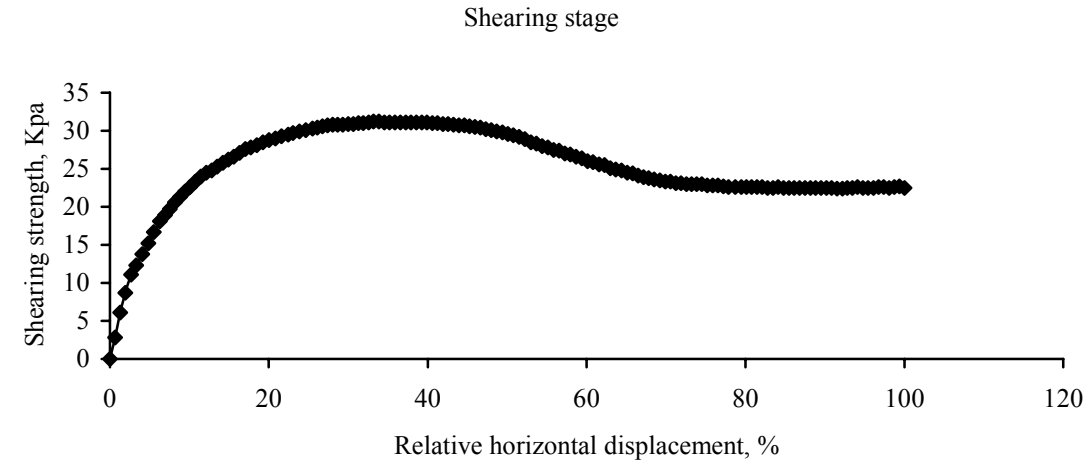

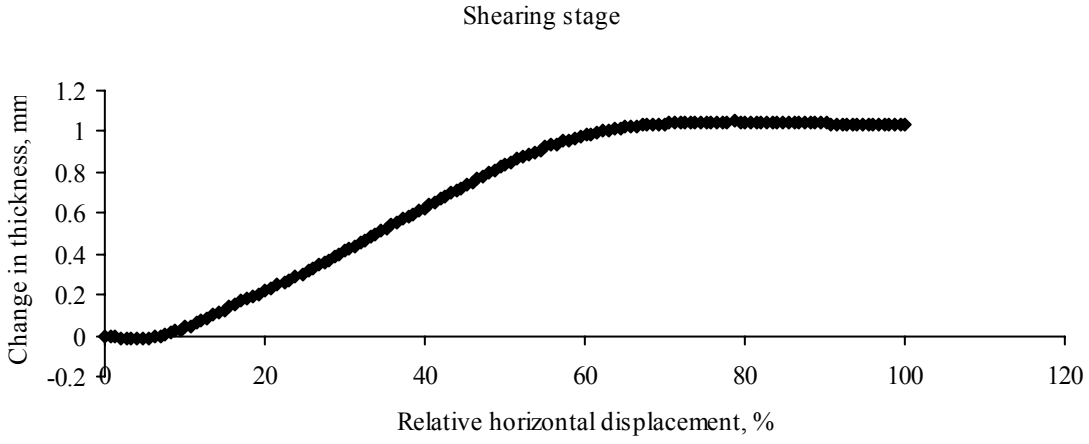

Figure B.5 30.9 kPa of normal stress was conducted in the untreated specimen with 85% of relative density, and data was recorded in (a) consolidation and (b) shearing stage, respectively. Note that vertical deformation, horizontal deformation, residual strength, and peak strength were -0.250 mm, 2.795 mm, 22.5 kPa and 31.1 kPa, respectively.

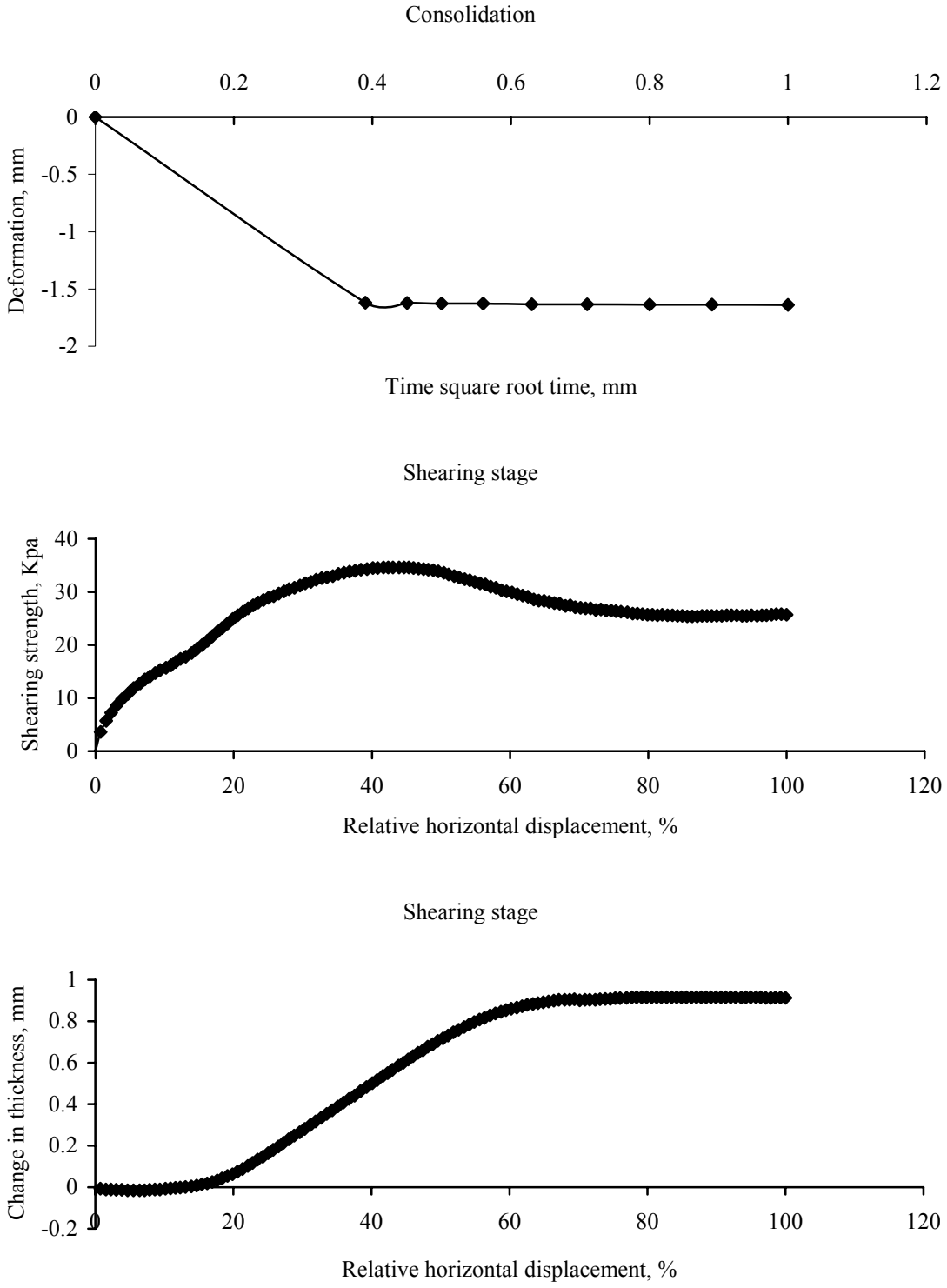

Figure B.6 40.7 kPa of normal stress was conducted in the untreated specimen with 85% of relative density, and data was recorded in (a) consolidation and (b) shearing stage, respectively. Note that vertical deformation, horizontal deformation, residual strength, and peak strength were -1.133 mm, 3.020 mm, 25.7 kPa and 34.5 kPa, respectively.

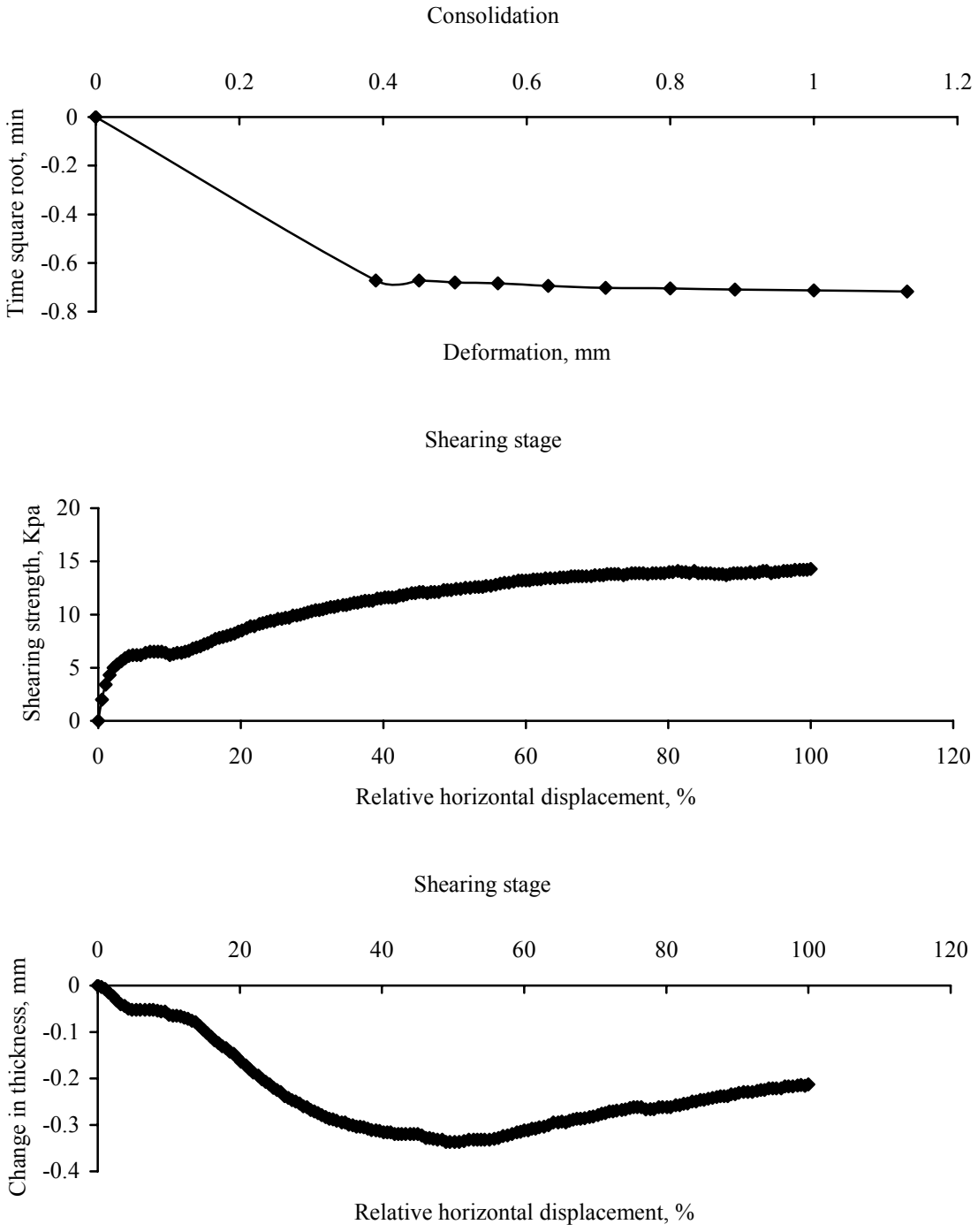

Figure B.7 21.1 kPa of normal stress was conducted in the specimen treated by 10^3 cells/mL of dead cells with 35% of relative density, and data was recorded in (a) consolidation and (b) shearing stage, respectively. Note that vertical deformation, horizontal deformation, and peak strength were -1.029 mm, 7.641 mm and 13.9 kPa, respectively.

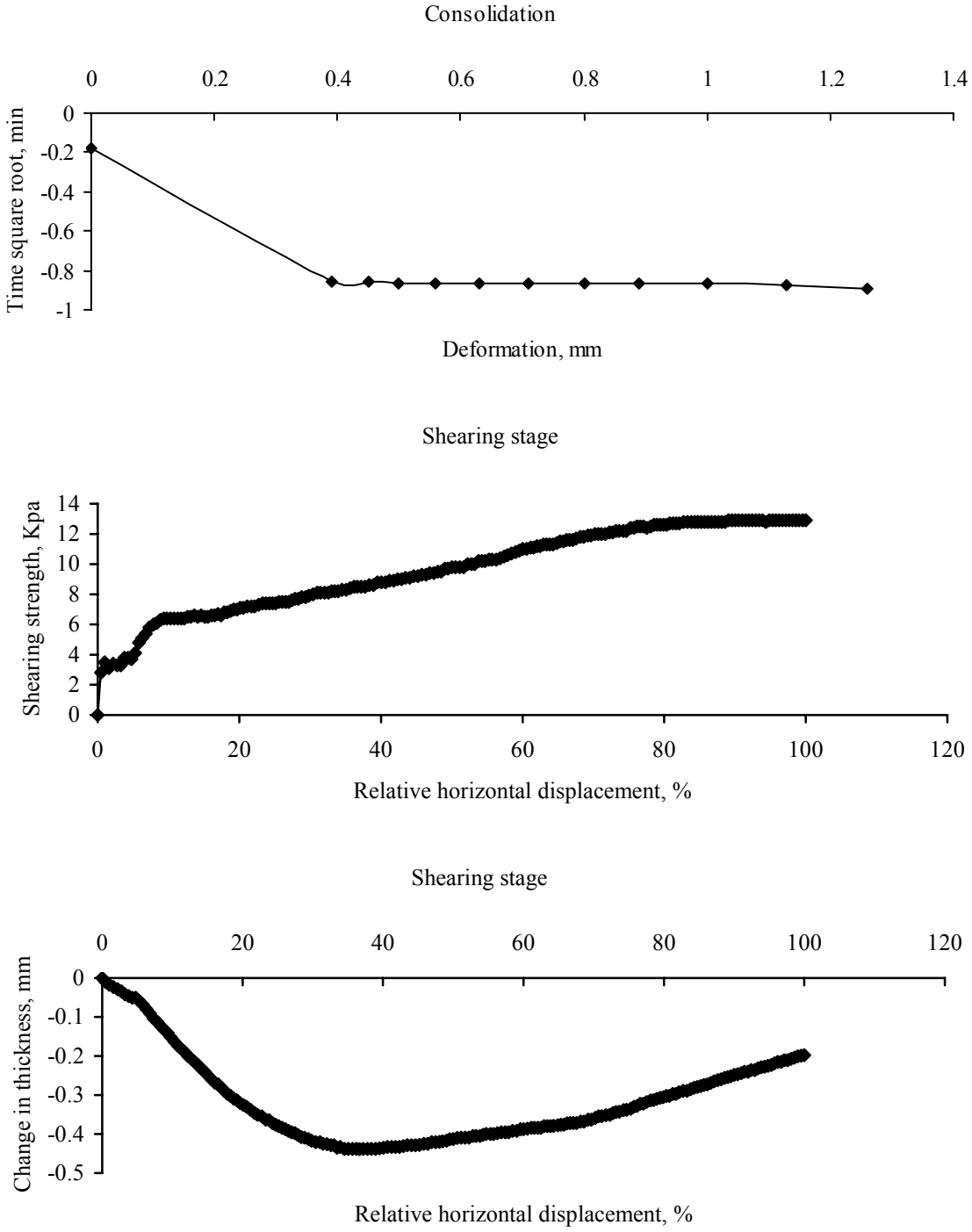

Figure B.8 16.2 kPa of normal stress was conducted in the specimen treated by 10^3 cells/mL of dead cells with 35% of relative density, and data was recorded in (a) consolidation and (b) shearing stage, respectively. Note that vertical deformation, horizontal deformation, and peak strength were -1.232 mm, 9.496 mm and 12.8 kPa, respectively.

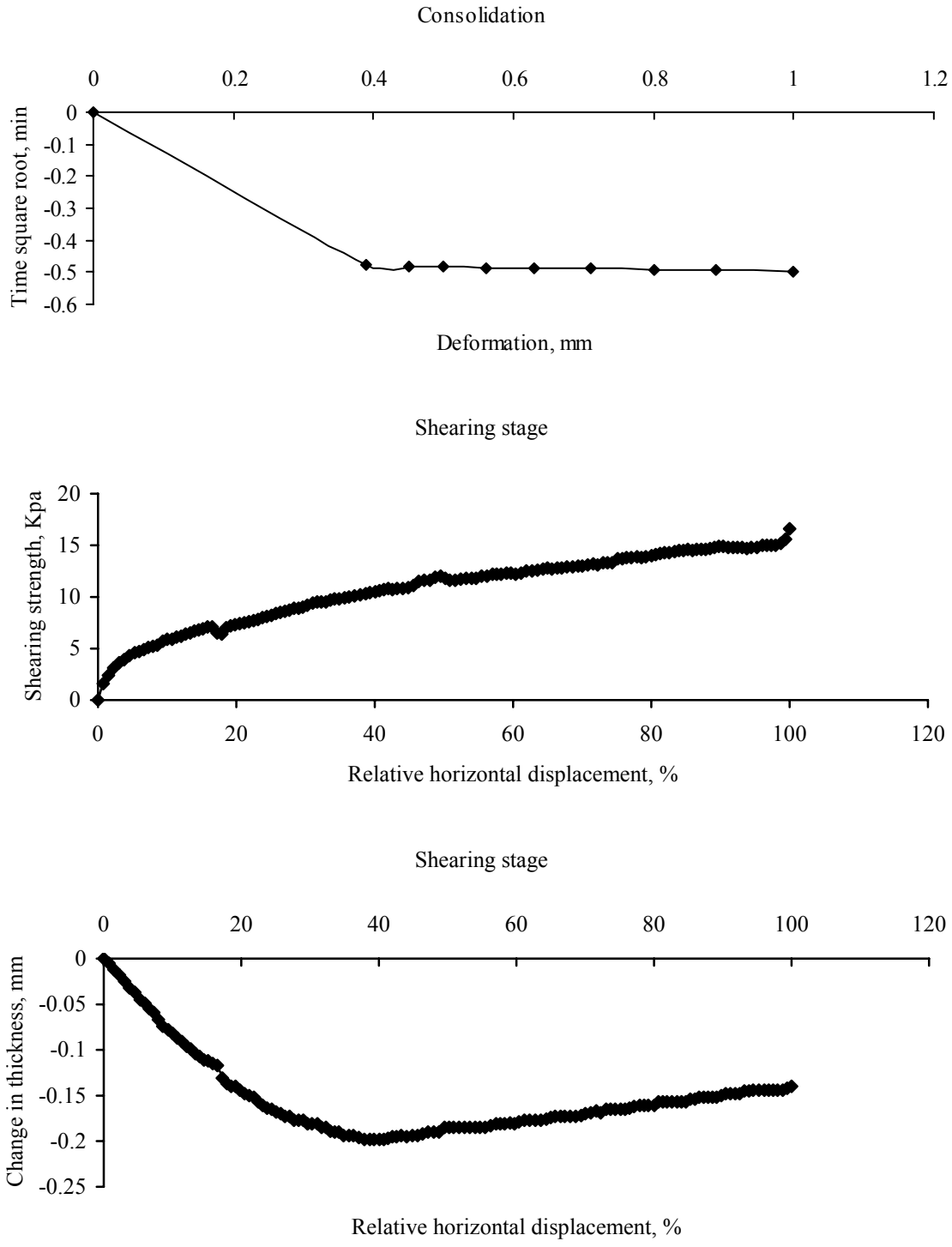

Figure B.9 21.1 kPa of normal stress was conducted in the specimen treated by 10^3 cells/mL of dead cells with 35% of relative density, and data was recorded in (a) consolidation and (b) shearing stage, respectively. Note that vertical deformation, horizontal deformation, and peak strength were -0.746 mm, 7.493 mm and 14.8 kPa, respectively.

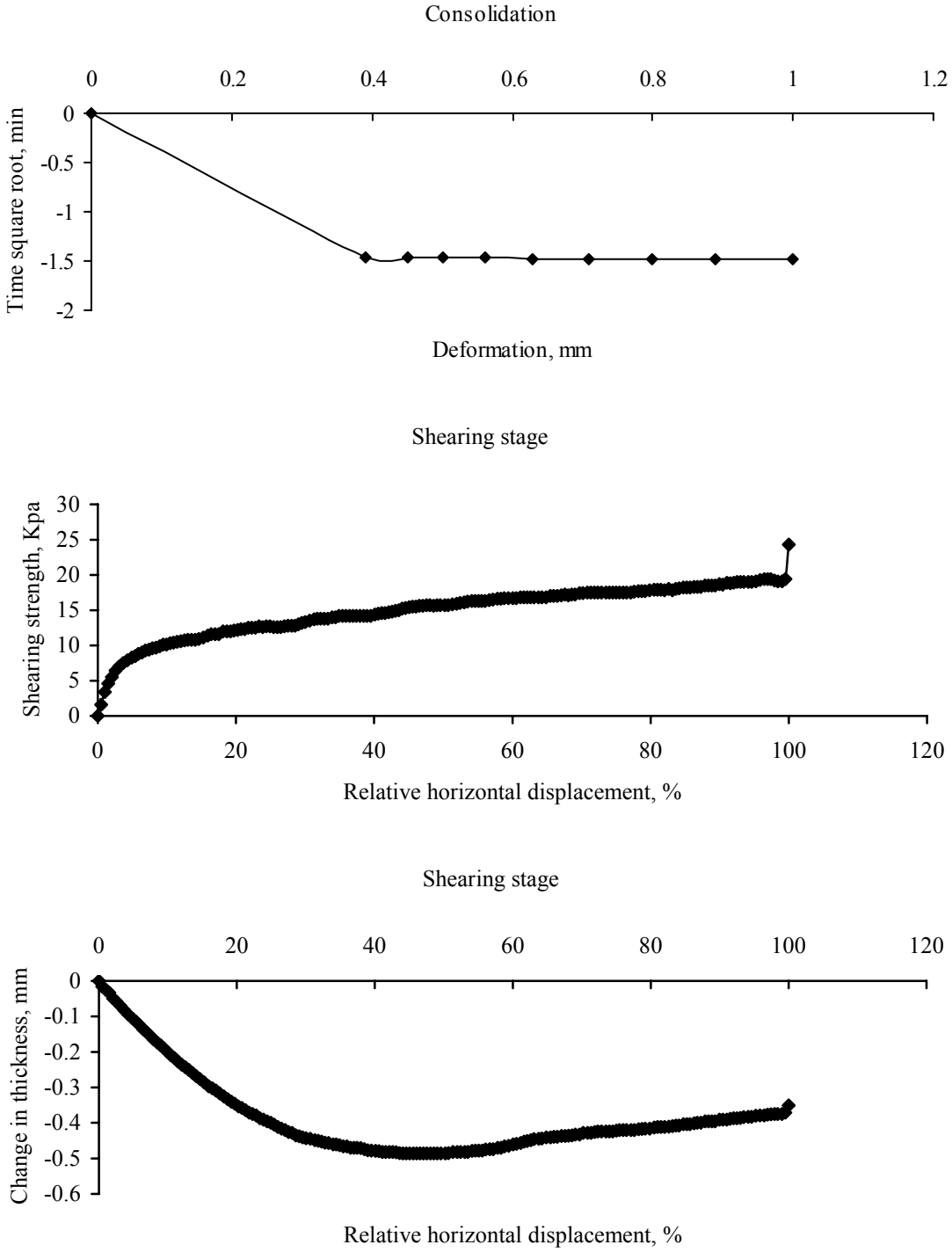

Figure B.10 30.9 kPa of normal stress was conducted in the specimen treated by 10^3 cells/mL of dead cells with 35% of relative density, and data was recorded in (a) consolidation and (b) shearing stage, respectively. Note that vertical deformation, horizontal deformation, and peak strength were -1.896 mm, 10.155 mm and 19.4 kPa, respectively.

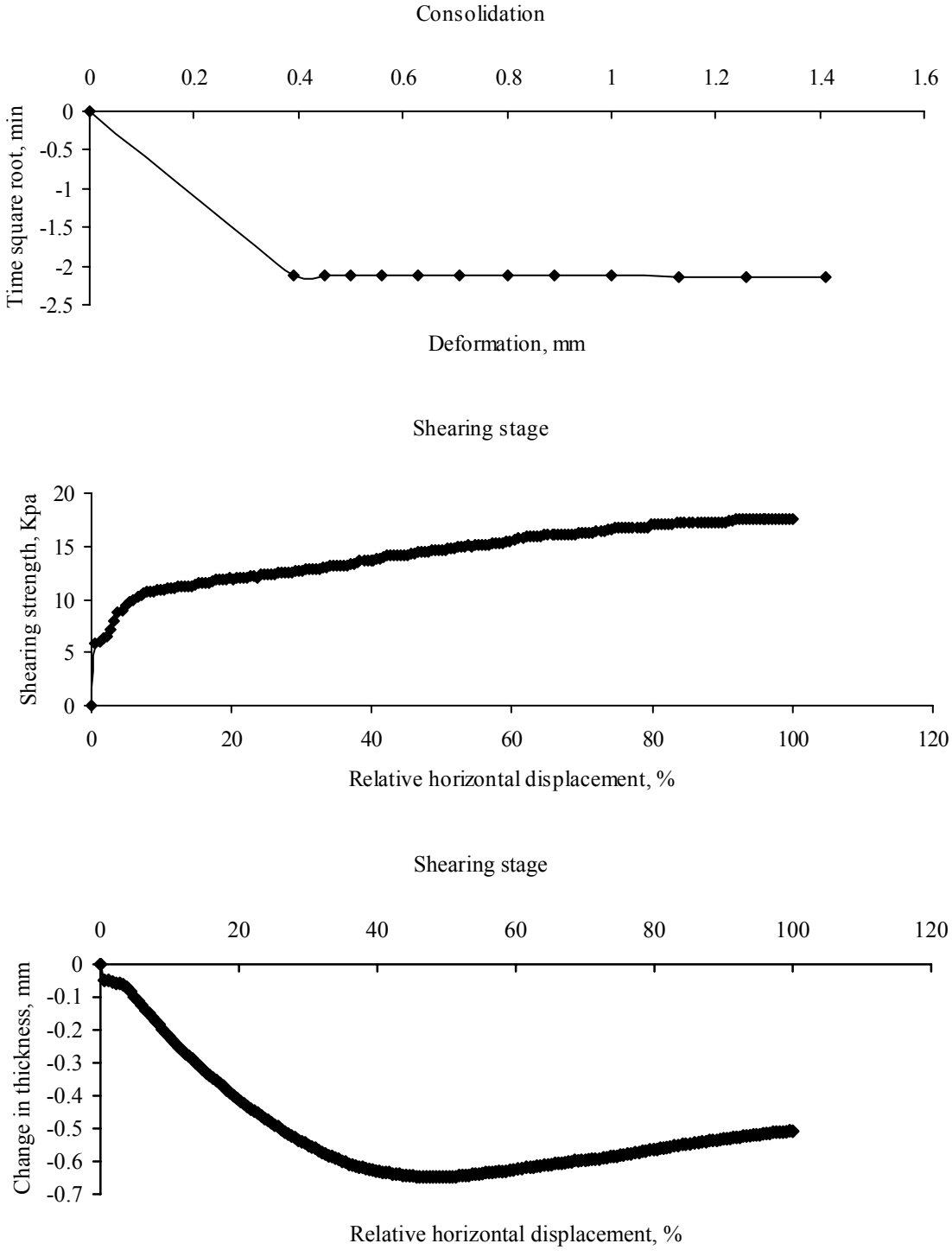

Figure B.11 30.9 kPa of normal stress was conducted in the specimen treated by 10^3 cells/mL of dead cells with 35% of relative density, and data was recorded in (a) consolidation and (b) shearing stage, respectively. Note that vertical deformation, horizontal deformation, and peak strength were -2.769 mm, 10.264 mm and 17.5 kPa, respectively.

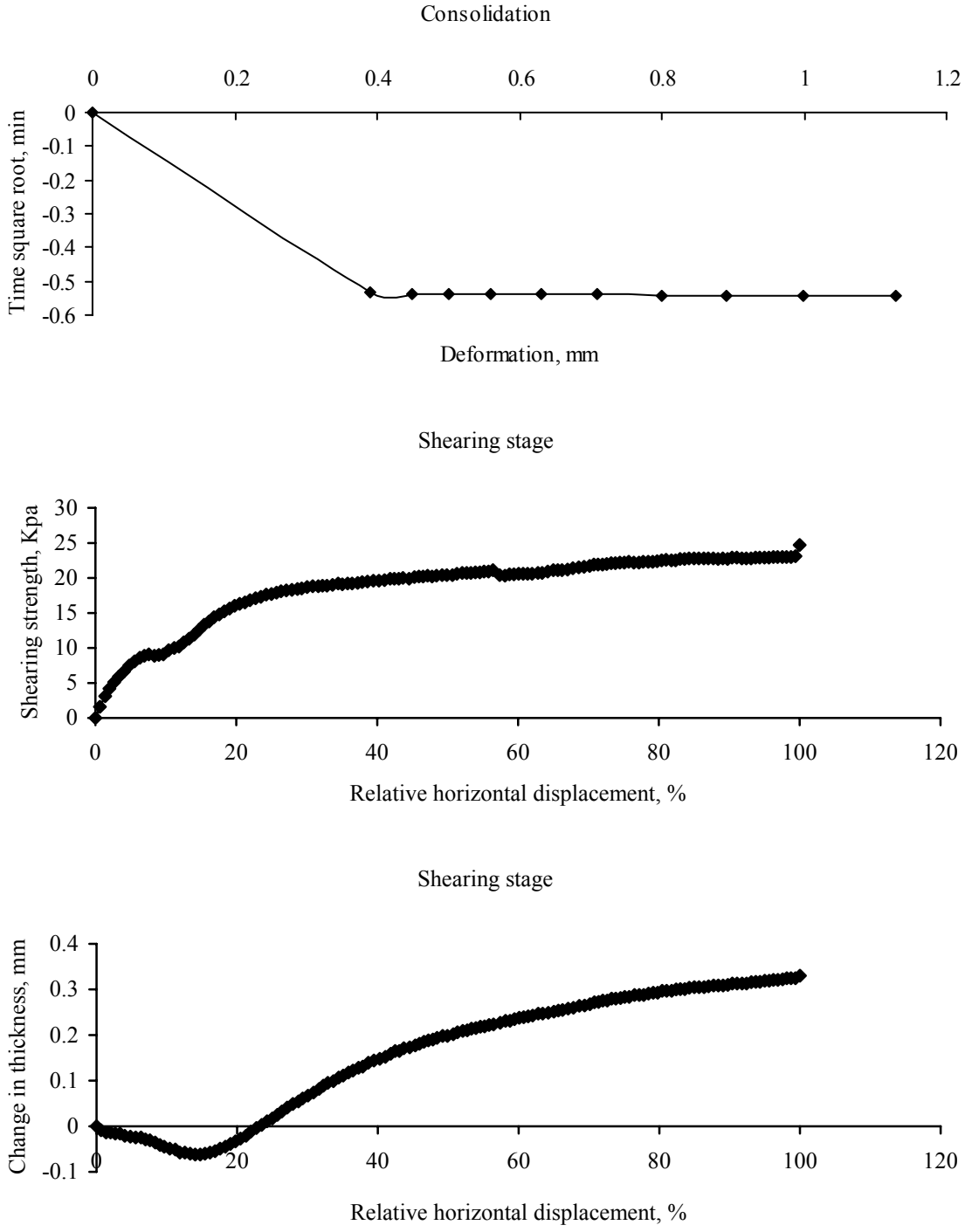

Figure B.12 30.9 kPa of normal stress was conducted in the specimen treated by 10^3 cells/mL of dead cells with 35% of relative density, and data was recorded in (a) consolidation and (b) shearing stage, respectively. Note that vertical deformation, horizontal deformation, and peak strength were -0.284 mm, 7.006 mm and 22.8 kPa, respectively.

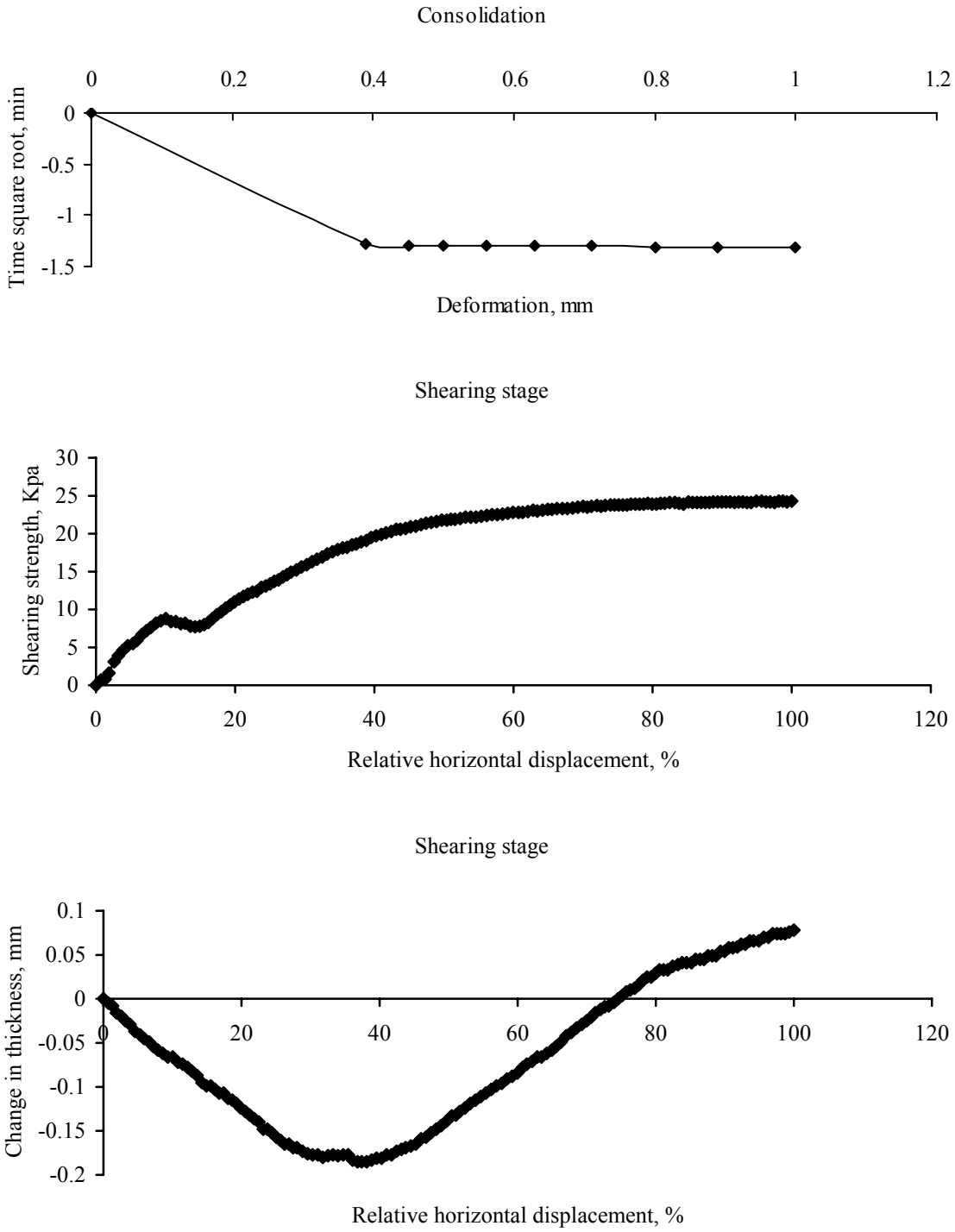

Figure B.13 40.7 kPa of normal stress was conducted in the specimen treated by 10^3 cells/mL of dead cells with 35% of relative density, and data was recorded in (a) consolidation and (b) shearing stage, respectively. Note that vertical deformation, horizontal deformation, and peak strength were -1.302 mm, 7.673 mm and 24.2 kPa, respectively.

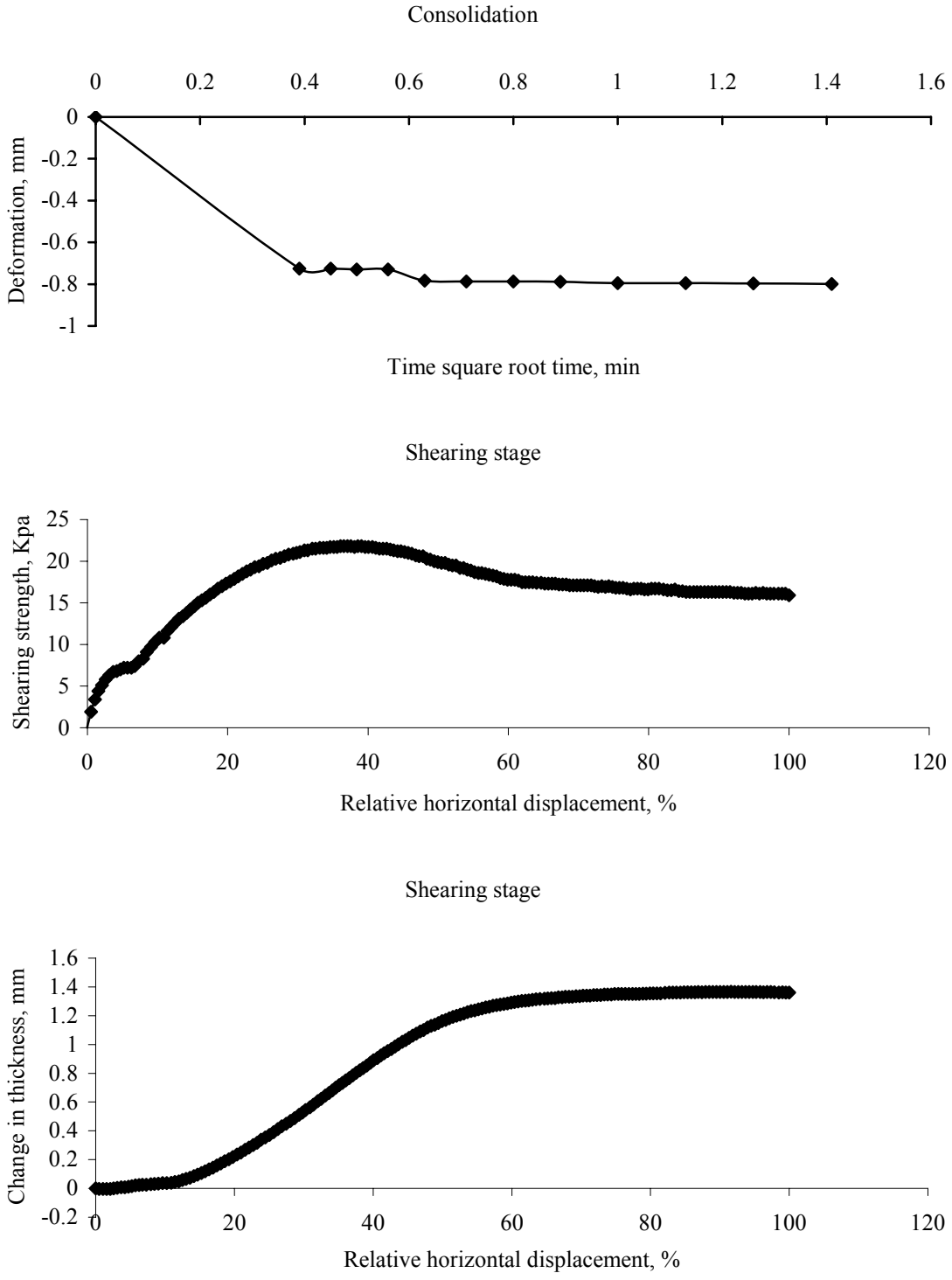

Figure B.14 21.1 kPa of normal stress was conducted in the specimen treated by 10^3 cells/mL of dead cells with 85% of relative density, and data was recorded in (a) consolidation and (b) shearing stage, respectively. Note that vertical deformation, horizontal deformation, residual strength and peak strength were -0.018 mm, 3.893 mm, 15.9 kPa and 21.8 kPa, respectively.

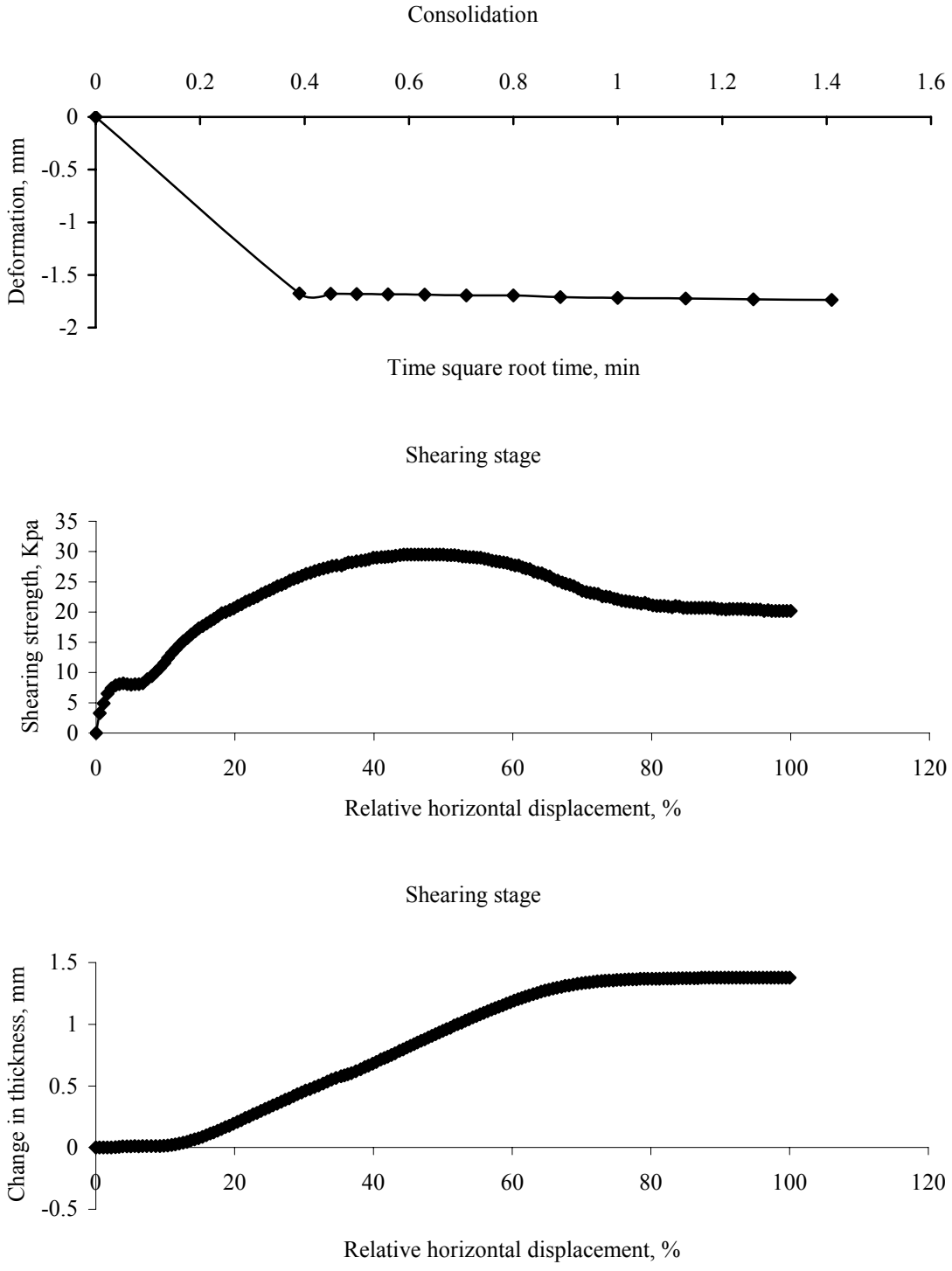

Figure B.15 30.9 kPa of normal stress was conducted in the specimen treated by 10^3 cells/mL of dead cells with 85% of relative density, and data was recorded in (a) consolidation and (b) shearing stage, respectively. Note that vertical deformation, horizontal deformation, residual strength and peak strength were -0.925 mm, 4.656 mm, 20.2 kPa and 29.5 kPa, respectively.

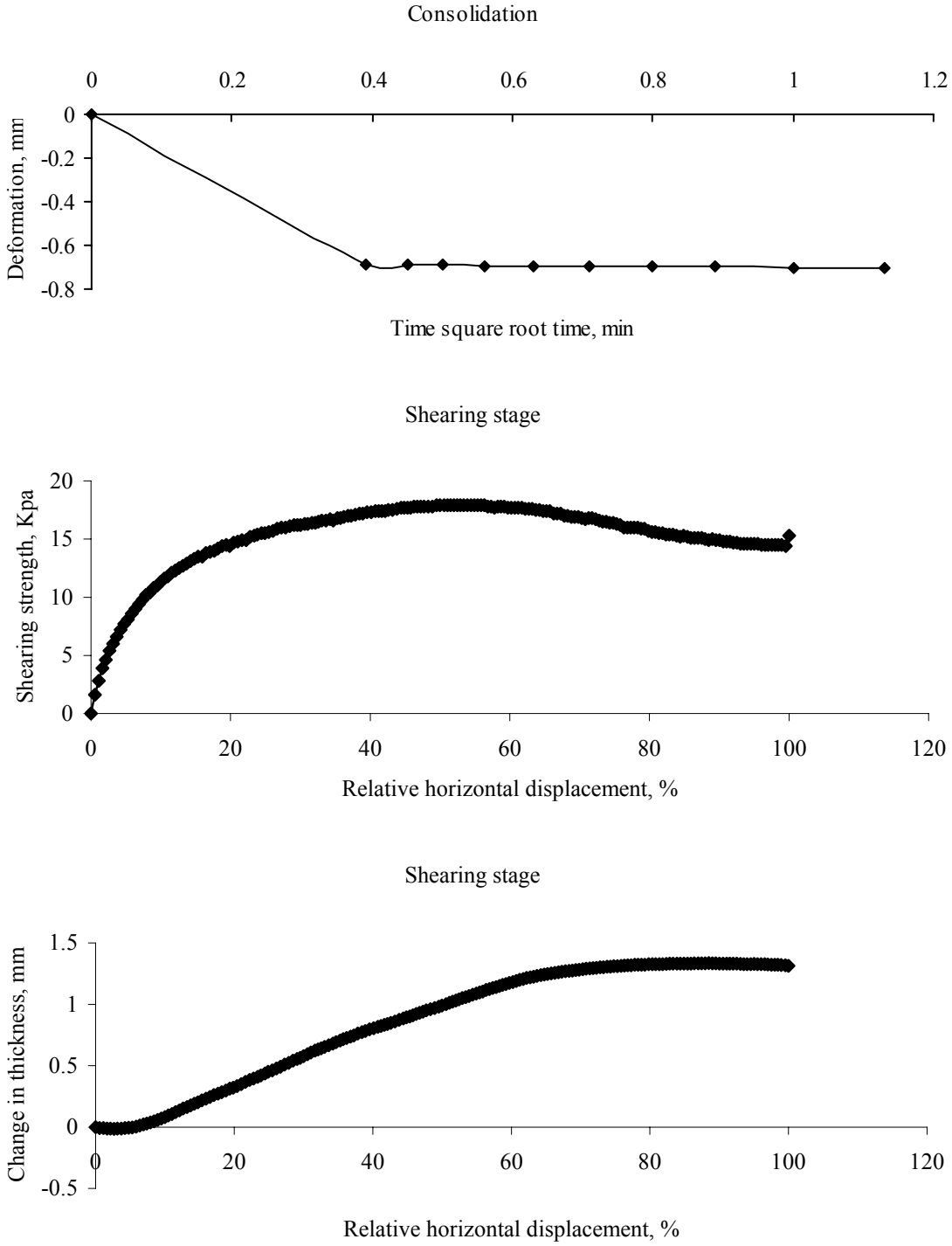

Figure B.16 16.2 kPa of normal stress was conducted in the specimen treated by 10^3 cells/mL of dead cells with 85% of relative density, and data was recorded in (a) consolidation and (b) shearing stage, respectively. Note that vertical deformation, horizontal deformation, residual strength and peak strength were 0.304 mm, 5.59 mm, 14.4 kPa and 17.9 kPa, respectively.

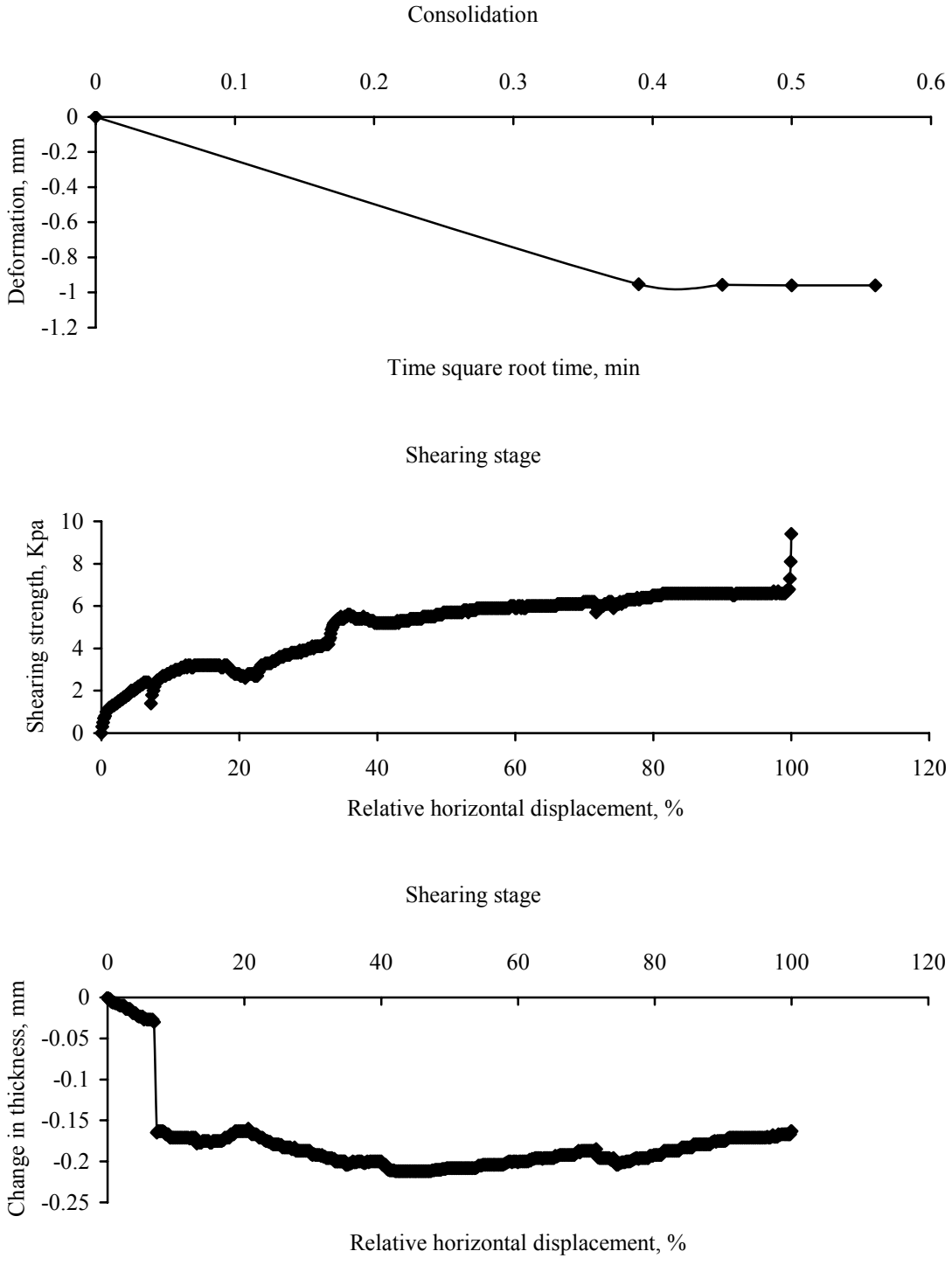

Figure B.17 11.3 kPa of normal stress was conducted in the specimen treated by 10^7 cells/mL of dead cells with 35% of relative density, and data was recorded in (a) consolidation and (b) shearing stage, respectively. Note that vertical deformation, horizontal deformation, and peak strength were -1.388 mm, 7.068 mm, and 6.6 kPa, respectively.

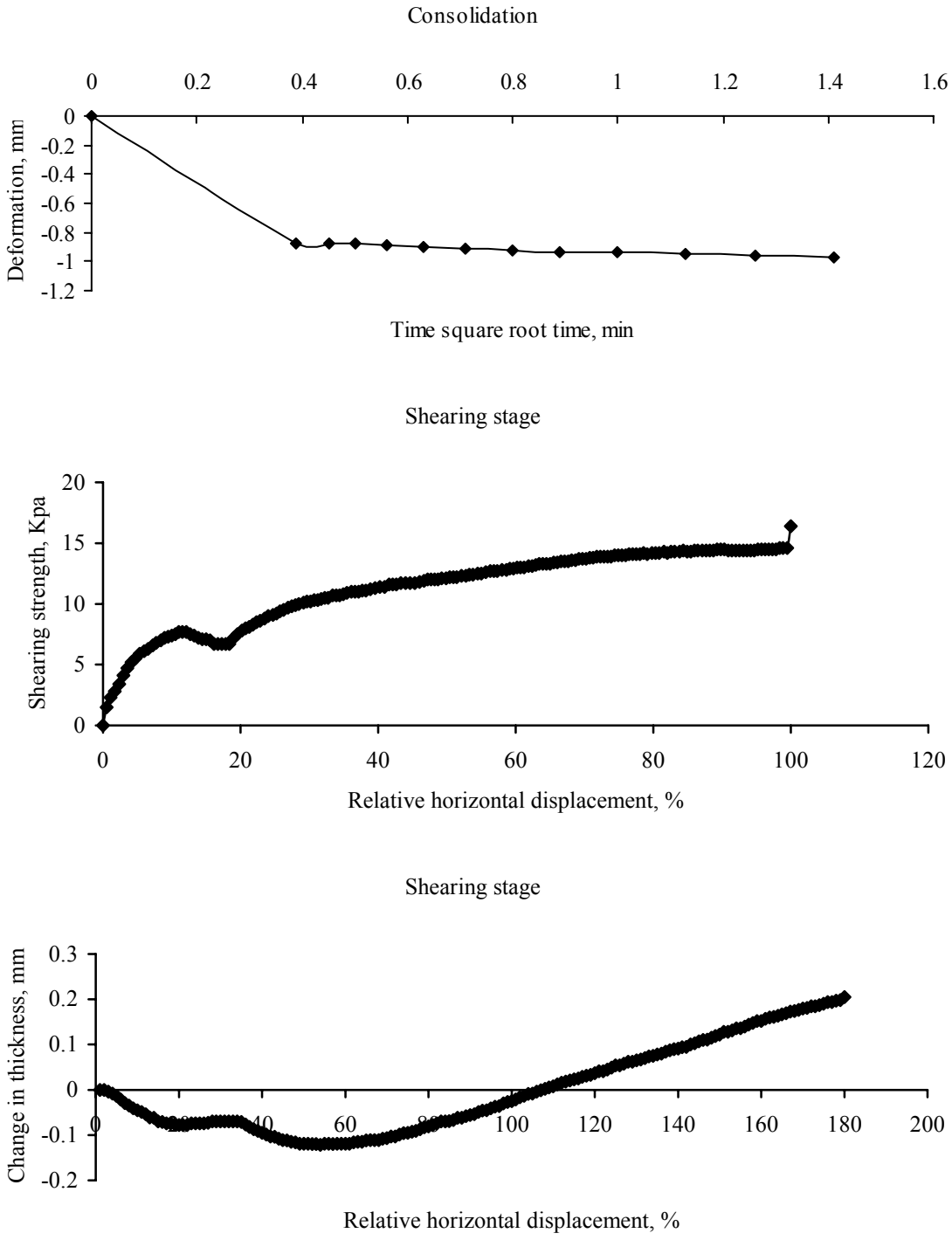

Figure B.18 21.1 kPa of normal stress was conducted in the specimen treated by 10^7 cells/mL of dead cells with 35% of relative density, and data was recorded in (a) consolidation and (b) shearing stage, respectively. Note that vertical deformation, horizontal deformation, and peak strength were -0.827 mm, 8.798 mm, and 14.5 kPa, respectively.

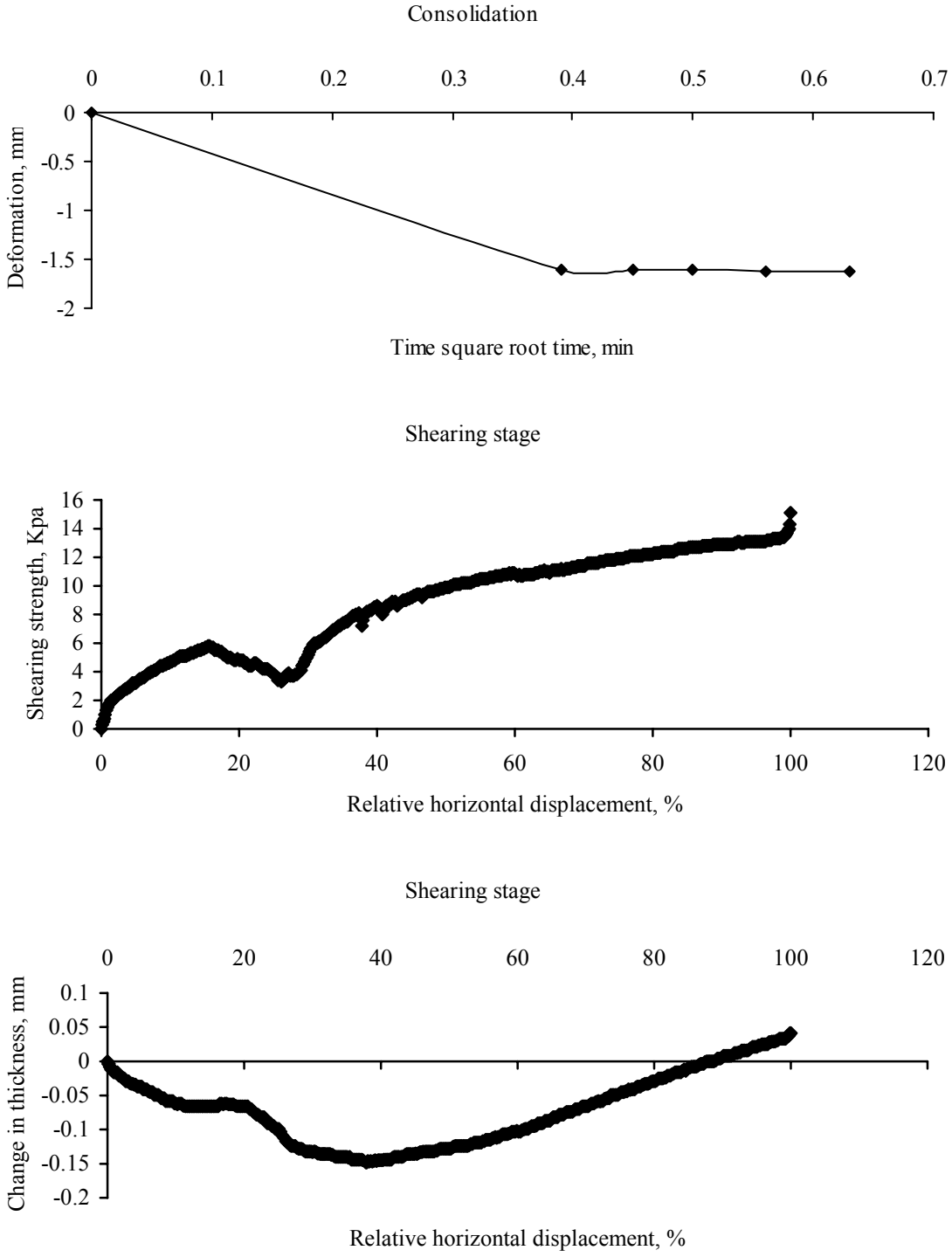

Figure B.19 21.1 kPa of normal stress was conducted in the specimen treated by 10^7 cells/mL of dead cells with 35% of relative density, and data was recorded in (a) consolidation and (b) shearing stage, respectively. Note that vertical deformation, horizontal deformation, and peak strength were -1.662 mm, 7.702 mm, and 13.3 kPa, respectively.

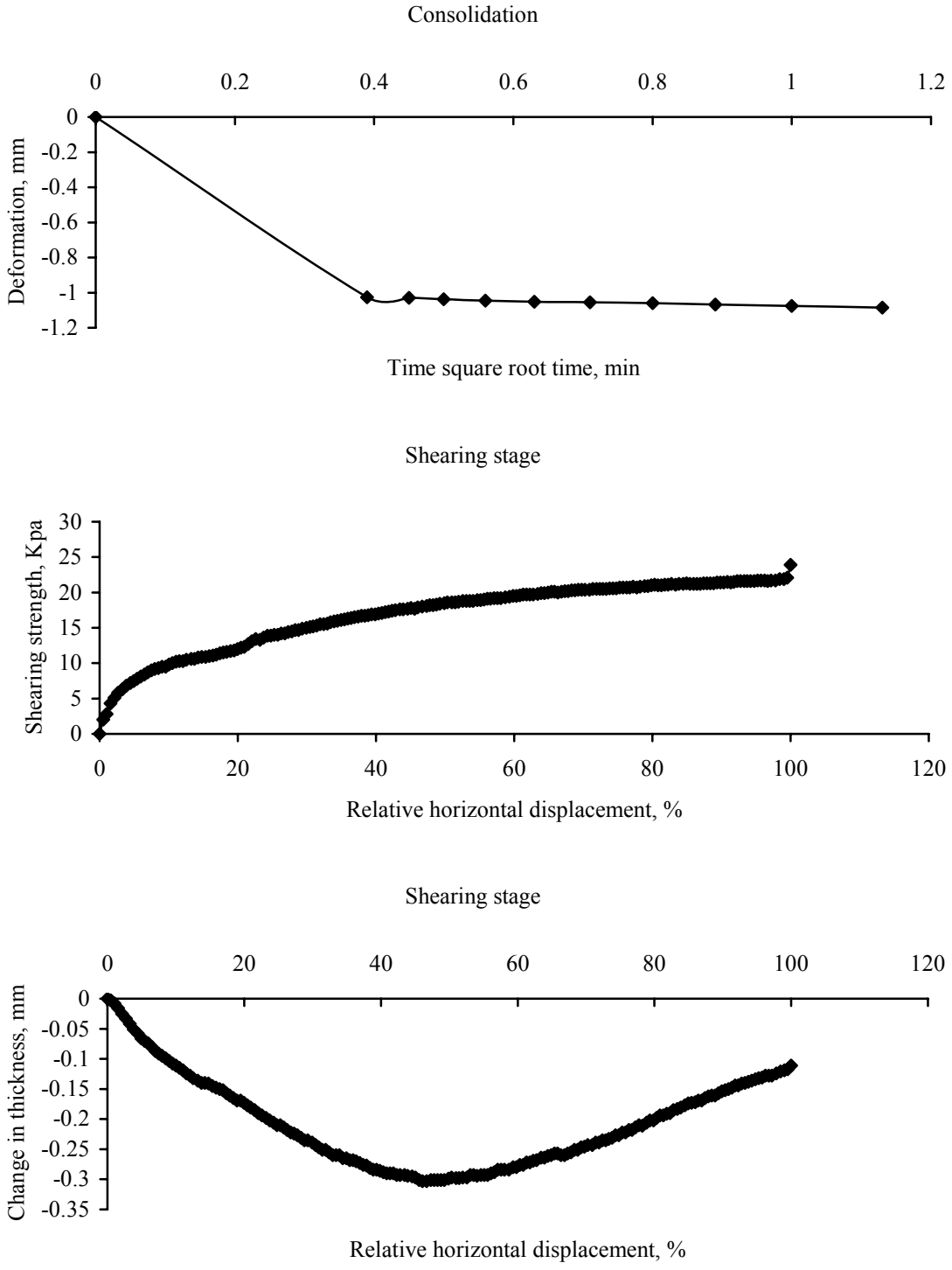

Figure B.20 30.9 kPa of normal stress was conducted in the specimen treated by 10^7 cells/mL of dead cells with 35% of relative density, and data was recorded in (a) consolidation and (b) shearing stage, respectively. Note that vertical deformation, horizontal deformation, and peak strength were -1.262 mm, 9.787 mm, and 21.6 kPa, respectively.

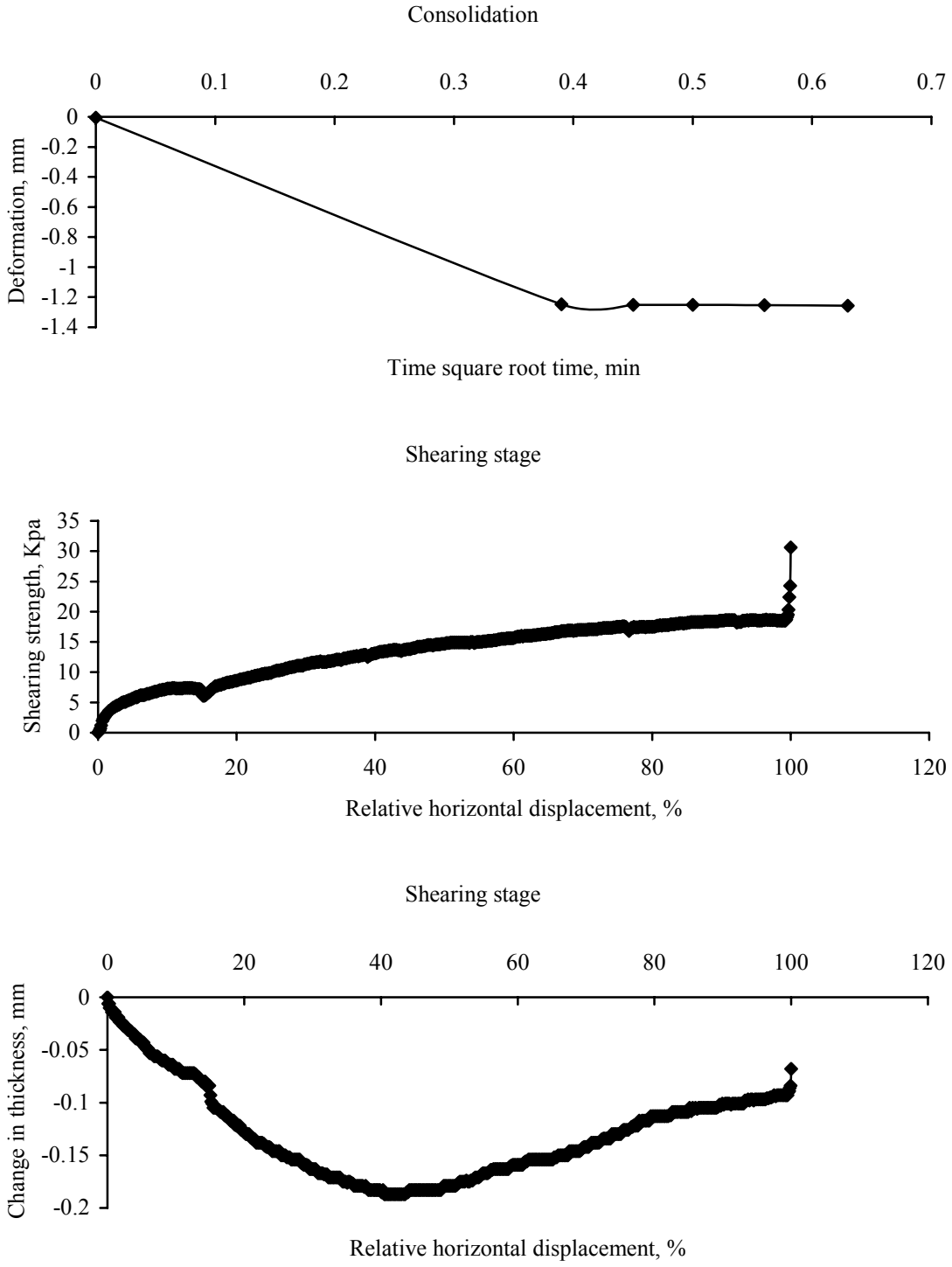

Figure B.21 30.9 kPa of normal stress was conducted in the specimen treated by 10^7 cells/mL of dead cells with 35% of relative density, and data was recorded in (a) consolidation and (b) shearing stage, respectively. Note that vertical deformation, horizontal deformation, and peak strength were -1.489 mm, 7.596 mm, and 18.6 kPa, respectively.

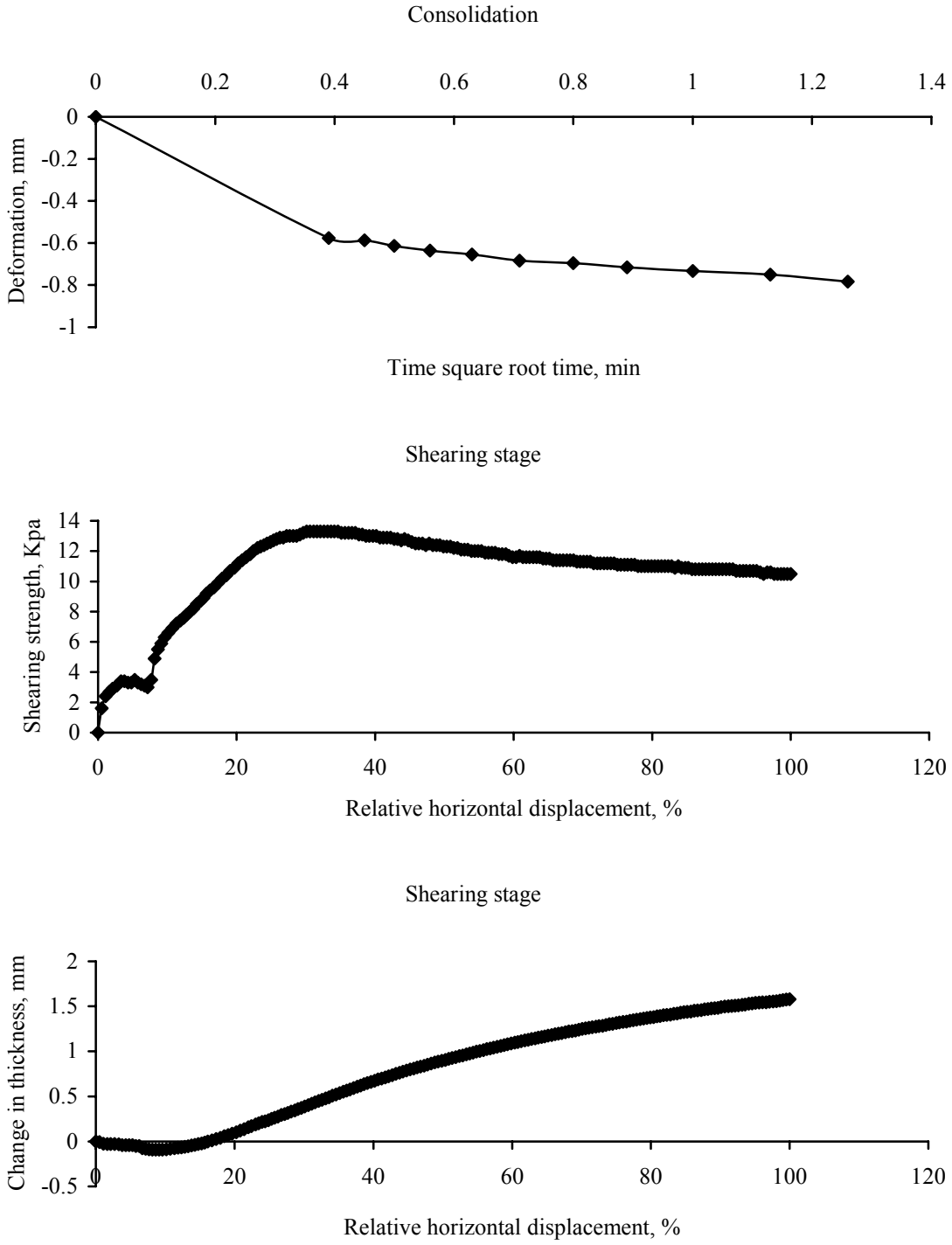

Figure B.22 11.3 kPa of normal stress was conducted in the specimen treated by 10^7 cells/mL of dead cells with 85% of relative density, and data was recorded in (a) consolidation and (b) shearing stage, respectively. Note that vertical deformation, horizontal deformation, residual strength and peak strength were -0.436 mm, 3.473 mm, 10.5 kPa, and 13.3 kPa, respectively.

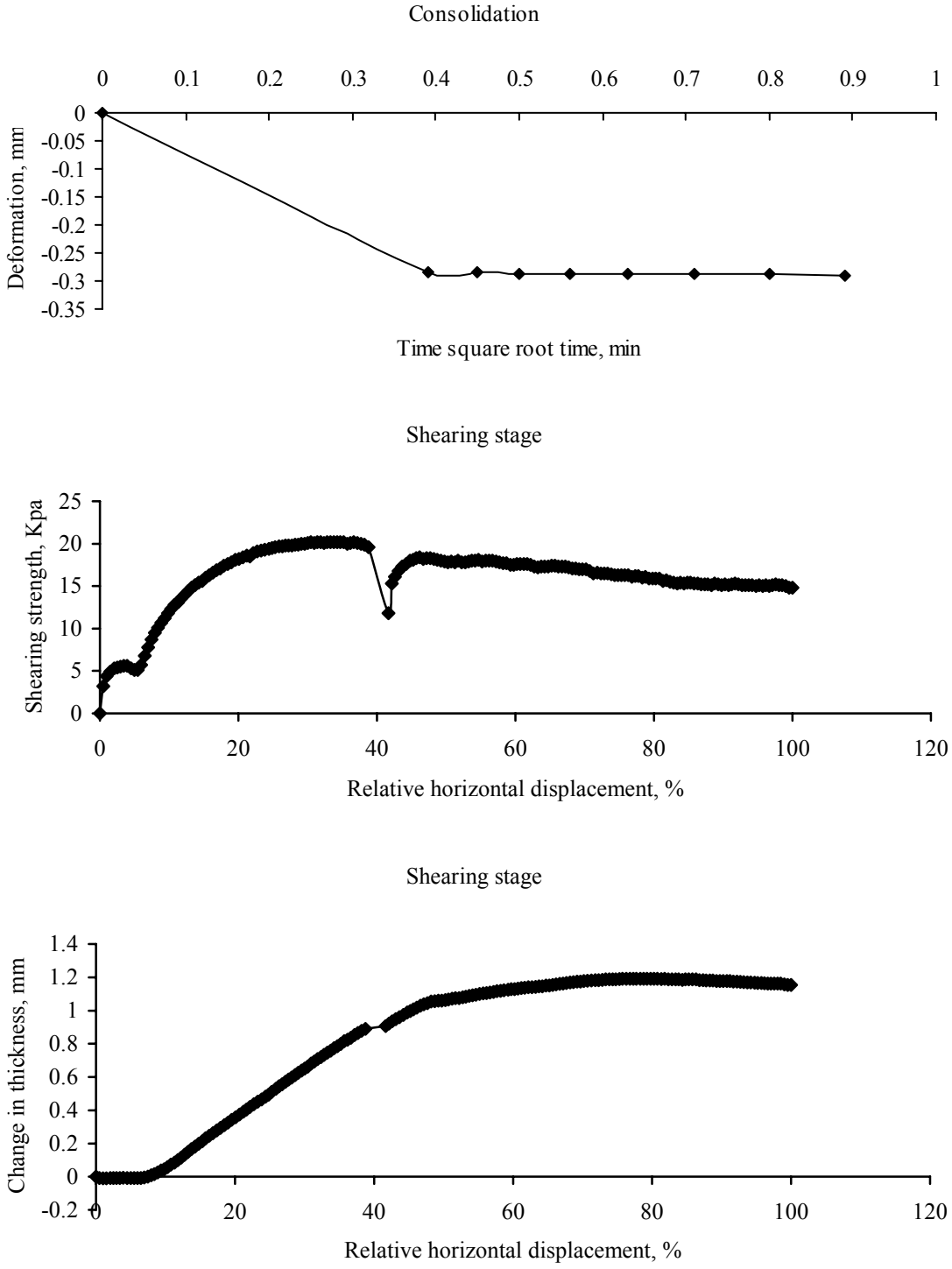

Figure B.23 16.2 kPa of normal stress was conducted in the specimen treated by 10^7 cells/mL of dead cells with 85% of relative density, and data was recorded in (a) consolidation and (b) shearing stage, respectively. Note that vertical deformation, horizontal deformation, residual strength and peak strength were 0.403 mm, 3.671 mm, 14.8 kPa, and 20.1 kPa, respectively.

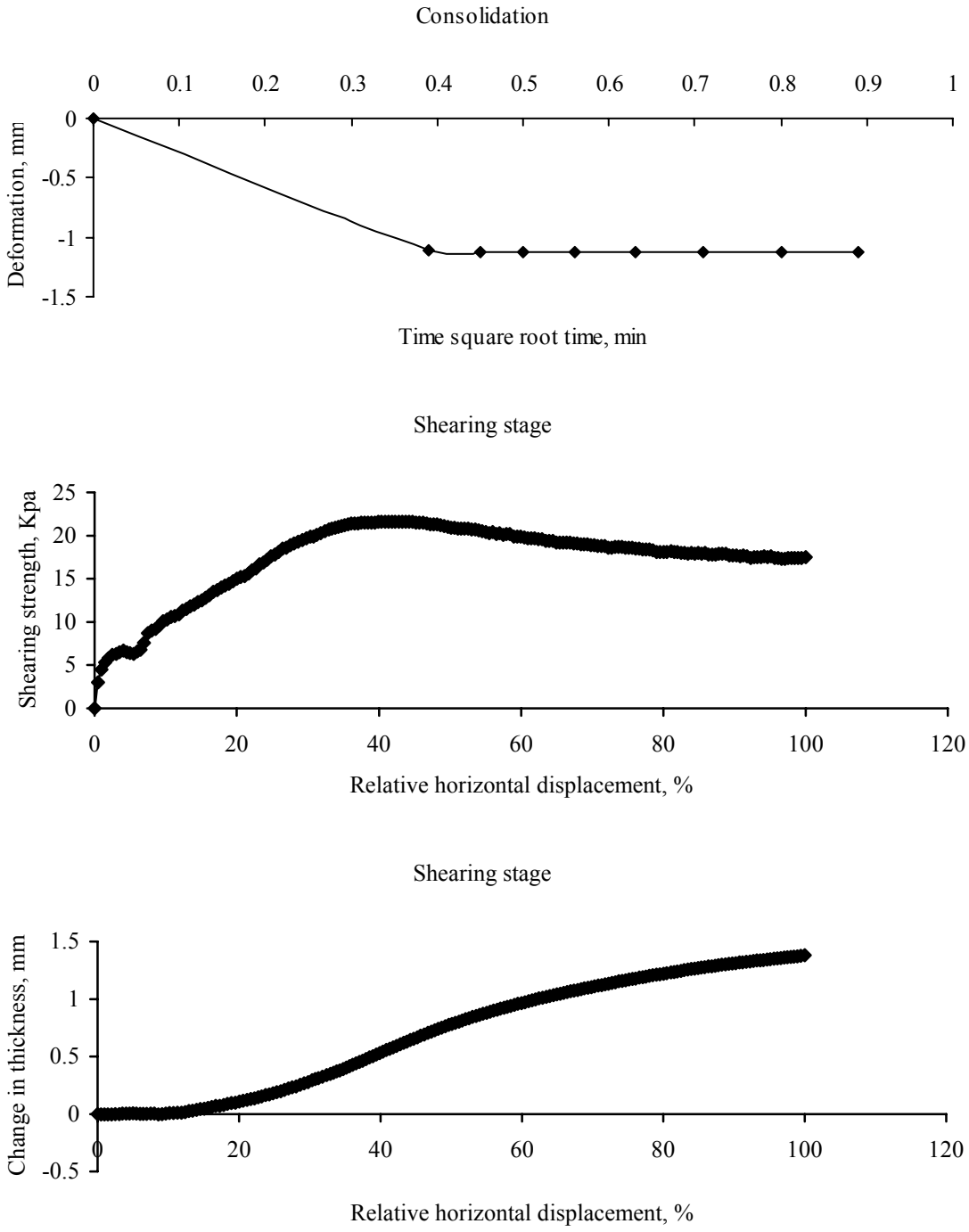

Figure B.24 21.1 kPa of normal stress was conducted in the specimen treated by 10^7 cells/mL of dead cells with 85% of relative density, and data was recorded in (a) consolidation and (b) shearing stage, respectively. Note that vertical deformation, horizontal deformation, residual strength and peak strength were -0.602 mm, 4.640 mm, 17.5 kPa, and 21.6 kPa, respectively.

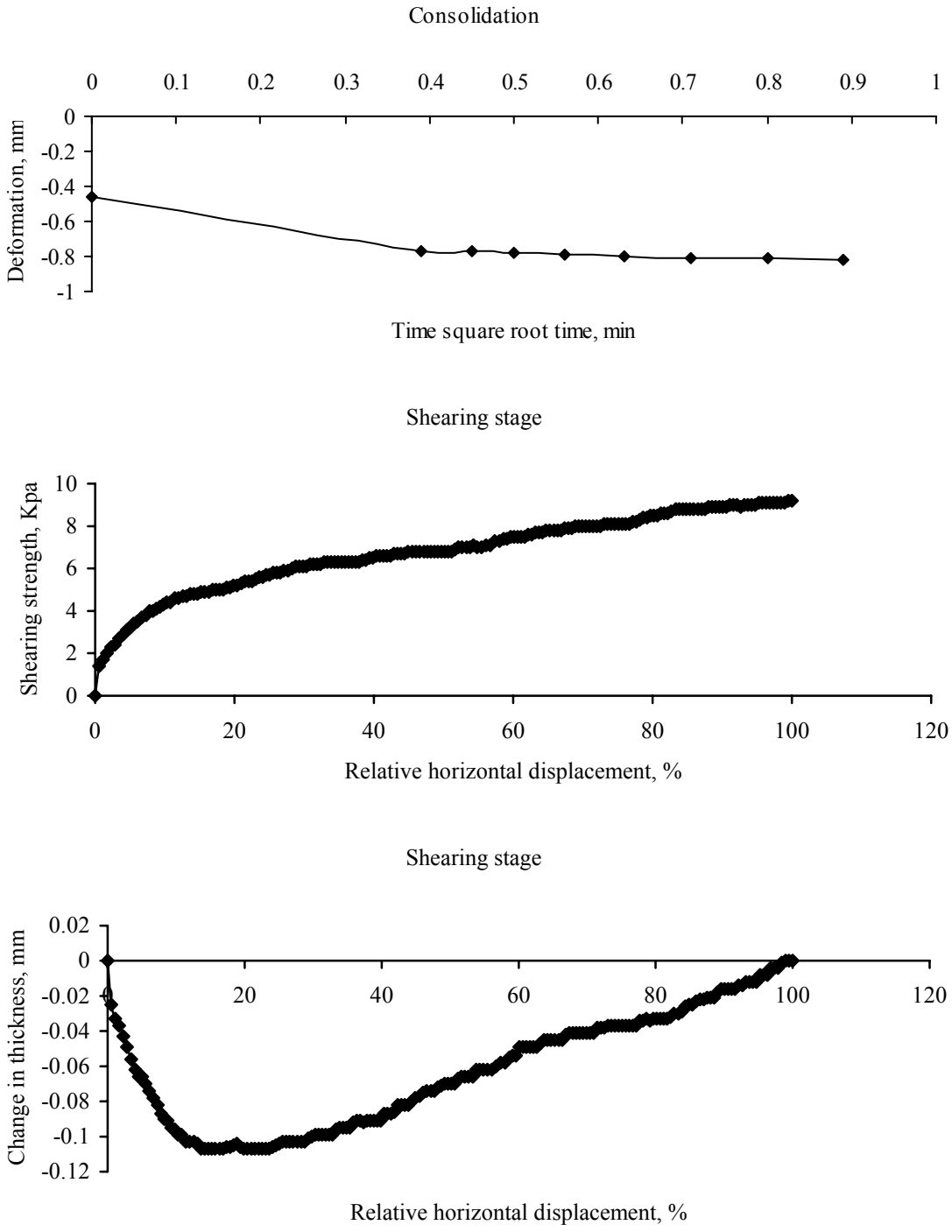

Figure B.25 11.3 kPa of normal stress was conducted in the specimen treated by 10^3 cells/mL of resting cells with 35% of relative density, and data was recorded in (a) consolidation and (b) shearing stage, respectively. Note that vertical deformation, horizontal deformation, and peak strength were -0.853 mm, 10.316 mm, and 9.2 kPa, respectively.

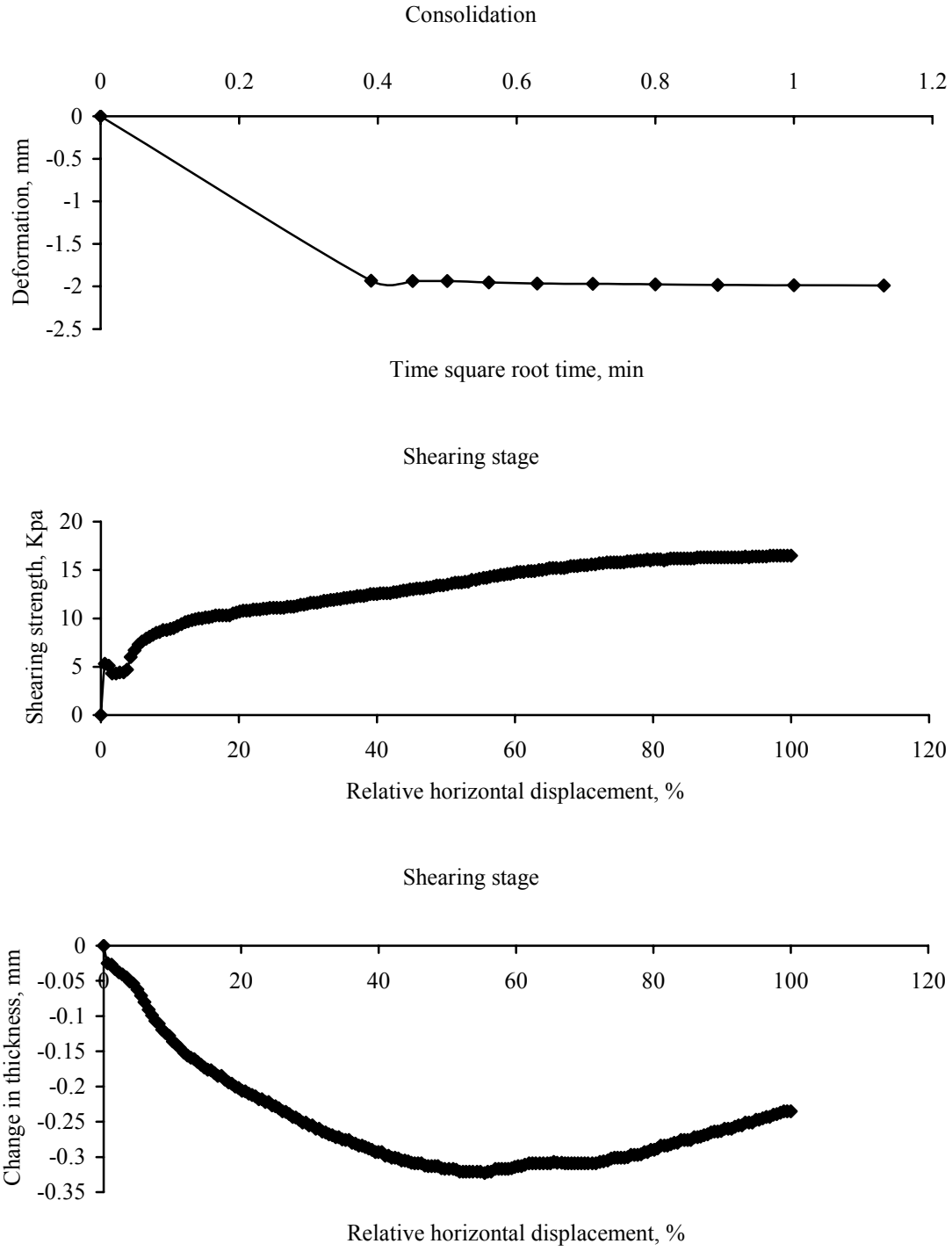

Figure B.26 26 kPa of normal stress was conducted in the specimen treated by 10^3 cells/mL of resting cells with 35% of relative density, and data was recorded in (a) consolidation and (b) shearing stage, respectively. Note that vertical deformation, horizontal deformation, and peak strength were -2.365 mm, 9.979 mm, and 16.4 kPa, respectively.

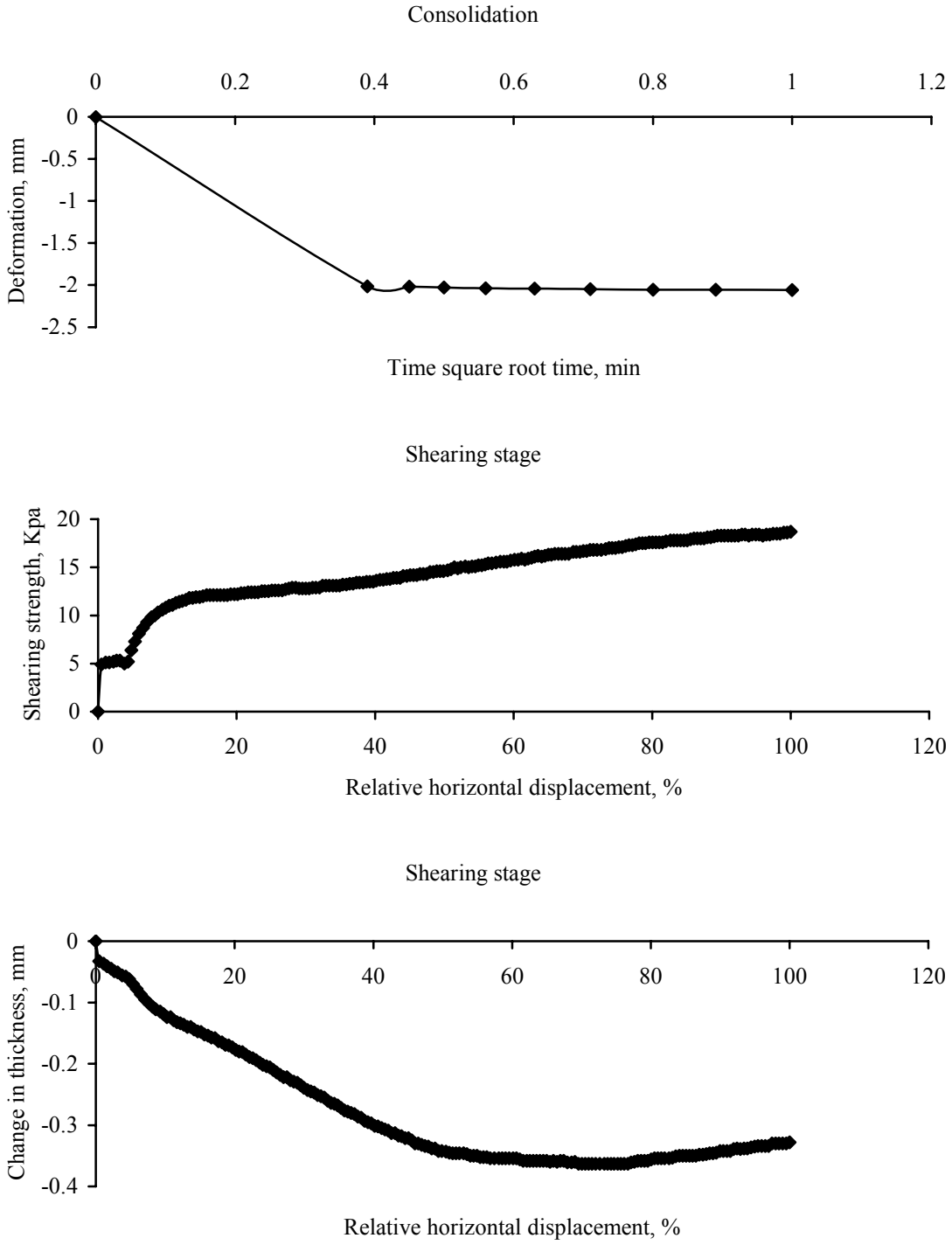

Figure B.27 30.9 kPa of normal stress was conducted in the specimen treated by 10^3 cells/mL of resting cells with 35% of relative density, and data was recorded in (a) consolidation and (b) shearing stage, respectively. Note that vertical deformation, horizontal deformation, and peak strength were -2.466 mm, 10.109 mm, and 18.4 kPa, respectively.

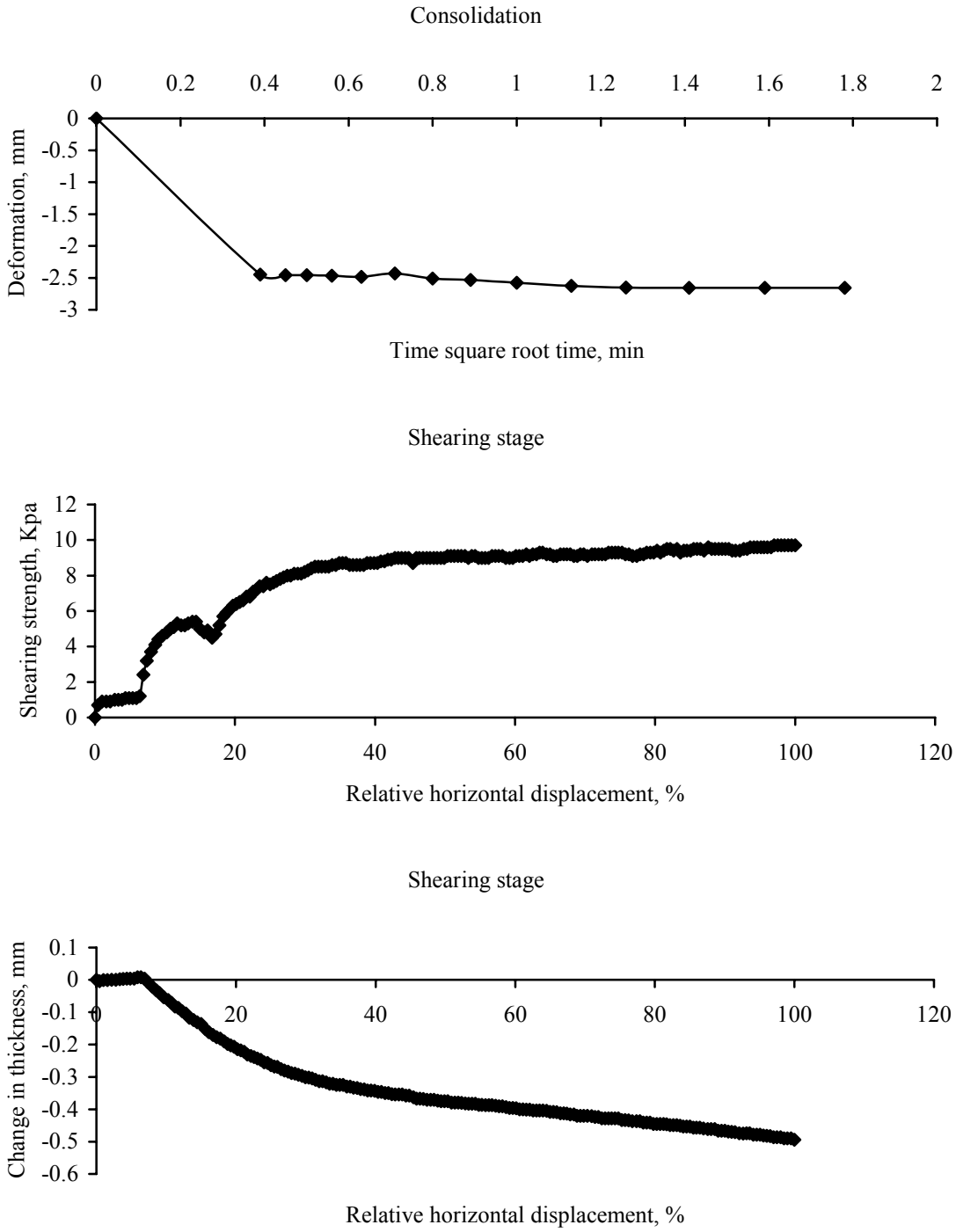

Figure B.28 21.1 kPa of normal stress was conducted in the specimen treated by 10^3 cells/mL of resting cells with 35% of relative density, and data was recorded in (a) consolidation and (b) shearing stage, respectively. Note that vertical deformation, horizontal deformation, and peak strength were -3.160 mm, 10.736 mm, and 9.7 kPa, respectively.

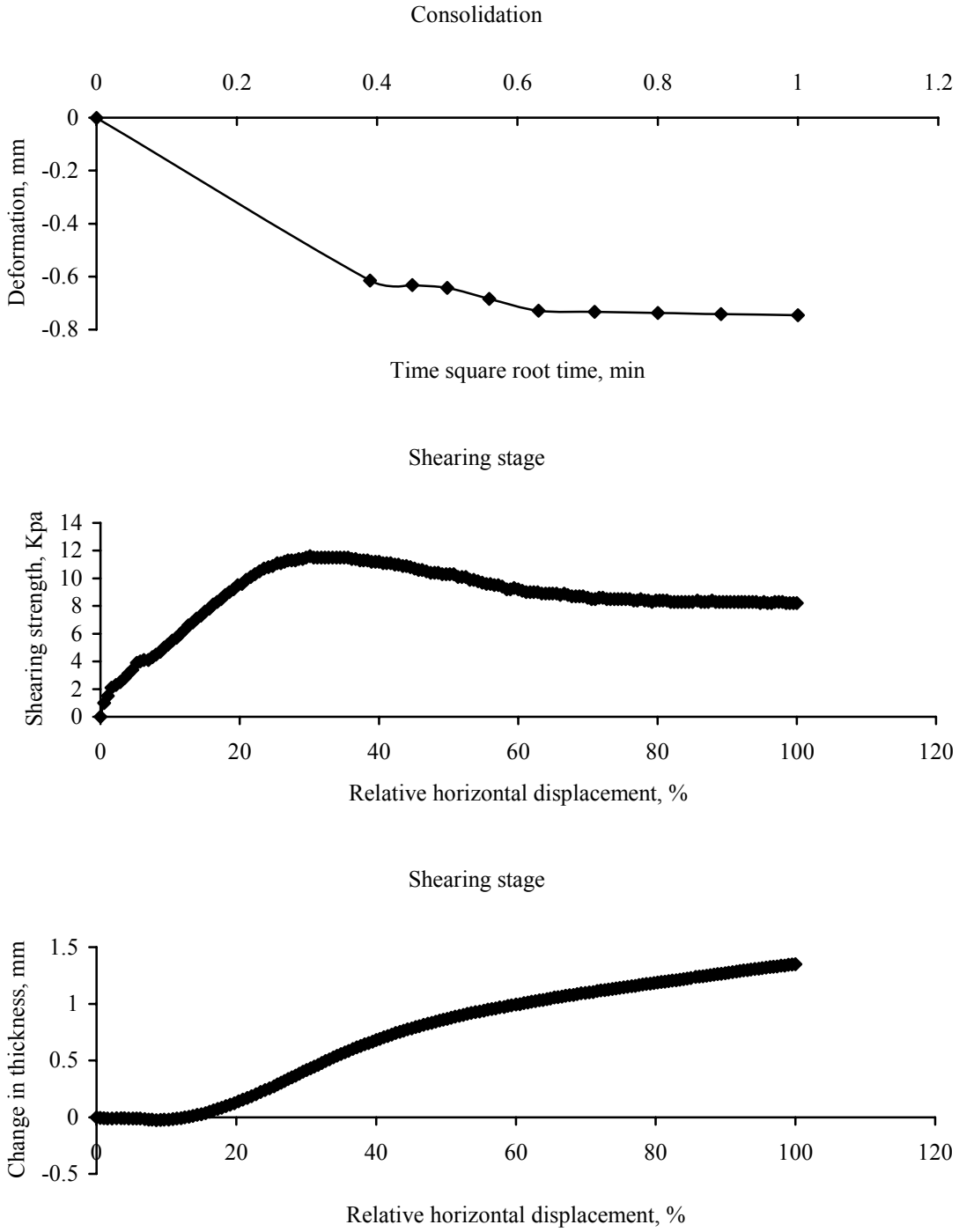

Figure B.29 11.3 kPa of normal stress was conducted in the specimen treated by 10^3 cells/mL of resting cells with 85% of relative density, and data was recorded in (a) consolidation and (b) shearing stage, respectively. Note that vertical deformation, horizontal deformation, residual strength, and peak strength were -0.309 mm, 3.219 mm, 8.2 kPa and 11.5 kPa, respectively.

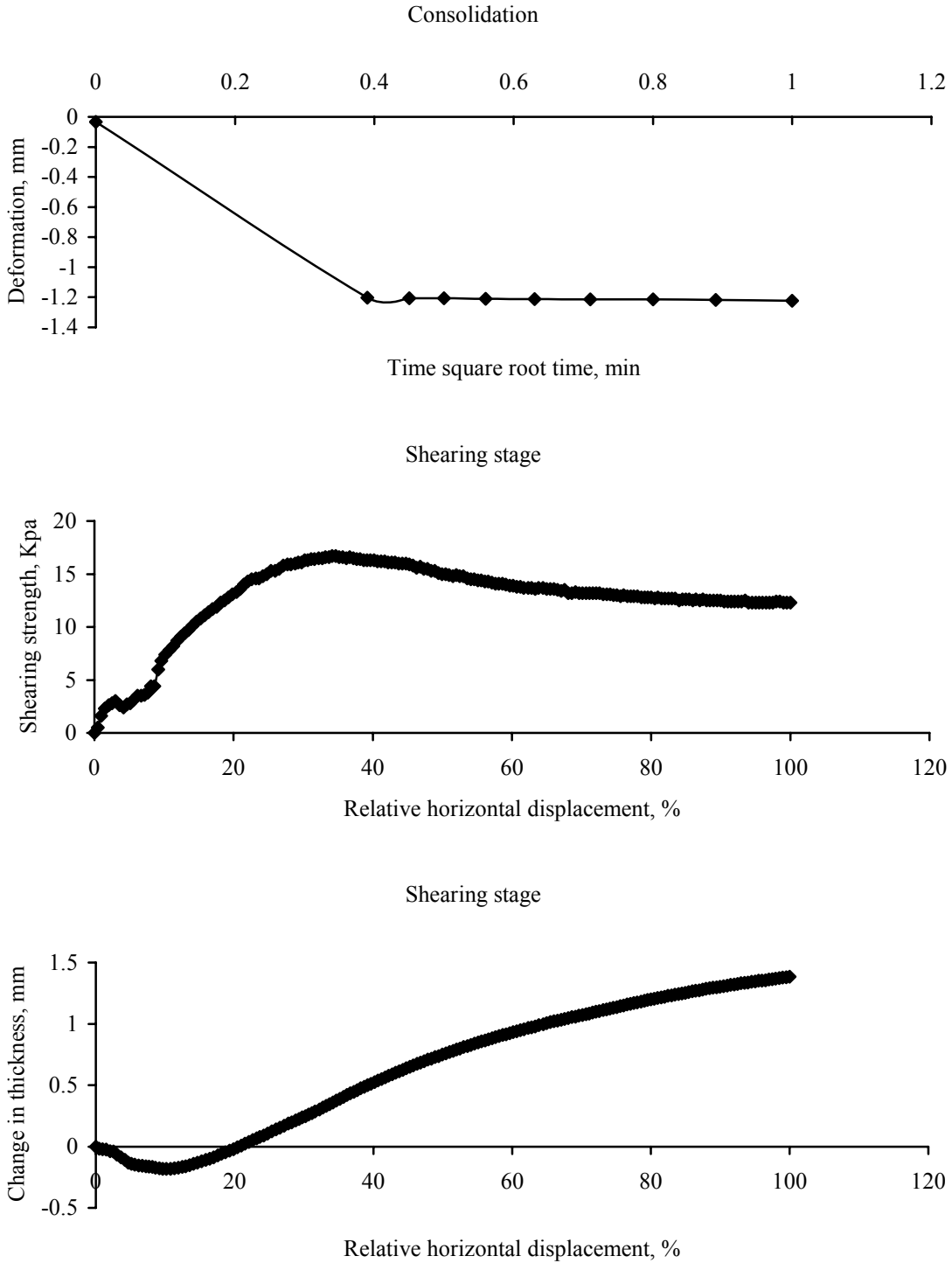

Figure B.30 16.2 kPa of normal stress was conducted in the specimen treated by 10^3 cells/mL of resting cells with 85% of relative density, and data was recorded in (a) consolidation and (b) shearing stage, respectively. Note that vertical deformation, horizontal deformation, residual strength, and peak strength were -0.972 mm, 3.746 mm, 12.3 kPa and 16.7 kPa, respectively.

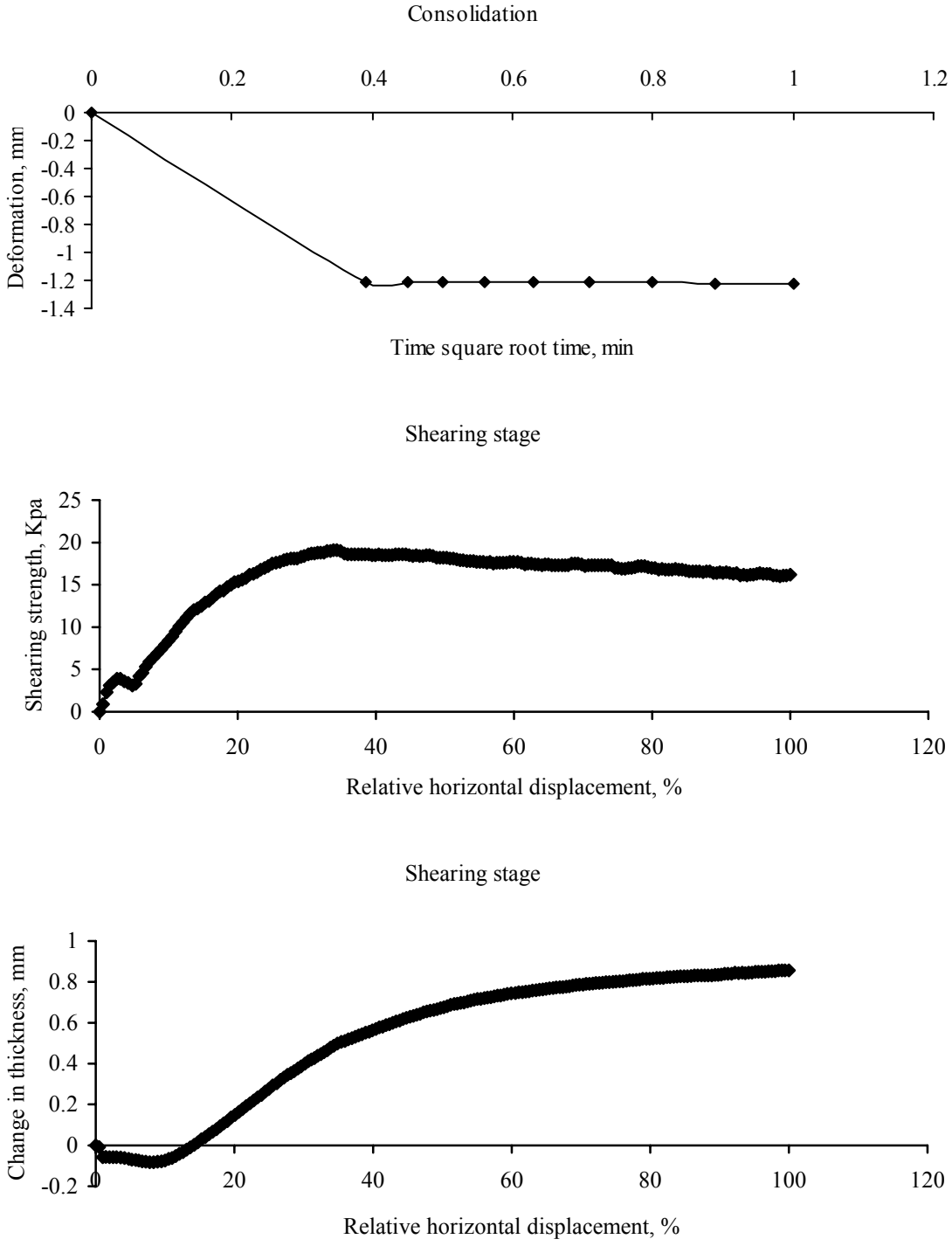

Figure B.31 21.1 kPa of normal stress was conducted in the specimen treated by 10^3 cells/mL of resting cells with 85% of relative density, and data was recorded in (a) consolidation and (b) shearing stage, respectively. Note that vertical deformation, horizontal deformation, residual strength, and peak strength were -0.812 mm, 3.809 mm, 16.2 kPa and 19.1 kPa, respectively.

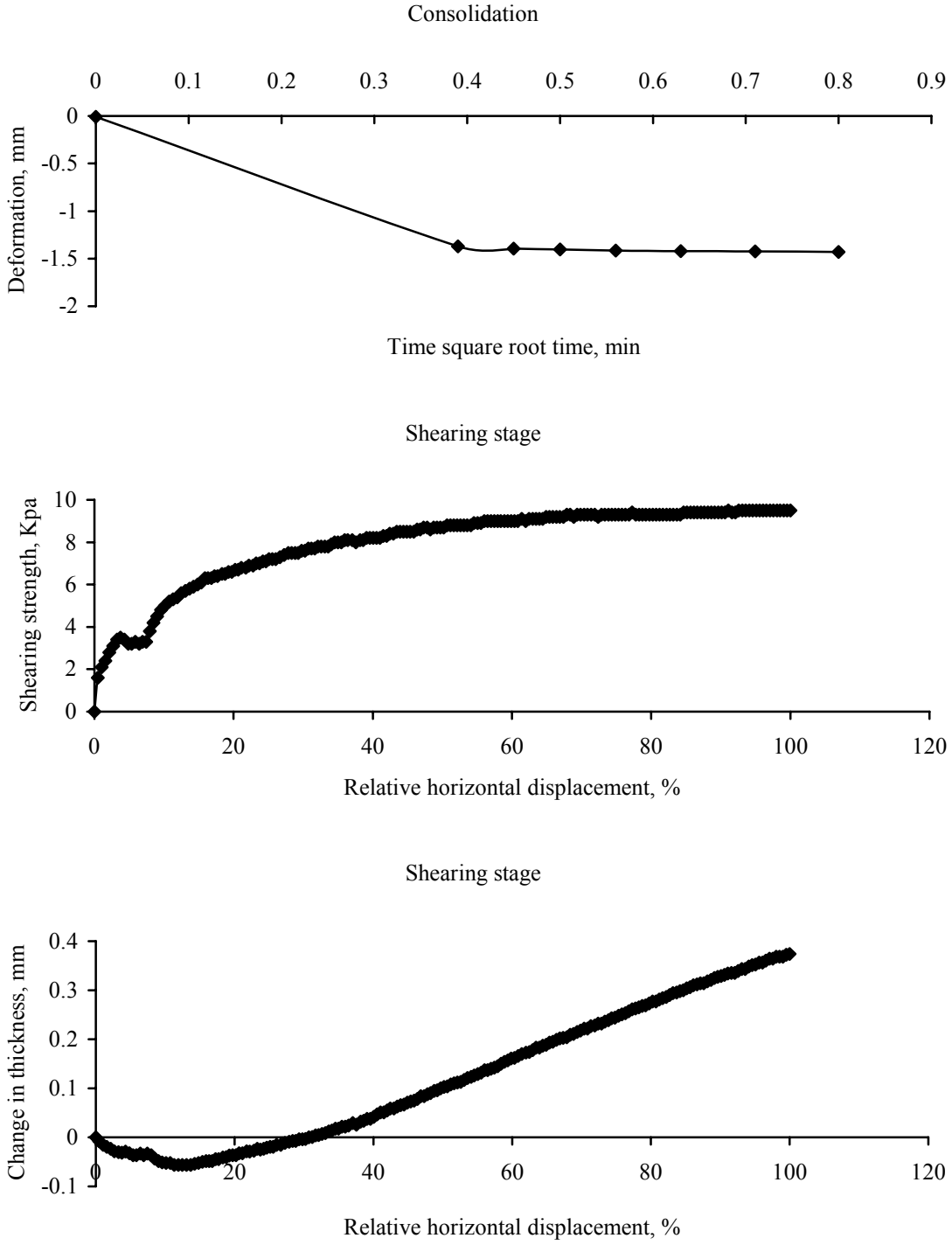

Figure B.32 11.3 kPa of normal stress was conducted in the specimen treated by 10^7 cells/mL of resting cells with 35% of relative density, and data was recorded in (a) consolidation and (b) shearing stage, respectively. Note that vertical deformation, horizontal deformation, and peak strength were -1.215 mm, 8,373 mm, and 9.3 kPa, respectively.

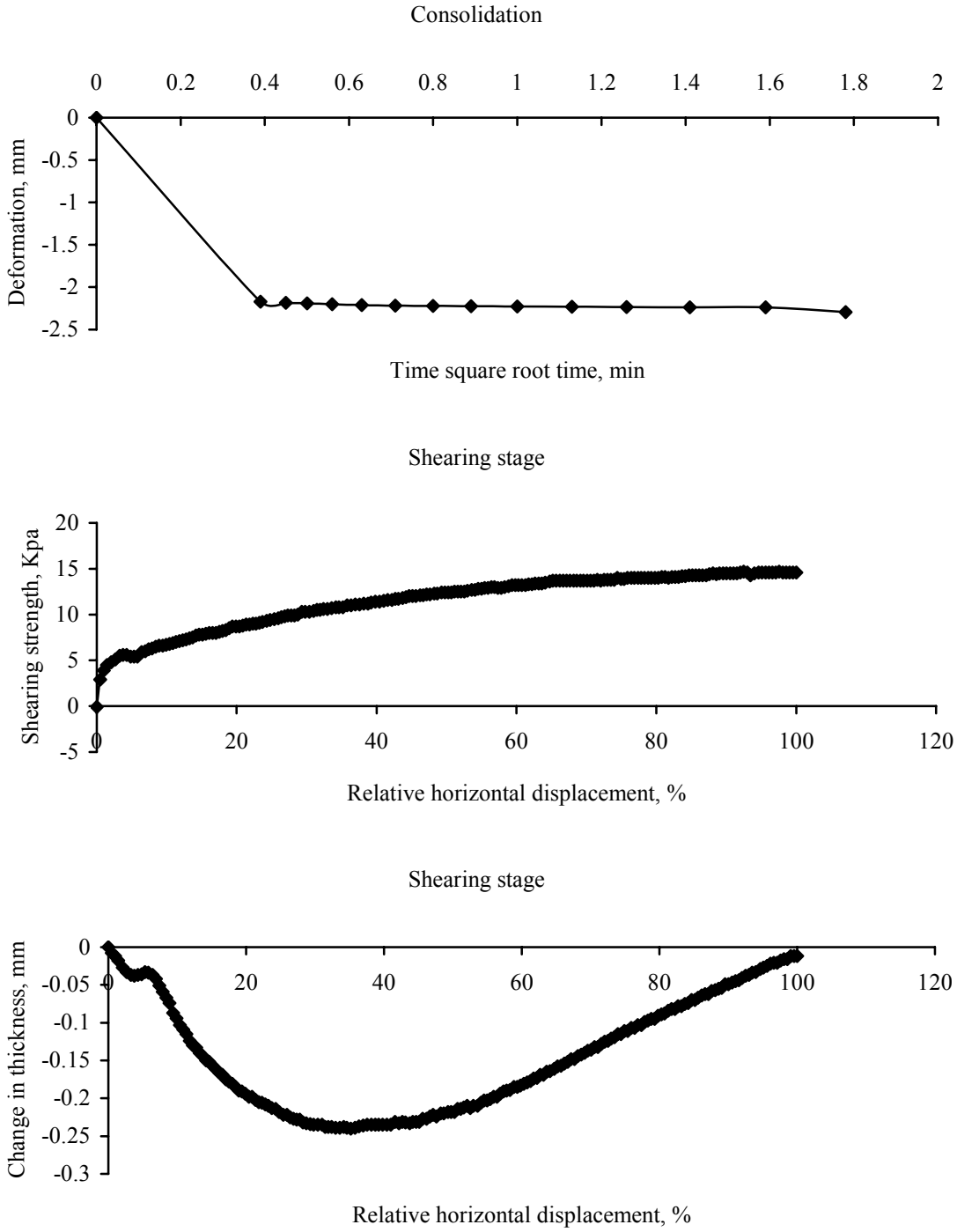

Figure B.33 21.1 kPa of normal stress was conducted in the specimen treated by 10^7 cells/mL of resting cells with 35% of relative density, and data was recorded in (a) consolidation and (b) shearing stage, respectively. Note that vertical deformation, horizontal deformation, and peak strength were -2.451 mm, 9.729 mm, and 14.5 kPa, respectively.

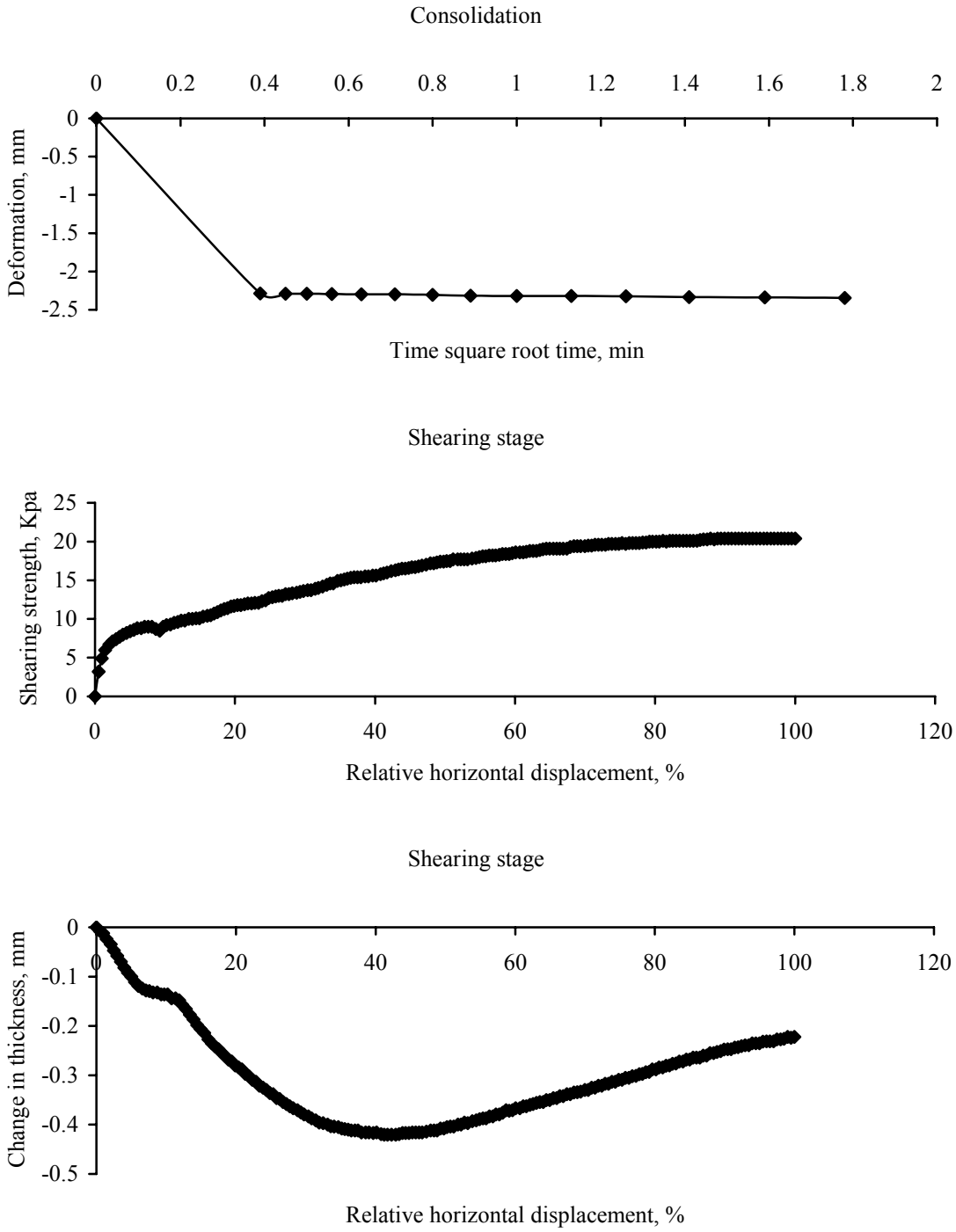

Figure B.34 30.9 kPa of normal stress was conducted in the specimen treated by 10^7 cells/mL of resting cells with 35% of relative density, and data was recorded in (a) consolidation and (b) shearing stage, respectively. Note that vertical deformation, horizontal deformation, and peak strength were -2.699 mm, 9.068 mm, and 20.1 kPa, respectively.

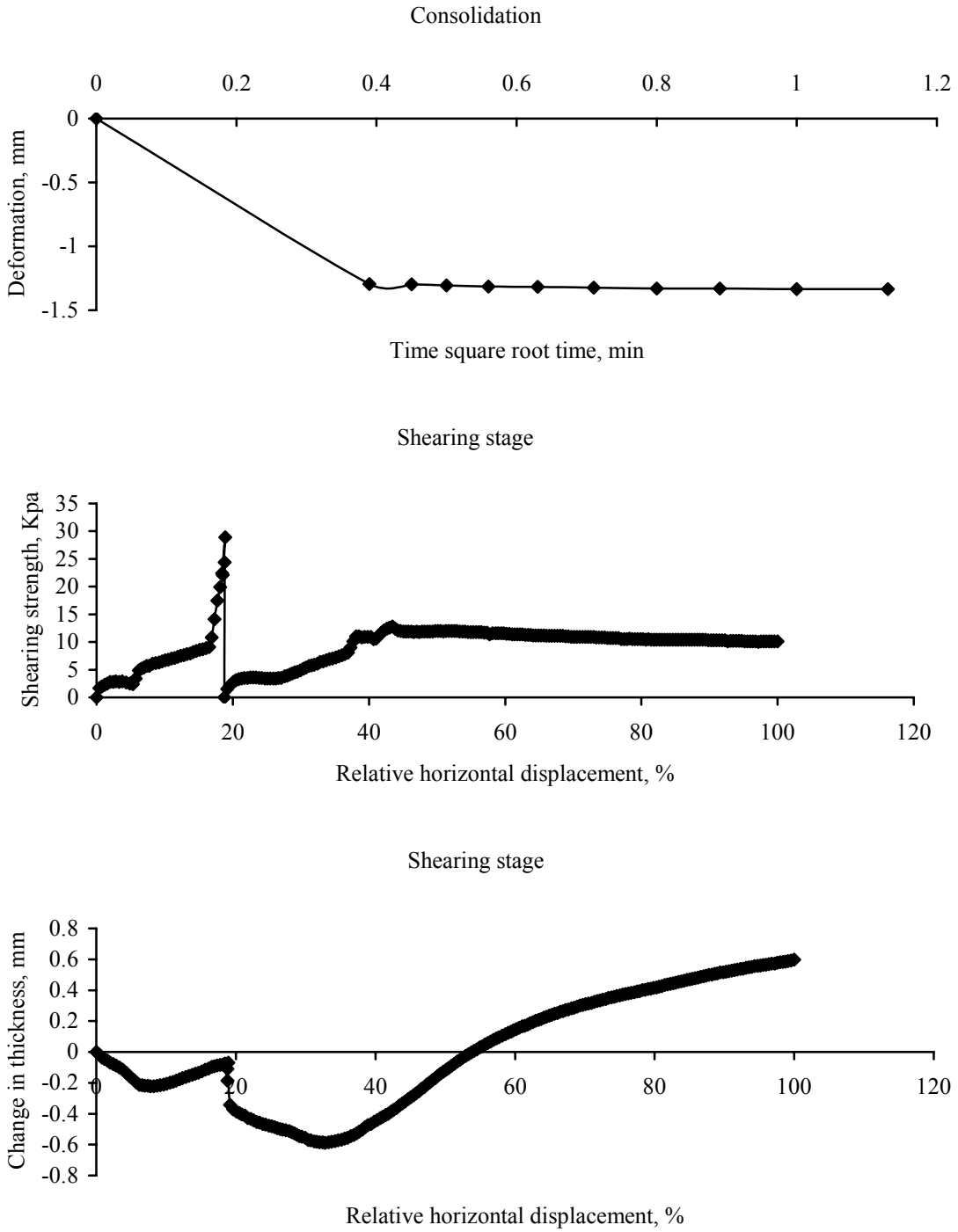

Figure B.35 11.3 kPa of normal stress was conducted in the specimen treated by 10^7 cells/mL of resting cells with 85% of relative density, and data was recorded in (a) consolidation and (b) shearing stage, respectively. Note that vertical deformation, horizontal deformation, residual strength and peak strength were -1.828 mm, 5.875 mm, 10.1 kPa and 12.6 kPa, respectively.

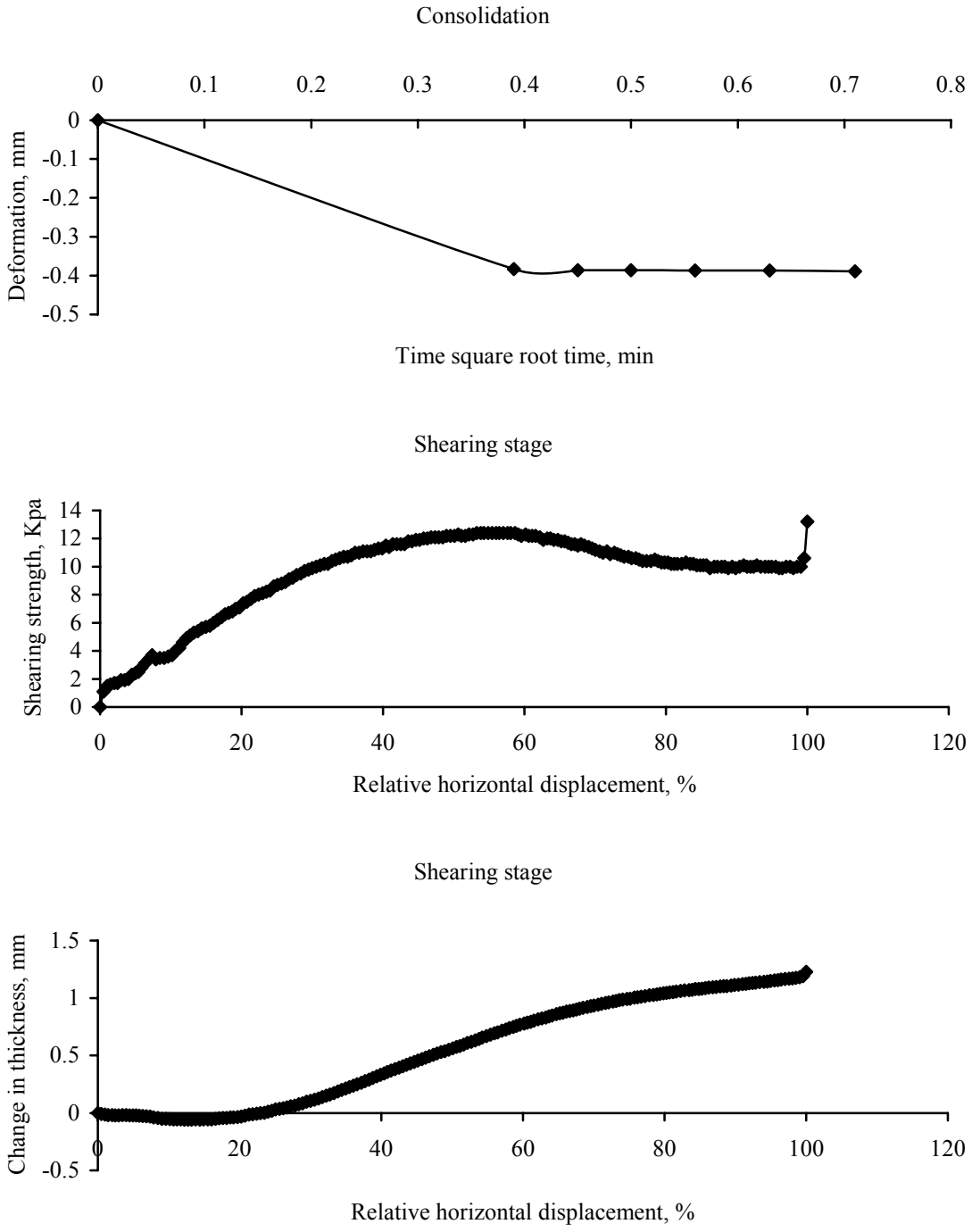

Figure B.36 11.3 kPa of normal stress was conducted in the specimen treated by 10^7 cells/mL of resting cells with 85% of relative density, and data was recorded in (a) consolidation and (b) shearing stage, respectively. Note that vertical deformation, horizontal deformation, residual strength and peak strength were -0.251 mm, 6.226 mm, 10 kPa and 12.4 kPa, respectively.

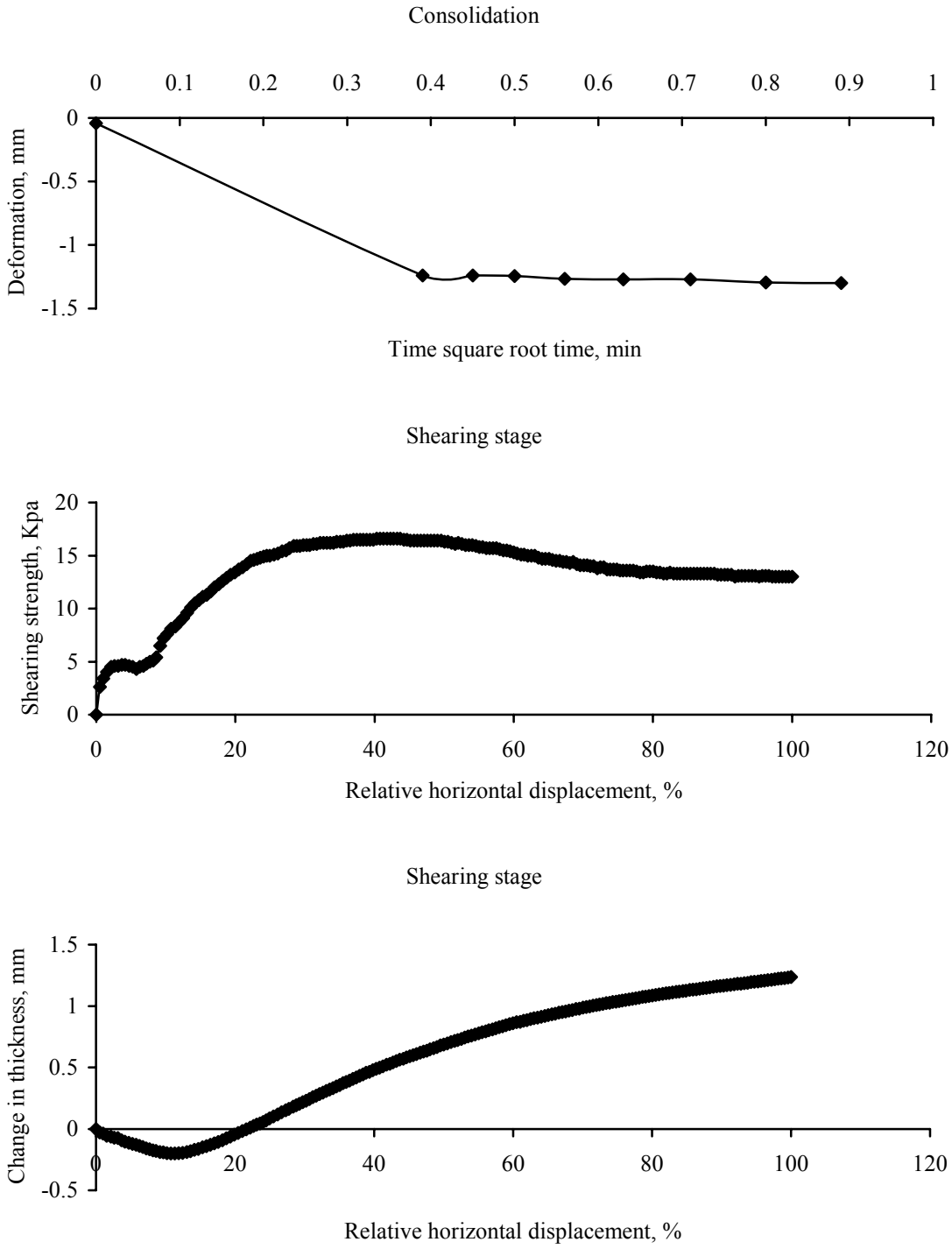

Figure B.37 16.2 kPa of normal stress was conducted in the specimen treated by 10^7 cells/mL of resting cells with 85% of relative density, and data was recorded in (a) consolidation and (b) shearing stage, respectively. Note that vertical deformation, horizontal deformation, residual strength and peak strength were -0.829 mm, 4.697 mm, 13 kPa and 16.6 kPa, respectively.

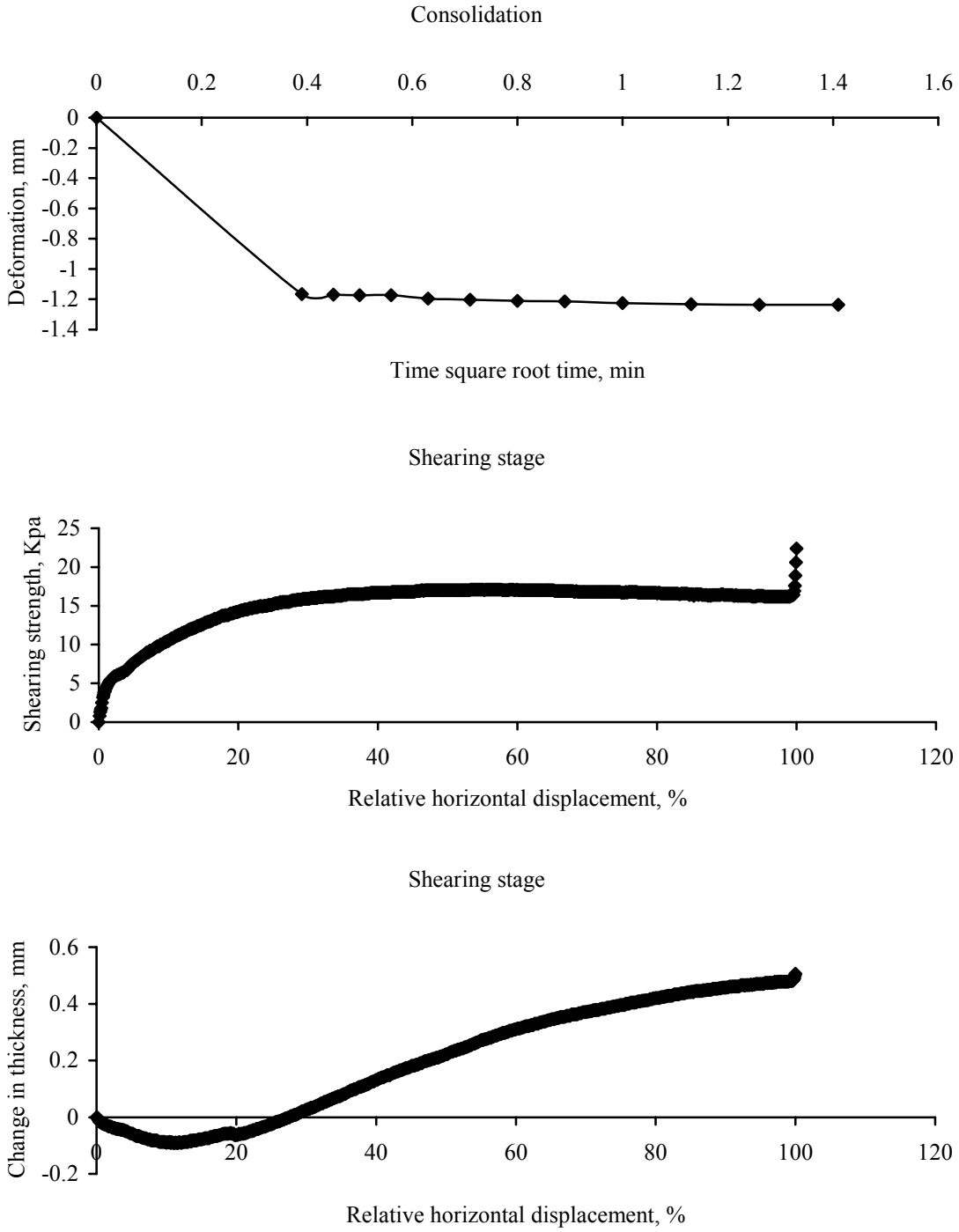

Figure B.38 21.1 kPa of normal stress was conducted in the specimen treated by 10^3 cells/mL of live cells with 35% of relative density, and data was recorded in (a) consolidation and (b) shearing stage, respectively. Note that vertical deformation, horizontal deformation, and peak strength were -1.051 mm, 5.190 mm, and 17.0 kPa, respectively.

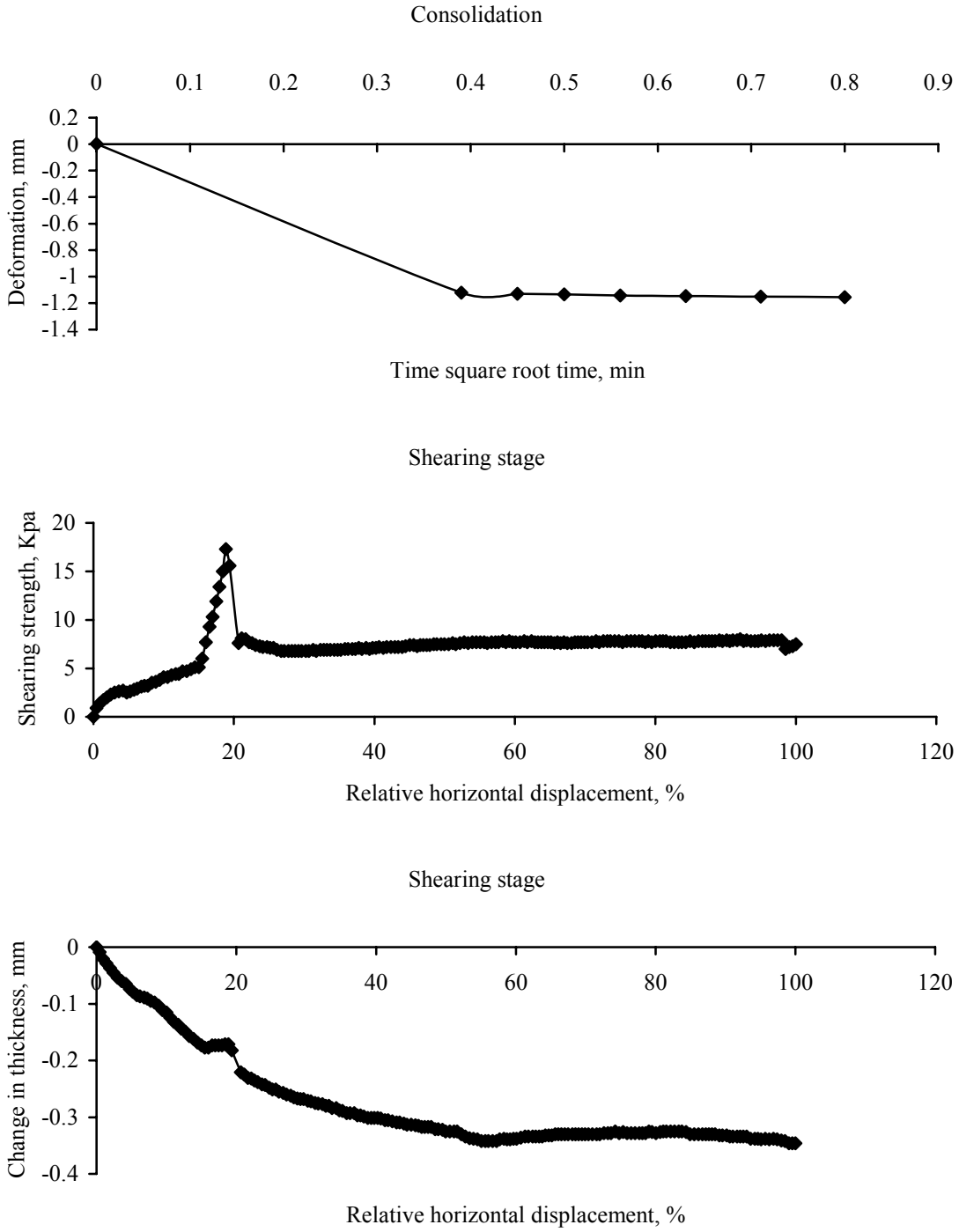

Figure B.39 11.3 kPa of normal stress was conducted in the specimen treated by 10^3 cells/mL of live cells with 35% of relative density, and data was recorded in (a) consolidation and (b) shearing stage, respectively. Note that vertical deformation, horizontal deformation, and peak strength were -1.671 mm, 8.865 mm, and 7.7 kPa, respectively.

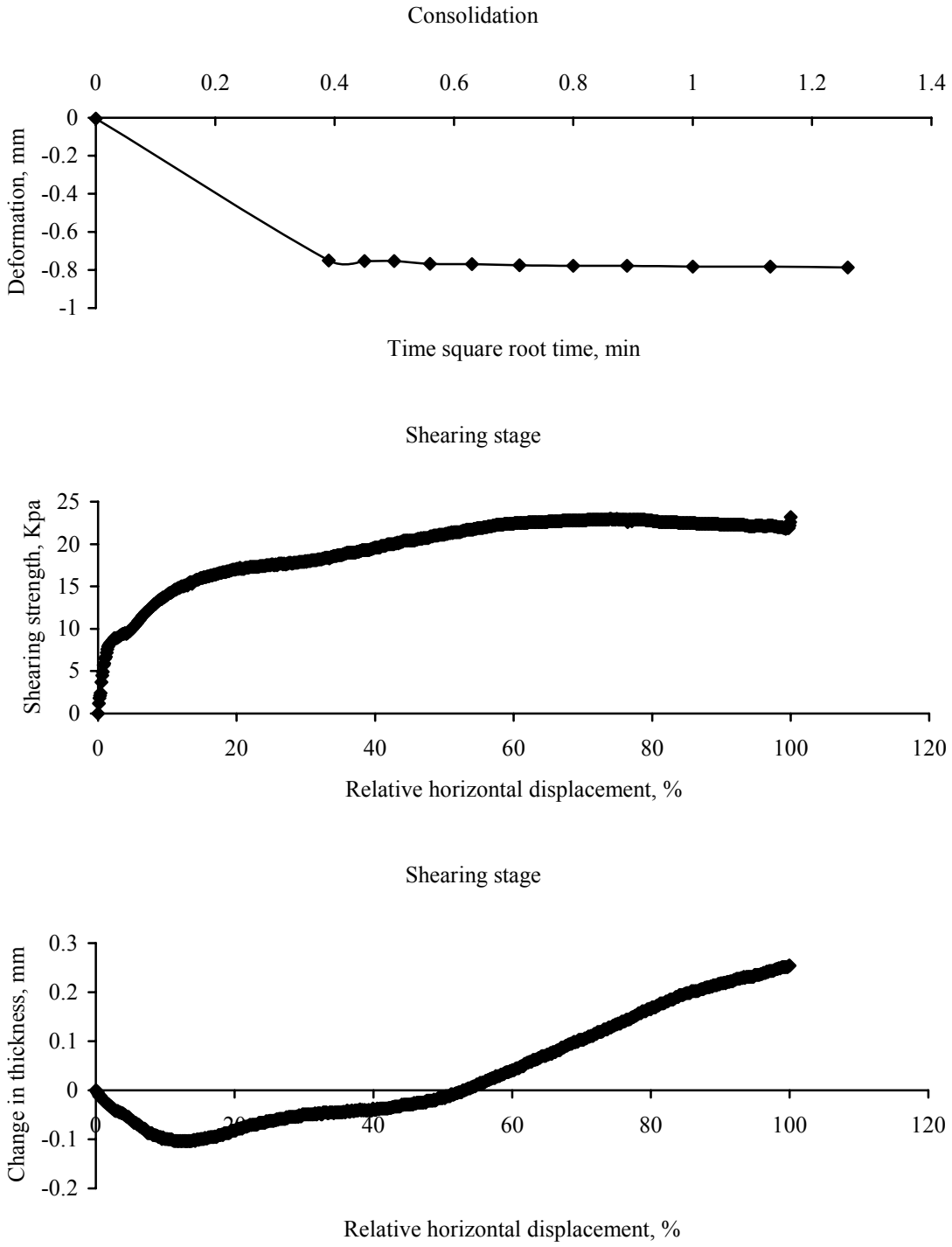

Figure B.40 30.9 kPa of normal stress was conducted in the specimen treated by 10^3 cells/mL of live cells with 35% of relative density, and data was recorded in (a) consolidation and (b) shearing stage, respectively. Note that vertical deformation, horizontal deformation, and peak strength were -0.726 mm, 7.379 mm, and 22.9 kPa, respectively.

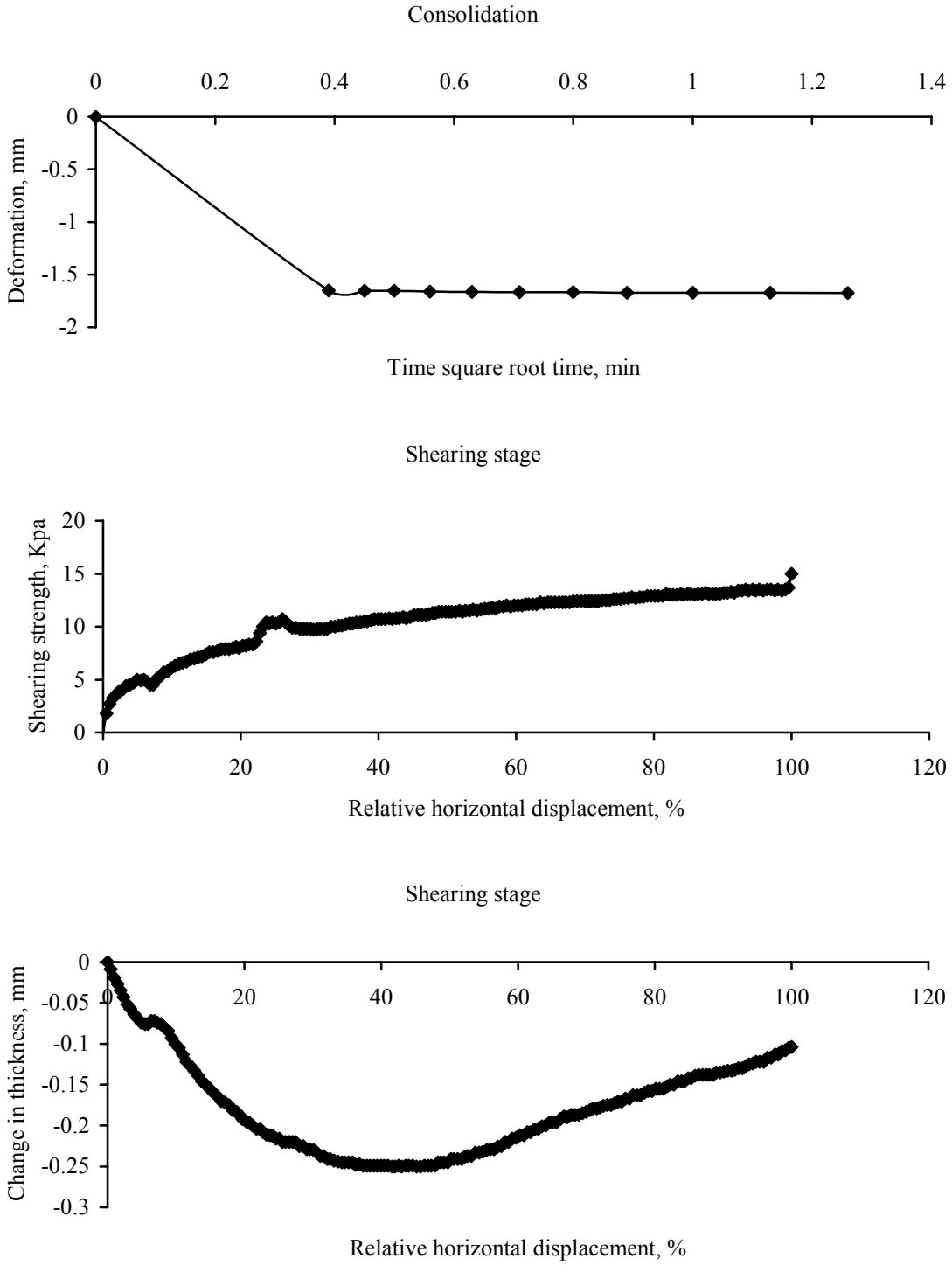

Figure B.41 21.1 kPa of normal stress was conducted in the specimen treated by 10^3 cells/mL of live cells with 35% of relative density, and data was recorded in (a) consolidation and (b) shearing stage, respectively. Note that vertical deformation, horizontal deformation, and peak strength were -1.862 mm, 10.989 mm, and 13.4 kPa, respectively.

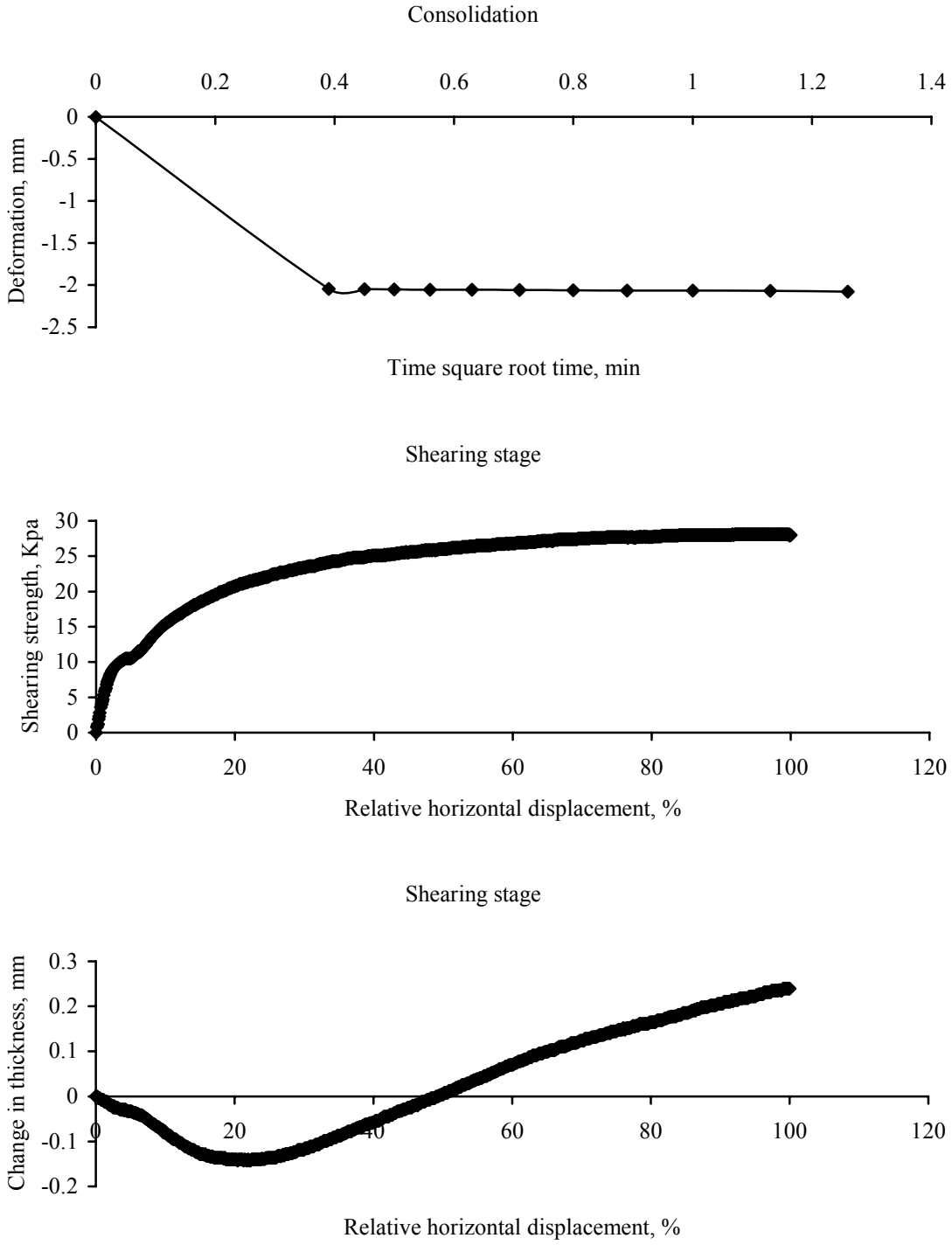

Figure B.42 40.7 kPa of normal stress was conducted in the specimen treated by 10^3 cells/mL of live cells with 35% of relative density, and data was recorded in (a) consolidation and (b) shearing stage, respectively. Note that vertical deformation, horizontal deformation, and peak strength were -2.031 mm, 8.709 mm, and 28 kPa, respectively.

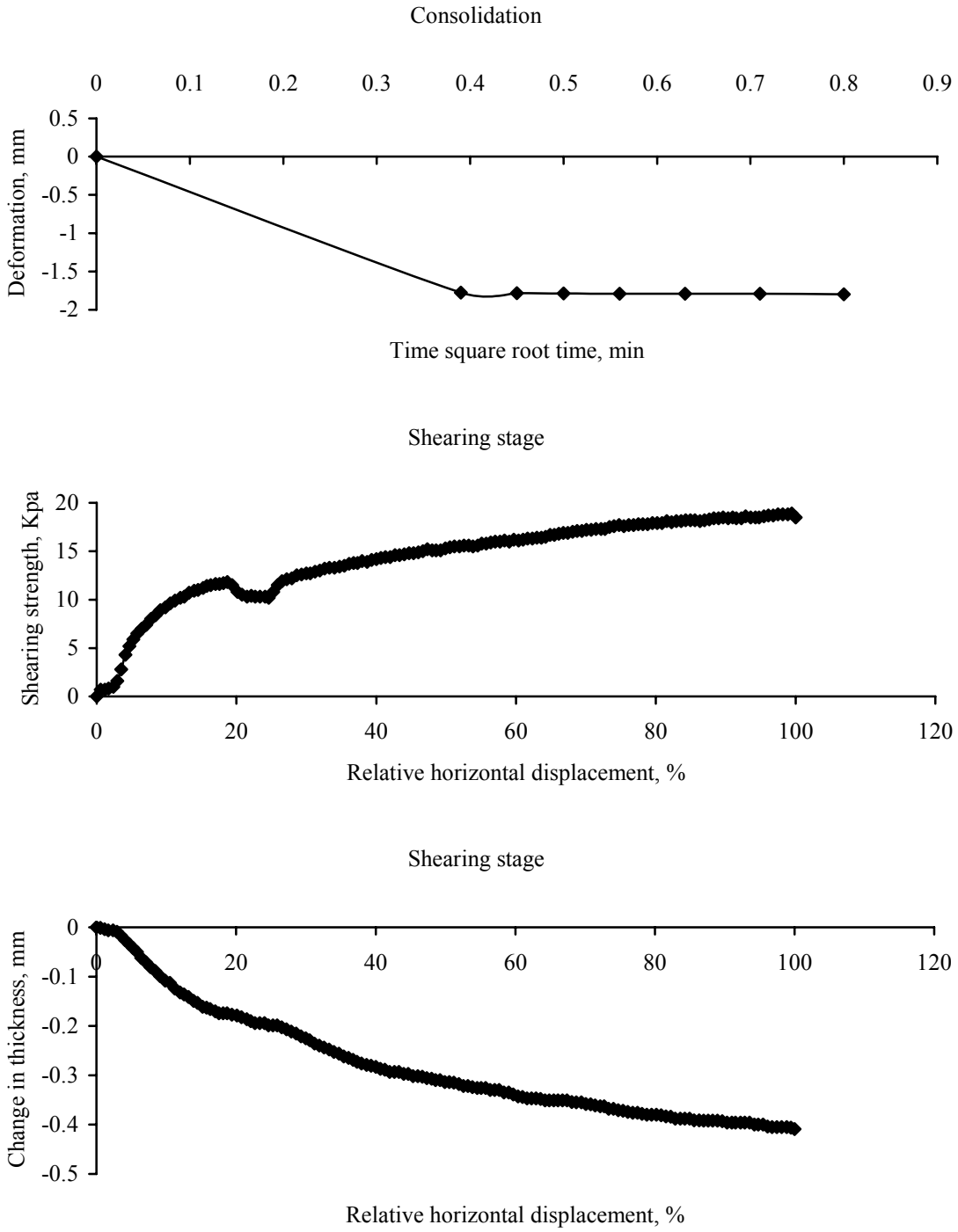

Figure B.43 30.9 kPa of normal stress was conducted in the specimen treated by 10^3 cells/mL of live cells with 35% of relative density, and data was recorded in (a) consolidation and (b) shearing stage, respectively. Note that vertical deformation, horizontal deformation, and peak strength were -2.288 mm, 9.216 mm, and 18.9 kPa, respectively.

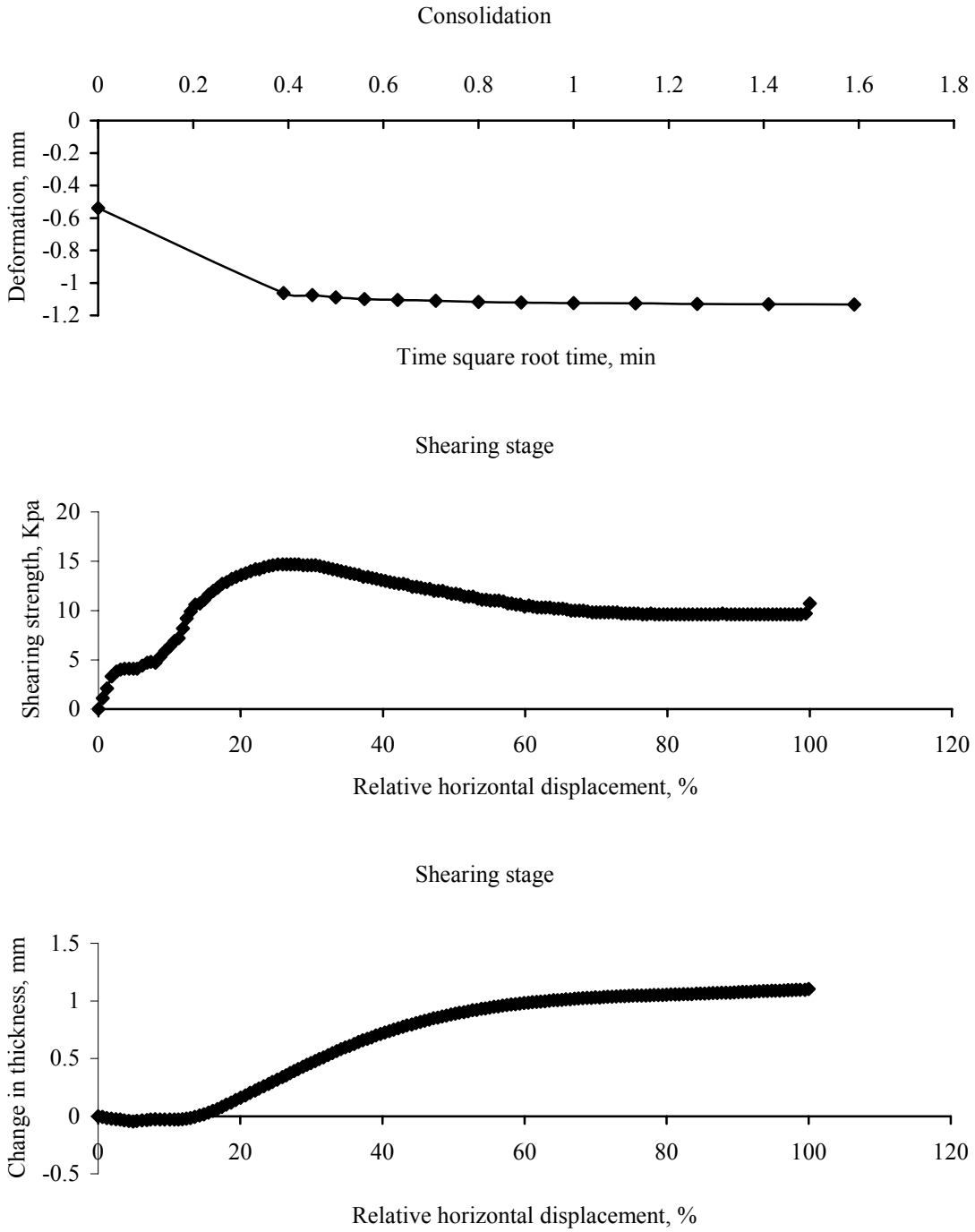

Figure B.44 11.3 kPa of normal stress was conducted in the specimen treated by 10^3 cells/mL of live cells with 85% of relative density, and data was recorded in (a) consolidation and (b) shearing stage, respectively. Note that vertical deformation, horizontal deformation, residual strength and peak strength were -0.878 mm, 2.452 mm, 9.7 kPa and 14.7 kPa, respectively.

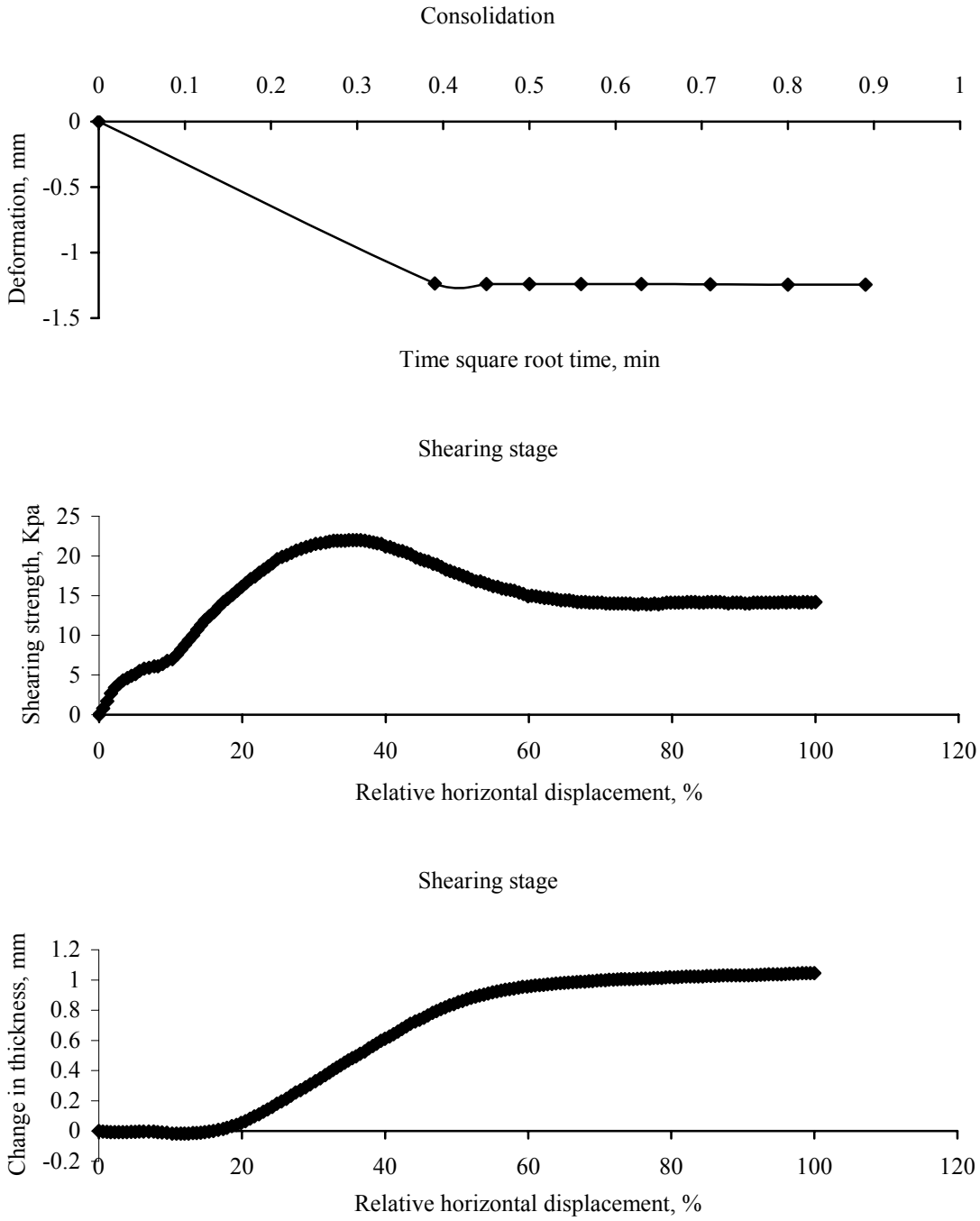

Figure B.45 21.1 kPa of normal stress was conducted in the specimen treated by 10^3 cells/mL of live cells with 85% of relative density, and data was recorded in (a) consolidation and (b) shearing stage, respectively. Note that vertical deformation, horizontal deformation, residual strength and peak strength were -0.78 mm, 3.277 mm, 14.2 kPa and 22 kPa, respectively.

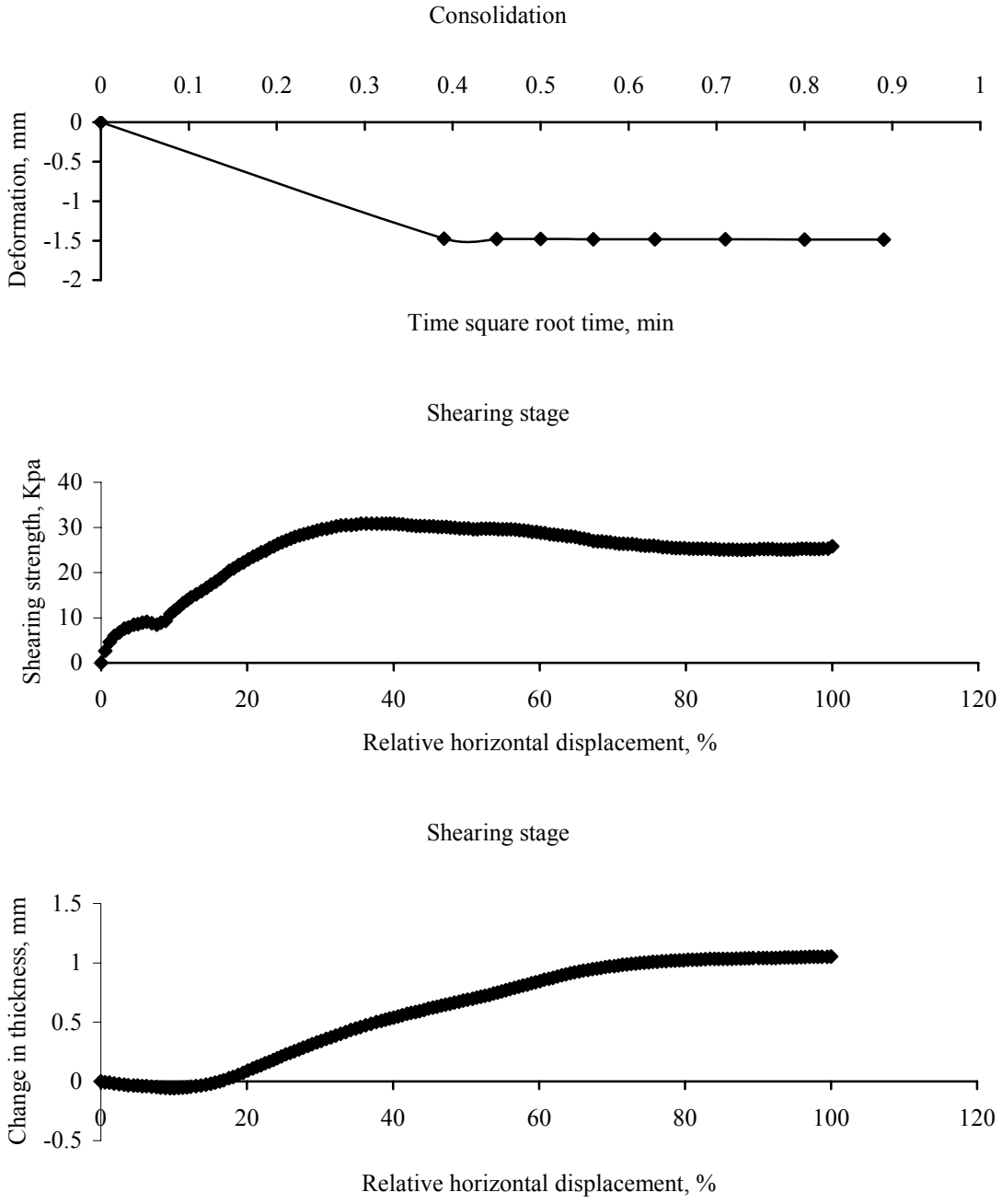

Figure B.46 30.9 kPa of normal stress was conducted in the specimen treated by 10^3 cells/mL of live cells with 85% of relative density, and data was recorded in (a) consolidation and (b) shearing stage, respectively. Note that vertical deformation, horizontal deformation, residual strength and peak strength were -1.015 mm, 3.36 mm, 25.2 kPa and 30.8 kPa, respectively.

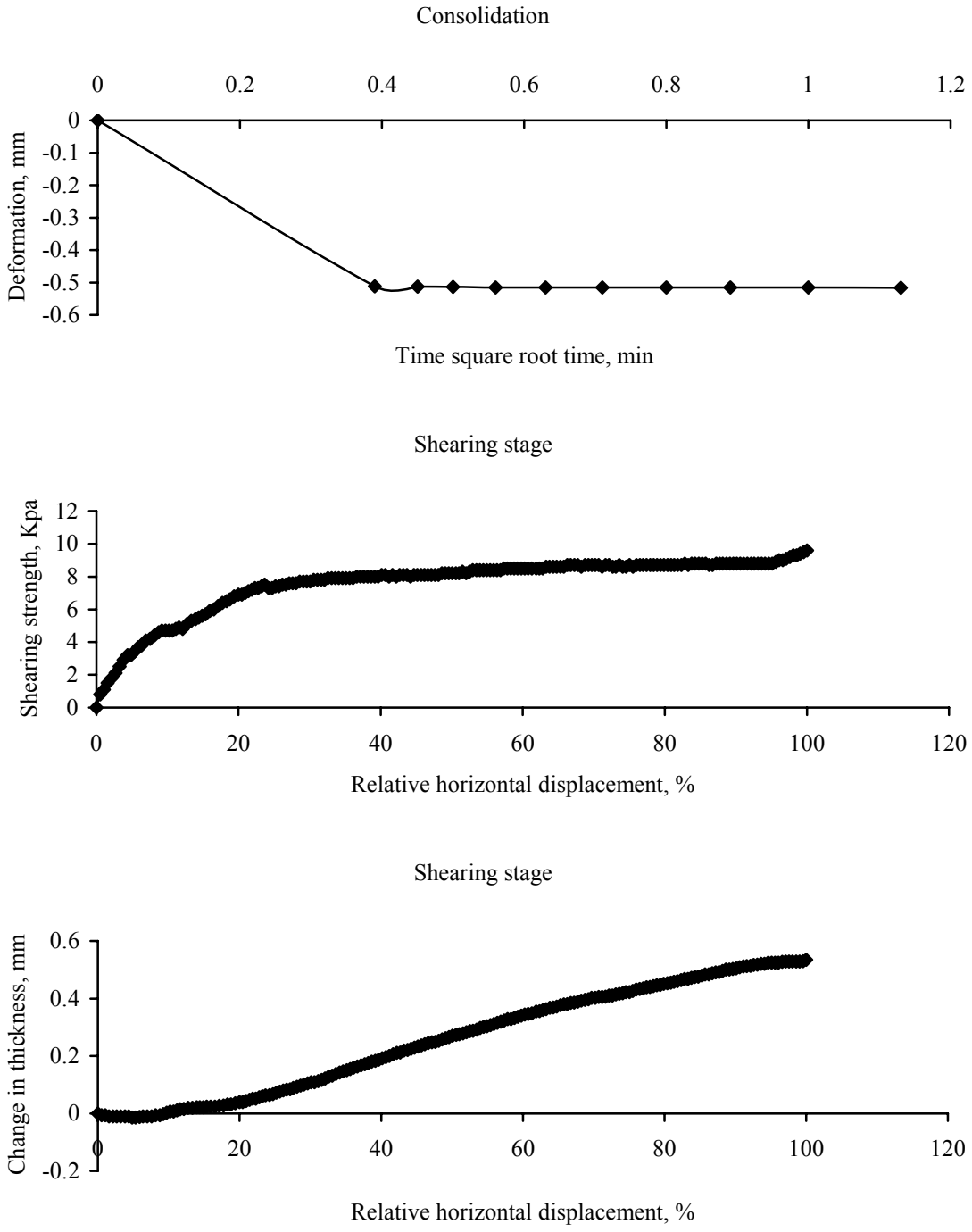

Figure B.47 11.3 kPa of normal stress was conducted in the specimen treated by 10^7 cells/mL of live cells with 35% of relative density, and data was recorded in (a) consolidation and (b) shearing stage, respectively. Note that vertical deformation, horizontal deformation, and peak strength were -0.181 mm, 7.287 mm, and 8.7 kPa, respectively.

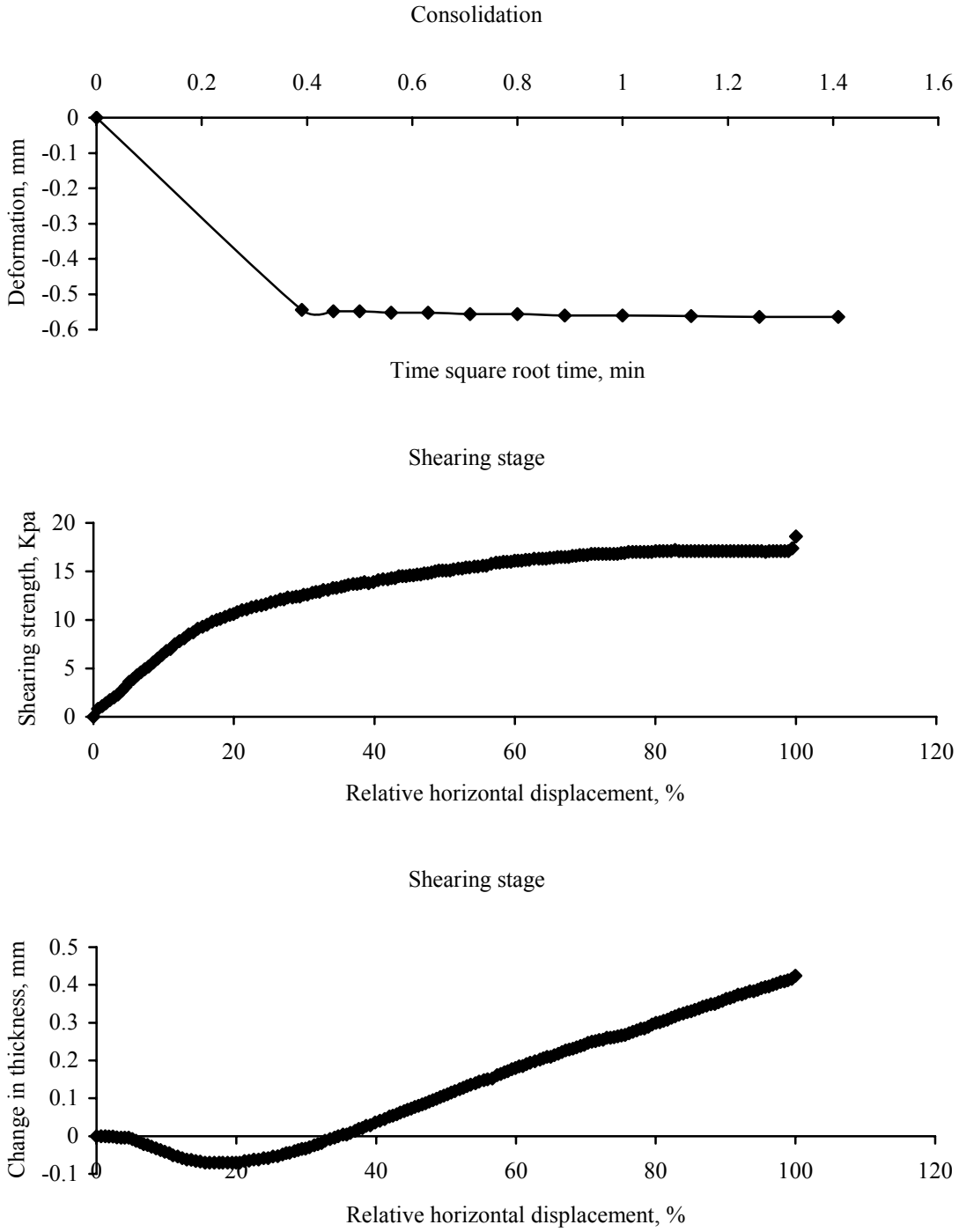

Figure B.48 21.1 kPa of normal stress was conducted in the specimen treated by 10^7 cells/mL of live cells with 35% of relative density, and data was recorded in (a) consolidation and (b) shearing stage, respectively. Note that vertical deformation, horizontal deformation, and peak strength were -0.379 mm, 7.419 mm, and 17 kPa, respectively.

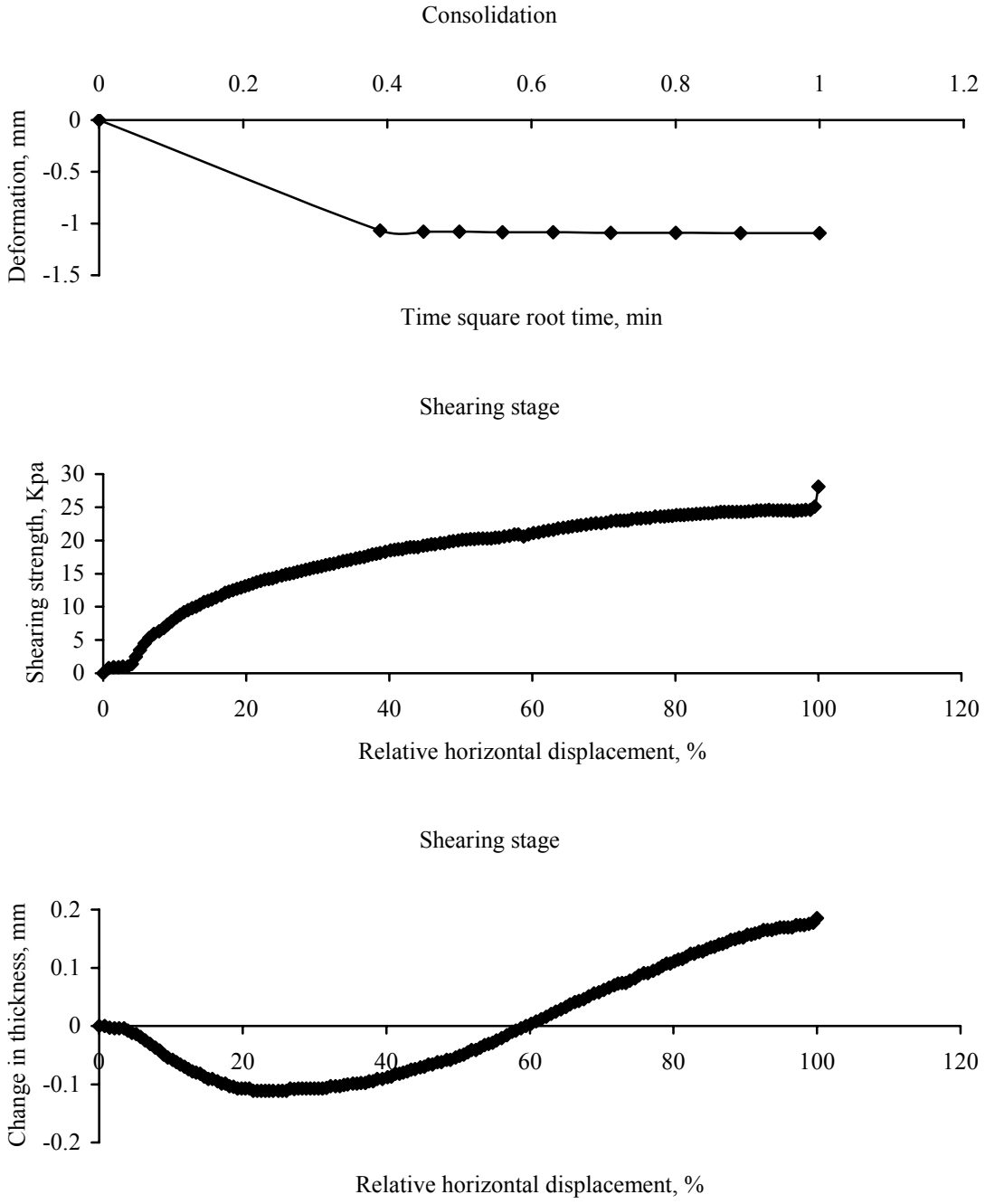

Figure B.49 30.9 kPa of normal stress was conducted in the specimen treated by 10^7 cells/mL of live cells with 35% of relative density, and data was recorded in (a) consolidation and (b) shearing stage, respectively. Note that vertical deformation, horizontal deformation, and peak strength were -1.022 mm, 8.888 mm, and 24.5 kPa, respectively.

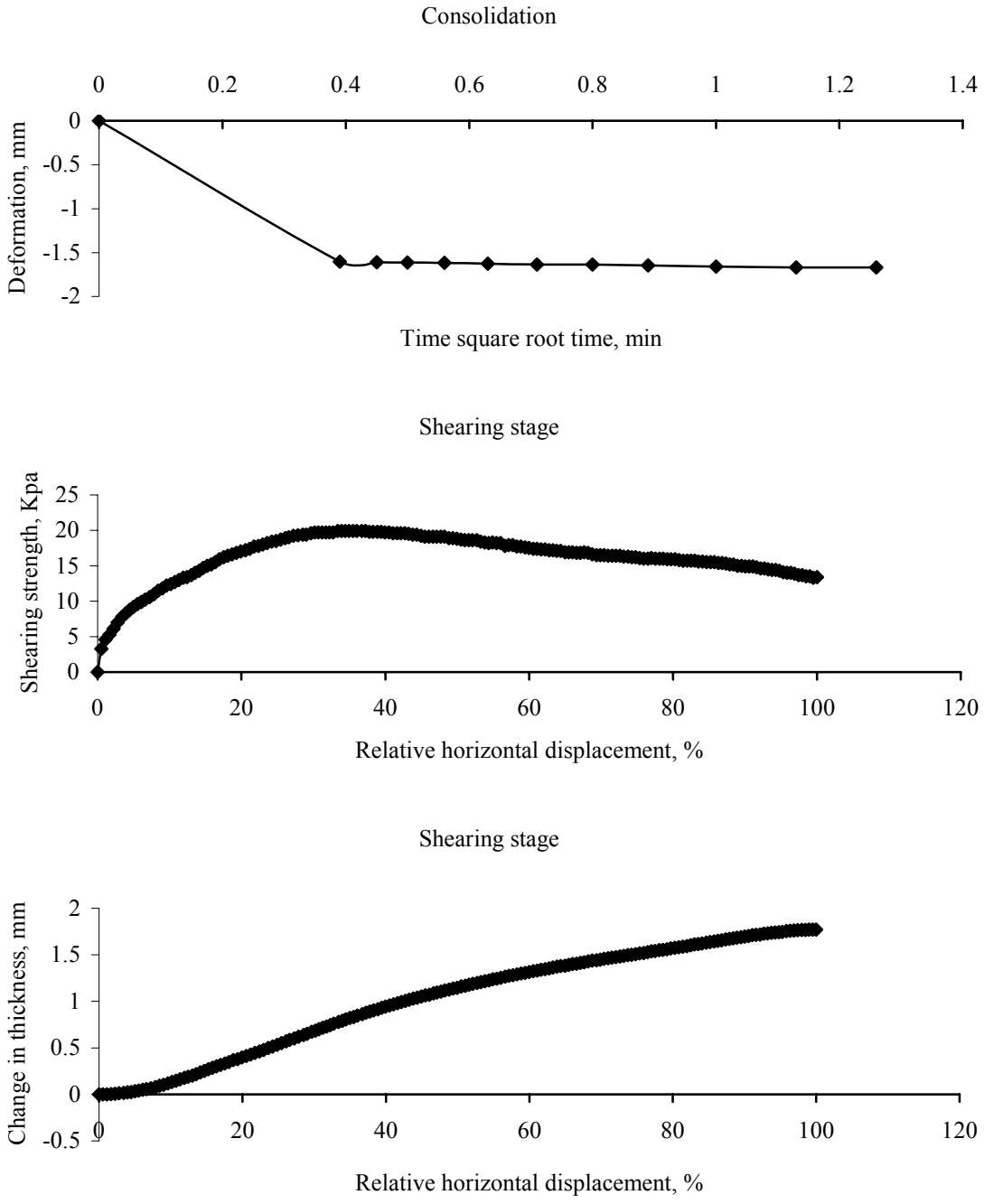

Figure B.50 21.1 kPa of normal stress was conducted in the specimen treated by 10^7 cells/mL of live cells with 85% of relative density, and data was recorded in (a) consolidation and (b) shearing stage, respectively. Note that vertical deformation, horizontal deformation, residual strength, and peak strength were -0.832 mm, 3.576 mm, 13.4 kPa and 19.9 kPa, respectively.

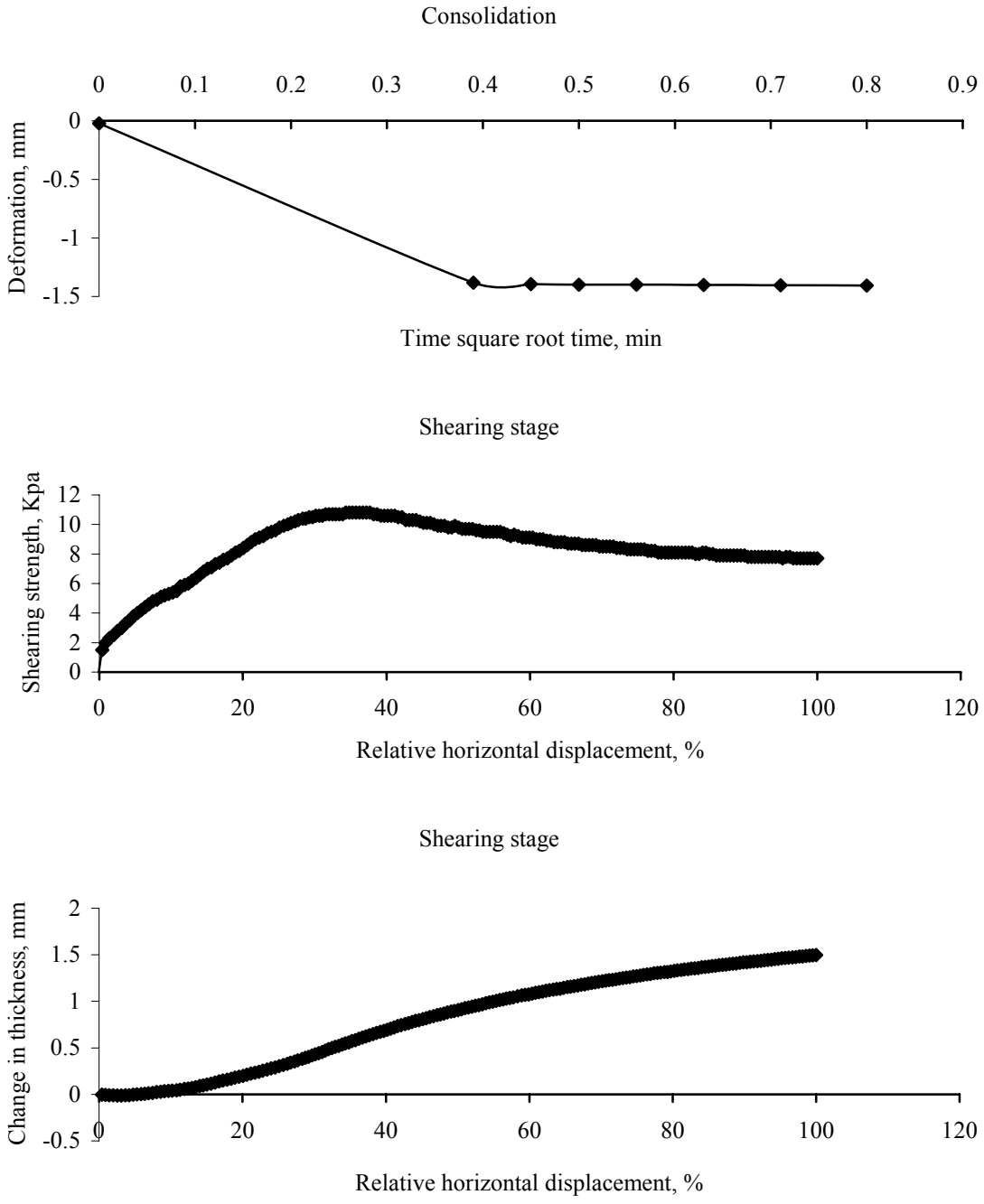

Figure B.51 11.3 kPa of normal stress was conducted in the specimen treated by 10^7 cells/mL of live cells with 85% of relative density, and data was recorded in (a) consolidation and (b) shearing stage, respectively. Note that vertical deformation, horizontal deformation, residual strength, and peak strength were -0.849 mm, 4.010 mm, 7.7 kPa and 10.8 kPa, respectively.

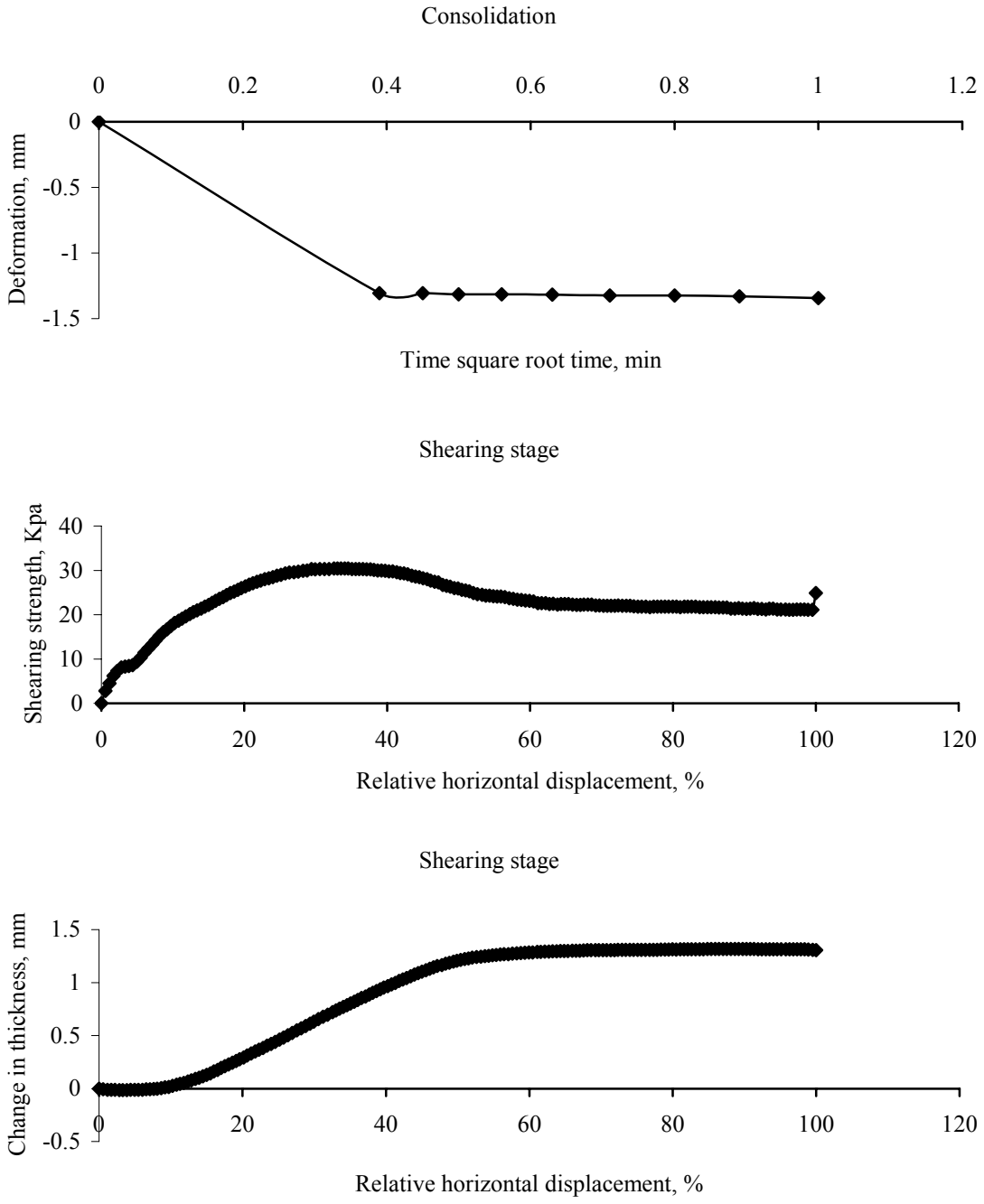

Figure B.52 30.9 kPa of normal stress was conducted in the specimen treated by 10^7 cells/mL of live cells with 85% of relative density, and data was recorded in (a) consolidation and (b) shearing stage, respectively. Note that vertical deformation, horizontal deformation, residual strength, and peak strength were -0.606 mm, 3.438 mm, 21.1 kPa and 30.4 kPa, respectively.

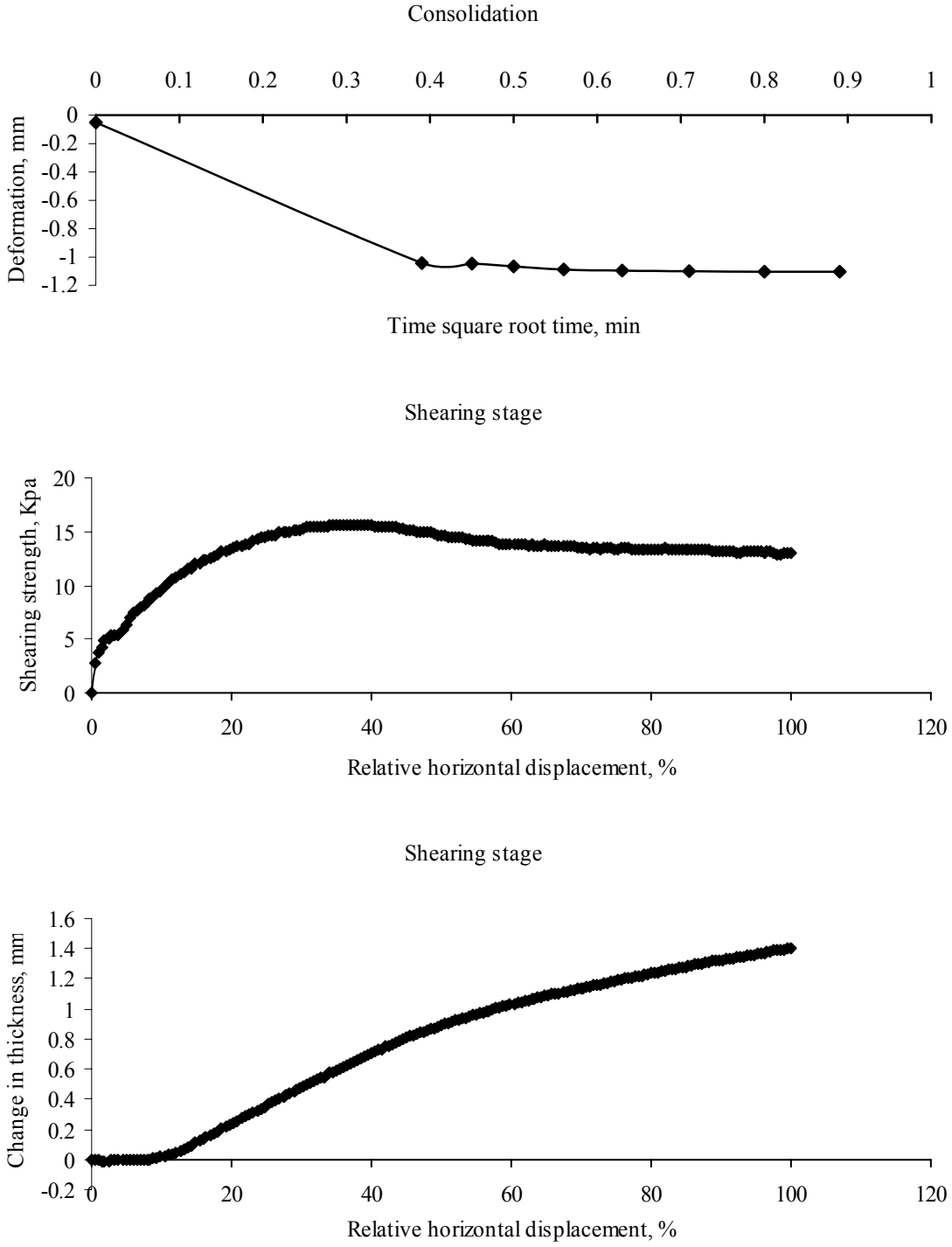

Figure B.53 16.2 kPa of normal stress was conducted in the specimen treated by 10^7 cells/mL of live cells with 85% of relative density, and data was recorded in (a) consolidation and (b) shearing stage, respectively. Note that vertical deformation, horizontal deformation, residual strength, and peak strength were -0.518 mm, 4.052 mm, 13 kPa and 15.6 kPa, respectively.

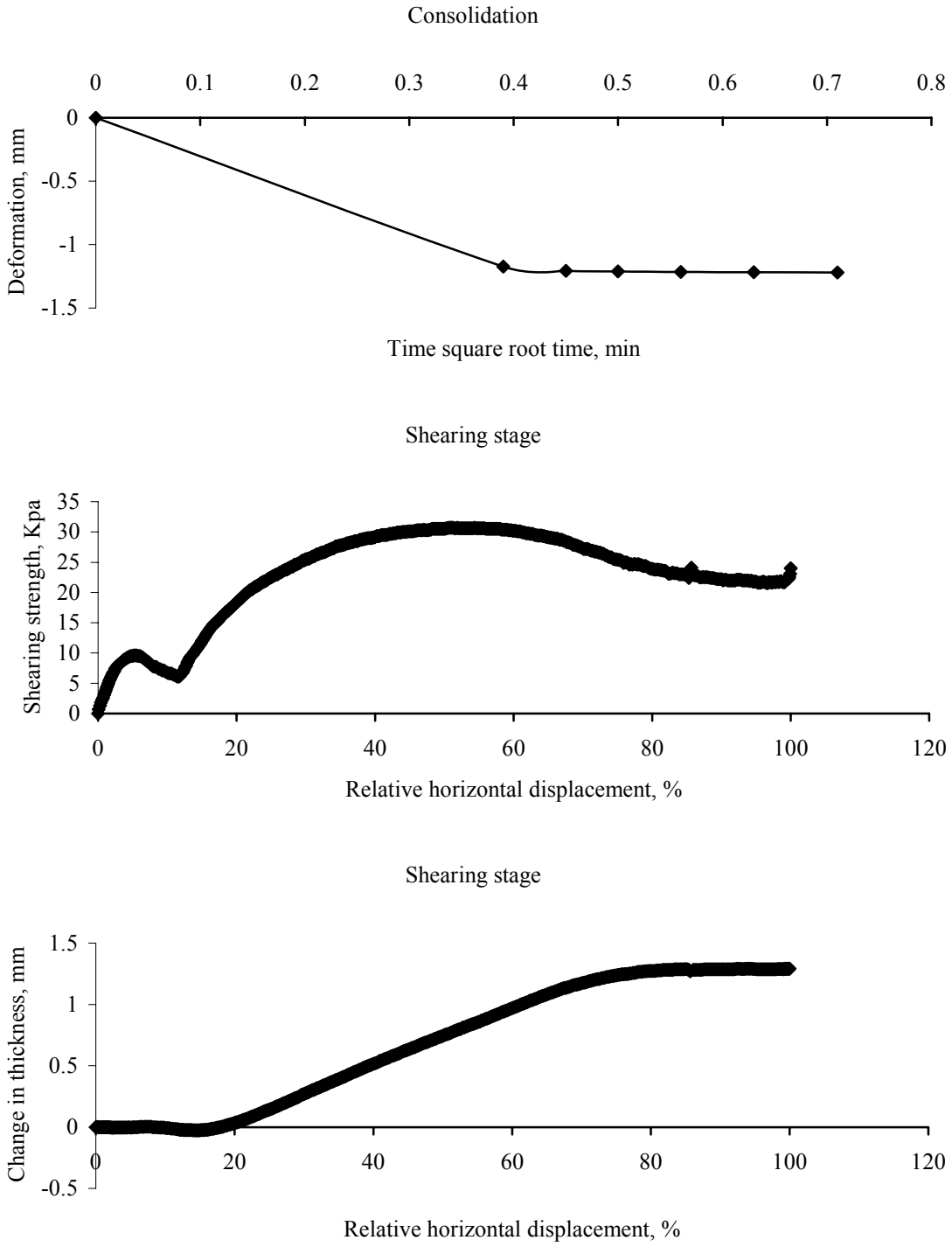

Figure B.54 30.9 kPa of normal stress was conducted in the specimen treated by 10^7 cells/mL of live cells with 85% of relative density, and data was recorded in (a) consolidation and (b) shearing stage, respectively. Note that vertical deformation, horizontal deformation, residual strength, and peak strength were -0.466 mm, 4.586 mm, 21.8 kPa and 30.6 kPa, respectively.

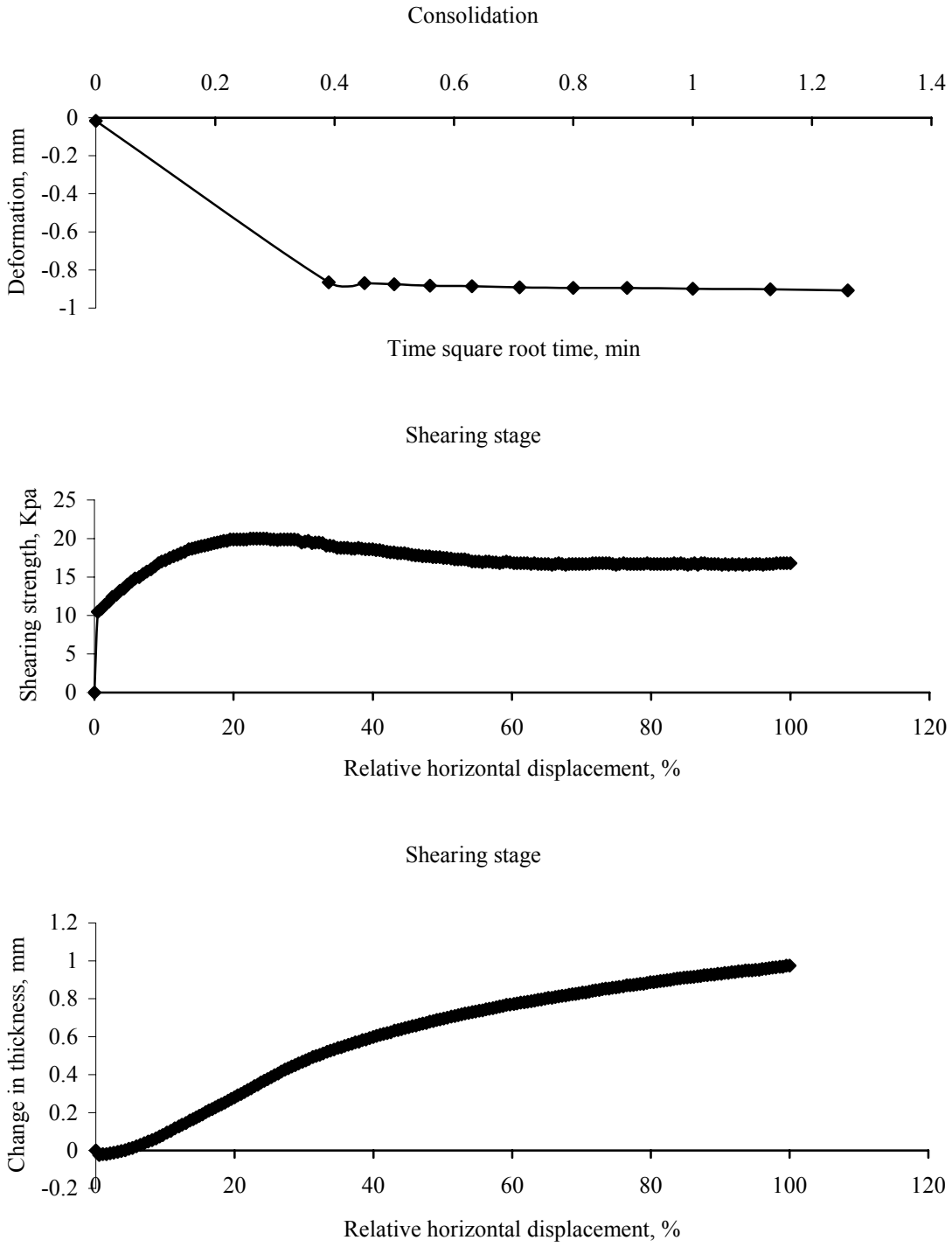

Figure B.55 26.0 kPa of normal stress was conducted in the specimen treated by 10^7 cells/mL of live cells with 85% of relative density, and data was recorded in (a) consolidation and (b) shearing stage, respectively. Note that vertical deformation, horizontal deformation, residual strength, and peak strength were -0.597 mm, 2.502 mm, 16.7 kPa and 20.0 kPa, respectively.

APPENDIX C

SCANNING ELECTRON MICROSCOPY ANALYSIS

In order to examine how calcareous crystals induced by microbes associate with sand particles and distribute within sand matrix, and how microbes attach onto sand particles, scanning electron microscopy (SEM) was conducted in untreated and live-cell treated sand. Generally, washing is one of specimen preparation stages in SEM procedure. However, in order to not disturb the association between precipitates and sand particles, treated sand samples were divided into the specimens with washing and without washing treatment. All images are listed as an order of untreated sand, treated sand without washing treatment, and treated sand with washing treatment. Finally, the identity of calcareous crystals was confirmed by Energy diffusion X-ray spectrometer (EDS).

(a)

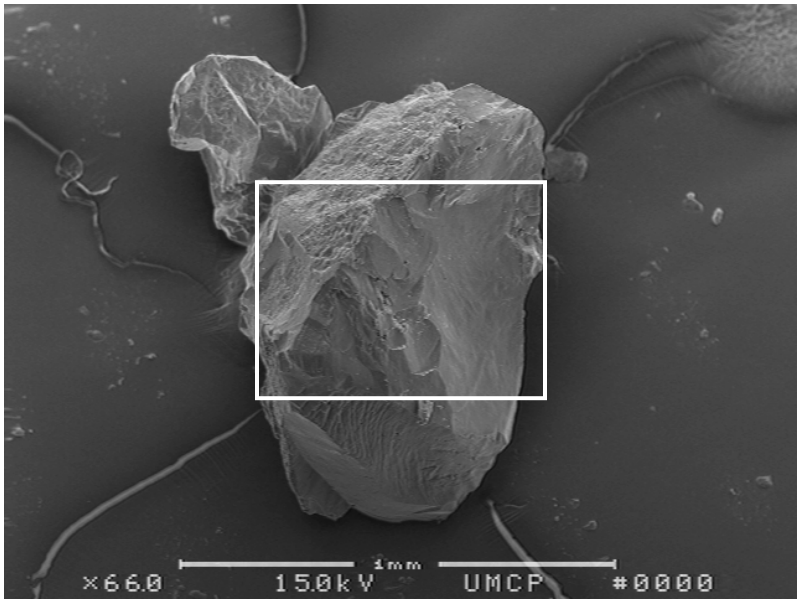

(b)

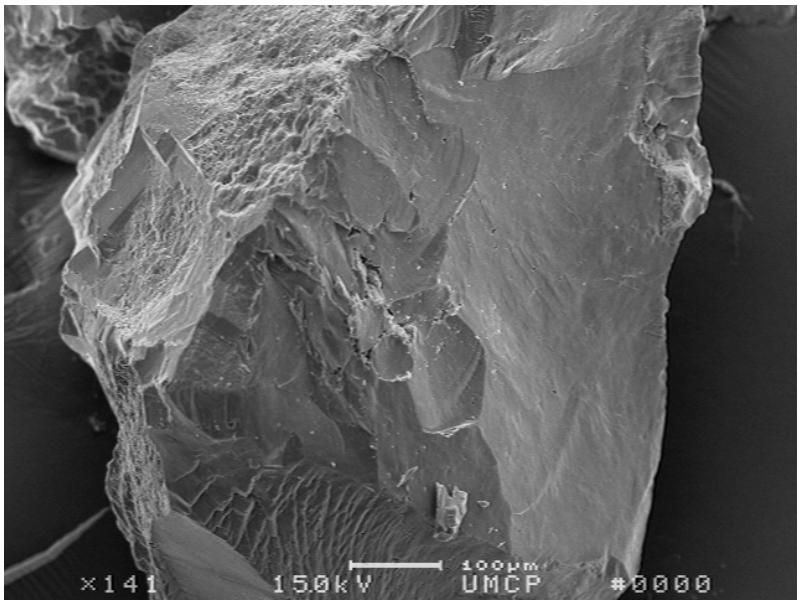

Figure C.1 Scanning electro micrographs of untreated sand in l mm of resolution (a), and focused on the surface of sand particle by using 100 µm of resolution (b). Note that untreated sand revealed rough and angled.

(a)

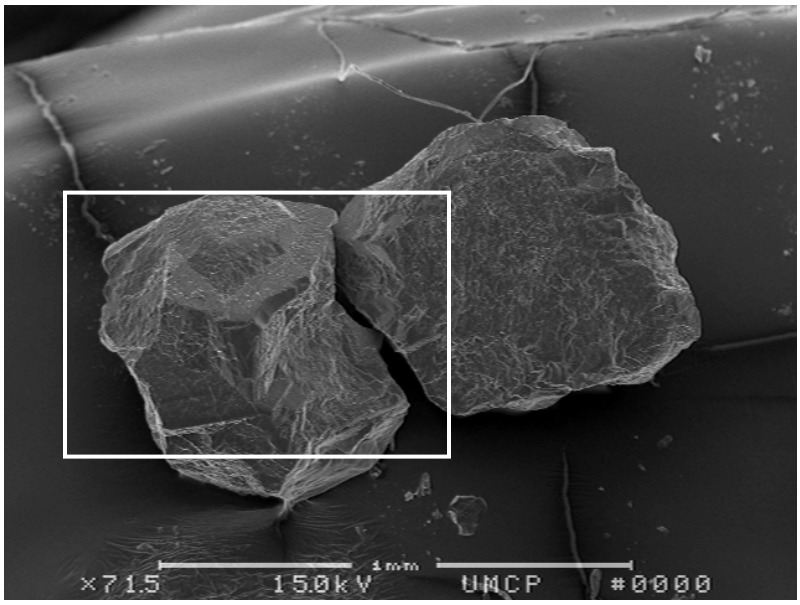

(b)

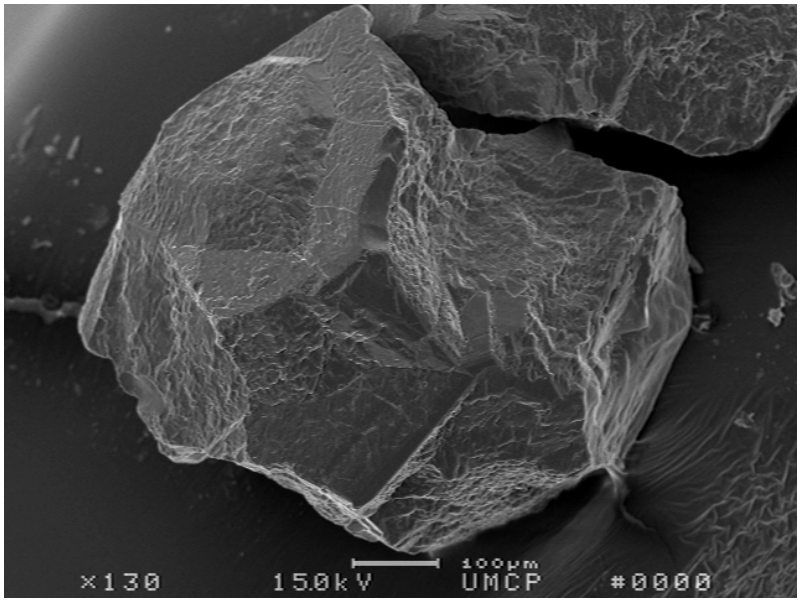

Figure C.2 Scanning electro micrographs of untreated sand in l mm of resolution (a), and focused on the surface of sand particle by using 100 μm of resolution (b). Note that the surface of untreated sand showed angled.

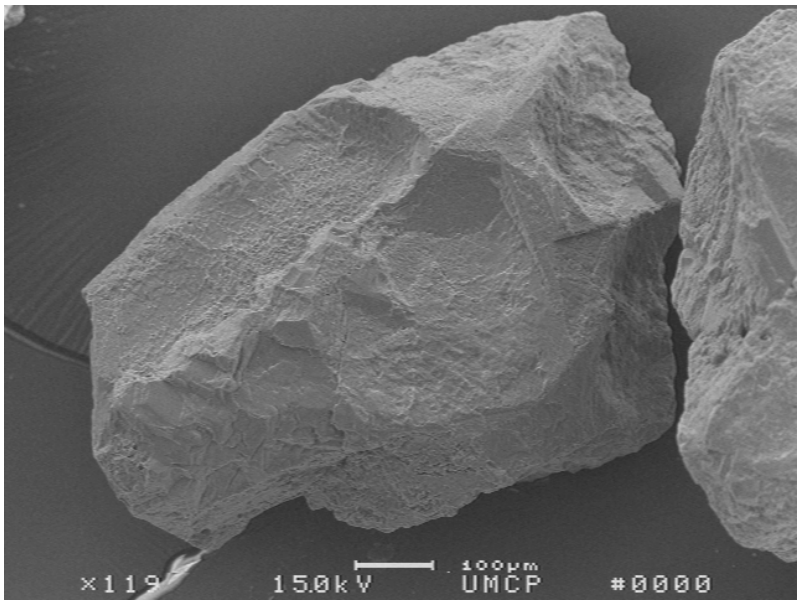

Figure C.3 Scanning electro micrographs of untreated sand in 100 µm of resolution. Note that the observation is similar to Figure C.1 and C.2.

(a)

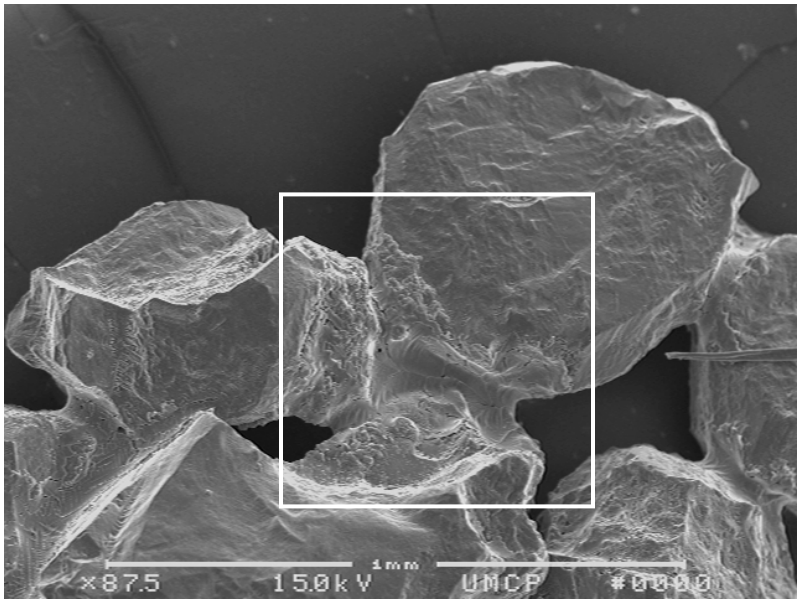

(b)

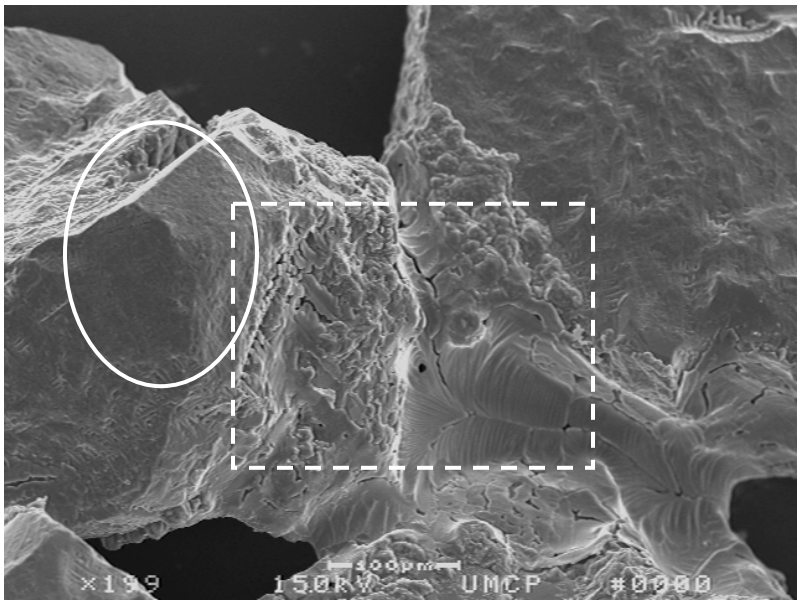

(c)

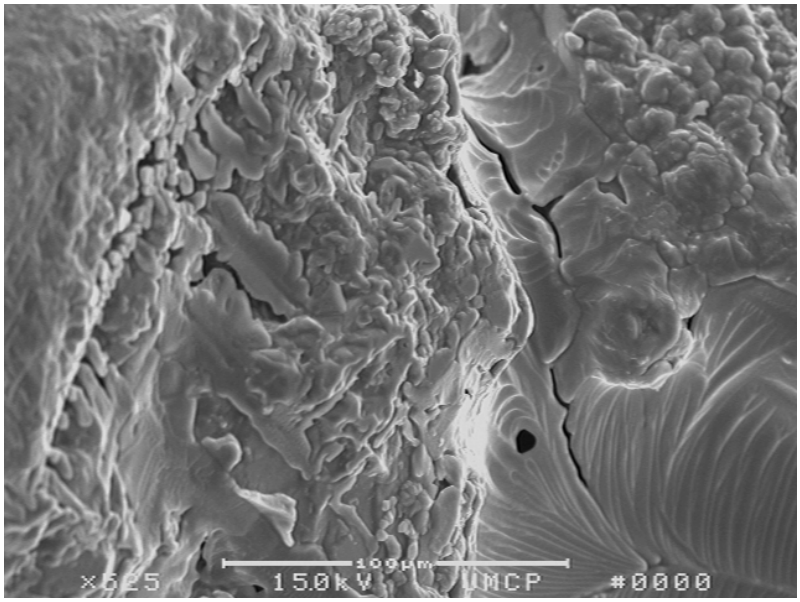

(d)

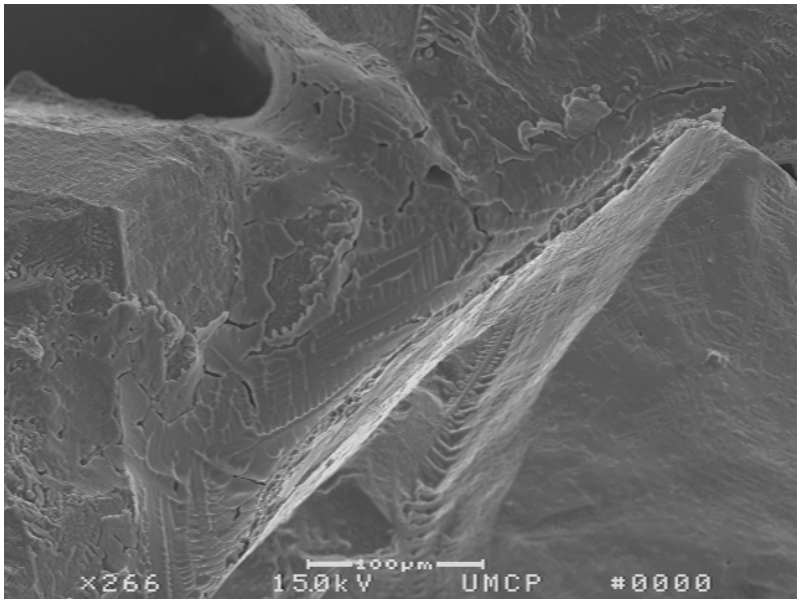

Figure C.4 Scanning electron micrographs of treated sand without washing in 1 mm of resolution (a), in 100 μm of resolution (b) which is focused on the area within solid square boundary from (a), in 100 μm of resolution (c) which is concentrated on the area within dotted square boundary from Figure C.4 (b) and in 100 μm of resolution (d) which is focused on the area within solid sphere boundary from Figure C.4 (b). Note that a heavy cementation formed between sand particles and on the surface of sand particle (see Fig. C.4 (a, c)), and those crystals show flaky morphologies between sand particles (see Fig. C.4 (b, d)).

(a)

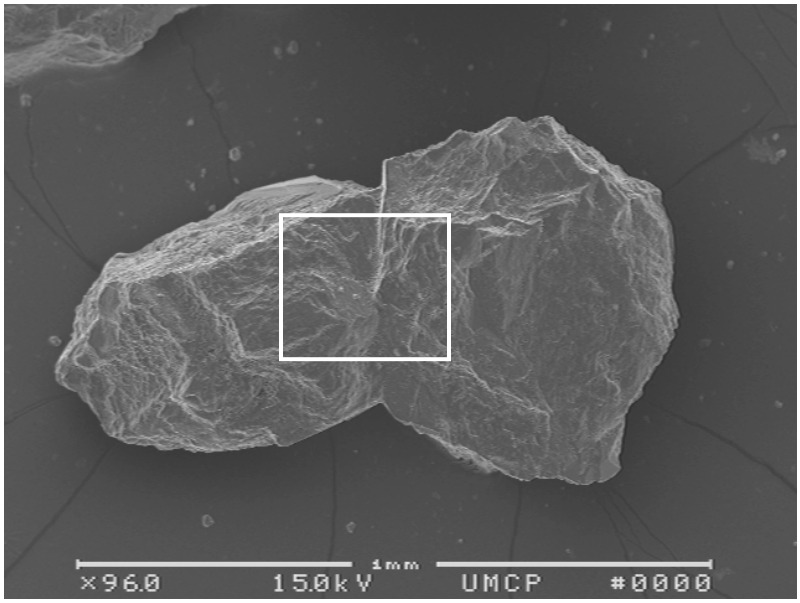

(b)

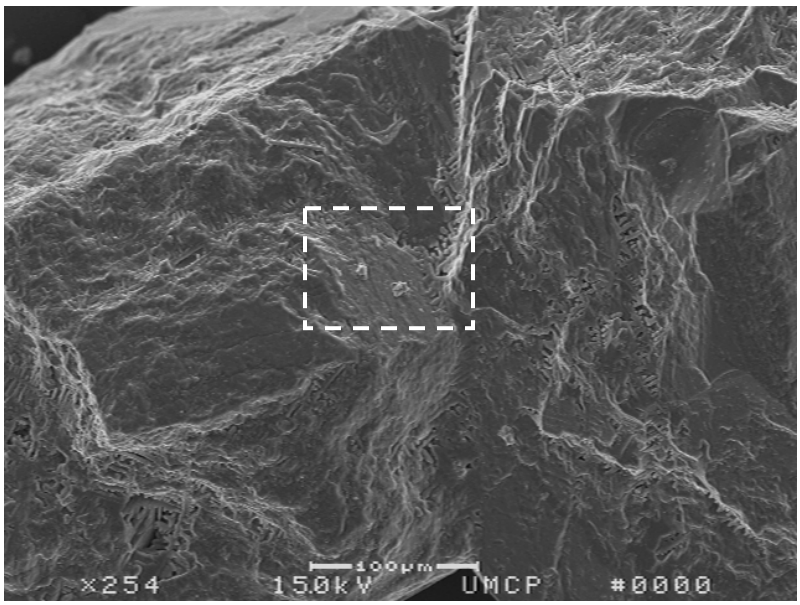

(c)

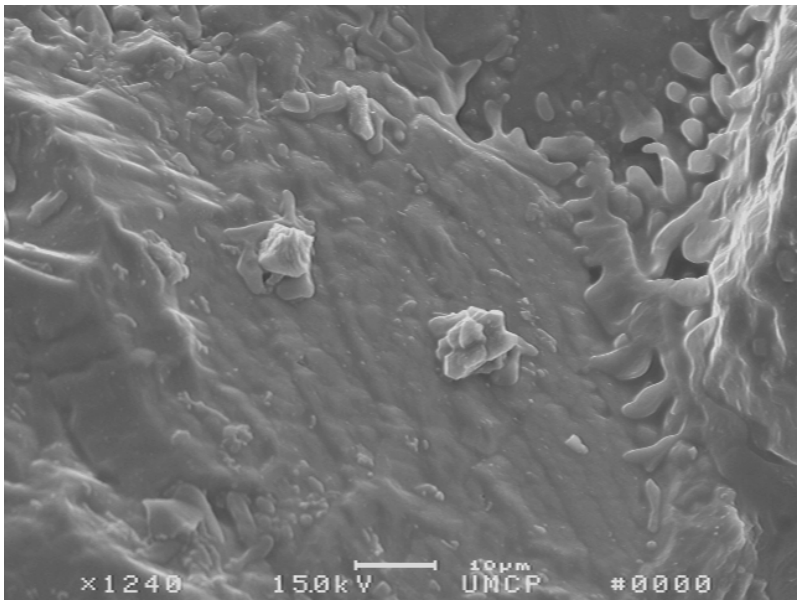

(d)

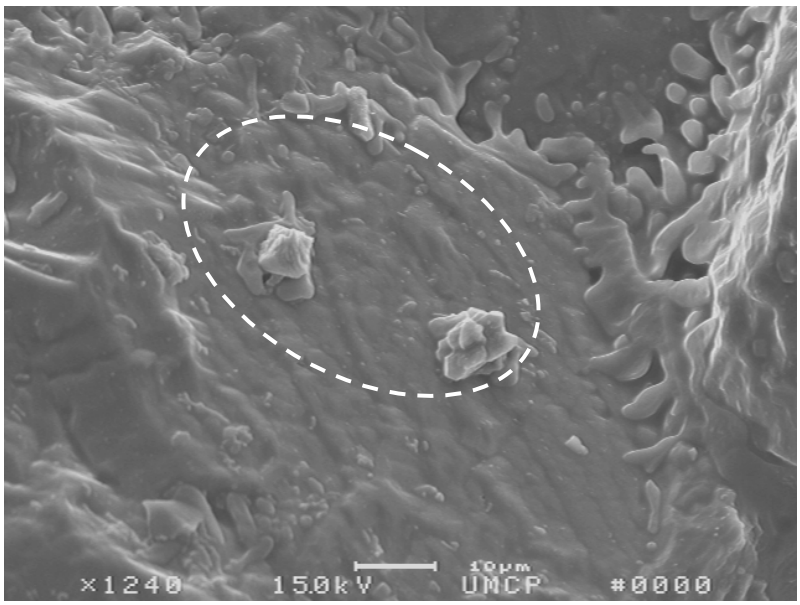

(e)

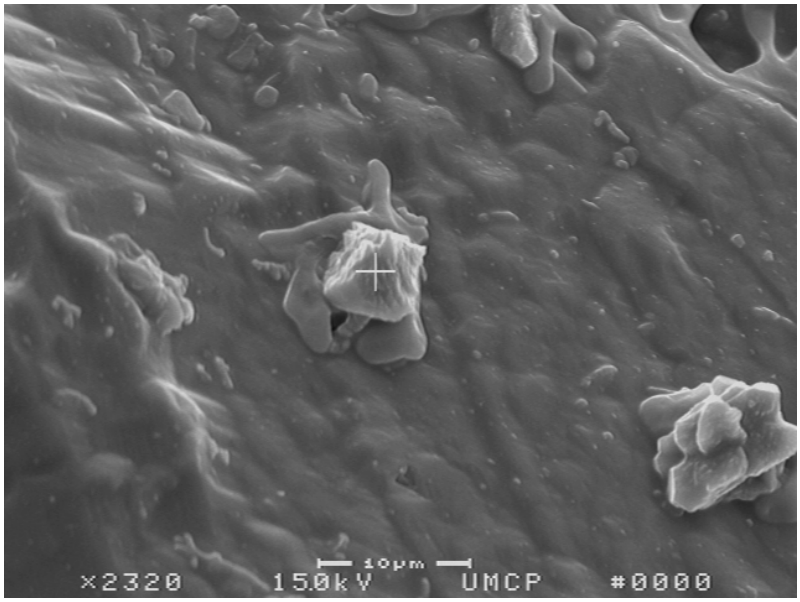

(f)

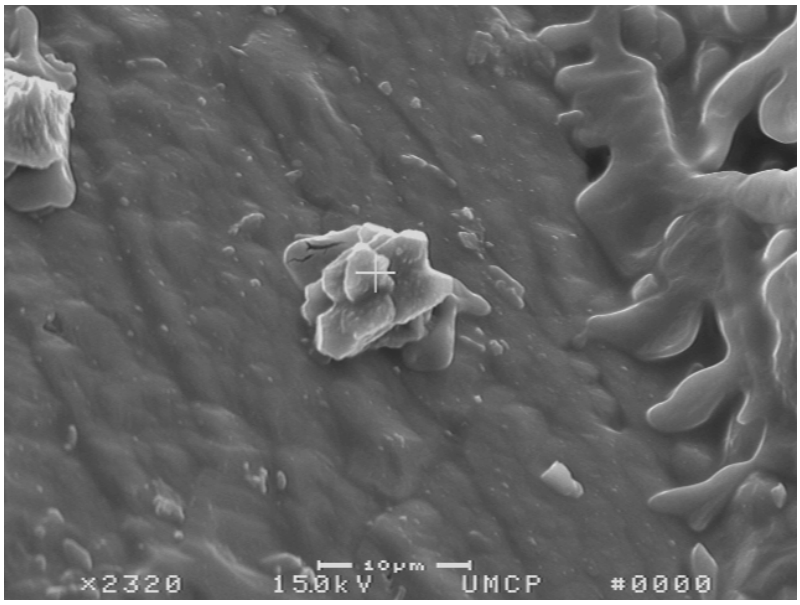

Figure C.5 Scanning electron micrographs of treated sand without washing in 1 mm of resolution (a), in 100 μm of resolution (b) which is focused on the area within solid square boundary from Figure C.5 (a), in 10 μm of resolution (c, d) which is concentrated on the area within dotted square boundary from Figure C.5 (b) and in 10 μm of resolution (e, f) which is focused on the area within solid sphere boundary from Figure C.5 (d). Note that a heavy cementation formed between sand particles and on the surface of sand particle, which is similar to the observation of Figure C.4.

(a)

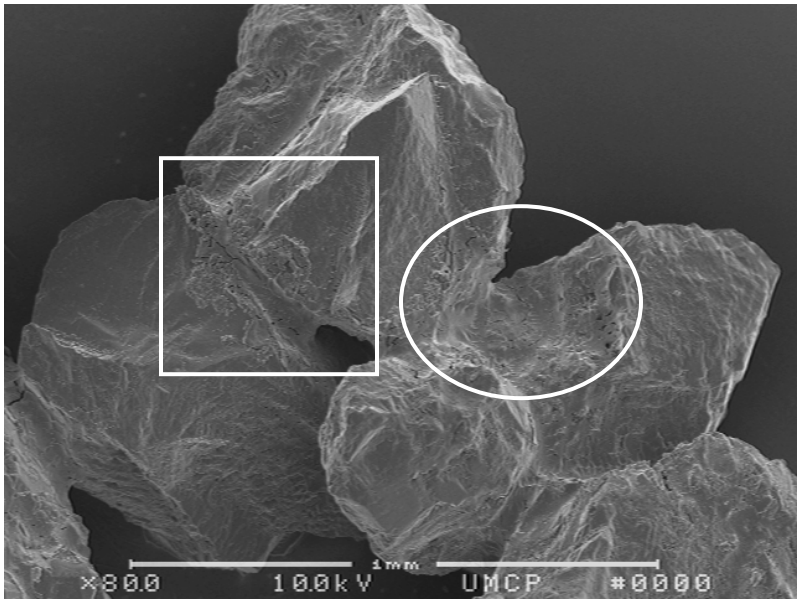

(b)

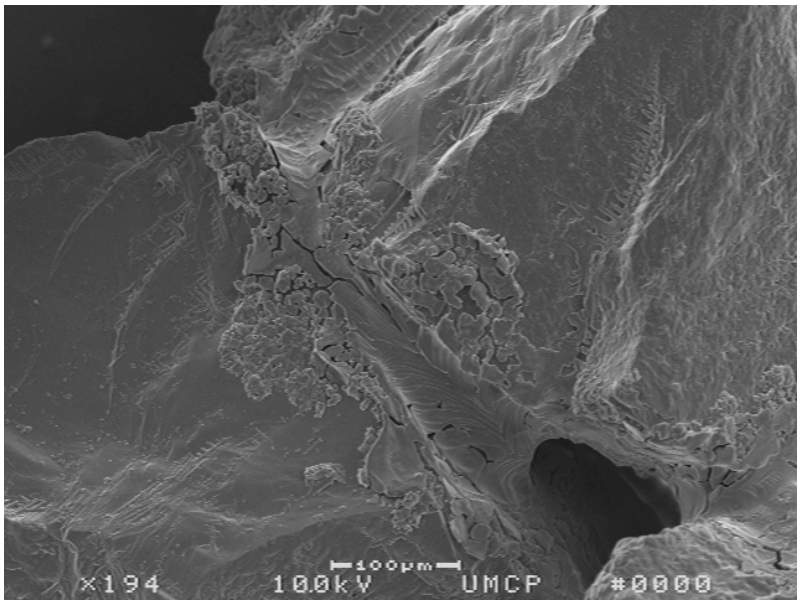

(c)

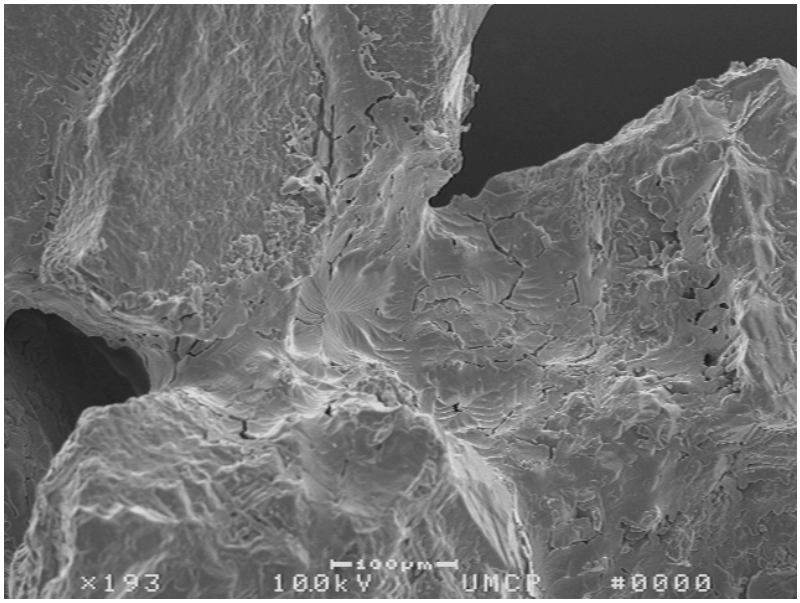

Figure C.6 Scanning electron micrographs of treated sand without washing in 1 mm of resolution (a), in 100 μm of resolution which is focused on the area within solid square boundary (b) and within solid square boundary (c) from Figure C.6 (a), respectively. Note that these observations are same with the images of Figure C.4.

(a)

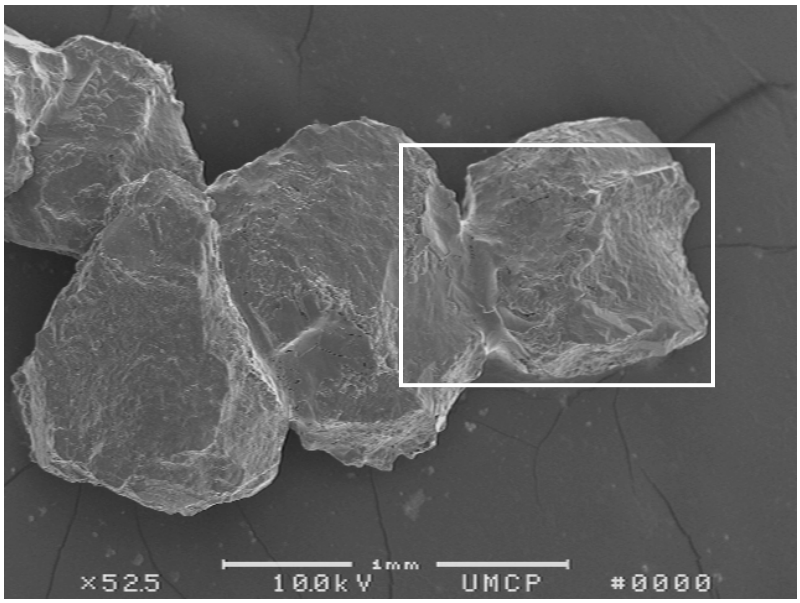

(b)

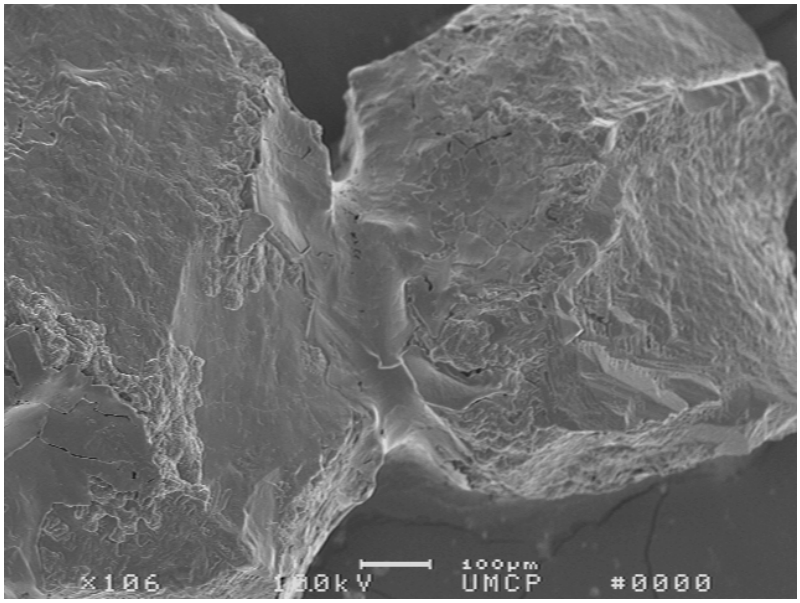

Figure C.7 Scanning electron micrographs of treated sand without washing in 1 mm of resolution (a), in 100 μm of resolution which is focused on the area within solid square boundary (b) from Figure C.7 (a). Note that these observations are same with the images of Figure C.4.

(a)

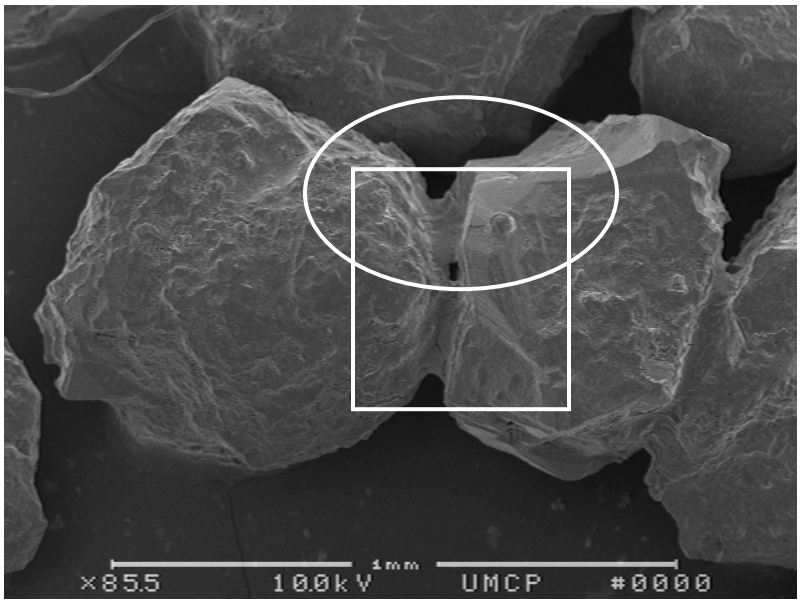

(b)

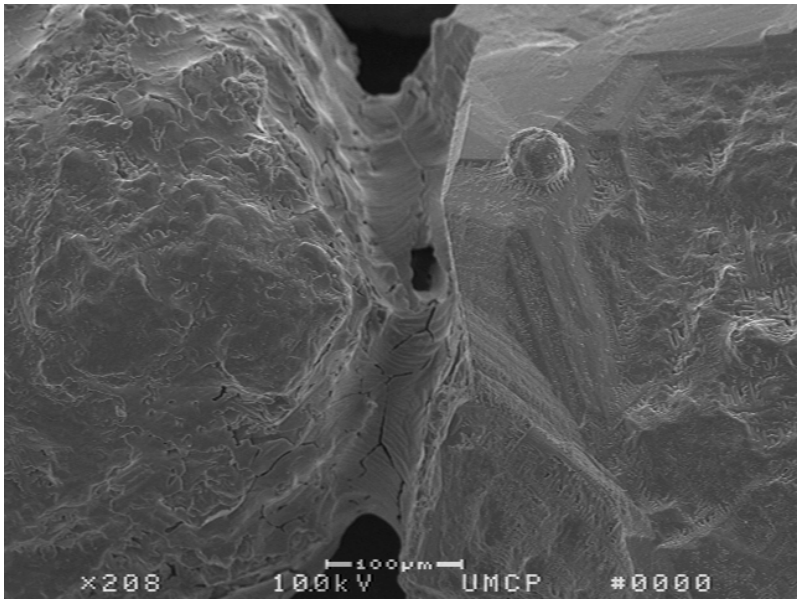

(c)

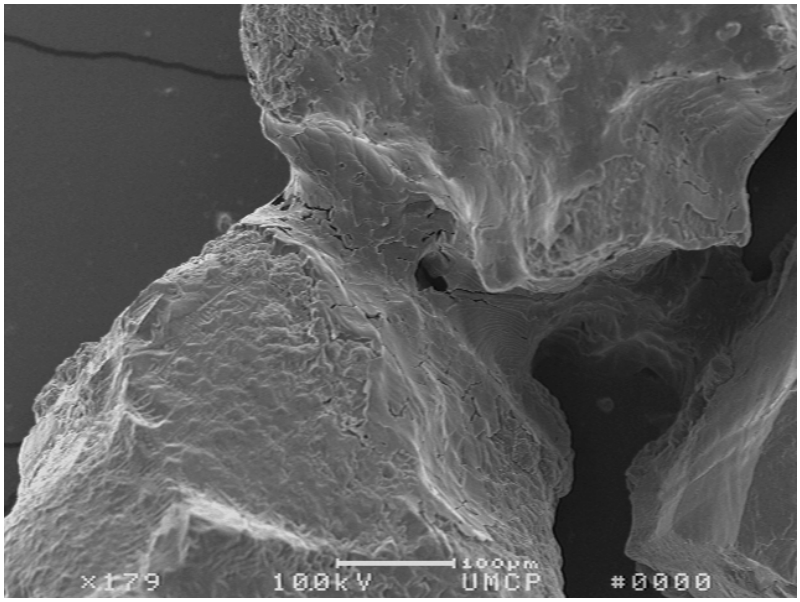

Figure C.8 Scanning electron micrographs of treated sand without washing in 1 mm of resolution (a), in 100 μm of resolution which is focused on the area within solid square boundary (b) and within solid square boundary (c) from Figure C.8 (a), respectively. Note that these observations are same with the images of Figure C.4.

(a)

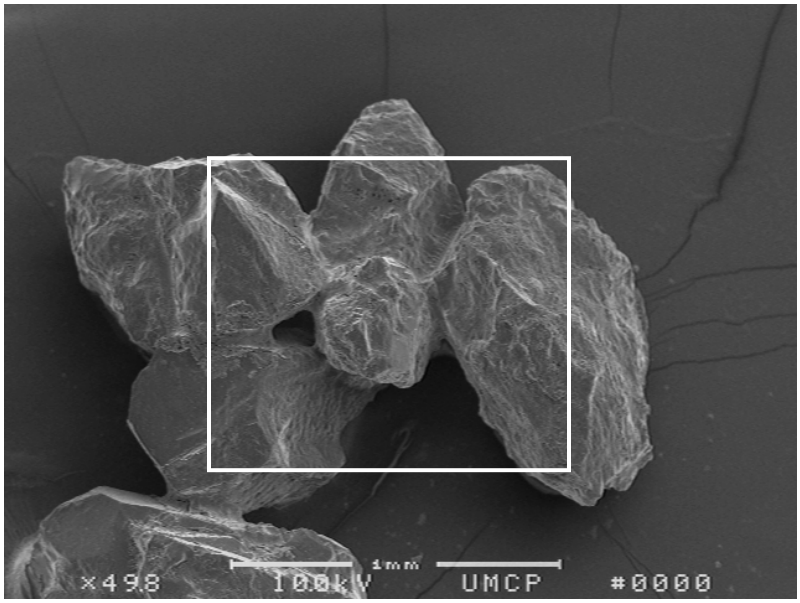

(b)

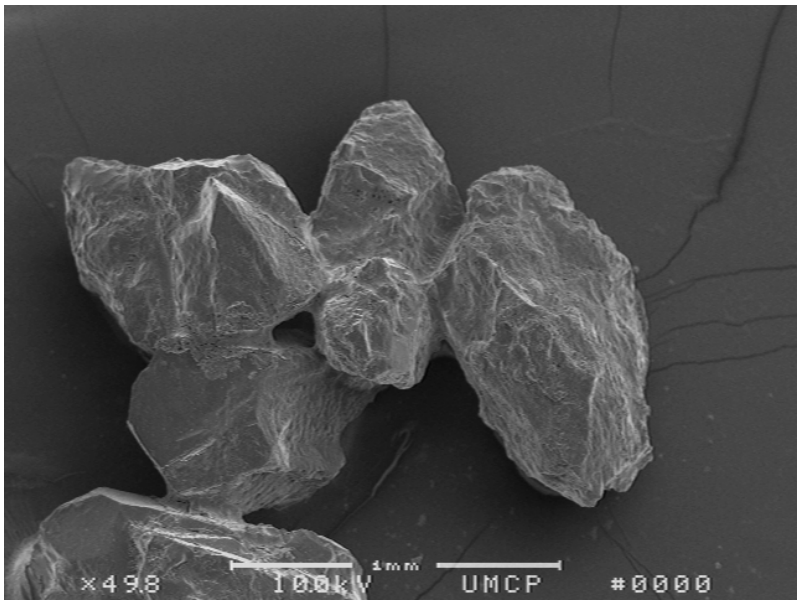

(c)

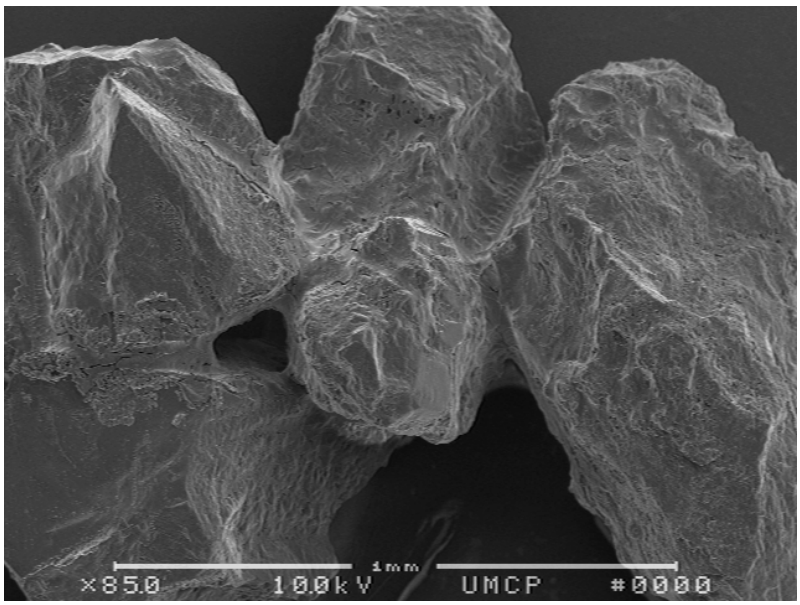

Figure C.9 Scanning electron micrographs of treated sand without washing in 1 mm of resolution (a, b) and in 1 mm of resolution that is focused on the area within solid square boundary (c) from Figure C.9 (a). Note that these observations are same with the images of Figure C.4.

(a)

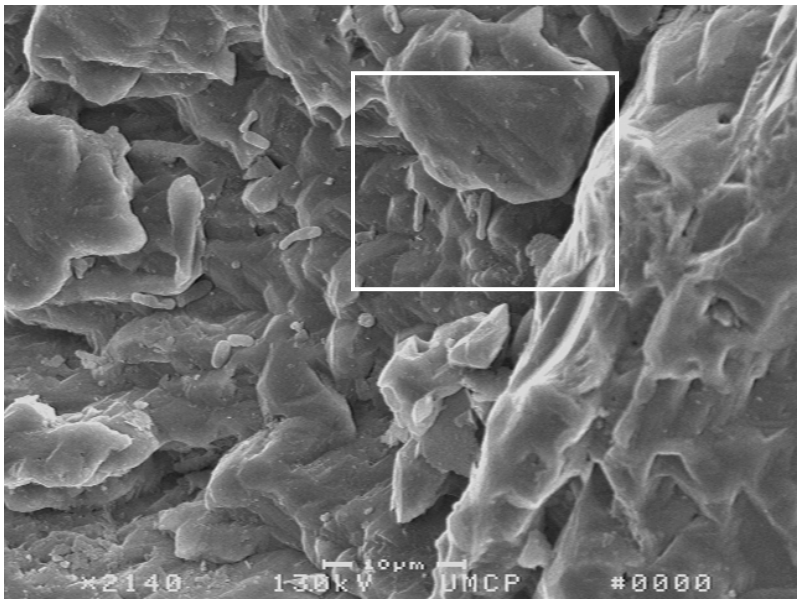

(b)

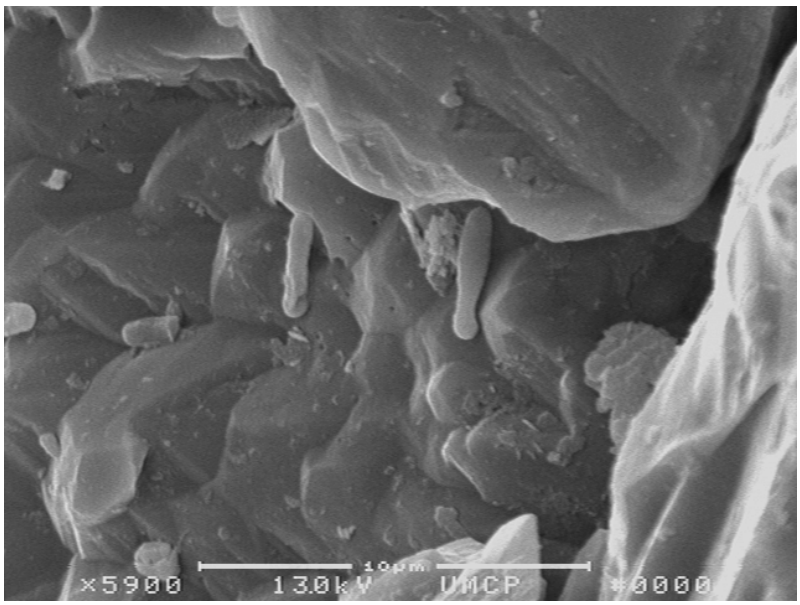

Figure C.10 Scanning electron micrographs of treated sand with washing in 10 μm of resolution (a) and in 10 μm of resolution that is focused on the area within solid square boundary (b) from Figure C.10 (a). Note that with washing treatment, the surface of sand particle revealed angled which is similar to untreated sand (see Figure C.1). Additionally, it is clear that microbes (i.e., rod-likeness in the images) are closely attached with sand particles.

(a)

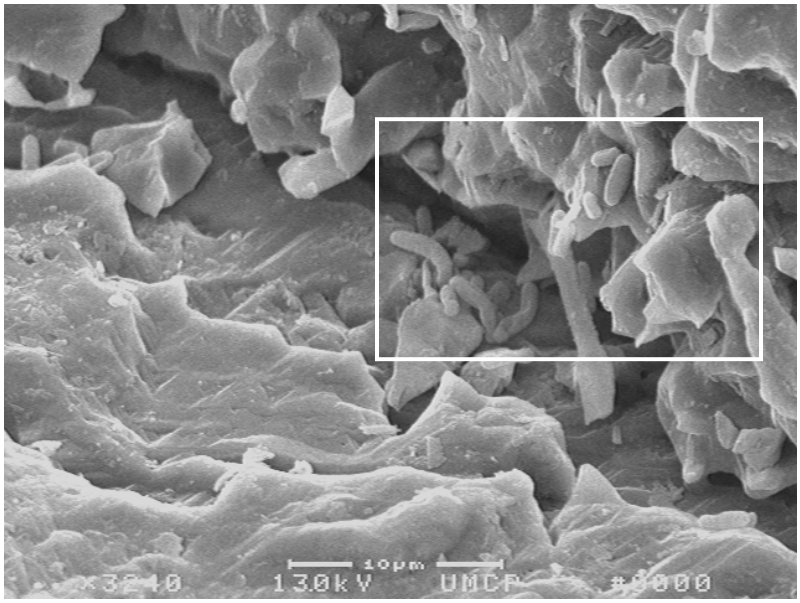

(b)

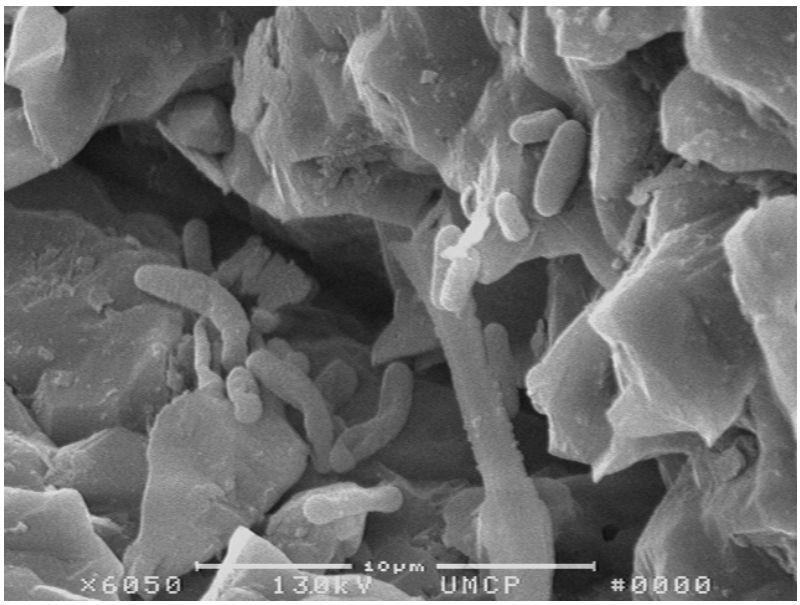

Figure C.11 Scanning electron micrographs of treated sand with washing in 10 μm of resolution (a) and in 10 μm of resolution that is focused on the area within solid square boundary (b) from Figure C.11 (a). Note that these observations are same with the images of Figure C.10.

(a)

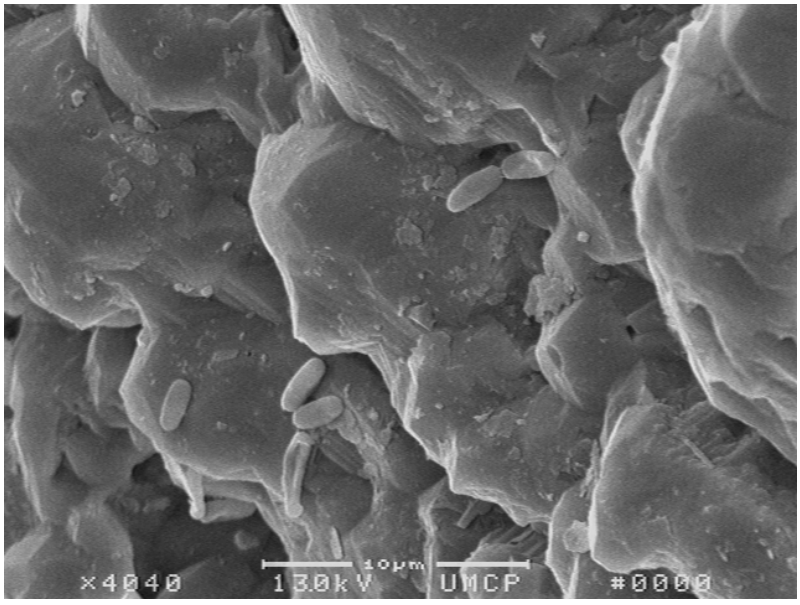

Figure C.12 Scanning electron micrographs of treated sand with washing in 10 μm of resolution. Note that these observations are same with the images of Figure C.10.

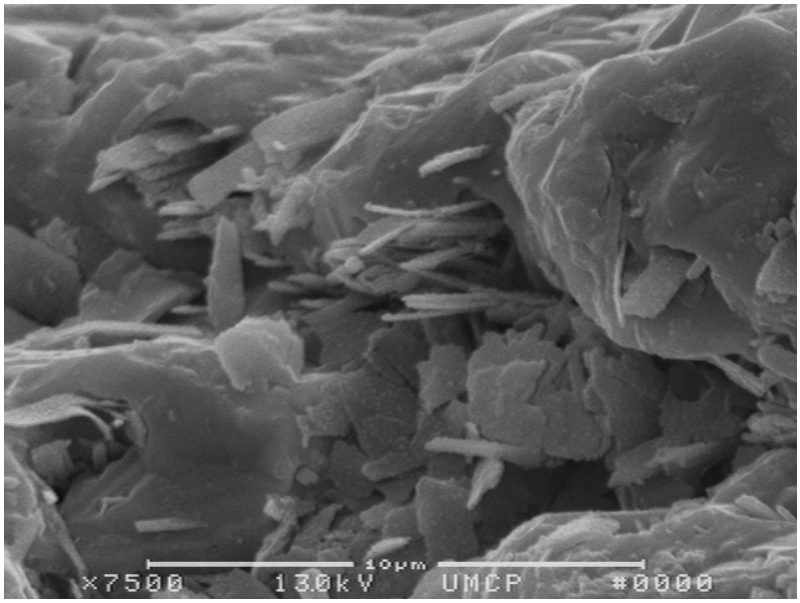

Figure C.13 Scanning electron micrographs of treated sand with washing in 10 μm of resolution. Note that some needle-likeness substances (i.e., maybe bacteria or crystals) formed within the gaps of the sand particle.

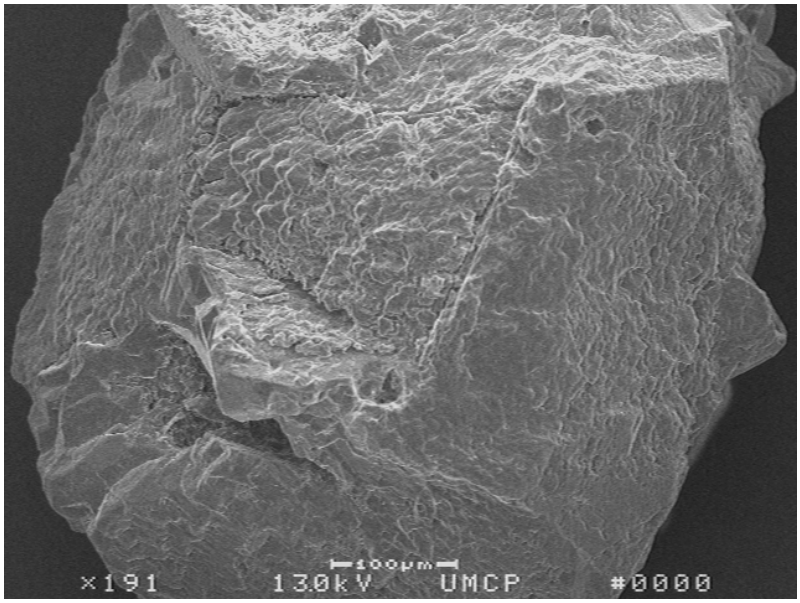

Figure C.14 Scanning electron micrographs of treated sand with washing in 100 μm of resolution. Note that as compared with untreated sand (Figure C.1), the surface of treated sand exhibits less angled and more irregular than that of untreated sand.

(a)

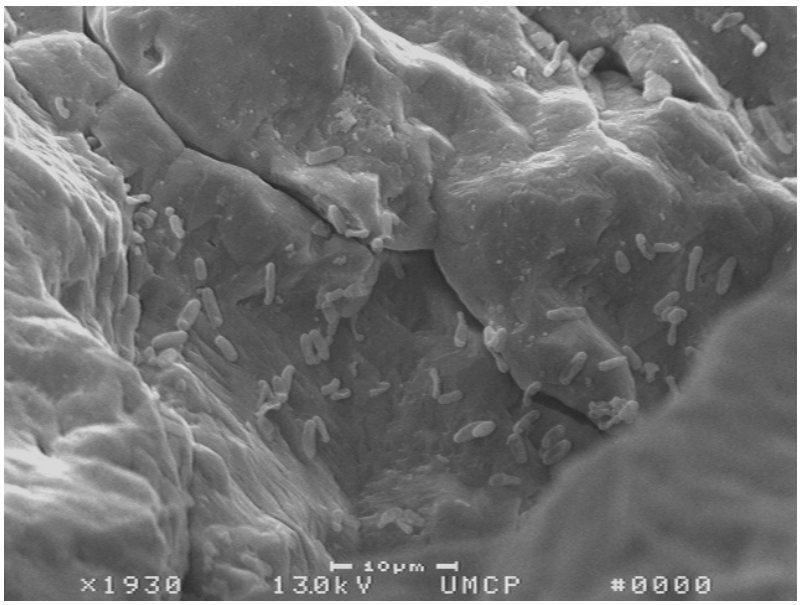

Figure C.15 Scanning electron micrographs of treated sand with washing in 10 μm of resolution. Note that these observations are same with the images of Figure C.10 and C.11.

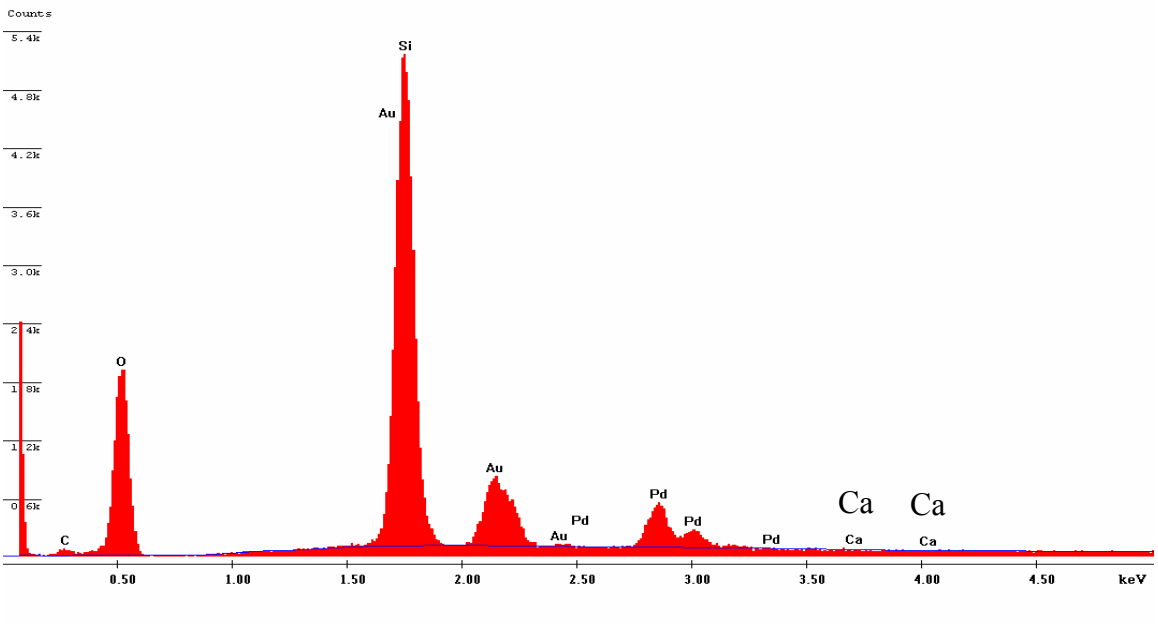

Figure C.16 Energy diffusion X-ray spectrometer (EDS) analysis of untreated sand from Figure C.1.

(a)

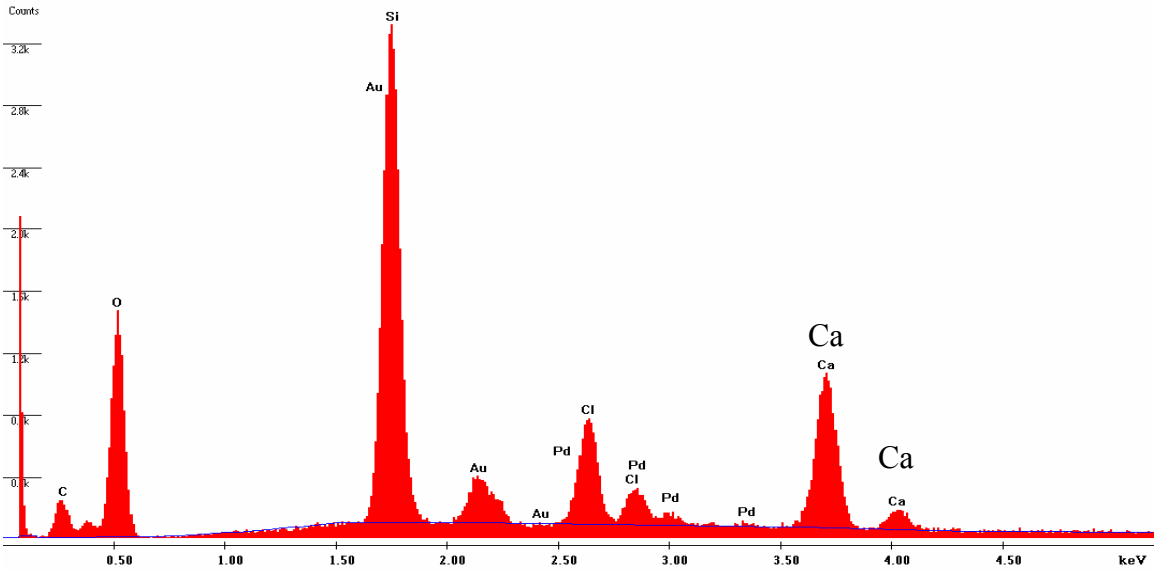

(b)

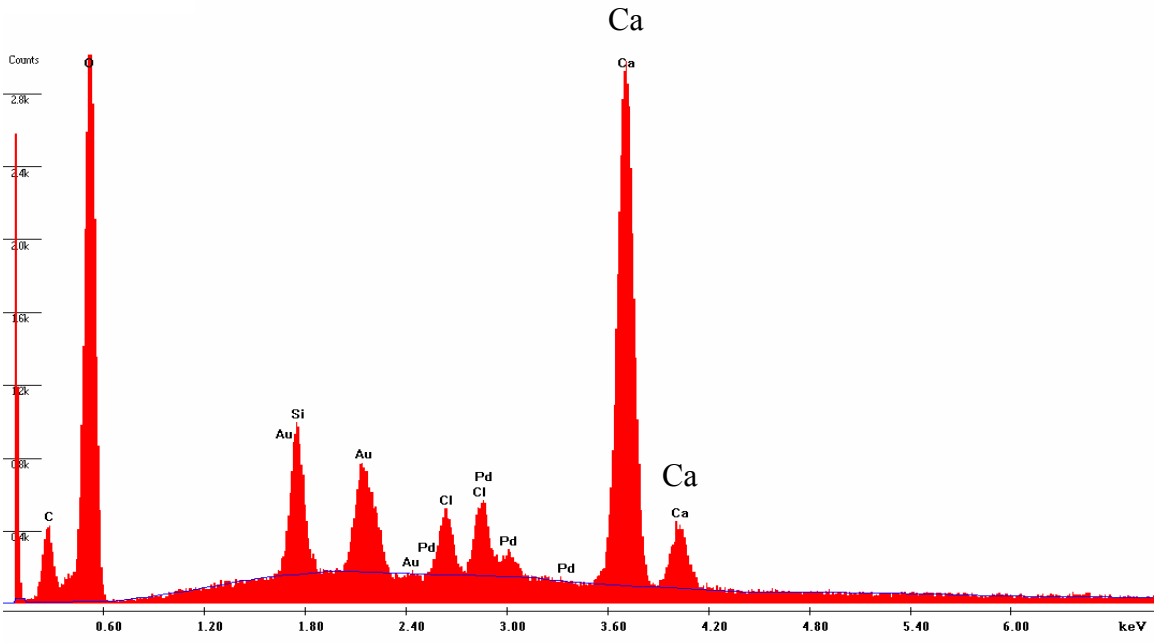

Figure C.17 Energy diffusion X-ray spectrometer (EDS) analysis of crystal (a, b) from Figure C.5 (e) and C.5 (f), respectively.

REFERENCES

AASHTO T 100, (2006). "Standard method of test for specific gravity of soils", *American Association of State Highway and Transportation Officials*.

AASHTO Designation T 193-93 (1993). "Standard Method of test for the California Bearing Ratio", Standard Specifications for Transportation Materials and Methods of Sampling and Testing, 16th Edition.

Ashford, S.A., Weaver, T.J., and Rollins, K.M. (200). "Pore pressure response of liquefied sand in full-scale lateral pile load tests", *Transportation Research Record*, Vol. 1808, No. 02-3631, pp. 21-29.

Al-Rawas, A.A., Hago, A.W., and Al-Sarmi, H. (2005). "Effect of lime, cement and Sarooj (artificial pozzolan) on the swelling potential of an expansive soil from Oman", *Building and Environment*, Vol. 40, pp. 681-687.

Ambarish, G. and Chillara, S. (2007). "Strength characteristics of class F fly ash modified with lime and gypsum", *Journal of Geotechnical and Geoenvironmental Engineering*, Vol. 133, pp. 757-766.

APHA, AWWA, and WEF. (1995). *"Standard methods for the examination of water and wastewater",* American Public Health Association, American Water Works Association, and Water Environment Federation, Washington, D.C.

ASTM D421-85 (2001). "Standard Practice for Dry Preparation of Soil Samples for Particle-Size Analysis and Determination of Soil Constants", *Annual Book of ASTM Standards*, V0l. 4.08, ASTM, Pennsylvania.

ASTM D422-63 (2001). "Standard test method for particle-size analysis of soils", *Annual Book of ASTM Standards*, V0l. 4.08, ASTM, Pennsylvania.

ASTM D854-06 (2001). "Standard Test Methods for Specific Gravity of Soil Solids by Water Pycnometer", *Annual Book of ASTM Standards*, V0l. 4.08, ASTM, Pennsylvania.

ASTM D4254 (2001). "Standard test methods for minimum index density and unit weight of soils and calculation of relative density", *Annual Book of ASTM Standards*, V0l. 4.08, ASTM, Pennsylvania.

ASTM D4253 (2001). "Standard test methods for maximum index density and unit weight of soils using a vibratory table", *Annual Book of ASTM Standards*, V0l. 4.08, ASTM, Pennsylvania.

Aydilek, A.H. and Edil, T.B. (2002). "Filtration performance of woven geotectiles with

wastewater treatment sludge", *Geosynthetics International*, Vol. 9, pp. 41-69.

Banat, IM. (1995). "Biosurfactants production and possible uses in microbial enhanced oil-recovery and oil pollution remediation- A review", *Bioresource Technology*, Vol. 51, pp. 1-12.

Banfield, J.F. and Nealson, K.H. (1997). *"Geomicrobiology: interactions between microbes and minerals. Review in mineralogy",* Vol. 35, Mineralogical Society of America, Washington, D.C.

Bang, S.S., Galinat, J.K., and Ramakrishnan, V. (2001). "Calcite precipitation induced by polyurethane-immobilized *Bacillus pasteurii*", *Enzyme and Microbial Technology*, Vol. 28, pp. 404-409.

Bang, S.S. (2004). "The present and future of biosealant in crack remediation," *Proceedings of the ICFRC International Conference on Fibre Composites, High Performance Concretes and Smart Materials*, Chennai, India, pp991-1001.

Bardet, J.P. (1997). "*Experimental soil mechanics*", Prentice-Hill, Inc., Upper Saddle River, New Jersey.

Bell, F.G. (1996). "Lime stabilization of clay minerals and soils", *Engineering Geology*, Vol. 42, pp. 223-237.

Beveridge, T.J., Makin, S.A., Kadurugamuwa, J.L., and Li, Z. (1997). "Interactions between biofilms and the environment", *FEMS Microbiology Review*, Vol. 20, pp. 291-303.

Broderick, G.P. and Daniel, E.E. (1990). "Stabilizing compacted clay against chemical attack", *Journal Geotechnical Engineering*, Vol. 16, pp. 1549-1567.

Boquet, E., Boronat, A., and Ramoscormenzana, A. (1973). "Production of calcite (calcium carbonate) crystals by soil bacteria is a general phenomenon", *Nature*, Vol. 246, pp. 527-529.

Bowles, J.E. (1992). "*Engineering properties of soils and their measurement*", McGraw-Hill, Fourth edition, pp. 201-227.

Buczynski, C. and Chafetz, H.S. (1991). "Habit of bacterially induced precipitates of calcium carbonate and the influence of medium viscosity on mineralogy", *Journal of Sedimentary Petrology*, Vol. 61, pp. 226-233.

Cabrera, M.L., Kissel, D.E., and Bock, B.R. (1991). "Urea hydrolysis in soil: effects of urea concentration and soil pH", *Soil Biology and Biochemistry*, Vol. 23, pp. 1121-1124.

Castanier, S., Le Metayer-Levrel, G., and Perthuisot, J.P. (1999). "Ca-carbonates precipitation and limestone genesis- the microbiologist point of view", *Sedimentary Geology*, Vol. 126, pp. 9-23.

Castanier, S., Le Métayer-Levrel, G., Orial, G., Loubiére, J.F., and Perthuisot, J.P. (2000). "Bacterial carbonatogenesis and application to preservation and restoration of historic property", *Of microbes and art: the role of microbial communities in the degradation and protection of cultural heritage*, Editors: Ciferri, O., Tiano, P., and Mastromei, G., Plenum, New York, N.Y. pp. 201-216.

Celestine, O. (2007). "Stabilization of clay using woodash", *Journal of Materials in Civil Engineering*, Vol. 19, pp. 14-18.

Ciurli, S., Marzador, C., Benini, S., Deiana, S., and Gessa, C. (1996). "Urease from the soil bacterium *Bacillus pasteurii*: immobilization on Ca-polygalacturonate", *Soil Biology and Biochemistry*, Vol. 28, pp. 811-817.

Consoli, N.C., Casagrande, D.T., Prietto, P.D.M., and Thomé, A. (2003). "Plate load test on fiber-reinforced soil", *Journal of Geotechnical and Geoenvironmental Engineering*, Vol. 129, pp. 951-955.

Consoli, N.C., Heineck, K.S., Casagrande, M.D.T., and Coop, M.R. (2007). "Shear strength behavior of fiber-reinforced sand considering triaxial tests under distinct stress paths", *Journal of Geotechnical and Geoenvironmental Engineering*, Vol. 133, pp. 1466-1469.

Cookson, J.T. (1995). *"Bioremediation engineering design and application"*, McGraw-Hill, Inc., pp. 1-9.

Day, J.L., Ramakrishnan, V., and Bang, S.S. (2003). "Microbiologically induced sealant for concrete crack remediation", *Proceedings of the 16th Engineering Mechanics Conference*, Seattle, Washington.

Défarge, C., Trichet, J., Jaunet, A., Robert, M., Tribble, J., and Sansone, F. (1996). "Texture of microbial sediments revealed by cryo-scanning electron microscopy", *Journal of Sedimentary Research*, Vol. 66, pp. 935-947.

Dejong, J.T., Friyzges, M.B., and Nüsslein, K. (2006). "Microbially induced cementation to control sand response to undrained shear", *Journal of Geotechnical and Geoenvironmental Engineering*, Vol. 11, pp. 1381-1392.

Dennis, M.L. and Turner, J.P. (1998). "Hydraulic conductivity of compacted soil treated with biofilm", *Journal of Geotechnical and Geoenvironmental Engineering*, Vol. 124, pp. 120-127.

Douglas, S. and Beveridge, T.J. (1998). "Mineral formation by bacteria in natural microbial communities", *FEMS Microbiol. Ecol.*, Vol. 26, pp. 79-88.

Ehrlich, H.L. (2002). "*Geomicrobiology*", 4th edition, Marcel Dekker, New York, N.Y.

Federal Emergency Management Agency (2005). *"Coastal construction manual: principles and practices of planning, siting, designing, constructing, and maintaining residential buildings in coastal areas"*, third edition, Washington, D.C.

Ferris, F.G., Stehmeier, L.G., Kantzas, A., and Mourits, F.M. (1996). "Bacteriogenic mineral plugging", *Journal of Canadian Petroleum Technology*, Vol. 35, pp. 56-61.

Ferris, F.G, Phoenix, V., Fujita, Y., and Smith, R.W. (2003). "Kinetics of calcite precipitation induced by ureolytic bacteria at 10 to 20℃ in artificial groundwater", *Geochimica et Cosmochimica Acta*, Vol. 67, pp. 1701-1722.

Folk, R. (1993). "SEM imaging of bacteria and nanobacteria in carbonate sediments and rocks", *Journal of Sedimentary Petrology*, Vol. 63, pp. 990-999.

Fujita, Y., Ferris, F.G., Lawson, R.D., Colwell, E.S., and Smith, R.W. (2000). "Calcium carbonate precipitation by ureolytic substrate bacteria", *Geomicrobiology Journal*, Vol. 17, pp. 305-318.

Gate, K., Aragona, K., Sabodish, M., and Gabr, M. (2001). "Adsorption/Desorption capacity of trichloroethylene (TCE) on till with high percent fines", *Journal of Transportation Research Board*, No. 1755, pp. 141-148.

Ghiorse, W.C. (1984). "Biology of iron-and manganese-depositing bacteria", *Annual Review of Microbiology*, Vol. 38, pp. 515-550.

Greenfield, L.J. (1963). "Metabolism and concentration of calcium and magnesium and precipitation of calcium carbonate by a marine bacterium", *Annals of the New York Academy of Science*, Vol. 109, pp. 23.

Gollapudi, U.K., Knytson, C.L., Bang, S.S., and Islam, M.R. (1995). "A new method for controlling leaching through permeable channels", *Chemosphere*, Vol. 30, pp. 695-705.

Gonzalez-Muñoz, M.T., Chekroun, K.B., Abound, A.B., Arias, J.M., and Rodriguez-Gallego, M. (2000). "Bacterially induced Mg-calcite formation: Role of Mg^{2+} in development of crystal morphology", *Journal of Sedimentary Petrology*, Vol. 70, pp. 559-564.

Gurel, I., Arica, M.Y., and Hasirci, V. (1997). "Immobilization of glucose oxidase and urease in hydrogel matrices", *Turkish Journal of Chemistry*, Vol. 21, pp. 387-393.

Hammes, F., Boon, N., Clement, G., and Villiers, J.D. (2003). "Molecular, biochemical and ecological characterization of a bio-catalytic calcification reactor", *Applied Microbiology and Biotechnology*, Vol. 62, pp. 191-201.

Hélène, T., Josée, D., Jacques, L., and Serge, L. (2002). "Influence of the nature of organic compounds on find soil stabilization with cement", *Canadian Geotechnical Journal*, Vol. 39, pp. 535-546.

Hill, D.D. and Sleep, B.E. (2002). "Effects of biofilm growth on flow and transport through a glass parallel plate fracture", *Journal of Contaminant Hydrology*, Vol. 56, pp. 227-246.

Hillgärtner, H. Dupraz, C., and Hug, W. (2001). "Microbially induced cementation of carbonate sands: are micritic meniscus cements good indicators of vadose diagenesis?", *Sedimentology*, Vol. 48, pp. 117-131.

Huang, Q.Y., Jiang, M.H., Yang, Z.J., and Li, X.Y. (1997). "Influence of several soil colloids on the adsorption and properties of urease enzyme", *Journal of Wuhan University of Technology-Materials Science Edition*, Vol. 12, pp. 25-32.

Jennings, P.A. (1975). *"A mathematical model for biological activity in expanded bed adsorption columns."* Ph.D. Dissertation, Department of Civil Engineering, University of Illinois, Urbana, IL.

Kantzas, A., Ferris, F.G., Stehmeier, L., Marentette, D.F., Jha, K.N., and Mourits, F.M. (1992). "A novel method of sand consolidation through bacteriogenic mineral plugging", *CIM 92-46, Proceedings of the CIM 1992 Annual Technical Conference*, Society of Canadian Institute of Mining, Metallurgy, and Petroleum, Calgary, Canada, 2, 1-15.

Klappa, C.F. (1979). "Calcified filaments in Quaternary calcretes: organo-mineral interactions in the subaerial vadose environment", *Journal of Sedimentary Petrology*, Vol. 49, pp. 955-968.

Klein, J. and Kluge, M. (1981). "Immobilization of microbial cells in polyurethane matrices", *Biotechnology Letters*, Vol. 3, pp. 65-70.

Knobel, L.L., Bartholomay, R.C., Cecil, L.D., Tucker, B.J., and Wegner, S.J. (1992). "Chemical constituents in the dissolved and suspended fractions of groundwater from selected sites", *Idaho National Engineering Laboratory and Vicinity, Idaho, 1989. Open-file Report*, pp. 92-51.

Konhauser, K.O. and Urrutia, M.M. (1999). "Bacterial clay authigenesis: A common biogeochemical process", *Chemical Geology*, Vol. 161, pp. 399-413.

Laspidou, C.S., Rittmann, B.E., and Karamanos, S.A. (2005). "Finite element modeling to expand the UMCCA model to describe biofilm mechanical behavior", *Water Science and Technology*, Vol. 52, pp. 161-166.

Lawton, E.C., Khire, M.V., and Fox, N.X. (1993). "Reinforcement of soils by multioriented geosynthestic inclusions", *Journal of Geotechnical Engineering*, Vol. 119, pp. 257-275.

Le Métayer-Levrel, G., Castanier, S., Orial, G., Loubiére, J.F., and Pertuisot, J.P. (1999). "Applications of bacterial carbonatogenesis to the protection and regeneration of limestones in buildings and historic patrimony", *Sedimentary Geology*, Vol. 26, pp. 25-34.

Lian, B., Hu, Q., Chen, J., Ji J., and Teng, H.H. (2006). "Carbonate biomineralization induced by soil bacterium Bacillus megaterium", *Geochimica et Cosmochimica Acta*, Vol. 70, pp. 5522-5535.

Maher, M.H. and Gray, D.H. (1990). "Static response of sands reinforced with randomly distributed fibers", *Journal of Geotechnical Engineering*, Vol. 116, pp. 1661-1677.

Makboul, H.E. and Ottow, J.C.G. (1979). "Short communication: Clay minerals and the Michaelis constant of *urease*", *Soil Biology and Biochemistry*, Vol. 11, pp. 683-686.

Martin, G.R., Yen, T.F., and Karimi, S. (1996). "Application of biopolymer technology in silty soil matrices to form impervious barriers", *Proceedings of the 7th Australia-New Zealand Geomechanics Conference*, Adelaide, Australia.

Michalowski, R.L., and Čermák, J. (2003). "Triaxial compression of sand reinforced with fibers", *Journal of Geotechnical and Geoenvironmental Engineering*, Vol. 129, pp. 125-136.

Mitchell, J.K. Hon, and Santamarina, J.C. (2005). "Biological considerations in geotechnical engineering", *Journal of Geotechnical and Geoenvironmental Engineering*, Vol. 131, pp. 1222-1233.

Mitchell, A. and Ferris, G.G. (2005). "The coprecipitation of Sr into calcite precipitation induced by bacterial ureolysis in artificial groundwater: Temperature and kinetic dependence", *Geochimica et Cosmochimica Acta*, Vol. 69, pp. 4199-4210.

Mobley, H.L.T. and Hausinger, R.P. (1989). "Microbial urease: significance, regulation and molecular characterization", *Microbiology Review*, Vol. 53, pp. 85-108.

Monger, H.C., Daugherty, L.A., Lindemann, W.C., and Liddell, C.M. (1991). "Microbial precipitation of pedogenic calcite", *Geology*, Vol. 19, pp. 997-1000.

Nielsen, T.H., Bonde, T.A., and Sørensen, J. (1998). "Significance of microbial urea turnover in N cycling of three Danish agricultural soils", *FEMS Microbiol. Ecol.*, Vol. 25, pp. 147-157.

Olivoera, I.B., Demond, A.H., and Salehzadeh, A. (1995). "Packing of the sands for the production of homogenous porous media", *Soil Science Society of America Journal*, Vol. 60, pp. 49-53.

Párraga, J., Rivadeneyra, M.A., Delgado, R., Iñiguez, J., Soriano M., and Delgado G. (1998). "Study of biomineral formation by bacteria from soil solution equilibrium", *Reactive and Functional Polymers*, Vol. 36, pp. 265-271.

Pettit, N.M., Smith, R.R., Freedman, R.B., and Burns, R.G. (1976). "Soil *urease*: activity, stability and kinetic properties, soil boil", *Biochemistry*, Vol. 8, pp. 479-484.

Phillips, S.E., Milnes, A.R., and Foster, R.C. (1987). "Calcified filaments: an example of biological influences in the formation of calcrete in South Australia", *Australian Journal Soil Research*, Vol. 25, pp. 405-428.

Picioreanu, C., Van, L.M.C.M., and Heilnen, J.J. (2000). "Effect of diffusive and convective substrate transport biofilm structure formation: a two-dimensional modeling study", *Biotechnology and bioengineering*, Vol. 69, pp. 504-515.

Rachhpal-Singh, and Nye, P.H. (1984). "The effect of soil pH and high urea concentrations on urease activity in soil", *Journal of Soil Science*, Vol. 35, pp. 519-527.

Raskin, L. (1993). *"Structural and functional analysis of anaerobic biofilm communities : an integrated molecular and modeling approach"*, Ph.D. thesis, University of Illinois at Urbana-Champaign.

Ramachandran, S.K., Ramakrishnan, V., and Bang, S.S. (2001). "Remediation of concrete using micro-organisms", *ACI material journal*, Vol. 98, pp. 3-9.

Rittmann, B.E. and McCarty, P.L. (1980a). "Model of steady-state kinetics", *Biotechnology and Bioengineering*, Vol. 22, pp. 2343-2357.

Rittmann, B.E. (1982a). "Comparative performance of biofilm reactor types", *Biotechnology and Bioengineering,* Vol. 24, pp. 1341-1370.

Rittmann, B.E. (1982b). "The effect of shear stress on loss rate", *Biotechnology and Bioengineering,* Vol. 24, pp. 501-506.

Rittmann, B.E., Crawford, L., and Tuck, C.K. (1986). "Insitu determination of kinetic-parameters for biofilms-isolation and characterization of oligotrophic biofilms",

Biotechnology and Bioengineering, Vol. 28, pp. 1753-1760.

Rittmann, B.E. (1993). "The significance of biofilms in porous-media", *Water Resources Research*, Vol. 29, pp. 2195-2202.

Rittmann, B.E. and McCarty, P.L. (2000). *"Environmental Biotechnology: Principles and Applications"*, McGraw-Hill.

Rodriguez-Navarro, C., Rodriguez-Gallego, M., Chekroun, K.B., and Gonzalez-Muñoz, M.T. (2003). "Conservation of ornamental stone by Myxococcus Xanthus-Induced carbonate biomineralization", *Applied and Environmental Microbiology*, Vol. 69, pp. 2182-2193.

Ross, N., Villemur, R., Deschênes, L., and Samson, R. (2001). "Clogging of limestone fracture by stimulating groundwater microbe", *Water Research*, Vol. 35, No. 8., pp. 2029-2037.

Sáez, P.B. and Rittmann, B.E. (1988). "An improved pseudo-analytical solution for steady state-biofilm kinetics", *Biotechnology and Bioengineering*, Vol. 32, pp. 379-385.

Sáez, P.B. and Rittmann, B.E. (1992). "Accurate pseudo-analytical solution for steady-state biofilms", *Biotechnology and Bioengineering*, Vol. 39, pp. 790-793.

Santoni, R.L. and Webster, S.L. (2001). "Airfields and roads construction using fiber stabilization of sands", *Journal of Transportation Engineering*, Vol. 127, pp. 96-104.

Santoni, R., Tingle, J.S., Webster, S.L. (2001). "Engineering properties of sand-fiber mixtures for road construction", *Journal of Geotechnical and Geoenvironmental Engineering*, Vol. 127, pp. 258-268.

Seagren, E.A. (1994). *"Quantitative evaluation of flushing and biodegredation for enhancing in situ dissolution of nonaqueous phase liquids"*, Ph.D dissertation, Univ. of Illinois, Urbana Champaign.

Seki, K., Miyazaki, T., and Nakano, M. (1998). "Effects of microorganisms on hydraulic conductivity decrease in infiltration", *European Journal of Soil Science*, Vol. 49, pp. 231-236.

Shackelford, C.D. and Jefferis, S.A. (2000). "Geoenvironmental engineering for in situ remediation", *International Conference on Geotechnical and Geoenvironmental Engineering (GeoEng2000),* Melbourne, Australia, Nov. 19-24, Technomic Publ. Co., Inc., Lancaster, PA, Vol. 1, pp. 121-185.

Silver, S., Toth, K., and Scribner, H. (1975). "Facilitated transport of calcium by cells and subcellular membranes of *Bacillus subtilis* and *Escherichia coli*", *Journal of*

Bacteriology, Vol. 12, pp. 880-885.

Skujins, J. and McLaren, A.D. (1969). "Assay of urease activity using ^{14}C-urea in stored, geologically preserved and irradiated soil", *Soil Biology Biochemistry*, Vol. 1, pp. 89-99.

Smith, M. and Compton, L. (2004). "Orign amd evolution of major salts in the Darling pans", *Applied Geochemistry*, Vol. 19, No. 5, pp. 645-664.

Stocks-Fisher, S., Galinat, J.K., and Bang, S.S. (1999). "Microbiological precipitation of $CaCO_3$", *Soil Biology and Biochemistry*, Vol. 31, pp. 1563-1571.

Swensen, B. and Bakken, L.R. (1998). "Nitrification potential and urease activity in a mineral subsoil", *Soil Biology and Biochemistry*, Vol. 30, pp. 1333-1341.

Takishima, K., Suga T., and Mamiya, G. (1988). "The structure of jack bean urease- The complete amino-acid sequence, limited proteolysis and reactive cysteine residues", *European Journal of Biochemistry*, Vol. 175, pp. 151-165.

Taylor, S.W. and Jaffé, P.R. (1990). "Substrate and biomass transport in a porous medium", *Water Resources Research*, Vol. 26, pp. 2181-2194.

Tiano, P., Biagiotti, L., and Mastromei, G. (1999). "Bacterial bio-mediated calcite precipitation for monumental stones conservation: methods of evaluations", *Journal of Microbiological Methods*, Vol. 36, pp. 139-145.

Tooth, A.F. and Fairchild, I.J. (2003). "Soil and barst aquifer hydrological controls on the geochemical evolution of speleothem-forming frip waters, Crag Cave, southwest Ireland", *Journal of Hydrology*, Vol. 273, No. 1, pp. 51-68.

Urzi, C., Carcia-Valles, M., Vendrell, M., and Pernice, A. (1999). "Biomineralization processes on rock and monument surfaces observed in field and in laboratory conditions", *Geomicrobiology Journal*, Vol. 16, No. 1, pp. 39-54.

US Army Corps of Engineers (1984). *"Soil stabilization for pavements"*, EM 1110-3-137, Washington DC.

Vandevivere, P. and Baveye, P. (1992). "Relationship between transport of bacteria and their clogging efficiency in sand columns", *Applied and Environmental Microbiology,* Vol. 58, pp. 2523-2530.

Venkatarama, R.B.V., Richardson, L., and Nanjunda, R.K.S. (2007). "Optimum soil grading for the soil-cement blocks", *Journal of Materials in Civil Engineering*, Vol. 19, pp. 139-148.

Waleed, A. (1995). *"Centrifuge modeling of sinkhole development in weakly cemented*

sand", Ph. D. Dissertation, Department of Civil and Environmental Engineering, University of Maryland College Park, College Park, MD.

Wang, X. and Ruchenstein, E. (1993). "Preparation of porous polyurethane particles and their use of enzyme immolbilization", *Biotechnology Progress*, Vol. 9, pp. 661-665.

Warren, L.A., Maurice, P.A., Parmar, N., and Ferris, F.G. (2001). "Microbially mediated calcium carbonate precipitation: implications for solid-phase capture of inorganic contaminants", *Geomicrobiology Journal*. Vol. 18, pp. 93-115.

Wartman, J. and Riemer, M. (2002). "The use of fly ash to alter the geotechnical properties of artificial model clay", *Proceeding of the Intl. Conference on Physical Modeling in Geotechnics*, St. John, Canada, July 2002.

Williamson, K.J. and McCarty, P.L. (1976). "Verification studies of the biofilm model for bacterial substrate utilization", *Journal Water Pollution Control Federation*, Vol. 48, pp. 281-289.